Uptake and intracellular delivery of nanoparticles into mammalian cells

Inaugural-Dissertation

to

obtain the academic degree

Doctor rerum naturalium (Dr. rer. nat.)

submitted to the Department of Biology, Chemistry and Pharmacy

of the

Freie Universität Berlin

by

Irene Schütz

born in

Fergana, Usbekistan

Berlin, July 2015

This thesis was prepared at the Institute of Chemistry and Biochemistry, Freie Universität Berlin and at the Leibniz-Institute for Molecular Pharmacology (FMP), Berlin-Buch under the supervision of Prof. Dr. Volker Haucke from April 2009 until June 2015.

1st Reviewer: Prof. Dr. Volker Haucke

2nd Reviewer: Prof. Dr. Eckart Rühl

Date of defense: December 16th 2015

I declare that my PhD thesis entitled “Uptake and intracellular delivery of nanoparticles into mammalian cells” has been written independently and with no other sources and aids than quoted.

Berlin, July 15th 2015

To the best sister in the world.

ACKNOWLEDGEMENTS

I would like to thank my supervisor Prof. Dr. Volker Haucke for giving me the opportunity to perform the work presented here. Thank you for your guidance and excellent support on my journey through the fields of biochemistry, cell biology, microscopy and nanotechnology. Your enthusiasm for science and your encouragement have been a constant source of motivation. During the time spent in your lab, I have not only extensively broaden my scientific horizon, but have also learned some valuable life lessons.

Furthermore, I would like to acknowledge the contributions of all collaborators: the groups of Prof. Dr. Eckart Rühl and Prof. Dr. Christina Graf for their commitment to the synthesis of silica nanoparticles and our collaboration within the SPP1313. I also want to thank Prof. Dr. Marcelo Calderón and Harald Krüger for the synthesis of TMPs, but more importantly for all the fruitful scientific discussions.

I would further like to thank all current and former members of the Haucke group for creating a unique scientific environment that has always been collaborative, inspiring and cheerful. Particularly, I want to say ‘thank you’ to a few special colleagues who became valuable friends: Wiebke Stahlschmidt (for not only being my initial chaperone in the lab, but all the good and bad times we shared), André Lampe (for all the intriguing technical discussions – with and without beer), Christina Kath (for constantly encouraging me to reach for higher goals) and Anela Vukoja (for good advice and the great Berlin action).

Finally, I want to thank all my other friends, near and far, and my family for their patience and support. And most importantly, I want to express my deepest gratitude to Manfred Bröring and my little sister Katharina Schütz for their love and never-ending support. Thank you for always believing in me!

DIRECTORY

SUMMARY

In the past two decades nanomaterials have become increasingly important in our daily life. Applications involving nanoparticle technology cover huge areas, such as the textile- and electronic industry, but particularly biomedicine. In fact, a high interest arose for pharmaceutical applications as nanoparticles hold great promise as therapeutic and diagnostic tools to advance detection and treatment of human diseases. For instance, the use of nanoparticle technology enabled remarkable improvements in the treatment of cancer, ranging from increased efficacy of cancer drug delivery to enhanced immunogenicity of cancer vaccines. Hence, it is necessary to fully understand the mechanisms of the interactions of nanoparticles with living cells. This knowledge will help to assess the biological consequences and to eventually design and engineer nanoparticles accordingly for individual pharmacological requirements.

In this study, we focused on the effects of the interaction of AHAPS(*N*-(6-aminohexyl)-aminopropyltrimethoxysilane)-functionalized silica nanoparticles (SiNPs) with human cervix carcinoma (HeLa) cells. We could show that these positively charged amino-functionalized nanoprobes were internalized largely via dynamin 2-dependent caveolar uptake, requiring an intact cytoskeletal network. Following cell entry SiNPs were targeted to late endosomal/ lysosomal compartments, where they accumulated and eventually led to reduced cell viability as demonstrated by MTT assays. The internalization of fluorescently labeled transferrin and epidermal growth factor (EGF) proceeded unaltered in SiNP-filled cells, as did the recycling of fluorescently labeled transferrin. In contrast, we observed that intralysosomal accumulation of SiNPs severly impaired the degradation of EGF. Moreover, levels of the autophagosomal marker LC3 (microtubule-associated protein light chain 3) along with autophagy-specific cargo protein p62 were elevated in SiNP-loaded cells. Given that lysosomes play an essential role in cell physiology crucial for the degradation of internalized cargo (e.g. EGF via degradative sorting) and aggregated proteins (e.g. p62 via autophagy), we examined lysosomal function. However, neither intralysosomal acidification nor intralysosomal hydrolase activity was determined to be responsible for the dysfunction of SiNP-filled lysosomes. We therefore propose that defective lysosomal degradation of autophagic and internalized subtrates results from inhibition of fusion between lysosomes and upstream compartments.

In a second project, we used FRET (fluorescence resonance energy transfer) to investigate intracellular drug release from a theranostic macromolecular prodrug (TMP) composed of a dendritic polyglycerol (PG) serving as polymeric nanocarrier, doxorubicin (Dox) and an

indodicarbocyanine dye (IDCC). While the PG and IDCC were linked via a tri-functional linker, the chemotherapeutic drug was attached to the delivery system via a pH-sensitive hydrazone bond. Additionally, Dox was located in close proximity to IDCC resulting in the quenching of Dox fluorescence via intramolecular FRET. After initial validation of the cell permeability of the PG-nanoparticles, we measured recovery of Dox fluorescence and evaluated its nuclear accumulation in live cell imaging experiments in HeLa cells. We were able to assure the pH-sensitive intracellular drug cleavage from the TMP by including two additional control conjugates, a non-cleavable, but quenched probe and a cleavable but non-quenching system. In summary, we could demonstrate that this functional probe can act as a reporter and help to understand drug release mechanisms and measure kinetics in real time.

ZUSAMMENFASSUNG

In den vergangenen zwanzig Jahren sind Nanomaterialien ein überaus wichtiger Bestandteil unseres täglichen Lebens geworden. Verfahren basierend auf der Nanopartikeltechnologie finden Anwendungen in verschiedensten Bereichen wie der Textil- und Elektronikindustrie, aber auch in der Biomedizin. In der Tat besteht ein spezielles Interesse an pharmazeutischen Applikationen, da Nanopartikel, eingesetzt als therapeutische und diagnostische Werkzeuge, helfen können die Detektion und vorallem Behandlung von Krankheiten voranzutreiben. Beispielsweise hat der Einsatz der Nanopartikeltechnologie beachtliche Fortschritte in der Behandlung von Krebs ermöglicht, unter anderem eine verbesserte Wirksamkeit im Transport von Krebsmedikamenten und eine erhöhte Immunogenität von Krebsimpfstoffen. Deshalb ist es überaus wichtig die zugrunde liegenden Interaktionsmechanismen zwischen Nanopartikeln und lebenden Zellen zu verstehen. Dieses Wissen wird helfen biologische Konsequenzen beurteilen und anschließend in das Design und die Konstruktion von Nanopartikeln übertragen zu können, die den individuellen pharmakologischen Anforderungen entsprechen.

Im Rahmen dieser Arbeit haben wir uns in erster Linie auf die Interaktion zwischen AHAPS(*N*-(6-aminohexyl)-aminopropyltrimethoxysilane)-funktionalisierten Siliziumoxidnano-partikeln (SiNP) mit humanen Gebärmutterkarzinomzellen (HeLa) fokussiert. Wir konnten zeigen, dass die positiv geladenen Aminogruppen-funktionalisierten Nanoproben hauptsächlich über die Dynamin 2-abhängige Caveolin-vermittelte Endozytose internalisiert wurden, unterstützt von einem funktionsfähigen Zytoskelettnetzwerk. Nach dem Zelleintritt wurden die SiNP in späte endosomale/ lysosomale Kompartimente transportiert, wo sie sich anreicherten und vermutlich die Zellviabilität beeinträchtigten, wie wir in MTT Tests zeigen konnten. Sowohl die Aufnahme von fluoreszenzmarkiertem Transferrin und epidermalem Wachstumsfaktor (EGF), als auch das Recycling von fluoreszenzmarkiertem Transferrin in SiNP-beladenen Zellen ging unverändert vonstatten. Demgegenüber haben wir festgestellt, dass die intralysosomale SiNP-Anreicherung den Abbau von EGF stark beeinträchtigt. Zusätzlich wurden in SiNP-akkumulierten Zellen dramatisch erhöhte Werte für den autophagosomalen Marker LC3 (microtubule-associated protein light chain 3), sowie für das autophagiespezifische Frachtprotein p62 gemessen. Da Lysosomen, als essentielle Bausteine für die Zellphysiologie, verantwortlich sind für den Abbau von internalisierten Bestandteilen (z.B. EGF über den degradativen Sortierungsprozess) und aggregierten Proteinen (z.B. p62 über Autophagie), haben wir die lysosomale Funktionalität untersucht. Wir konnten jedoch weder die intralysosomale Ansäuerung, noch die Aktivität von intralysosomalen Hydrolasen als

Ursache für die Fehlfunktion von SiNP-beladenen Lysosomen identifizieren. Deshalb vermuten wir, dass der mangelhafte lysosomale Abbau von autophagosomalen und internalisierten Substraten auf die Inhibition der Fusion zwischen Lysosomen und vorgeschalteten Kompartimenten zurückzuführen ist.

Parallel dazu haben wir mittels FRET (Fluoreszenz Resonanz Energie Transfer) die intrazelluläre Wirkstofffreisetzung eines theranostischen makromolekularen Propharmakons (TMP) untersucht, das aus einem dendritischen Polyglycerol (PG) als polymerem Nanotransporter, Doxorubicin (Dox) und einem Indodicarbocyaninfarbstoff (IDCC) zusammengesetzt war. Alle Komponenten wurden über einen trifunktionalen Linker miteinander vernetzt, wobei wichtig ist, dass der chemotherapeutische Wirkstoff über eine pH-sensitive Hydrazonbindung an das Transportsystem gebunden war. Zusätzlich wurde das Dox in sehr kurzem Abstand zum IDCC positioniert, so dass eine Auslöschung der Doxorubicinfluoreszenz (Quenching) über intramolekularen FRET gewährleistet wurde. Nach einer anfänglichen Validierung der Zellpermeabilität der PG-Nanopartikel haben wir Lebendzellexperimente in HeLa Zellen durchgeführt und dabei die wiederhergestellte Doxorubicinfluoreszenz und seine nukleäre Akkumulierung ermittelt und ausgewertet. Durch den Einsatz von zwei zusätzlichen Kontrollkonjugaten, wovon eines nicht-spaltbar, aber gequencht und das andere spaltbar, jedoch nicht-gequencht wurde, waren wir in der Lage die ermittelten Erkenntnisse über die pH-sensitive intrazelluläre Wirkstofffreisetzung abzusichern. Zusammengefasst konnten wir zeigen, dass diese funktionale Probe als Reporter fungieren und dabei helfen kann Mechanismen zur Wirkstofffreisetzung zu verstehen und ihre Kinetiken in Echtzeit zu erfassen.

1 INTRODUCTION

1.1 Endocytic pathways

Regulated processes are required for the maintenance of cellular and organismal homeostasis. The plasma membrane, a highly dynamic structure, serves as a major control point that coordinates the exchange of molecules between the extracellular environment and the cell interior. Small molecules (e.g. ions, sugars or amino acids) pass across the membrane via channels or integral membrane protein pumps, whereas larger molecules must be transported in plasma membrane-derived invaginations into cells. This procedure, known as endocytosis, is classified as phagocytosis ('cell eating') and pinocytosis ('cell drinking'). Phagocytosis is a process restricted to specialized cells by which large particles such as pathogens or cell debris are internalized. Pinocytosis in contrast is conducted in all cells following mechanistically diverse pathways to maintain complex physiological processes such as neurotransmission, signal transduction, immune surveillance and antigen-presentation (Figure 1.1) (Conner & Schmid, 2003; Niedergang & Chavrier, 2004).

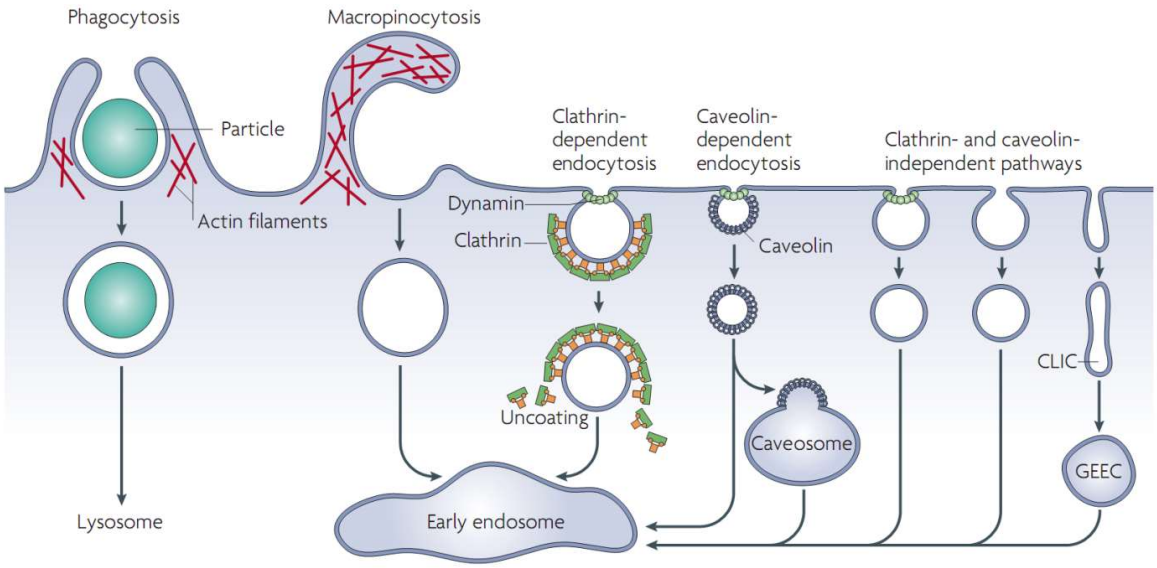

Figure 1.1 Pathways of endocytosis. Actin-dependent internalization of large particles and fluids occurs via phagocytosis and macropinocytosis, respectively. Both clathrin- and caveolin-dependent endocytosis involve coat proteins and undergo dynamin-driven fission. Additional pathways distinct from clathrin- and caveolin-mediated endocytosis might also be dynamin-dependent. Internalized cargoes are often delivered to early endosomes via vesicular (clathrin- or caveolin-coated vesicles) or tubular structures (clathrin- and dynamin-independent carriers, CLICs). Some pathways include intermediate compartments, such as caveosomes or glycosyl phosphatidylinositol-anchored protein-enriched early endosomal compartments (GEECs), to which cargo is first transported on the way to the early endosome (Mayor & Pagano, 2007).

Three pinocytic entry routes which are distinct from each other (clathrin-dependent endocytosis, caveolin-dependent endocytosis, and clathrin- and caveolin-independent endocytosis) will be further described below (Figure 1.2)(Hansen & Nichols, 2009).

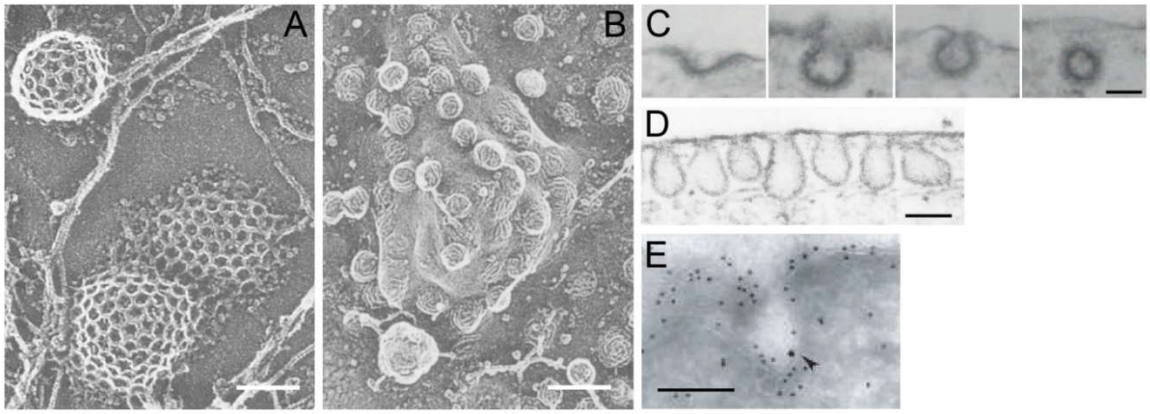

Figure 1.2 Electron micrographs from early endocytic intermediates of clathrin-dependent and –independent pathways. (**A**) Clathrin lattices on the inner surface of a chick fibroblast. Scale bar, 100 nm. (Heuser & Anderson, 1989) (**B**) Deep-etch view of caveolae from human fibroblasts subjected to 1 M NaCl for 15 min at 4°C. Scale bar, 250 nm. (Rothberg et al, 1992) (**C**) Stages of clathrin-coated pit (CCP) formation: membrane invagination, U-shaped CCP, Ω-shaped constricted CCP and free clathrin-coated vesicle (CCV). Scale bar, 100 nm. (Posor et al, 2013) (**D**) Thin section view from human fibroblast caveolae. Scale bar, 250 nm. (Rothberg et al, 1992) (**E**) Ultra-thin cryosections of COS7 cells expressing flotillin-1-GFP (15 nm gold secondary) and endocytosed subunit B of cholera toxin (CTxB)-FITC (10 nm gold-conjugated secondary). Scale bar, 200 nm. (Glebov et al, 2006)

1.1.1 Clathrin-mediated endocytosis

This pinocytic entry route is the best characterized endocytic pathway and essential for fundamental processes as neurotransmission and signal transduction by controlling and regulating surface protein levels. Clathrin-dependent endocytosis is responsible for the receptor-mediated uptake of essential nutrients, such as low-density lipoprotein, transferrin, and growth factors (Brodsky, 2012; Doherty & McMahon, 2009). This pathway is also hijacked by bacteria, viruses and toxins to gain access to the interior of the cell (Dong M. et al, 2003; Rust et al, 2004; Veiga & Cossart, 2005).

The clathrin-coated vesicle cycle, which is crucial for a persistent function of clathrin-mediated endocytosis (CME), can be categorized in five steps (Figure 1.3; see also Figure 1.2 C): nucleation, cargo selection, coat assembly, scission and uncoating (McMahon & Boucrot, 2011).

The initial phase of the creation of a clathrin-coated pit (CCP) requires the formation of a membrane invagination. FCH domain-only proteins (FCHo 1/2) bind to phosphatidylinositol-4,5-bisphosphate ($PI(4,5)P_2$), a plasma membrane-specific lipid, and subsequently recruit EGFR pathway substrate 15 (Eps15) and intersectins (Henne et al, 2010). FCHo proteins are able to bind to low curvatures via their F-BAR (Bin-Amphiphysin-Rvs) domain, where they initiate the generation of a CCP due to their membrane-binding activity.

This protein assembly then recruits adaptor protein 2 (AP-2) to the plasma membrane (Collins B. M. et al, 2002; Pechstein et al, 2010), where it coordinates cargo selection together with other cargo-specific adaptor proteins (collectively known as CLASPs, clathrin-associated sorting proteins) (Traub, 2009). As AP-2 binds both cargo and clathrin, it acts as a major interaction hub in clathrin-coated vesicle (CCV) formation (Wieffer et al, 2009).

After cargo selection the clathrin coat is assembled by recruitment of clathrin triskelia (Figure 1.2 A) (Brodsky, 2012). Clathrin polymerization not only leads to the formation of a vesicle coat but also results in stabilization of the membrane curvature (Hinrichsen et al, 2006). Additionally, accessory proteins such as Eps15 and epsin are directed to the rim of the maturing vesicle, where they contribute to membrane bending (Ford et al, 2002; Tebar et al, 1996).

The scission of a nascent vesicle is initiated by a constriction driven by BAR domain-containing proteins, such as amphiphysin, endophilin and sorting nexin 9 (SNX9), which gather preferably at the neck of the clathrin cage (Ferguson S. M. et al, 2009; Posor et al, 2013; Sundborger et al, 2011; Wigge et al, 1997). BAR proteins recruit the GTPase dynamin via their SRC homology 3 (SH3) domains to the vesicle neck, where it mediates further constriction followed by the scission of the vesicle from the plasma membrane (Hinshaw & Schmid, 1995; Roux et al, 2006; Sweitzer & Hinshaw, 1998). Fission of the CCV requires multiple rounds of GTP binding and hydrolysis (Faelber et al, 2011).

Finally, uncoating of the detached vesicle is facilitated by auxilin, which binds to the clathrin terminal domain after vesicle budding (Massol et al, 2006; Scheele et al, 2001; Ungewickell et al, 1995). It then recruits the ATPase heat shock cognate 70 (Hsc70) to the foot of a clathrin tripod for the ATP dependent disassembly of the clathrin coat (Rapoport et al, 2008; Schlossman et al, 1984; Xing et al, 2010). Destabilization of the clathrin coat results in release of clathrin triskelia (Bocking et al, 2011; Rothnie et al, 2011). In addition, a change in lipid composition mediated by the 5-phosphatase synaptojanin is crucial for the uncoating of CCVs (Cremona et al, 1999).

A new cycle of clathrin-coated vesicle formation can take place after uncoating and release of all components of the clathrin machinery (Taylor et al, 2011).

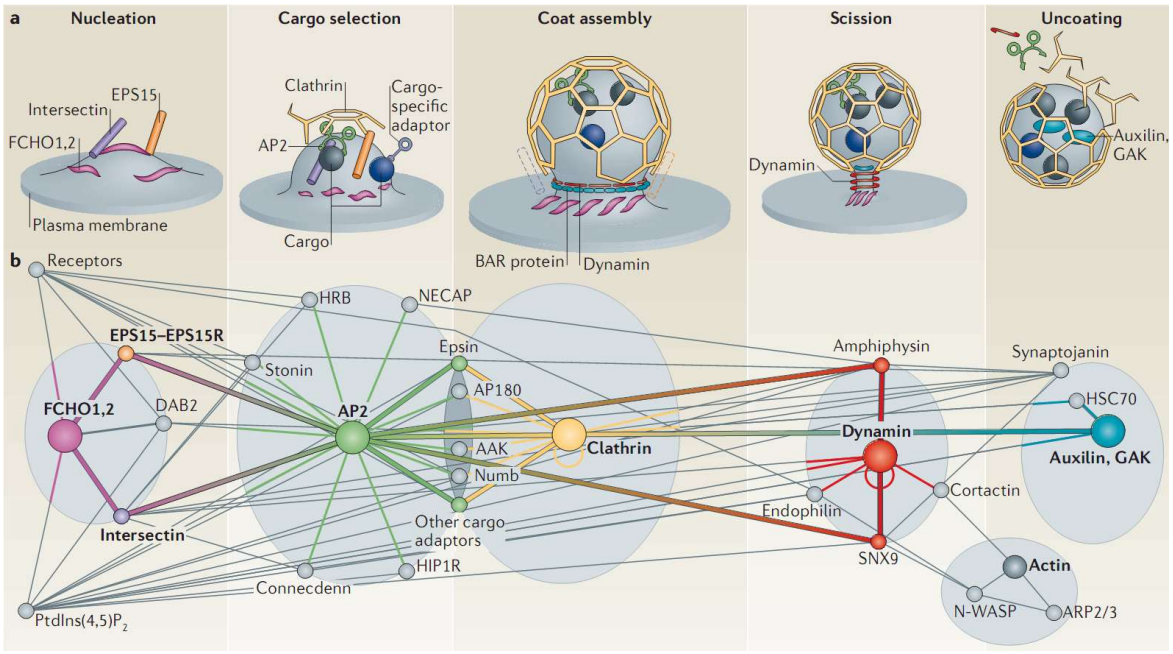

Figure 1.3 The clathrin-coated vesicle cycle. The assembly and disassembly of the clathrin machinery involved in clathrin-coated vesicle formation can be subdivided into five steps: nucleation, cargo selection, coat assembly, scission and uncoating. Consult the text above for detailed information about the processes. Taken from (McMahon & Boucrot, 2011)

1.1.2 Dynamin 2-dependent caveolar endocytosis

The best-described clathrin-independent endocytic route is the caveolin-dependent pathway (Kirkham & Parton, 2005; Mayor & Pagano, 2007). Cavolae are highly characteristic bulb-like shaped plasma membrane invaginations of 60-80 nm surrounded by a caveolin protein coat (Figure 1.2 B and D) (Rothberg et al, 1992). Caveolin 1 (also called (VIP)21, vesicular integral membrane protein), one of three caveolin proteins and the most abundant component of caveolae, is inserted in the inner leaflet of the plasma membrane (Dietzen et al, 1995). There, it is surrounded by four additional structural elements termed cavins 1-4 (Hansen & Nichols, 2010; Hill M. M. et al, 2008; Liu L. et al, 2008). These cytoplasmic proteins form heteromeric complexes that are recruited to caveolae, where they associate with both phosphatidylserine and caveolin 1 (Gustincich et al, 1999; Hayer et al, 2010). Moreover, the BAR domain protein pacsin 2 (PKC and casein kinase substrate in neurons 2, also termed syndapin 2) and the ATPase EHD2 (Eps-15 homology domain-containing protein 2) are also present in caveolae. EHD2 binds to $PI(4,5)P_2$, which is

enriched in the plasma membrane around the caveolar opening and associates with caveolae via an amino acid stretch located on its G-domain (Daumke et al, 2007; Fujita et al, 2009; Moren et al, 2012; Stoeber et al, 2012). The curvature sensing protein pacsin 2 then binds dimers of EHD2 and additionally interacts with dynamin via its SH3 domain and with caveolin 1 via its N-terminus (Hansen et al, 2011; Senju et al, 2011).

Caveolin-mediated uptake (Figure 1.4) is highly dependent on cholesterol content and the cytoskeleton (Breen et al, 2012; Richter et al, 2008; Sharma et al, 2004; Wickstrom et al, 2010). Although known for many years, this endocytic process remains a subject of controversy as specific cargo for this endocytic pathway is still under debate (Milici et al, 1987; Parton & del Pozo, 2013; Shvets et al, 2014). Simian virus 40 (SV40) was long thought to be internalized exclusively via caveolin-mediated endocytosis, but is now known to take a caveolin-independent pathway (Damm et al, 2005; Ewers et al, 2010; Pelkmans et al, 2001). Nevertheless, several studies point at dynamin as being crucial for the budding of caveolae from the plasma membrane (Henley et al, 1998; Oh P. et al, 1998).

However, caveolae not only play a central role in caveolin-mediated endocytosis, but have also been shown to be pivotal in lipid regulation (Asterholm et al, 2012; Fernandez-Rojo et al, 2012), signal transmission (Collins B. M. et al, 2012; Okamoto T. et al, 1998), in cell protective mechanosensing (Dulhunty & Franzini-Armstrong, 1975; Sinha et al, 2011) and in remodeling of the extracellular environment (Goetz et al, 2011; Nassoy & Lamaze, 2012).

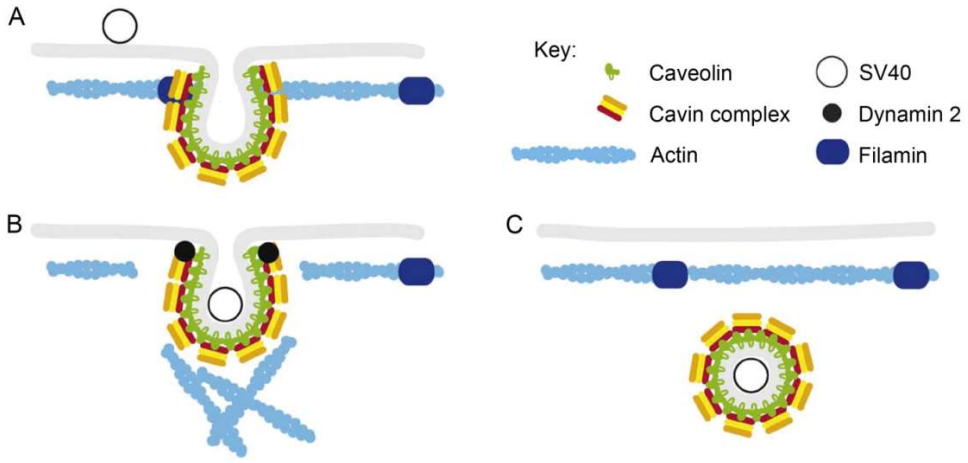

Figure 1.4 Scheme of caveolar-mediated endocytosis. (**A**) Static caveolar structures are closely associated with the actin cytoskeleton via binding to filamin. Caveolin, inserted in the inner leaflet of the plasma membrane is surrounded by the cavin complex. (**B**) Entry of SV40 triggers multiple signaling events leading to the recruitment of dynamin, which is crucial for the budding of vesicles from the plasma membrane. Signaling also initiates a burst of actin polymerization adjacent to virus-loaded caveolae, which might be important for the inward movement of forming caveolar vesicles.

(**C**) After scission, the released caveolar vesicle will eventually fuse with caveosomes or early endosomes. Modified from (Hansen & Nichols, 2010)

1.1.3 Flotillin internalization via CLIC/ GEEC intermediates

Another variant of clathrin-independent endocytosis involves flotillin proteins and CLIC/ GEEC (clathrin-independent carriers/ GPI-enriched early endosomal compartments) structures (Doherty & McMahon, 2009; Hansen & Nichols, 2009). Flotillin 1 and flotillin 2 (also referred to as reggie 2 and reggie 1, respectively) are integral membrane proteins that form microdomains in the plasma membrane upon oligomerization (Otto & Nichols, 2011; Solis et al, 2007). Similar to caveolins, they are tightly associated with the membrane via hairpins inserted into the inner leaflet (Morrow & Parton, 2005). Flotillin microdomains have been proposed to represent an additional clathrin-independent endocytic pathway. This was corroborated by studies indicating that the internalization of GPI-anchored protein CD59 and cholera toxin (CTx)-binding glycosphingolipid GM1 (monosialotetrahexosylganglioside) took place in a flotillin- and dynamin-dependent fashion independent of clathrin or caveolin (Figure 1.2 E) (Frick et al, 2007; Glebov et al, 2006). Nontheless, others suggested that flotillin-mediated uptake proceeds dynamin-independent (Carcea et al, 2010). Furthermore, early CLIC/ GEEC intermediates were found to be concentrated in flotillin protein although cargo internalization was flotillin-independent (Lundmark et al, 2008). CLICs were observed to form vesicular and tubular structures which, are transported to GEECs independent of dynamin-mediated scission (Kirkham et al, 2005).

In addition to endocytosis, flotillins have been implicated in signal transduction and cytoskeleton regulation, with yet unknown molecular mechanisms (Meister & Tikkanen, 2014; Otto & Nichols, 2011).

1.1.4 Role of cytoskeletal elements in endocytosis

1.1.4.1 Actin filaments

Actin plays an important role in CME, where it participates at multiple stages of the clathrin-coated vesicle cycle (see chapter 1.1.1) and facilitates the formation of CCVs by providing energy for vesicle budding and scission (Figure 1.5) (Kaksonen et al, 2003; Merrifield et al, 2002; Mooren et al, 2012). Cortactin or N-WASP (neural Wiskott-Aldrich syndrome protein) first orchestrate the ARP2/3 (actin-related protein 2/3) complex to the clathrin network, where it then initiates the recruitment and nucleation of actin into actin filaments (Benesch

et al, 2005; Campellone & Welch, 2010; Cao et al, 2003; Helgeson & Nolen, 2013; Perrais & Merrifield, 2005). TIRF (total internal reflection fluorescence) microscopy studies uncovered actin as a late component of the clathrin network since its assembly begins at the time of membrane scission (Boettner et al, 2012; Taylor et al, 2011). Additionally, actin was shown to facilitate budding and scission of large vesicles, such as those formed at the plasma membrane during bacterial and viral infection (Cureton et al, 2009; Veiga et al, 2007).

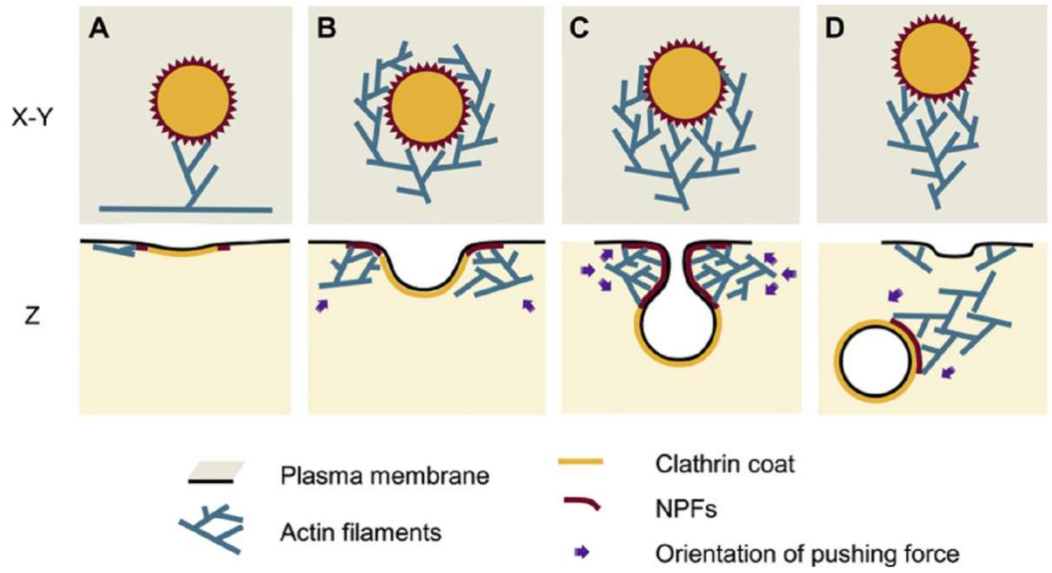

Figure 1.5 Model for the role of actin in CME – shown en face (X-Y) and in profile (Z). (**A**) Nucleation-promoting factors (NPFs), first recruited to the periphery of the clathrin coat, activate ARP2/3, which then initiates actin assembly. (**B**) An expanding actin network surrounds the clathrin-coated structure and possibly drives its lateral movement. (**C**) The dendritic actin network sitting at the neck of the CCP promotes constriction and elongation. (**D**) The actin network finally reorganizes into a comet tail and facilitates the inward movement of the vesicle away from the plasma membrane. Taken from (Collins A. et al, 2011)

An essential role for actin is also given in caveolar-mediated endocytosis, except that there are different key players involved in the recruitment of actin and the formation of actin stress fibers, respectively (Figure 1.6) (Mundy et al, 2002; Parton & del Pozo, 2013; Richter et al, 2008). Filamin A, one of the most prominent actin-crosslinking proteins, was shown to stabilize caveolin 1-positive structures at the plasma membrane by binding them to actin stress fibers. Thereby, it regulates caveolae dynamics upon phosphorylation mediated by protein kinase C α (PKCα) (Muriel et al, 2011). However, to promote internalization of caveolae additional proteins such as Abl (Abelson murine leukemia) tyrosine kinase and the formin mDia1 (mammalian diaphanous 1) are required (Hernandez et al, 2004;

Watanabe N. et al, 1999). Abl regulates the actin-linked caveolin 1 pool and its correct spatial organization, whereas mDia1, an actin regulator downstream of Abl, controls organization and inwards trafficking of caveolae (Echarri et al, 2012).

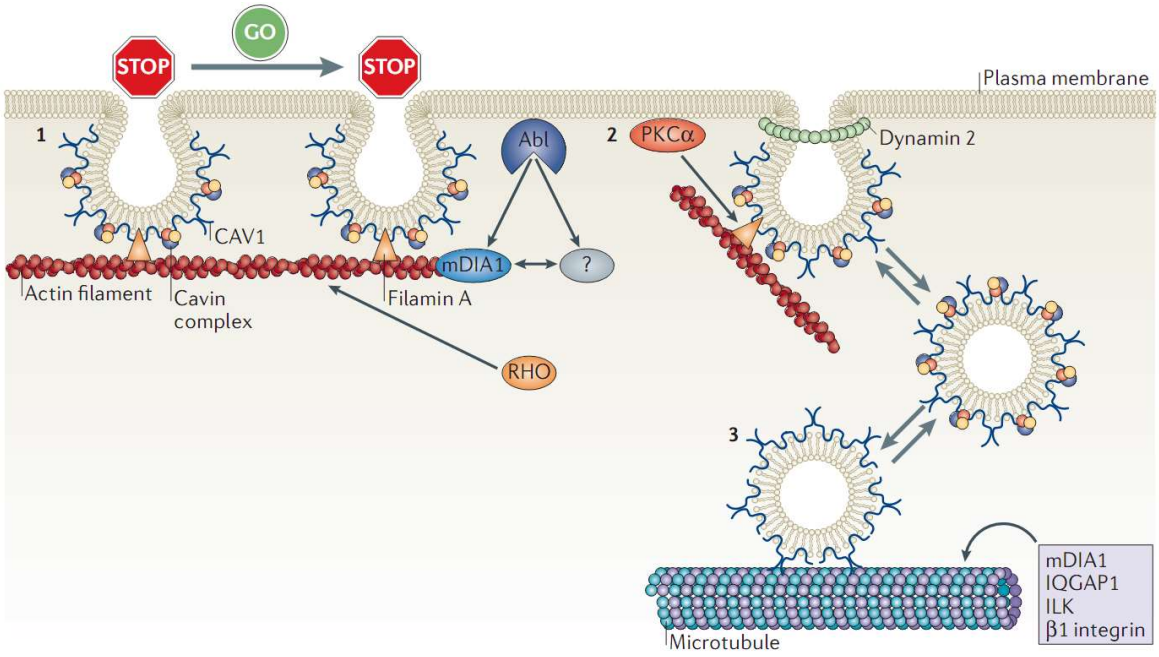

Figure 1.6 Involvement of the cytoskeleton in caveolae movement and endocytosis. Lateral movement of caveolae (indicated as 'STOP' and 'GO') is regulated by filamin A and by the Abl tyrosine kinase-mDia1 pathway that controls actin stress fiber dynamics (1). Internalization of caveolar structures is controlled by dynamin 2, protein kinase C α-mediated phosphorylation of filamin A and actin in the first step, and by microtubules in the second (2). Trafficking of caveolar vesicles is microtubule-dependent (see also chapter 1.1.4.2). β1 integrin, ILK (integrin-linked kinase), IQGAP1 (IQ motif-containing GTPase-activating protein 1) and mDia1 (mammalian diaphanous 1) promote the stabilization of microtubules and conduct the translocation of caveolae from one cytoskeletal system to the other (Dobbins et al). Taken from (Parton & del Pozo, 2013)

Although flotillins have been shown to interact with and modulate the cytoskeleton in a variety of cellular processes, there is no evidence that actin is involved in flotillin-dependent endocytosis (Langhorst et al, 2007; Ludwig et al, 2010; Otto & Nichols, 2011). Interactions between flotillin microdomains and actin or actin-associated proteins have been shown to be important for cell polarization, chemotaxis, cell motility, cell signaling and cell-cell adhesion (Affentranger et al, 2011; Malaga-Trillo et al, 2009; Rajendran et al, 2009; Rossy et al, 2009).

1.1.4.2 Microtubules

Microtubules (MT) participate in various fundamental cellular processes, including vesicular trafficking and cell migration (Doherty & McMahon, 2008; Etienne-Manneville, 2013). Clathrin-dependent and –independent endocytosis of integrins, trans-membrane receptors that connect the extracellular matrix (ECM) with the cytoskeleton, represents an essential step in cell migration (Margadant et al, 2011). Several studies have shown that depletion of clathrin machinery components, such as clathrin, dynamin 2 and clathrin adaptors like AP-2 or Dab-2 (Disabled-2) result in an increased integrin surface expression and reduced cell migration (Chao & Kunz, 2009; Ezratty et al, 2009; Ezratty et al, 2005; Teckchandani et al, 2009). However, the recruitment of clathrin machinery components to focal adhesions is independent of MTs (Etienne-Manneville, 2013).

In contrast, in the caveolar membrane system MTs are essential for caveolin transport, caveolae formation and caveolar vesicle trafficking from the plasma membrane into the cell interior and back (Figure 1.6) (Parton & del Pozo, 2013; Wickström et al, 2010). In particular, β1 integrin, a cell surface receptor, and integrin-linked kinase (ILK) an integrin-binding protein that regulates actin reorganization downstream of integrins, form a complex, which recruits the actin-binding scaffold protein IQGAP1 (IQ motif-containing GTPase-activating protein 1) to the cell cortex, where IQGAP1 interacts with its downstream effector mDia1 (see chapter 1.1.4.1) to promote local MT stabilization (Wickström et al, 2010). Importantly, the IQGAP1-mDia1 complex binding both actin and MTs represents a crossing point for the transition of pinched-off caveolar vesicles from actin fibers onto MTs for further inward trafficking (see Figure 1.6) (Brandt et al, 2007; Brown & Sacks, 2006; Ishizaki et al, 2001).

1.2 Endosome maturation

Surface receptors and other proteins can be internalized into cells via different pinocytic pathway mechanisms all involving the budding of carrier vesicles from the plasma membrane (PM) (see chapter 1.1). These vesicles eventually fuse to generate early endosomes (EEs), which function as key sorting stations in eukaryotic cells. From there the majority of proteins is recycled back to the PM directly or indirectly via recycling endosomes, while others are transported toward the lysosomal system for degradation and the trans-Golgi network (TGN). The development of early endosomes to late endosomes (LEs)/ lysosomes, a process referred to as endosomal maturation, involves major changes in protein or lipid composition and rising acidification of the endosomal lumenal milieu, with

pHs ranging from ≈6.8 to ≈4.5 (Huotari & Helenius, 2011; Maxfield & Yamashiro, 1987; Scott et al, 2014).

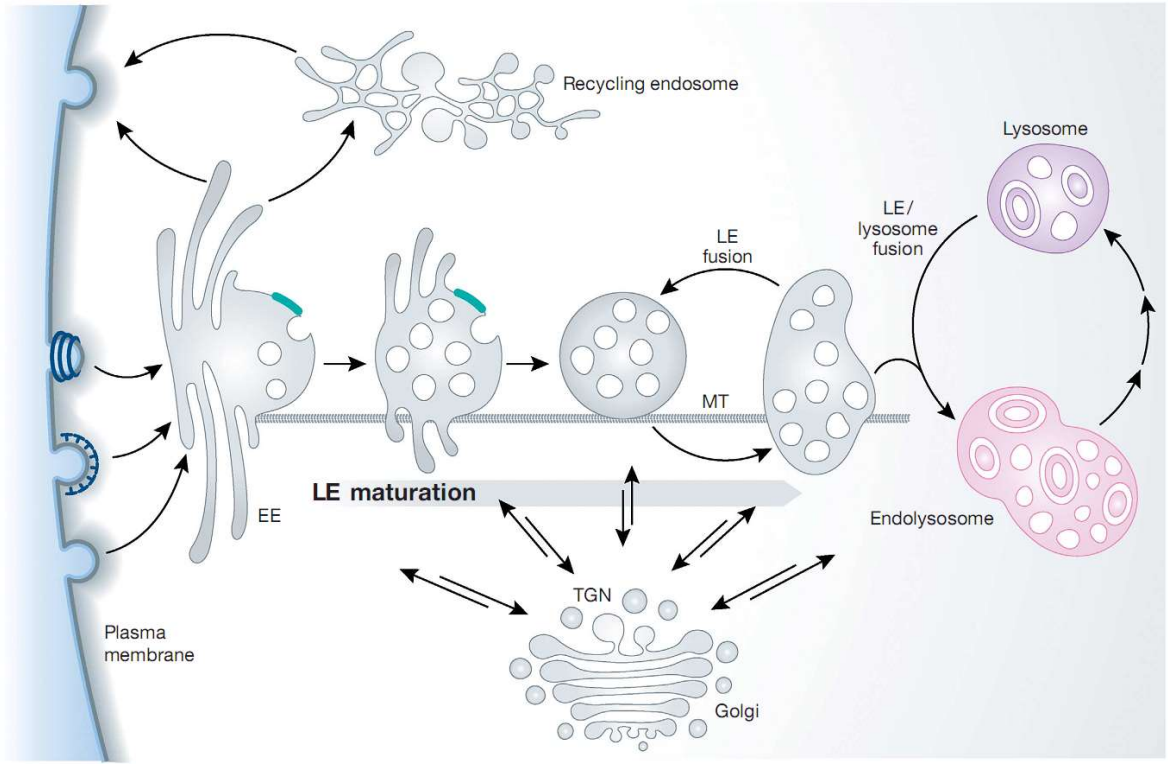

Figure 1.7 Endosome maturation. Cargo containing vesicles eventually fuse into early endosomes (EEs) after endocytosis. Proteins are then sorted either into a recycling pathway back to the PM or are routed toward the degradative pathway, that involves a comprehensive maturation process of EEs into late endosomes (LEs)/ lysosomes. Taken from (Huotari & Helenius, 2011)

All endocytosed material, internalized via clathrin-dependent and –independent pathways (see chapter 1.1), converge into the formation of EEs, which serve as the main sorting station and the starting point for LE maturation (Huotari & Helenius, 2011). Cytosolic proteins associate with the cytosolic surface of EE membranes and help to define their identity and functional properties. Beside the tethering factor EEA1 (early endosome antigen 1) and the GTPase Rab5, the phosphoinositol-3-phosphate (PI3P), a lipid generated by the phosphatidyl 3-kinase (PI(3)K) Vps34 (vacuolar protein sorting)/ p150, is characteristic for EE identity (Behnia & Munro, 2005; Gruenberg, 2001). EEs are mildly acidic with a pH in the range of 6.8 – 6.1 and appear in complex structures containing tubular and vacuolar elements (Lakadamyali et al, 2006; Maxfield & Yamashiro, 1987; van Meel & Klumperman, 2008). This mosaic of subdomains differs in protein composition and function, e.g. Rab 4 is involved in the rapid and direct recycling of surface receptors to the PM, whereas Rab 11 participates in the slow recycling route via recycling endosomes (Galvez et al, 2012; Zerial & McBride, 2001). Cargo destined for lysosomal degradation is sorted

into intralumenal vesicles (ILVs) by components of the ESCRT (endosomal sorting complex required for transport) machinery (Raiborg & Stenmark, 2009). Particularly, the Hrs subunit of the ESCRT-0 complex is recruited to EE membranes via its PI3P-binding FYVE domain, where it binds ubiquitylated cargo (Hurley & Stenmark, 2011). Subsequently, mediated by the action of ESCRT-I, ESCRT-II and ESCRT-III, ubiquitylated cargo is sequestered and sorted into newly formed ILVs (Henne et al, 2011). Simultaneously with recycling and degradation, retrograde transport between endosomes and the TGN continuously establishes delivery and removal of components during endosome maturation. Mediators of this traffic route are Rab family proteins (Rab7 and Rab9) and the multimeric retromer complex (Bonifacino & Hurley, 2008; Pfeffer, 2009).

Internalized material destined for degradation is sorted into vacuolar domains (namely ILVs) inside the EEs, which then mature to LEs (also known as MVBs). This maturation process is essential for the separation of the EE/ recycling pathway from the LE/ lysosome cycle and is accompanied by a multitude of changes, such as exchange and conversion of membrane components, formation of additional ILVs, drop in lumenal pH and movement to the perinuclear area (Huotari & Helenius, 2011). The exchange of the GTPase Rab5 to Rab7 on the maturing endosome determines the conversion from EE to LE and is regulated by the SAND-1/Mon1-Ccz1 complex (Kinchen & Ravichandran, 2010; Poteryaev et al, 2010; Wang C. W. et al, 2002). Importantly, the GTPase exchange itself is crucial for the recruitment of retromer complex and the replacement of CORVET (class C core vacuole/ endosome tethering) with the HOPS (homotypic fusion and vacuole protein sorting) complex, both of which establish the regulation of SNARE (soluble *N*-ethylmaleimide-sensitive factor attachment receptor) docking/ fusion proteins for EEs and LEs, respectively (Nickerson et al, 2009; Rojas et al, 2008; Solinger & Spang, 2013). Another important step in endosome maturation is the conversion of membrane lipids generated by a phosphatidyl 3-phosphate 5-kinase, PIKfyve, that phosphorylates PI3P to PI(3,5)P_2 (phosphatidylinositol-3,5-bisphosphate), lipids distinctive for EE and LE membranes, respectively (Odorizzi et al, 1998; Vicinanza et al, 2008). As mentioned earlier, the ESCRT machinery mediates protein sorting and ILV formation, and is therefore indispensable for MVB biogenesis (Henne et al, 2011). Increasing acidification of the LE (pH ranging from 6.0 – 4.8) important for hydrolytic reactions inside of LEs/ lysosomes is established by the large and complex proton pump V-ATPase, that consists of one membrane-associated V_o complex serving as a membrane pore for protons, and a cytosolic V_1 complex responsible for ATP-hydrolysis (Forgac, 2007; Marshansky & Futai, 2008). Acidified LEs/ MVBs are then rapidly transported via microtubules to the perinuclear area where they fuse with other LEs and lysosomes to form larger bodies (Luzio et al, 2007; Soppina et al, 2009). Mature LEs and lysosomes with a low

lumenal pH around 4.5 contain lysosomal membrane proteins such as LAMP1 (lysosome-associated membrane protein 1) and acid hydrolases that maintain the degradation process of constantly delivered cargo (see chapter 1.4) (Maxfield & Yamashiro, 1987; Schwake et al, 2013).

In addition to the described endocytic membrane transport, autophagy (see chapter 1.3) represents another route to deliver material into the lysosomal system destined for degradation (Scott et al, 2014).

1.2.1 Endocytic recycling of transferrin receptor

The blood plasma glycoprotein transferrin (Tf) and its receptor (TfR) are regulators of iron uptake and a source for hemoglobin synthesis (Jandl et al, 1959). Due to specific binding sites Tf is able to bind up to two Fe^{3+}-ions very tightly, but reversibly (Holmberg & Laurell, 1947). To avoid binding competition to iron-free Tf (apo-Tf) on the cell surface, interaction with TfR is only possible in an iron-bearing state (holo-Tf) (Aisen, 2004).

After binding of Tf to the TfR, its uptake proceeds via CME (see chapter 1.1.1), shown by depletion of essential components of the clathrin machinery, such as AP-2, $PI(4,5)P_2$, dynamin 2, cortactin and clathrin itself, which results in a significant reduction of Tf/ TfR internalization (Abe et al, 2008; Brodsky, 2012; Hill T. A. et al, 2009; Macia et al, 2006; Motley et al, 2003; von Kleist et al, 2011; Zoncu et al, 2007). Following endocytosis, vesicles with ligand-loaded TfR subsequently fuse with EEs, including both the static and dynamic population of EEs (Mayle et al, 2012). As demonstrated by live-cell microscopy static EEs (Rab5-associated) exhibit slow maturation kinetics, whereas dynamic EEs (Rab5- and Rab7-associated) display fast kinetics (Figure 1.8) (Lakadamyali et al, 2006). Due to the weakly acidic early endosomal pH iron (Fe^{3+}) is released from the ligand and transported as Fe^{2+} across the endosomal membrane via the divalent metal transporter (DTM1), while transferrin remains associated to its receptor (Fleming et al, 1998; Steere et al, 2012). Then, TfR is sorted into tubular structures of the EE and segregated from cargo that remains in endosomes for degradation. This sorting event was suggested to be Rab4-dependent (van der Sluijs et al, 1992). However, depletion of Rab4 using a siRNA-approach resulted in increased Tf recycling to the cell surface (Deneka et al, 2003). Vesicles separate from these tubules and deliver TfR either directly to the plasma membrane or indirectly via the endocytic recycling compartment (ERC) (Maxfield & McGraw, 2004). There is evidence that trafficking from early/ sorting endosomes to the ERC might be dependent on Sorting Nexin 4 (SNX4) and Rab22a GTPase activity (Magadan et al, 2006; Traer et al, 2007). Certainly,

transport from the ERC to the plasma membrane was shown to be strongly dependent on Rab11 (Ren M. et al, 1998; Ullrich et al, 1996). Whether Rab8, Rab35 and Arf6 GTPases are involved in Tf/ TfR recycling remains a subject of debate (Grant & Donaldson, 2009; Mayle et al, 2012). Finally, after returning to the cell surface Tf is released from its receptor facing near neutral pH of 7.4, ready for a new cycle of iron transport.

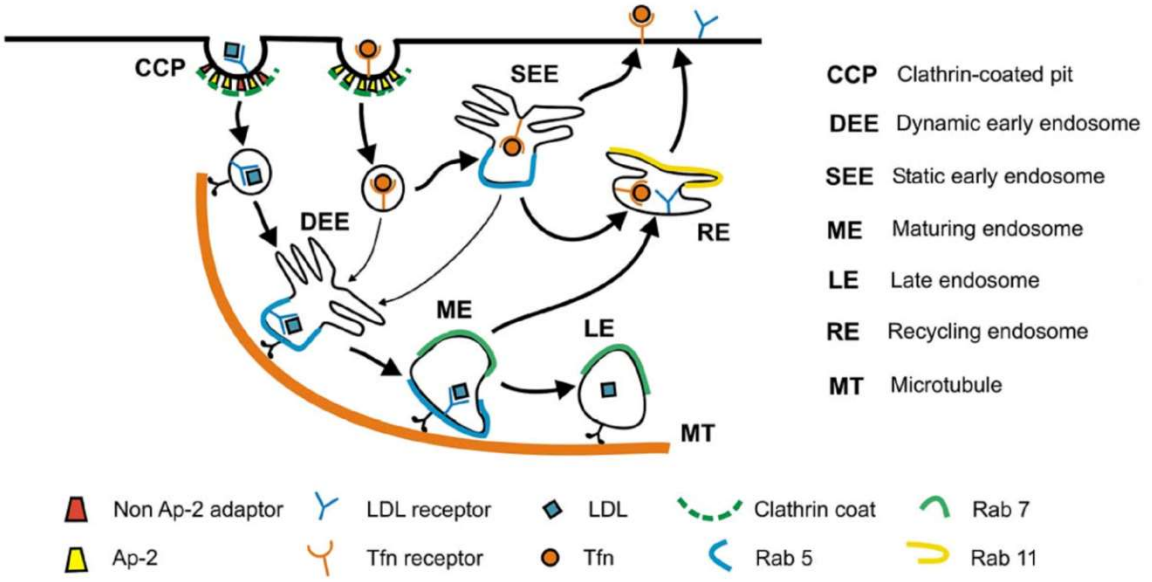

Figure 1.8 Early endosomal sorting of transferrin receptor (TfR). Tf bound TfR enters cells via CME. Subsequently vesicles containing TfR fuse with static and dynamic populations of EEs. TfR is then sorted into tubular structures and transported back to the cell surface. Recycling proceeds either fast (directly from EE to PM) or slow via recycling endosomes. Modified from (Lakadamyali et al, 2006)

1.2.2 Endosomal sorting of epidermal growth factor receptor

The transmembraneous glycoprotein EGFR is one of four members of the erbB family of receptor tyrosine kinases (RTKs) (Herbst, 2004). Ligand binding induces autophosphorylation and subsequent activation of signal transduction pathways. These signaling events regulate numerous cellular processes, such as proliferation, growth and survival (Yarden, 2001). Also, EGFRs are important targets for cancer therapy due to the fact that they are frequently overexpressed or mutated in various cancers (Witsch et al, 2010; Yarden & Sliwkowski, 2001).

Monomeric EGFR is autoinhibited and becomes activated upon ligand binding, thereby exposing its dimerization interface (Ferguson K. M. et al, 2003; Schlessinger, 2002). There are six known ligands for EGFR of which EGF (epidermal growth factor) and TGFα

(transforming growth factor α) are the best characterized. Following ligand binding, cytoplasmic tyrosine kinase domains of dimerized EGFRs then transphosphorylate the opposing monomer resulting in the recruitment of signaling modulators (Ferguson K. M. et al, 2003). Additionally, E3 ubiquitin ligase c-Cbl (named after Casitas B-lineage lymphoma) is recruited, which together with E2 ubiquitin-conjugating enzymes Ube2D1-4 (Ubc4/5 homolog, yeast) controls the downregulation of EGFR by ubiquitination (Jensen et al, 1995; Levkowitz et al, 1998; Schmidt & Dikic, 2005; Umebayashi et al, 2008).

Internalization of EGFR can be mediated via several alternative pathways depending on the extent of ubiquitination, although CME is predominant (Goh et al, 2010; Sigismund et al, 2005). Apart from tyrosine kinase activity of the EGFR, the interaction with the Cbl-CIN85-endophilin complex, comprising the ubiquitin ligase Cbl, the adaptor protein CIN85 (Cbl-interacting protein of 85 kDa) and endophilin (a regulatory component of clathrin-coated vesicles), is crucial for receptor internalization (Sorkina et al, 2002; Soubeyran et al, 2002). Ubiquitination of the EGFR is not strictly needed for its endocytosis, but it certainly is required for the activation of downstream signaling cascades, such as the MAPK (mitogen-activated protein kinase) pathway (Goh et al, 2010; Oda et al, 2005; Pearson et al, 2001). Internalized EGFR is then either recycled back to the PM or transported to lysosomes for degradation, depending on the associated ligand (Hurley & Stenmark, 2011). TGFα for instance dissociates from the EGFR at mildly acidic pH as found within endosomes, which leads to a deubiquitination of the receptor and its recycling to the cell surface. In contrast, EGF remains bound to EGFR due to a higher affinity at this pH, ensuring sustained receptor activation and resulting in lysosomal sorting via the MVB pathway (Madshus & Stang, 2009). Importantly ubiquitination of ligand-activated EGFR mediated by c-Cbl is pivotal for sorting into the degradative pathway (Huang et al, 2006). Similarly essential for the sorting of ubiquitinated EGFR is the ESCRT machinery as depletion of various ESCRT components resulted in strong inhibition of EGFR degradation (Babst et al, 2000; Bache et al, 2003; Bishop et al, 2002; Malerod et al, 2007; Raiborg et al, 2008; Raiborg & Stenmark, 2009). Prior to sorting of EGFR into ILVs or recycling to the PM, deubiquitination of the receptor is required (Hurley & Stenmark, 2011). AMSH [associated molecule with the SH3 domain (Src homology 3 domain) of STAM (signal transducing adapter molecule)] and USP8/UBPY (ubiquitin-specific protease 8), so called deubiquitinating enzymes (DUBs), were shown to cleave ubiquitin moieties from the EGFR (Clague & Urbe, 2006). Both DUBs competitively interact with ESCRT components and bind to both ESCRT-0 and ESCRT-III (Urbe et al, 2006). Particularly, AMSH was suggested to act at an earlier stage, whereas USP8 is involved in the regulation at the early and late stages dictating receptor fate (Alwan & van Leeuwen, 2007; Berlin et al, 2010; McCullough et al, 2004). Following deubiquitination and

sorting of EGFR into ILVs, MVBs subsequently fuse with lysosomes and deliver their content for degradation.

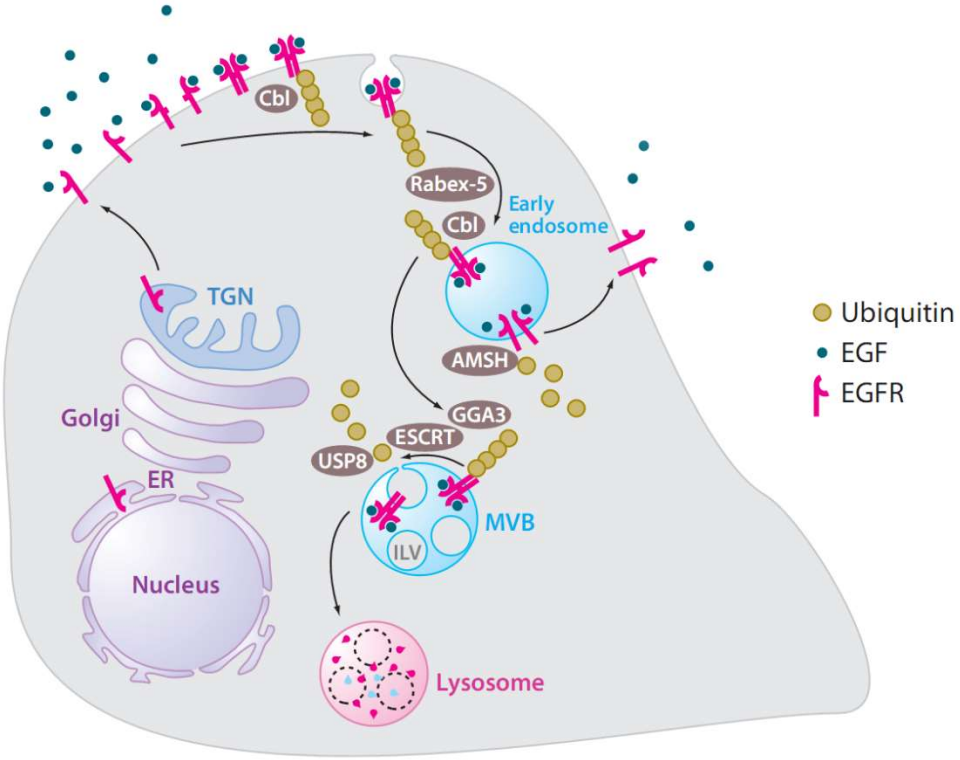

Figure 1.9 Endosomal sorting of EGFR. EGF binds to EGFR generating a conformational change, which makes the dimerization interface of the receptor accessible. Phosphorylation of the cytosolic tails of the dimerized receptors initiates signaling cascades and promotes receptor ubiquitination by the E3 ubiquitin ligase Cbl. Internalized receptors are transported to early endosomes where they are sorted either into the recycling or the degradative pathway. If ligands dissociate from the receptors at mildly acidic pH, the receptors become deubiquitinated by a DUB, leading to recycling. Still activated and ubiquitinated receptors are recognized by the ESCRT (endosomal sorting complex required for transport) machinery. Prior to sorting into ILVs, receptors undergo deubiquitination. Fusion of a MVB with a lysosome leads to degradation of EGFR and ligand. Taken from (Hurley & Stenmark, 2011)

1.3 Autophagy

This evolutionarily conserved pathway can be described as a ‘self-eating’ process, which is dedicated to the turnover of cytoplasmic components to retain cellular homeostasis. Particularly, misfolded or long-lived proteins, dispensable or damaged organelles, and invading microorganisms are degraded to produce metabolites for reuse as a nutrient and energy source (Figure 1.10). However, autophagy also represents the simplest form of a

cells adaptation to starvation. Meanwhile, evidence has been substantiated that autophagy has great impact on diverse fields of cell physiology such as neurodegeneration, immunity, cancer, development and ageing (Boya et al, 2013; Mizushima et al, 2008; Yang Z. & Klionsky, 2010a).

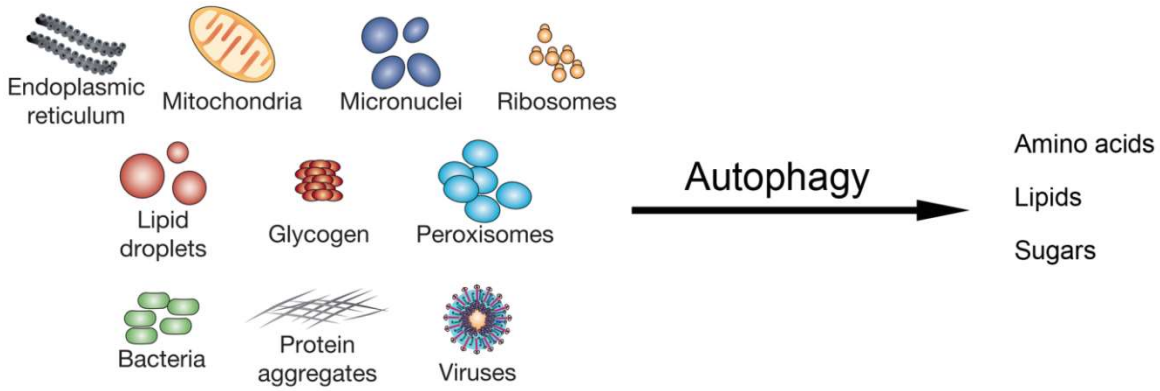

Figure 1.10 Turnover of cytoplasmic material via autophagy. Damaged or dispensable organelles, protein aggregates or invading microorganisms are discarded to provide metabolites as a recycled source of nutrients and energy for the maintenance of cell homeostasis. Modified from (Boya et al, 2013)

1.3.1 Various types of autophagy

Autophagy is a common term for pathways that include the delivery of cytoplasmic components to the lysosome for degradation. Three classes of autophagy have been defined: macroautophagy, microautophagy and chaperone-mediated autophagy (CMA) (Figure 1.11) (Mizushima & Komatsu, 2011).

Characteristic for macroautophagy is the formation of 'autophagosomes', double-membrane vesicles. There, an initially forming isolation membrane (IM, also called phagophore) sequesters cytoplasmic components, including soluble materials and organelles, to form an autophagosome, which then fuses with a lysosome to become an autolysosome (Figure 1.11, see also chapter 1.3.2) (Mizushima & Komatsu, 2011). In selective macroautophagy intracellular protein aggregates or organelles, such as mitochondria, ribosomes, lipid droplets or ER (endoplasmic reticulum) membranes are specifically targeted for degradation (also referred to as aggrephagy and organellophagy, respectively) (Lamark & Johansen, 2012; Okamoto K., 2014).

During selective microautophagy soluble cytosolic cargo is internalized directly into lysosomes by inward invagination of the lysosomal membrane. This process strictly relies

on Hsc70-assisted cargo selection and delivery, and secondly on the ESCRT complex components I and III-mediated vesicle formation (Figure 1.11) (Sahu et al, 2011). Membrane dynamics may proceed similar to ESCRT-dependent MVB formation (Mizushima & Komatsu, 2011).

In contrast to macro- or microautophagy, CMA does not involve any membrane re-organization. Substrates for CMA, which contain a KFERQ-like pentapeptide, are individually recognized by the cytosolic chaperone Hsc70 and co-chaperones and delivered to lysosomes. There, the chaperone/cargo complex binds to LAMP2A (lysosome-associated membrane protein type 2A), a transmembrane protein, which acts as a receptor located in the lysosomal membrane. After unfolding, the substrate protein is translocated into the lysosomal lumen through a multimeric translocation complex, comprised of several LAMP2A-molecules, and degraded (Figure 1.11) (Kaushik & Cuervo, 2012).

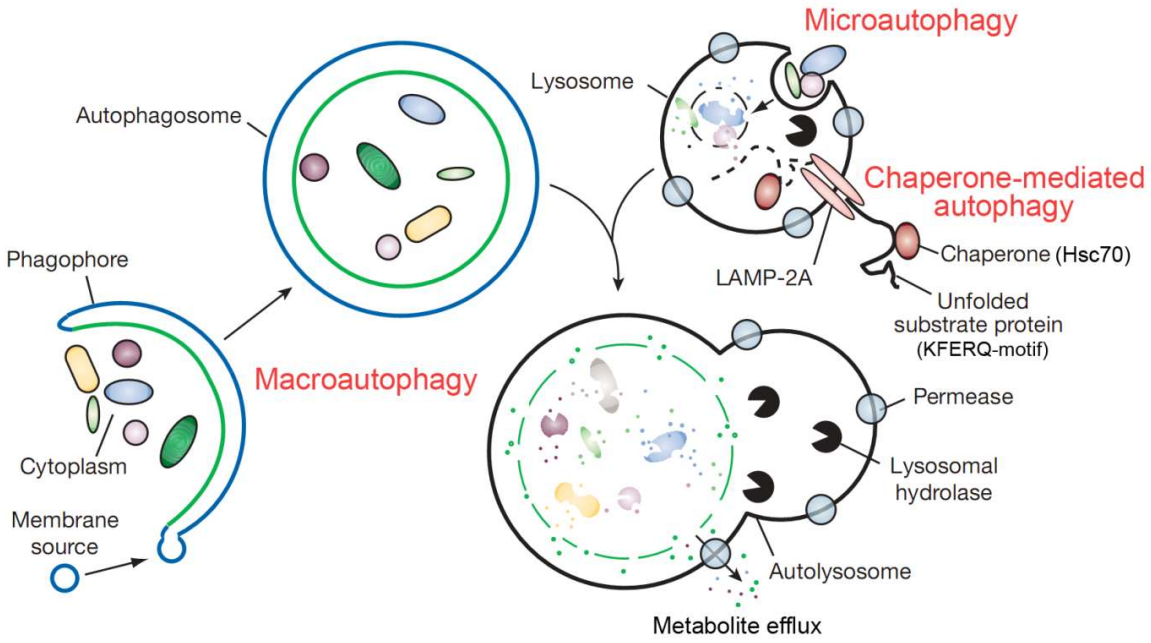

Figure 1.11 Three different types of autophagy. Macroautophagy involves the formation of a double-membrane vesicle (termed autophagosome). An initially formed isolation membrane (termed phagophore) engulfs cytoplasmic material resulting in autophagosome formation. To deliver their lumenal content for degradation autophagosomes fuse with lysosomes and become autolysosomes. During microautophagy lysosomes sequester soluble cytosolic proteins directly by invagination of vesicle-like structures, which are then degraded. Chaperone-mediated autophagy (CMA) is a selective autophagosomal pathway. Proteins with a KFERQ-like pentapeptide are recognized by Hsc70 and co-chaperones and delivered to lysosomes, where the chaperone/cargo-complex binds to LAMP2A. The substrate is first unfolded and then translocated into the lysosomal lumen through a multimeric translocation complex. Decomposed cargo is transported into the cytoplasm and reused as a nutrient and energy source. Modified from (Mizushima et al, 2008)

1.3.2 Regulation of autophagosome formation

Since the discovery of the first *ATG* (autophagy-related) genes in yeast in the 90s', not only has our understanding of the molecular machinery of mammalian autophagy tremendously gained, but also its importance for human physiology and disease (Cuervo, 2008; Mizushima et al, 2008; Orrenius et al, 2013). Autophagy is regulated through diverse mechanisms, including starvation and stress, with depletion of amino acids and/ or growth factors being most effective for autophagy induction (Mizushima et al, 2011; Rubinsztein et al, 2012a). Starvation inactivates mTOR complex 1 (mTORC1, mammalian target of rapamycin complex 1), a protein complex implicated in various cellular signaling pathways and the best-characterized regulator of autophagy, leading to the induction of autophagy by phosphorylation of ULK1 and ULK2 (UNC-51-like kinases 1/2) (Chan et al, 2007; Zoncu et al, 2011b). Alternatively, ULK1/2 (orthologs of Atg1 in yeast) can be phosphorylated by AMPK [AMP(5' adenosine monophophate)-activated protein kinase] in response to glucose starvation resulting in autophagy activation, hence autophagosome formation (Alers et al, 2012; Kim J. et al, 2011). ULK1 and ULK2 are the major components of the ULK complex, which itself is essential for phagophore initiation. In particular, inception and establishment of a phagophore strictly requires two large macromolecular complexes, ULK and PI3K complex, and two ubiquitin-like protein conjugation systems (LC3 and Atg16L) (Mizushima et al, 2011; Rubinsztein et al, 2012b; Yang Z. & Klionsky, 2010b). Additionally, two transmembrane proteins, Atg9L1/2 (orthologs of Atg9 in yeast) and Atg2A/B (orthologs of yeast Atg2), were shown to be indispensable for phagophore formation and closure, respectively (Figure 1.12) (Lamb et al, 2013).

Autophagosome formation begins with the assembly of a subset of Atg proteins ('core' molecular machinery) at the phagophore assembly site (PAS) (Suzuki et al, 2007; Xie & Klionsky, 2007). ULK complex, composed of ULK1 and ULK2, mAtg13 (mammalian homolog of Atg13), Atg101 and the scaffold protein FIP200 (FAK (focal adhesion kinase) family interacting protein of 200 kDa; an ortholog of Atg17 in yeast), is constitutively formed irrespective of nutrient conditions and translocates from the cytoplasm to the PAS upon autophagy induction (Mizushima, 2010; Mizushima et al, 2011).

Equally important for autophagosome formation is the PI3K (phosphatidylinositol 3-kinase) complex (also known as Beclin 1 complex), consistent of PI3K/ hVps34 (human vacuolar protein sorting 34 homolog of Vps34 in yeast), p150/ hVps15 (human Vps15 is homologous to Vps15 in yeast), Beclin 1 (an ortholog of yeast Atg6/Vps30), Atg14L [also known as Barkor (Beclin 1-associated autophagy-related key regulator); homolog of Atg14 in yeast] and the mammalian-specific scaffold protein AMBRA1 (activating molecule in Beclin 1-

related autophagy 1) (Lamb et al, 2013; Mizushima et al, 2011). Atg14L, an autophagy-specific factor, recruits the class III kinase hVps34 to the PAS, which in turn produces the lipid PI3P for autophagosomal membranes (Obara et al, 2008; Sun Q. et al, 2008; Zhong et al, 2009). PI3K activity is also regulated by the serine/threonine kinase p150/ hVps15 (Lindmo et al, 2008). PI3P lipid levels are kept in balance by phosphatidylinositol 3-phosphatases MTMR3 (myotubularin-related phosphatase 3) and MTMR14 (also known as Jumpy) (Taguchi-Atarashi et al, 2010; Vergne et al, 2009).

Evidently, ULK and PI3K complexes interact, thereby inducing the nucleation of the isolation membrane at an autophagosome-specific PI3P pool (Russell et al, 2013), where additional Atg proteins and PI3P effectors, such as Atg2A/B (orthologs of yeast Atg2) (Velikkakath et al, 2012), DFCP1 (double FYVE-containing protein 1) (Axe et al, 2008) and WIPI 1-4 (WD-repeat protein interacting with phosphoinositides; four mammalian proteins homologous to Atg18 and Atg21 in yeast) (Watanabe Y. et al, 2012), are suggested to be involved in autophagosome formation, but with yet not fully determined functions (Itakura & Mizushima, 2010; Matsunaga et al, 2010; Mizushima et al, 2011).

Furthermore, ubiquitin-like proteins LC3, GABARAP (γ-aminobutyric-acid-type-A-receptor-associated protein) and GATE-16 (Golgi-associated ATPase enhancer of 16 kDa) (orthologs of Atg8 in yeast) are important for autophagosome formation. These proteins are precursors that undergo further modifications at the C-terminus mediated by additional Atg proteins. Atg4, a cysteine protease, cleaves off one amino acid at the C-terminus leaving a glycine-exposed LC3 (cytosolic LC3-I), which is then first activated by the E1-like enzyme Atg7, and subsequently transferred to the E2-like enzyme Atg3. A final reaction leads to the covalently phosphatidylethanolamine (PE)-conjugated LC3 (LC3-II) that remains residual in both the isolation membrane and the autophagosomal membrane until fusion with a lysosome (Geng & Klionsky, 2008; Yang Z. & Klionsky, 2010b). Clearly, lipidation of LC3 is essential for expansion of the isolation membrane and autophagosome formation (Mizushima et al, 2011). In addition, as lipidated LC3 remains incorporated in the autophagosomal membrane, it is widely used as a specific marker for autophagosomes (Klionsky et al, 2012; Mizushima et al, 2010; Zhou et al, 2012).

The second conjugation system is the Atg16L1 complex, composed of Atg12, Atg5 and Atg16L1/2 (homologous to Atg16). Atg7 (E1-like enzyme) and Atg10 (E2-like enzyme) first mediate the conjugation of Atg12 to Atg5. Then, an additional non-covalent interaction between the Atg12-Atg5 conjugate with Atg16L1, followed by homo-oligomerization, completes the multimeric complex that associates with phagophores but falls off completed autophagosomes (Geng & Klionsky, 2008; Rubinsztein et al, 2012b). The two ubiquitin-like

protein conjugation systems are closely interconnected (Kaufmann et al, 2014; Mizushima et al, 2011).

In addition, Atg9L1 (ortholog of Atg9), the only transmembrane Atg protein, was suggested to act as a carrier for the supply of lipids and other components to expand the autophagosomal membrane (Orsi et al, 2012; Yamamoto et al, 2012).

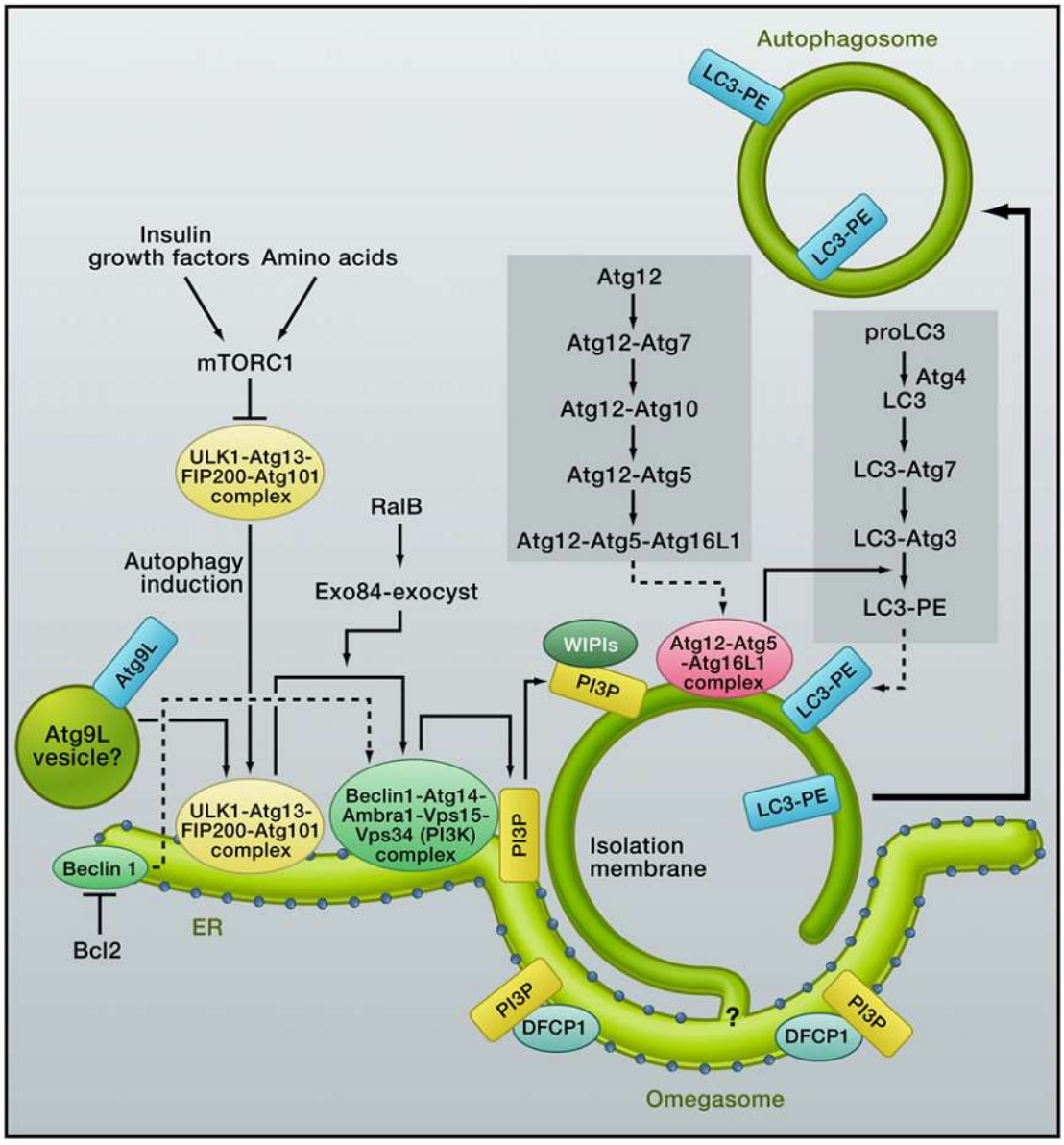

Figure 1.12 Autophagosome formation in mammalian cells. Autophagy can be induced upon nutrient deprivation. There, inhibition of mTORC1 leads to the activation of two multimeric protein complexes, ULK and PI3K complex. Equally important are two ubiquitin-like protein conjugation systems (LC3 and Atg16L). These components supported by the action of additional transmembrane proteins such as Atg9L, DFCP1 and WIPIs help to initiate and form autophagosomes. Taken from (Mizushima & Komatsu, 2011)

1.3.3 Autophagy in diseases

Autophagy has been shown to be critical for survival under starvation conditions and to serve as a quality-control machinery for cytoplasmic components at a basal level (Mizushima & Komatsu, 2011). Autophagy-deficient yeast cells for instance display rapidly decreasing intracellular amino acid levels when cultured in nitrogen-free medium (Onodera & Ohsumi, 2005). Also, mice lacking essential Atg genes (*Atg3* (Sou et al, 2008), *Atg5* (Kuma et al, 2004), *Atg7* (Komatsu et al, 2005), *Atg9* (Saitoh et al, 2009), *Atg16L1* (Saitoh et al, 2008)) exhibit reduced amino acid levels and die at the neonatal stage.

'Self eating' plays an essential role during differentiation and organismal development as drastic cellular and tissue remodeling processes are accomplished (Mizushima & Levine, 2010). In early embryogenesis it provides nutrients and selectively eliminates pre-existing materials, such as paternal mitochondria (Al Rawi et al, 2011; Sato & Sato, 2011; Tsukamoto et al, 2008).

Defective autophagy is practically always accompanied by an accumulation of polyubiquitinated proteins (Mizushima & Levine, 2010). Both p62 (also known as sequestosome 1/ SQSTM1) and NBR1 (neighbor of Brca1 gene) contain not only a LC3-interacting region (LIR) but also a ubiquitin-associated (UBA) domain (Pankiv et al, 2007; Waters et al, 2009). They have been proposed to act as autophagy receptors for the degradation of ubiquitinated cargo, such as protein aggregates, damaged mitochondria or ubiquitin-tagged microbes (Johansen & Lamark, 2011; Komatsu & Ichimura, 2010; Weidberg et al, 2011).

Aside from the role of nutrient supply, basal autophagy is indispensable for the maintenance of tissue homeostasis (Mizushima & Komatsu, 2011). Malfunctional autophagy frequently leads to the formation and accumulation of protein aggregates in tissues. In liver for instance p62 and ubiquitin positive aggregates cause severe hepatomegaly (enlarged liver) and hepatocytic hypertrophy, resulting in hepatitis (Komatsu et al, 2005). Neurologic deficits and substantial loss of neurons accompanied by the formation of inclusion bodies were monitored in autophagy-depleted brains. There, pathogenic protein aggregates of α-synuclein cause Parkinson disease, whereas polyglutamine (polyQ)-containing proteins result in Huntington disease and spinocerebellar ataxia (Nixon, 2013; Rubinsztein, 2006). Furthermore, mutated forms of autophagy were reported to affect heart tissue, muscles, bone and numerous other organs leading to severe diseases (Mizushima & Komatsu, 2011; Mizushima et al, 2008; Orrenius et al, 2013; Sandri et al, 2013).

Additionally, there is evidence that autophagy is implicated in cancer progression (Mizushima & Komatsu, 2011). In non-tumor cells or in early stages of tumor cell development autophagy maintains the role of a tumor suppressor as damaged or malfunctional organelles are constantly removed. Once a tumor has developed, autophagy becomes essential for cancer cell survival and is therefore a highly relevant target for cancer treatment (Amaravadi et al, 2011; Mathew et al, 2007; White, 2012).

1.4 Lysosomal system

Lysosomes are often simply termed as the recycling bins of the cell, responsible for the degradation and recycling of material. Meanwhile, however, it became evident that lysosomes cover a much broader spectrum of functions beside nutrient supply, such as energy metabolism, secretion, plasma membrane repair and signaling (Settembre et al, 2013). For simplification, lysosomal functions can be subdivided into three major categories: degradation, secretion and signaling (Figure 1.13).

These acidified organelles receive subtrates for degradation from different pathways (see continuous lines in Figure 1.13). Extracellular endocytosed cargo (see chapter 1.1) is first transported to EEs, from where it is further routed into the degradative pathway (see chapter 1.2). Proteins destined for degradation, such as EGF-bound EGFR (see chapter 1.2.2), are sorted into ILVs of MVBs, which subsequently fuse with pre-existing lysosomes (Luzio et al, 2010; Luzio et al, 2009; Saftig & Klumperman, 2009). Importantly, endosome-to-lysosome maturation is accompanied by a progressive decline of intralumenal pH from initially above 6 to 4.5 generated by a proton-pumping V-type (vacuolar-type) ATPase (Mindell, 2012; Saftig & Klumperman, 2009). Also, intralumenal acidification is substantial for the uptake of acid hydrolases by MPRs (mannose 6-phosphate receptors) (Griffiths et al, 1988). Intracellular substrates on the other hand reach the degradative organelles via autophagy (see chapter 1.3), where autophagosomes fuse with lysosomes to enable decomposition of engulfed material (Kaushik & Cuervo, 2012; Mijaljica et al, 2011; Mizushima & Komatsu, 2011).

Secretion of lysosomal proteins, also known as lysosomal exocytosis (dashed lines in Figure 1.13), has not only been shown to mediate physiological processes in specialized cells, such as melanocyte function in pigmentation, platelet function in coagulation and hydrolase release by spermatozoa during fertilization, but is now also recognized as a ubiquitous process important for plasma membrane repair and in defending bacterial infection (Andrews, 2000; Reddy et al, 2001; Ren Q. et al, 2008; Roy et al, 2004;

Stinchcombe et al, 2004; Tulsiani et al, 1998). This Ca^{2+}- and synaptotagmin VII (Syt VII; a Ca^{2+} sensor located on lysosomes)-dependent process requires SNARE proteins. Implicated are the lysosomal vesicle-SNARE (v-SNARE) VAMP7 (vesicle-associated membrane protein 7; also known as synaptobrevin) and the two plasma membrane-associated target-SNAREs (t-SNAREs) SNAP-23 (synaptosome-associated protein of 23 kDa) and syntaxin 4. In addition, several Rab proteins and the lysosomal membrane associated Ca^{2+} channel MCOLN1 (Mucolipin 1; a lysosomal nonselective cation channel that is mutated in mucolipidosis IV) help to mediate the release of typical lysosomal proteins (Jahn & Scheller, 2006; Medina et al, 2011; Rao et al, 2004; Rodriguez et al, 1997; Verhage & Toonen, 2007).

Lysosomal signaling (see dotted lines in Figure 1.13), mediated by an intricate signaling machinery [referred to as LYNUS (lysosome nutrient sensing)], is involved in nutrient sensing processes and pathways that relate to cell metabolism and growth (Settembre et al, 2012). The LYNUS machinery comprises the V-ATPase complex, which mediates the initial step in lysosomal signaling, mTORC1 and additional protein complexes located on the lysosomal surface (Cang et al, 2013; Settembre et al, 2013; Zoncu et al, 2011a). Interestingly, mTORC1, an established regulator of autophagy and cell growth, acts here as a balance control between biosynthetic and catabolic states (Laplante & Sabatini, 2012; Zoncu et al, 2011b).

Although there is still need to understand the detailed mechanisms of lysosome function under different physiological conditions, there is clear evidence that lysosomal biogenesis and function underlie a global transcriptional regulation mediated by the transcription factor EB (TFEB) (Sardiello et al, 2009; Settembre et al, 2011).

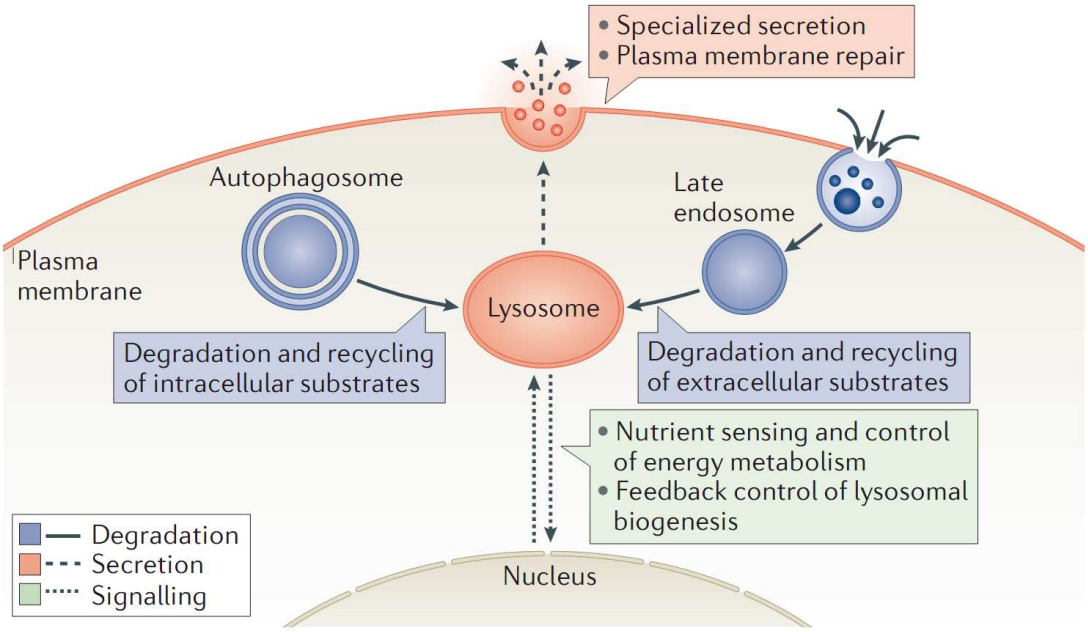

Figure 1.13 Main lysosomal functions summarized in three categories: degradation (continuous lines), secretion (dashed lines) and signaling (dotted lines). Extracellular endocytosed substrates and intracellular material conducted via autophagy are delivered to lysosomes for degradation. Lysosomal exocytosis is important for plasma membrane repair and does not only occur in specialized cells. Lysosomal signaling is mTORC1-dependent and underlies transcriptional regulation by TFEB (transcription factor EB). Taken from (Settembre et al, 2013)

1.4.1 Lysosome structure

Lysosomal biogenesis is based on a complex maturation process from EE to LE and lysosomes under constant exchange of membraneous and soluble components (Braulke & Bonifacino, 2009; Saftig & Klumperman, 2009). Lysosomes have a single-lipid bilayer with an approximately 8 nm thick polysaccharide-based coat on the inner side to avoid degradation of the lysosomal membrane by lumenal acid hydrolases (see Figure 1.14) (Wilke et al, 2012). In addition, this so called glycocalyx, consistent of highly glycosylated structural membrane proteins as LAMP1, separates the rest of the cell from the aggressive acidic environment as lysosomal hydrolases exhibit the highest activity at acidic pH (Guha & Padh, 2008; Mego, 1971; Sajid & McKerrow, 2002). Acidification of the lysosomal lumen is thereby generated by the v-type ATPase, which transports protons across the membrane under ATP hydrolysis (Marshansky & Futai, 2008). Furthermore, proteins required for fusion with other organelles, as well as for transport of metabolites, ions and soluble substrates reside in the lysosomal membrane (Settembre et al, 2013). Rab GTPases (Rab5 and Rab7) and a specific set of SNARE proteins, including VAMP7 , VAMP8, VTI1B (vesicle transport

through interaction with t-SNAREs homolog 1B), syntaxin 7 and syntaxin 8, mediate lysosomal trafficking and fusion events (Itakura et al, 2012; Jahn & Scheller, 2006; Pryor et al, 2004; Rink et al, 2005; Wang T. et al, 2011). Ion transport across the lysosomal membrane is maintained by ion channels such as MCOLN1 (also known as TRPML1), a nonselective cation channel, that participates in Ca^{2+} signaling during lysosomal fusion, and CLC7, a Cl^- channel, that contributes to lysosomal acidification (Dong X. P. et al, 2008; Kasper et al, 2005). Niemann-Pick C1 protein 1 (NPC1) is responsible for cholesterol export, whereas LAAT1 (lysosomal amino acid transporter 1) shuttles lysine and arginine across the membrane (Carstea et al, 1997; Liu B. et al, 2012). Similarly important, numerous soluble hydrolases, including sulphatases, glycosidases, peptidases, phosphatases, lipases and nucleases, targeted and transported into the lysosome by receptors such as MPR or LIMP2 (lysosome integral membrane protein 2; also known as SCARB2), are responsible for the degradation of substrates (Ghosh et al, 2003; Huynh et al, 2007; Reczek et al, 2007; Saftig & Klumperman, 2009; Settembre et al, 2013). A few lysosomal proteins will be discussed in further detail below.

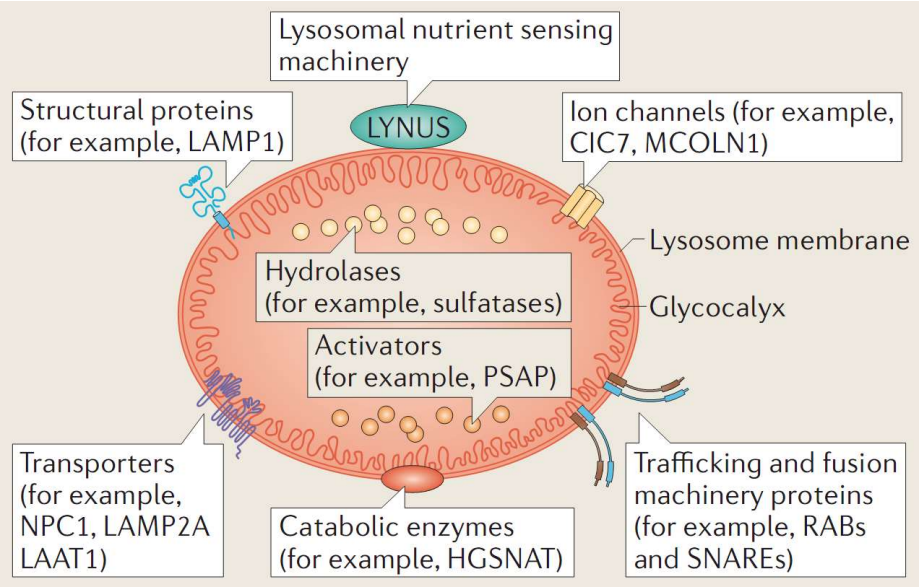

Figure 1.14 Lysosome structure. The single-lipid bilayer of lysosomes contains integral and peripheral membrane proteins, such as transporters and ion channels. The highly acidic lysosomal lumen is populated by soluble proteins as hydrolases required for substrate degradation. Taken from (Settembre et al, 2013)

1.4.1.1 Lysosomal membrane proteins (LMPs)

The most abundant integral membrane proteins in the lysosome are LAMP1 and LAMP2. Both proteins share a considerable sequence homology, whith three existing isoforms of

LAMP2 (LAMP2A, B and C). Their C-terminal cytosolic tail is rather short (11 amino acids) compared to the large, heavily glycolysated lumenal domain, which greatly contributes to the stability and integrity of the lysosome (Schwake et al, 2013; Wilke et al, 2012). LAMP1 is mainly involved in lysosomal trafficking as it mediates the attachment of lysosomes to the transport machinery (Andrejewski et al, 1999; Settembre et al, 2013). In contrast LAMP2A serves as a transporter for cytosolic proteins into the lysosome during chaperone-mediated autophagy (Kaushik & Cuervo, 2012). Additionally, LAMPs are required for the regulation of lysosome motility and fusion with other organelles and the plasma membrane (Huynh et al, 2007; Yogalingam et al, 2008).

Another abundant LMP is CD63 (also known as LAMP3), a conserved member of the tetraspanin family (Pols & Klumperman, 2009). The majority of CD63 is located on late endosomes and lysosomes. Importantly, lysosomal targeting of Syt VII, which itself is indispensable for lysosomal exocytosis and plasma membrane repair, is highly dependent on palmitoylation of CD63 (Flannery et al, 2010). In addition, CD63 is present on exosomes, which are considered important for antigen presentation (Escola et al, 1998).

1.4.1.2 Soluble proteins

The highly acidic lysosomal lumen is populated by more than 50 soluble proteins with proteolytic activity mainly involved in protein degradation. Most hydrolytic enzymes belong to the cathepsin family of proteases, which can further be subdivided into serine, aspartic or cysteine cathepsins depending on the catalytic type (Müller et al, 2012). Proteases are synthesized as inactive proenzymes, undergoing post-tranlational modification before being transported by receptors such as MPR or LIMP2 towards the lysosome, where they are finally processed into catalytically active enzymes (Conus & Simon, 2008; Saftig & Klumperman, 2009). Cathepsin B and L, the two most abundant lysosomal proteolytic enzymes, are the major proteases involved in the turnover of intracellular organelles, e.g. autophagolysosomes (Claus et al, 1998; Müller et al, 2012; Turk et al, 2000).

1.4.2 Lysosome-related diseases

Lysosomal storage disorders (LSDs) arise from lysosomal hydrolase deficiencies, some of which are treatable nowadays. In particular, impaired lysosomal function followed by the lack of degradation leads to a progressive accumulation of material in lysosomes (Cox & Cachon-Gonzalez, 2012). However, mutations in genes encoding for LMPs were also

shown to cause diseases ranging from severe visceral symptoms to neurodegeneration (Ballabio & Gieselmann, 2009; Schwake et al, 2013). For instance, mutations in genes encoding for the ion channel MCOLN1 cause mucolipidosis type IV leading to psyochomotor retardation and retinal degeneration. Mutations in CLC7, a protein that is involved in inherited osteopetrosis, might lead to neurodegeneration (Bargal et al, 2000; Kasper et al, 2005; Weinert et al, 2010). Mutated LAMP2A is responsible for Danon disease, a disorder characterized by skeletal and cardiac myopathy and mental retardation (Nishino et al, 2000). Further, NPC1 that is mutated in Niemann-Pick disease type C1 leads to hepatic dysfunction, ataxia, spasticity and dementia (Lloyd-Evans et al, 2008).

Therapeutic strategies often concentrate on either restoration or replacement of the activity of defective lysosomal enzymes. Another therapeutic option is targeting the substrate synthesis inhibition. Nevertheless, any strategy faces limitations and has to be evaluated strictly disease-specific (Settembre et al, 2013).

1.5 Nanoparticles

Nanotechnology is a research area investigating or engineering items that are smaller than 100 nm in at least one dimension (Figure 1.15). Hence, objects like nanoplates or very thin surface coatings (<100 nm in one dimension), nanowires or nanotubes (<100 nm in two dimensions) and nanoparticles (<100 nm in three dimensions) are covered by the umbrella term nano-objects or nanomaterials. Downsizing macroscaled materials often generates new physical and chemical properties at the nanoscale level. Thus, the principles of quantum physics rather than classical fundamentals of physics do apply. Aside from a tremendous enlargement of the surface area, which is accompanied by an increased chemical reactivity, also changes in optical, electrical or magnetic properties are observed. The chemical composition of synthetically manufactured nanomaterials ranges from noble metals (e.g. gold, silver), and metal composites (e.g. TiO_2, SiO_2, Quantum Dots (QDs)) to non-metals (e.g. C-tubes, BNs, polymeric materials) (Knauer & Stauber, 2009).

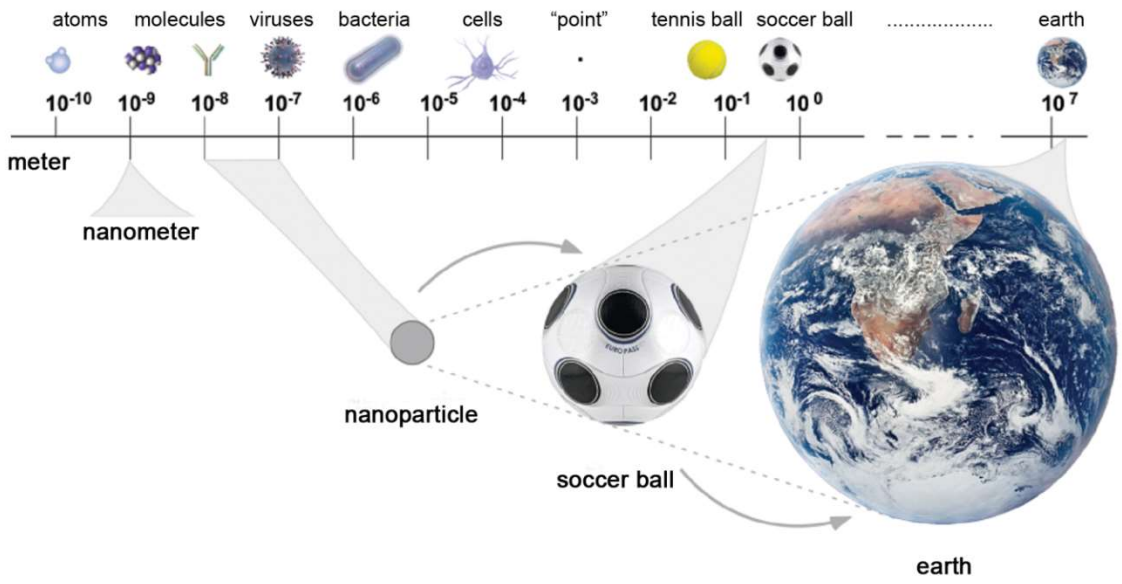

Figure 1.15 Scale of things. The size of nanoparticles in relation to a soccer ball is like that of the ball in relation to the earth. Modified from (Knauer & Stauber, 2009)

More than a decade ago, industrial and commercial use of nanomaterials has come to the center of attention (Salata, 2004). Meanwhile, nanoscaled TiO_2 and SiO_2 have become essential components in cosmetics (e.g. sunscreen) or as food additives (e.g. soup powders) (Das et al, 2009; Dekkers et al, 2011; Park et al, 2009). In sunscreens for instance, both oxides are utilized due to their ability to reflect ultraviolet light more efficiently than micro-sized particles (Nabeshi et al, 2011). The electronic industry uses nanomaterials to create printable, wearable or even disposable electronics (Bauer & Kaltenbrunner, 2014). Zhong and coworkers for instance created a metal-free carbon nanotube fiber-based generator that can be woven into self-powered garment and thereby enables a variety of applications for health and medicine, for example in supporting monitoring physiological and biomechanical signals from the human body (Zhong et al, 2014). Yet another interesting application of nano-objects in the textile industry is the use of nano-silver and oxidized nanodiamonds, both of which were shown to exhibit bactericidal activity: applied onto fibers they create odor-resistent clothing (Chernousova & Epple, 2013; Wehling et al, 2014). Furthermore, nanomaterials showed great performance as imaging, diagnostic and drug delivery tools in biomedical applications (Chapman et al, 2013; Ke et al, 2010; Ruedas-Rama et al, 2012; Wang A. Z. et al, 2008). There, polymer- and lipid-based nanoparticles are in use for a long time as siRNA transport vehicles and even gained recognition in cancer therapy (Gilleron et al, 2013; Haag & Kratz, 2006; Lee H. et al, 2012a; Sahay et al, 2013).

Nonetheless, with the increasing utilization of nanomaterials, especially in biological systems, the question arises whether nano-sized materials might generate undesirable

consequences affecting environmental health and safety (Oberdörster et al, 2009; Warheit, 2010). Thus, possible harmful effects emerging from interactions with biological systems remain to be elucidated in further detail.

1.5.1 Silica based nanoparticles

Silicon dioxide (SiO_2) is commonly referred to as 'silica' and appears in two structures, crystalline and amorphous. Quartz is the most familiar crystalline form aside from manufactured porous porosil. Amorphous forms of silica occur naturally as minerals (e.g. opal or silica glass) or are synthetically produced, such as silica nanoparticles (Figure 1.16).

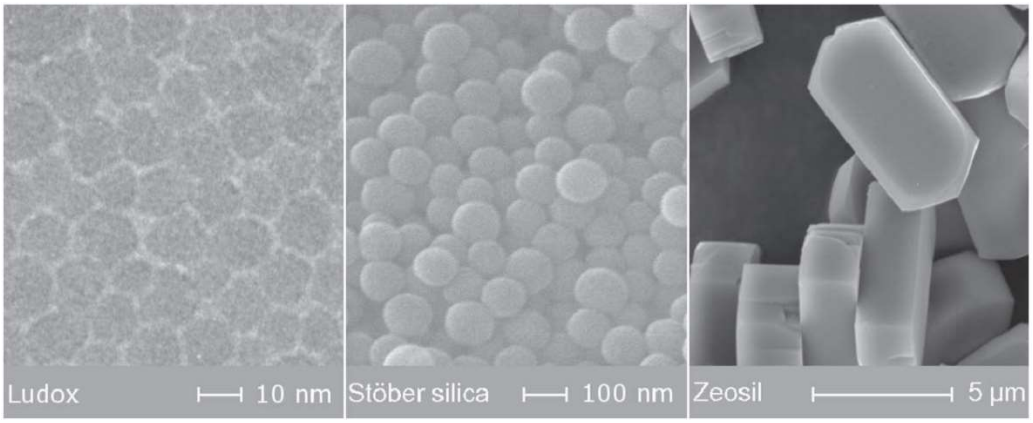

Figure 1.16 Classification of natural and synthetic silica nanoparticles. Amorphous (left and middle) and crystalline (right) nanosilica. Taken from (Napierska et al, 2010)

Nowadays various established techniques to produce nano-sized silica particles exist, one of which is the so called Stöber process (Napierska et al, 2010). This procedure enables to synthesize monodisperse spherical amorphous silica particles with adjustable size and porosity. Alkyl silicates are hydrolyzed in ethanol with catalytic amounts of ammonia under subsequent condensation of silicic acid (Stöber et al, 1968).

Silica nanoparticles have gained broad attention in industry as additives to ink and varnishes, to food and cosmetics or as catalysts to enhance reaction performance (Al Rawi et al, 2011; Dekkers et al, 2011; Napierska et al, 2010; OECD 2005). In addition, silica nanoparticles have attracted researchers from the biotechnological and pharmaceutical industry to develop suitable applications in the fields of delivery (e.g. DNA, drugs) and cancer therapy (Barik et al, 2008; Slowing, II et al, 2008; Trewyn et al, 2007; Yang P. et al, 2012). Nevertheless, understanding the mechanisms of action and dealing with potential health effects of silica nanomaterials remains essential. Whether silica nanoparticles are able to enter cells is certainly one important issue to investigate.

1.5.1.1 Cellular internalization

Extracellular material can enter cells via different uptake mechanisms (see chapter 1.1). How silica-based nanoparticles enter cells is still a highly controversial field of research as their internalization is dependent on multiple factors, such as particle size, shape, as well as surface chemistry and topology (Figure 1.17) (Canton & Battaglia, 2012). The degree of particle uptake depends also on particle concentration, time of exposure and used cell type (Rabolli et al, 2010; Wu S. H. et al, 2011a).

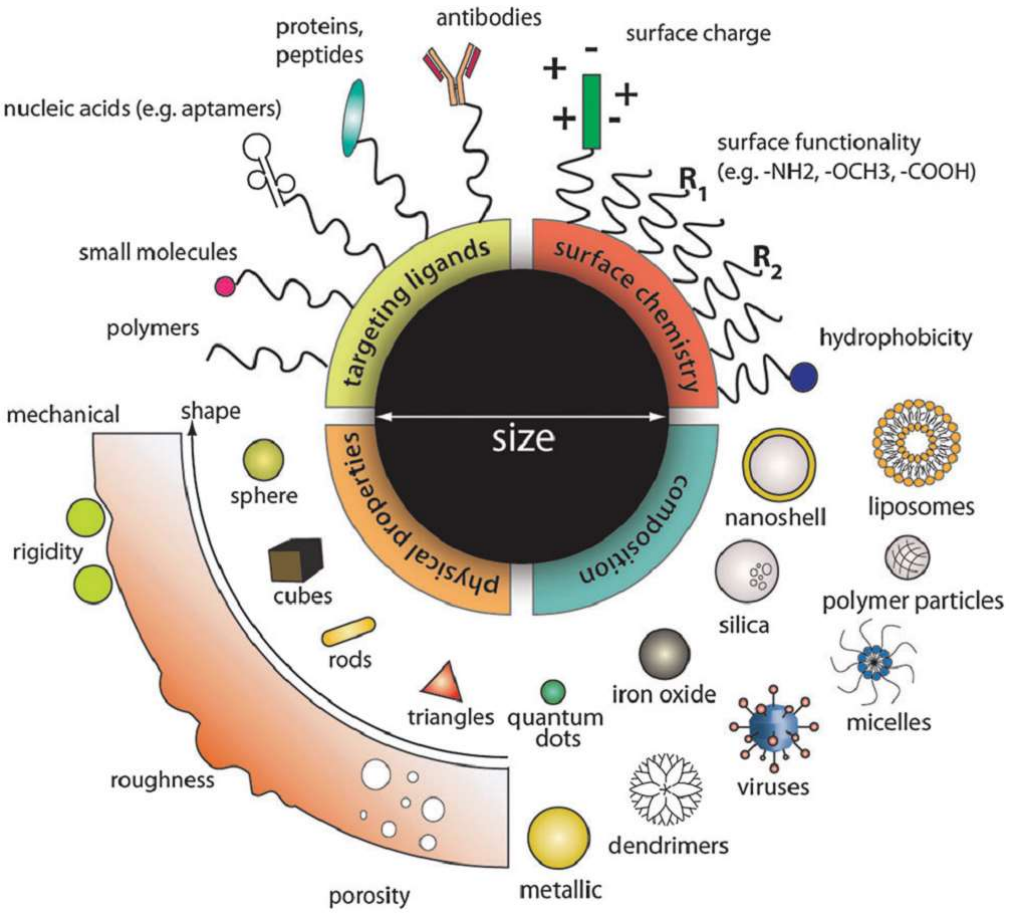

Figure 1.17 Nanoparticle design for intracellular applications. Adjusting different physical and chemical properties enables the modular assembly of artificial nanoparticles for specific intracellular applications as contrast agents or drug delivery vehicles. Taken from (Chou et al, 2011)

The size of silica nanoparticles developed for intracellular applications ranges from a few to hundreds of nanometers. Theoretical and experimental models dealing with size-contingent nanoparticle endocytosis demonstrate a size-depedency for particles with an optimal radius at around 20 nm to 30 nm; uptake efficiency decreases for both bigger and smaller particles (Canton & Battaglia, 2012; Chaudhuri et al, 2011). In agreement, results obtained for artificial glycoviruses, quantum dots, latex beads or gold nanoparticles show the most

efficient internalization for particles around the optimum diameter of 40 nm to 60 nm (Chithrani et al, 2006; Jiang et al, 2008; Ma et al, 2011; Nakai et al, 2003; Osaki et al, 2004; Rejman et al, 2004; Shan et al, 2011). The same is true for silica nanoparticles as demonstrated by an experimental study based on flow cytometry and mass spectrometry data (Lu et al, 2009; Shapero et al, 2011). Although some studies indicate a better uptake efficiency for bigger instead of smaller nanoparticles, 100 nm and 50 nm respectively, the majority of publications confirms a higher internalization rate for silica nanoparticles with an average size (diameter) around 50 nm (Docter et al, 2014; Gan et al, 2012; Napierska et al, 2009; Oh W. K. et al, 2010).

An additional factor that might influence particle internalization rates is their shape, which, among others, comprises spherical, cylindrical and rod-like formats (see Figure 1.17) (Champion & Mitragotri, 2006; Ferrari, 2008). For instance, higher virulence of tubular viruses such as the Ebola and the Marburg virus was proposed to result from particle shape (Ascenzi et al, 2008; Dolnik et al, 2008). Also, studies investigating monodisperse cationic hydrogel particles show a preference for an uptake of rod-like (high aspect ratio) compared to cubic-shaped (low aspect ratio) particles in HeLa cells, whereas studies comparing rod-like and spherical particles demonstrate a higher uptake efficiency for nanoparticle spheres (Chithrani & Chan, 2007; Chithrani et al, 2006; Dasgupta et al, 2014; Gratton et al, 2008; Yoo & Mitragotri, 2010). On the other hand, several studies either found no difference or even contrary internalization rates, pointing to the dominating roles of surface functionalization and cell type (Herd et al, 2011; Hutter et al, 2010; Qiu et al, 2010).

Surface chemistry and surface topology of nanoparticles are considered to be crucial aspects for cellular internalization as functional groups are the primary interactors with the biological surrounding (Canton & Battaglia, 2012; Fröhlich, 2012; Verma & Stellacci, 2010). Functional groups can differ in charge and hydrophobicity and can cover the nanoparticle surface in an uneven topological arrangement. Therefore, numerous investigations were performed in a wide selection of cell types to evaluate the cellular internalization rate of neutral as well as negatively (anionic) and positively (cationic) charged nanoparticles (Cho et al, 2009; Perumal et al, 2008). As most cells express negatively charged proteoglycans on their surface, lower internalization rates were repeatedly demonstrated for neutral and negatively charged nanoparticles than for positively charged particles (Graf et al, 2012; Harush-Frenkel et al, 2007; Mislick & Baldeschwieler, 1996; Rancan et al, 2012; Slowing I. et al, 2006). One explanation might be enhanced membrane permeability that can be induced by a substantial interaction of cationic species, such as cationic liposomes, polypeptides and amine-containing polymers, with the negatively charged cell membrane leading to the formation of nanoscale holes (Al-Jamal et al, 2008; Chou et al, 2011; Herrero

et al, 2009; Ohsaki et al, 2002). Interestingly, cellular toxicity was frequently enhanced in cells upon treatment with positively charged nanospheres in contrast to nanoparticles with a net negative surface charge (Xia et al, 2006; Xia et al, 2008). Nevertheless, the arrangement of functional groups on the nanoparticle surface may also affect their uptake mechanisms as demonstrated for gold and polymer nanoparticles (LoPresti et al, 2011; Massignani et al, 2009; Verma et al, 2008).

In addition, fusion of so-called cell-penetrating peptides (CPP) or fusogenic motifs, mostly short polycationic or amphiphilic peptides, to the nanoparticle surface may facilitate cellular internalization (Gupta et al, 2005; Verma & Stellacci, 2010). Their sequences are often based on natural sequences, e.g. protein-transduction domains of viruses (Chou et al, 2011; Zorko & Langel, 2005).

Finally, nanoparticle surfaces can be equipped with particular moieties to enable targeting towards specific cell types. These nanomaterials armed with ligands such as small molecules, antibodies or proteins with high affinities to cell surface antigens or membrane receptors are nowadays widely used for cancer therapy (Chou et al, 2011; Errico, 2013).

1.5.1.2 Silica nanoparticles for biomedical applications and potential health effects

The rapidly developing field of nanomedicine pursues the design and synthesis of drug delivery vehicles that primarily fulfill compelling requirements such as ample drug loading, efficient transport across physiological barriers, and safe and sustainable cure of diseases. Silica nanoparticles as one representative among other inorganic nanomaterials (Figure 1.18) hold great promise for applications in medicine mainly as delivery vehicles, but also as imaging and diagnosis tools (Peer et al, 2007; Tang & Cheng, 2013).

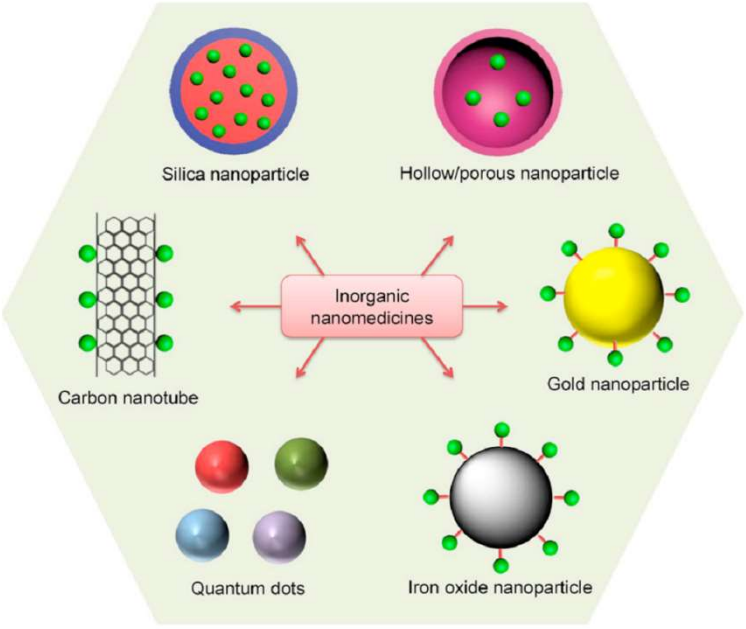

Figure 1.18 Inorganic nanomaterials for cancer diagnosis and therapy. Small green dots represent the chemotherapeutic agent or diagnostic probe. Taken from (Tang & Cheng, 2013)

Artificial transport systems help to overcome limitations of small molecular drugs and biopharmaceutical proteins, such as lack of specific targeting, instability against proteolytic degradation or low solubility. As silica nanoparticles exhibit unique properties, among them excellent biocompatibility and the ease of large-scale synthesis, they have attracted significant interest. Hence, bioactive molecules (e.g. doxorubicin or insulin) are often either encapsulated (non-covalent binding) into a silica matrix or conjugated (covalent binding) to a silica-based nanoparticle backbone (Yang P. et al, 2012).

One important application of silica nanoparticles in medicinal therapy, particularly in photodynamic therapy (PDT), is favourable as a less toxic and minimally invasive alternative to chemo- and radiotherapy (Couleaud et al, 2010). Another option is the use as transfection agent for *in vitro* gene delivery (Luo & Saltzman, 2000). Silica-based nanocarriers are also highly suitable for molecular imaging techniques such as fluorescence imaging or magnetic resonance imaging (MRI) (Ruedas-Rama et al, 2012; Tang & Cheng, 2013).

Although silica nanoparticles have great impact on both medicinal therapy and diagnosis, important issues encompassing the safety and toxicity of such nanocarriers *in vitro* and *in vivo* needs to be elucidated in further detail (Dwivedi et al, 2009; Stern et al, 2012). Even though some *in vitro* studies reveal low or no cytotoxicity at all upon silica nanoparticle exposure, numerous studies indicate serious implications for regular cellular activities, including enhanced ROS (reactive oxygen species) production, upregulation of autophagic processes, and apoptosis (Mamaeva et al, 2013; Napierska et al, 2010). Moreover, *in vivo*

investigations performed in different animal models displayed inconsistent results. In particular, flies exhibited no negative effects after oral administration of silica nanoparticles, whereas the same particles caused severe embryonic malformations in zebrafish (Barandeh et al, 2012; Duan et al, 2013). Similarly, pregnant mice intravenously injected with silica nanoparticles experienced complications leading to smaller fetuses than in untreated animals (Yamashita et al, 2011).

Even though silica nanomaterials possess exceptional properties rendering them highly interesting for biomedical applications, the elucidation of a complete toxicity profile and a potential environmental impact remains inevitable.

1.5.2 Polymer based nanoparticles

Organic nanomaterials, molecularly engineered polymer constructs of nano-size, have pioneered the field of nanomedicine. Starting with the synthesis of first polymers, that went into clinical testing in the 1960s, proceeding with the elaboration of new conjugates, including polymer-drug conjugates, polymeric micelles and PEGylated proteins [proteins carrying poly(ethylene glycol)], the entire field of 'polymer therapeutics' has emerged productively over the past decades (see Figure 1.19, chapter 1.5.2.2) (Duncan, 2003).

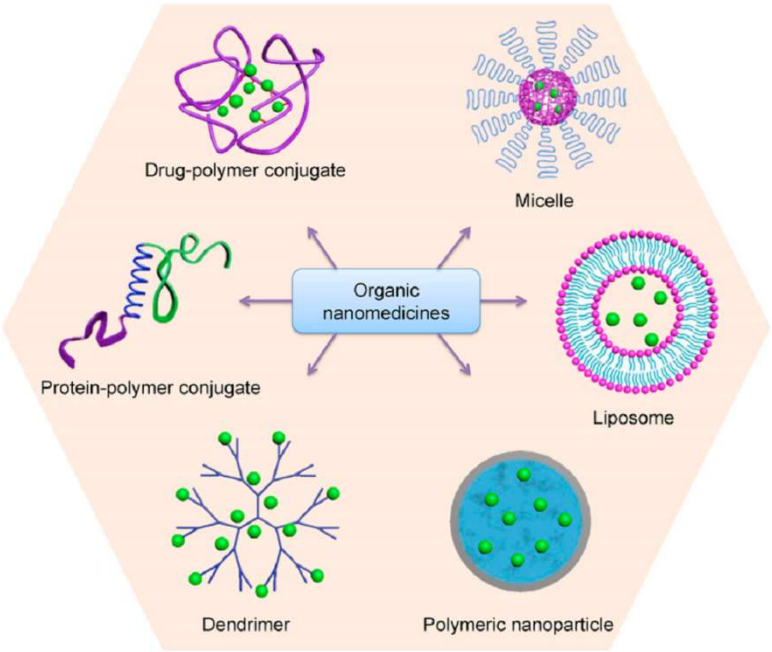

Figure 1.19 Organic nanomaterials for cancer diagnosis and therapy. Small green dots represent chemotherapeutic agents or diagnostic probes. Taken from (Tang & Cheng, 2013)

With PEGylation of proteins leading to increased manufacturing of important medical products, acceptance of the entire field of polymer therapeutics grew (Pasut & Veronese, 2012). The appearance of dendrimers (repetitively hyperbranched molecules) in the 1980s, opened the architectural design of polymer therapeutics towards the third dimension, also leading to the synthesis of polymeric nanospheres (or polymer based nanoparticles) (Duncan & Vicent, 2013). Nowadays, dendritic polyglycerol conjugates among others are frequently in use as polymeric nano-sized delivery systems (Khandare et al, 2012). Yet, such nanocarriers are not only being developed to transport agents for therapeutic or diagnostic purposes, but may also carry both functions in combination. These so called theranostic prodrugs that incorporate both capabilities could help gaining information about their trafficking pathways and delivery kinetics while curing disease. Therefore, such tools hold great promise to advance the biomedical field toward personalized medicine (Kelkar & Reineke, 2011).

1.5.2.1 Drug release mechanisms

The main goal of drug delivery systems is to effectively overcome limitations of conventional therapeutics. Therefore, vehicles of biologically relevant size need to be equipped with targeting moieties to selectively accumulate in diseased organs to minimize damage of healthy tissue (Cheng et al, 2012). In addition, it is desirable to provide controlled and sustainable drug release at the site of action. For an enhanced local therapeutic effect, detachment of the pharmaceutical can be activated endogenously or by external stimuli (Figure 1.20) (Kim C. S. et al, 2013).

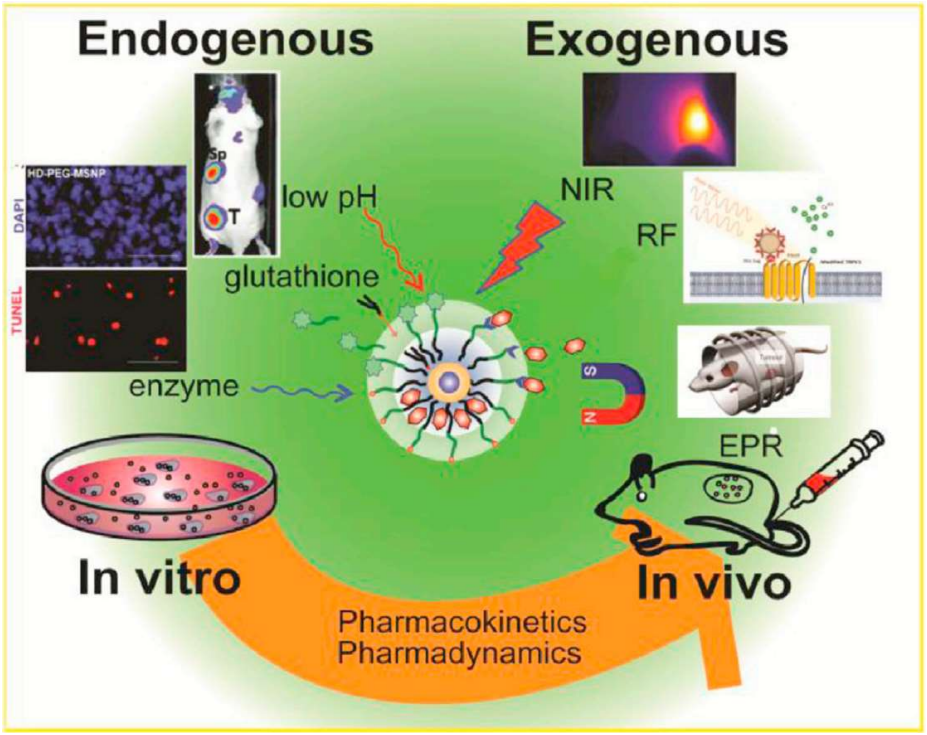

Figure 1.20 Triggered drug release mechanisms for nanomaterials. Cleavage of attached bioactive agents can be achieved via endogenous (pH-, redox- or enzymatic-triggered) or exogenous (light- or magnetic field-activated) stimulation. Taken from (Kim C. S. et al, 2013)

Biologically controlled drug release can be achieved exploiting various possibilities, such as pH changes, enzymatic cleavage or redox reaction (Ambrogio et al, 2011). Aside from intracellular acidification that takes place during endosome maturation (see chapter 1.2), inadequate supply of oxygen and nutrients to tumor tissue leads to an excessive production of lactic and carbonic acid resulting in lower extracellular pH values compared to healthy tissue (Minchinton & Tannock, 2006). Thus, chemotherapeutics attached via a pH-sensitive linker can selectively be dispensed into diseased organs and released from the nanodevice (Calderón et al, 2011; Krüger et al, 2014). Enzymatic cleavage emerged as an additional option for controlled drug release as protein levels of certain enzymes, usually proteolytic enzymes, differ considerably from those in healthy tissue (Koblinski et al, 2000; Singh et al, 2011). Furthermore, taking into account that the intracellular free thiol concentration (mainly glutathione) is manifold higher compared to the extracellular environment, nanocarrier-containing drugs connected through disulfide bonds represent a promising system for selective intracellular delivery (Santra et al, 2011). The tripeptide glutathione is not only an important cysteine reservoir, but also serves as the main intracellular antioxidant (Sies, 1999).

Exogenous stimulation on the other hand can additionally activate the nanocarrier itself as demonstrated by hyperthermia treatment (Lee J. H. et al, 2011). Here, heat production can

be achieved by radio frequency activation or magnetic field induction. Moreover, light (near-UV or near-infrared) can be applied to break photo-cleavable bonds for drug release or to activate a photosensitizer that locally applied turns endogenous oxygen into cytotoxic ROS (Choi et al, 2011; Kim C. S. et al, 2013).

1.5.2.2 Polymer therapeutics for nanomedicine application

The first synthetic polymer drugs were based on natural extracts, particularly polyanions and polysulfates, which possess antiviral and antitumor activity. Initial attempts to pass clinical trials with an anticancer agent (known as DIVEMA) failed due to its severe toxicity, which was clearly associated with molecular weight of the polymer and intravenous administration (Duncan, 2003). Since then, numerous modified polysaccharides, synthetic polypeptides and polymers were successfully introduced into the market (Dhal et al, 2009). The development of the first polymer–drug conjugates based on co-polymeric HPMA (N-(2-Hydroxypropyl)methacrylamide) in the late 1970s/early 1980s was a breakthrough that led to the design of various clinically relevant conjugates mostly for chemotherapy, including polymer–drug, polymer–protein and polymer–aptamer conjugates (Duncan & Vicent, 2010). In addition, pioneering work on protein PEGylation has started in the 1970s and since has gained clinical value with products like PEG-adenosine deaminase (ADAGEN, Enzon) to treat X-linked severe combined immunogenicity syndrome, PEG-L-asparaginase (ONCASPAR, Enzon) to cure acute lymphoblastic leukeamia or PEG-interferon-α conjugates as medication for hepatitis C (Duncan, 2003; Duncan & Vicent, 2013). However, among these diverse polymeric structures, dendritic polymer architecture has provided advantages for drug delivery applications compared to linear polymers, including defined multivalency, high density of functional groups, low polydispersity and globular shape (Khandare et al, 2012). Aside from PAMAM (polyamidoamine) dendrimers, which are commercially available but still under critical investigation, and other dendritic molecules, dendrimers based on polyglycerol present an ideal platform for nanomedicine application. Although dendritic polyglycerols were coupled to different bioactive agents and exhibited anti-inflammatory (ibuprofen), antitumor (doxorubicin or methotrexate), antithrombotic (short peptide sequence consisting of Arg–Gly–Asp), and antimicrobial activity (chitosan conjugated), clinical suitability is still under evaluation (Calderón et al, 2010).

1.6 Aims of this study

Preliminary work about the colloidal stability of silica nanoparticles in physiological media identified AHAPS-functionalized silica nanoparticles as the candidates with the best uptake efficiency into HeLa cells. Based on this result, the first part of my study focuses on the investigation of these positively charged silica nanoparticles interacting with HeLa cells. In particular, we aimed at characterizing their internalization mechanism and potential intracellular effects on trafficking, autophagy and lysosomal degradation using cell biological and biochemical methods as well as optical imaging.

The second part of my work concentrates on the monitoring of pH-triggered doxorubicin release from a theranostic macromolecular prodrug (TMP) via fluorescence resonance energy transfer (FRET). Dendritic polyglycerol nanoparticles served here as the drug delivery system.

2 MATERIAL AND METHODS

2.1 Materials

2.1.1 Chemicals and consumables

Chemicals were purchased from Carl Roth GmbH, Gibco, Sigma-Aldrich, Thermo Scientific, Life Technologies (Invitrogen), and Merck. The supplier for reagents used in specific applications is mentioned in the respective methods section. Consumables were obtained from Sarstedt, GE Healthcare, Schott, and Greiner.

2.1.2 Molecular weight standards

Marker	Composition	Supplier
Prestained protein marker	175, 80, 58, 46, 30, 25, 17, 7 kDa protein bands	New England Bio Labs Inc.
Page Ruler Plus Prestained	250, 130, 100, 70, 55, 35, 25, 15, 10 kDa protein bands	Thermo Fisher Scientific (Fermentas)

2.1.3 Buffers, media and solutions

All solutions and buffers were prepared with ultrapure water (ddH_2O). The pH was adjusted using NaOH or HCl if not mentioned otherwise.

Biochemistry	
PMSF stock solution	100 mM in DMSO (dimethyl sulfoxide)
20 % Triton X-100	20 % (w/v) Triton X-100 in ddH_2O
20 % Tween 80	20 % (w/v) Tween 80 in ddH_2O
Cell lysis buffer	20 mM HEPES pH 7.4 100 mM KCl 2 mM $MgCl_2$ 1 % (v/v) Triton X-100 1 mM PMSF 3 µl/ ml protease inhibitor cocktail (Sigma)

	(1 % (v/v) phosphatase inhibitor cocktail 1+2 for analysis of phosphorylated proteins)
Cell lysis buffer (Autophagy assay)	20 mM HEPES pH 7.4 100 mM KCl 4 mM $MgCl_2$ 2 % (v/v) Triton X-100 1 mM PMSF 3 µl/ml protease inhibitor cocktail (Sigma)
2x Bradford reagent	70 mg (w/v) Coomassie G250 100 ml 85 % H_3PO_4 50 ml ethanol ad 500 ml ddH_2O, filtered
APS	10 % (w/v) APS (ammonium peroxodisulfate) in ddH_2O
6x SDS-PAGE sample buffer	375 mM Tris pH 6.8 60 % (v/v) glycerol 30 % (v/v) β-mercaptoethanol 18 % (w/v) SDS added bromophenol blue
4x SDS-PAGE separating buffer	1.5 M Tris pH 8.8 0.4 % (w/v) SDS
4x SDS-PAGE stacking buffer	0.5 M Tris pH 6.8 0.4 % (w/v) SDS
10x SDS-PAGE running buffer	246 mM Tris pH 8.8 1.92 M glycine 1 % (w/v) SDS
1x semi-dry transfer buffer	1x SDS-PAGE running buffer 10-20 % methanol
1x wet transfer buffer	20 % Methanol 380 mM glycine 50 mM Tris pH 8.8 1.92 mM SDS
Ponceau staining solution	0.2 % (w/v) Ponceau S 1 % (v/v) acetic acid
Ponceau de-staining solution	1 % (v/v) acetic acid

10x TBS	200 mM Tris, 1.4 M NaCl pH 7.6
IB blocking solution	3 % (w/v) non-fat dry milk in TBS
IB antibody solution	3 % (w/v) BSA (bovine serum albumin) 0.05 % Tween (20 %) 0.01% (w/v) NaN_3 in 1x TBS
IB stripping buffer	62.5 mM Tris pH 6.8 2 % (w/v) SDS add β-mercaptoethanol immediately before use (78 µl to 10 ml buffer)

Cell Biology	
DMEM (Dulbecco's modified Eagle's medium)	1 g/ l glucose w/o L-Glutamine (Gibco)
Fetal calf serum (FCS)	heat inactivated from Gibco
L-Glutamine	200 mM L-Glutamine in 0.85 % NaCl solution (Lonza)
Antibiotitcs	Penicillin (10000 U/ ml)/ Streptomycin (10 mg/ ml) from Gibco
Trypsin / EDTA	200 mg/ l Versene (EDTA), 170000 U Trypsin/ l (Lonza)
Cell culture medium	DMEM 10 % (v/v) FCS 1 % (v/v) Antibiotics 1 % (v/v) L-Glutamine
Starvation medium	DMEM (w/o additives)
Optimem	from Gibco
HBSS (Hank's balanced salt solution)	$+Ca^{2+}$ $+Mg^{2+}$(Gibco)
Imaging buffer	HBSS 0.2 % (v/v) FCS 10 mM HEPES pH 7.4

10x PBS	1.37 M NaCl 27 mMKCl 43 mM Na_2HPO_4 14 mM NaH_2PO_4 pH 7.4
Fixation buffer (PFA)	4 % (w/v) paraformaldehyde 4 % (w/v) sucrose In 1x PBS
1 M sodium phosphate buffer (100 ml)	77.4 ml 1 M Na_2HPO_4 22.6 ml 1 M NaH_2PO_4 pH 7.4
Goat serum dilution buffer (GSDB)	30 % (v/v) goatserum 15 mM sodium phosphate buffer pH 7.4 100 mM NaCl 0.06 % (v/v) TritonX-100 (20 %)
IF washing buffer	GSDB w/o goat serum

2.1.4 Nanoparticle probes

Silica nanoprobes	**Surface functionalization**	**FITC labeling**
NPs-AHAPS	N-(6-Aminohexyl)-aminopropyltrimethoxysilane	-
NPs-AHAPS	N-(6-Aminohexyl)-aminopropyltrimethoxysilane	+
NPs-APS	(3-Aminopropyl)trimethoxysilane	+
NPs-GP	APS coupled with N-guanylpyrazole	+
NPs-non	non-functionalized	+
NPs-PEG	2-[Methoxy(polyethyleneoxy)$_n$propyl]trimethoxysilane, n=6-9	+

Silica nanoprobes were always freshly transferred from ethanol into water before performing cell biological experiments. Ethanol was removed from the dispersion by centrifugation for at least 120 min at 1000 xg, T = 20°C. The sediment containing the functionalized silica nanoparticles was redispersed in ultrapure water using ultrasonication for 15 min. This procedure was repeated at least two times to ensure that the ethanol content in the sample is negligible (<0.5 vol %).

Polymer conjugate	Cleavage	FRET
TMP	+	+
Non-cleavable ctrl	-	+
Non-quenching ctrl	+	-

2.1.5 Small interfering RNA oligonucleotides

Oligonucleotides were obtained as a lyophilized powder and dissolved to a concentration of 100 µM in RNAse-free buffer.

siRNA	Sequence	Supplier
caveolin 1	5'-CCUGAUUGAGAUUCAGUGC-3' (Nichols, 2002)	MWG Biotech
caveolin 1 smartpool	5'-CUAAACACCUCAACGAUGA-3' 5'-GCAAAUACGUAGACUCGGA-3' 5'-GCAGUUGUACCAUGCAUUA-3' 5'-GCAUCAACUUGCAGAAAGA-3'	Dharmacon
clathrin heavy chain	5'-AUCCAAUUCGAAGACCAAU-3'	MWG Biotech
dynamin 2	5'-GCAACUGACCAACCACAUCTT-3'	MWG Biotech
flotillin 1	5'-CACACUGACCCUCAAUGUC-3' (Glebov et al, 2006)	MWG Biotech
scrambled (ctrl)	5'-GTAACTGTCGGCTCGTGGT-3'	MWG Biotech

2.1.6 Primary antibodies

Antigen	Species	Clone	IF	IB	Source
AP-1γ-adaptin	Mouse	100/3	1:100	-	Sigma (A4200)
β-actin	Mouse	ac15	-	1:5000	Sigma (A-5441)
Caveolin 1	Mouse		-	1:1000	BD transduction (611436)
Caveolin 1	Rabbit	(N-20)	1:100	1:500	Santa Cruz (sc-894)
CD63	Mouse	RFAC4	1:100	-	Millipore (CBL553)
Clathrin heavy chain	Mouse	TD1	-	1:500	homemade

Dynamin1+2	Mouse	41	-	1:500	BD Biosciences (610245)
EEA1	Mouse		1:100	-	BD transduction (610456)
EGF receptor	Rabbit	D38B1	-	1:1000	Cell signaling (4267S)
phospho-EGF receptor	Rabbit	D7A5	-	1:1000	Cell signaling (3777S)
Erk 1/2	Mouse	9B3	-	1:2000	Abcam (ab36991)
phospho-Erk 1/2	Mouse	MAPK-YT	-	1:5000	Sigma (M8159)
Flotillin 1	Mouse		-	1:250	BD transduction (610820)
Hsp70	Mouse		-	1:5000	Affinity Bioreagents (MA 3006)
LAMP1	Mouse	CD107a/H4A3	1:200	-	BD Pharmingen
LAMP2A	Rabbit		1:100	-	Abcam (18528)
LC3	Mouse	4E10	1:100	-	MBL international (M152-3)
LC3	Rabbit		-	1:1000	Novus Biochemical (NB600-1384)
CI-M6PR	Mouse	2G11	1:100	-	Affinity Bioreagents (MA1-066)
p62 lck	Mouse	3	1:400	1:1000	BD transduction (610832)
p70S6K	Rabbit	49D7	-	1:1000	Cell Signaling (2708)
phospho-p70 S6K (T389)	Rabbit	108D2	-	1:1000	Cell Signaling (9234)
Oregon Green	Rabbit		1:500	-	Invitrogen (A-889)
Tubulin	Mouse	B5-1-2	1:500	-	Sigma (T5168)
ULK1	Rabbit	D8H5	-	1:1000	Cell Signaling (8054)
phospho-ULK1 (S757)	Rabbit		-	1:1000	Cell Signaling (6888)

2.1.7 Secondary antibodies

Antibody	conjugate	IF	IB	Source
GαM^{HRP}	HRP-conjugated goat anti-mouse IgG	-	1:5000	Dianova
GαR^{HRP}	HRP-conjugated goat anti-rabbit IgG	-	1:5000	Dianova
GαM^{405}	CF^{TM} goat anti-mouse IgG	1:100	-	Biotium
GαM^{488}	Alexa Fluor® 488 goat anti-mouse IgG	1:100	-	Invitrogen
GαM^{568}	Alexa Fluor® 568 goat anti-mouse IgG	1:100	-	Invitrogen
GαM^{647}	Alexa Fluor® 647 goat anti-mouse IgG	1:100	-	Invitrogen
GαR^{405}	CF^{TM} goat anti-rabbit IgG	1:100	-	Biotium
GαR^{488}	Alexa Fluor® 488 goat anti-rabbit IgG	1:100	-	Invitrogen
GαR^{568}	Alexa Fluor® 568 goat anti-rabbit IgG	1:100	-	Invitrogen
GαR^{647}	Alexa Fluor® 647 goat anti-rabbit IgG	1:100	-	Invitrogen

2.1.8 Fluorescent probes

Fluorescent probes	Source
Alexa Fluor®568phalloidin	Invitrogen
Alexa Fluor®568 conjugated transferrin (Tf^{568})	Invitrogen
Alexa Fluor®647 conjugated EGF (EGF^{647})	Invitrogen
Alexa Fluor®647 conjugated transferrin (Tf^{647})	Invitrogen
DAPI (4', 6-Diamindino-2-phenylindole dihydrochloride)	Sigma
Hoechst 33342	Immunochemistry Technologies, LLC
Magic Red^{TM}Cathepsin B MR-$(RR)_2$	Immunochemistry Technologies, LLC
Magic Red^{TM}Cathepsin L MR-$(FR)_2$	Immunochemistry Technologies, LLC
LysoTracker® Red DND-99	Invitrogen
Oregon Green® 488, dextran 10,000 MW (OGD^{488})	Invitrogen

2.2 Devices and equipment

Device	Model	Company
Autoclave	Systec model V-65	Systec (Wettenberg)
Centrifuge	Eppendorf 5417-R	Eppendorf (Hamburg)
Incubator for tissue culture	Heraeus	Thermo Electron (Langenselbold)
Magnetic stirrer	RCT basic	IKA-Werke (Staufen)
Microscopes	Axiovert 200/ 200M	Carl Zeiss (Jena)
	LSM780	Carl Zeiss (Jena)
	Nikon Ti Eclipse	Nikon (Düsseldorf)
	Olympus CKX31	Olympus (Hamburg)
pH meter & electrode	Five Easy FE 20, LE438	Mettler-Toledo (Gießen)
Plate reader	GeniosPro	Tecan AG (Männedorf)
Power Supply	Standard Power Pack P25	Whatman Biometra (Göttingen)
Semi-dry blotter	Fastblot B44	Whatman Biometra (Göttingen)
Spectrophotometer	Eppendorf Bio Photometer	Eppendorf (Hamburg)
Ultrasonic unit	Sonorex RK103H, 560 W	Bandelin (Berlin et al)
Water Purification System	arium® advance	Sartorius (Göttingen)
Wet transfer blotter	Mini Trans-Blot® Electrophoretic transfer	Biorad (München)

2.3 Software and online tools

Software	Source
Adobe Acrobat	Adobe Systems (San José, USA)
Adobe Illustrator	Adobe Systems (San José, USA)
Adobe Photoshop	Adobe Systems (San José, USA)

EndNote X5	Thomson Reuters (Philadelphia, USA)
Fluorescence Spectra Viewer	http://www.lifetechnologies.com/de/de/home/life-science/cell-analysis/labeling-chemistry/fluorescence-spectraviewer.html
GraphPadQuickCalcs t test calculator	http://www.graphpad.com/quickcalcs/ttest1.cfm
ImageJ / Fiji	Wayne Rasband (NIH, USA) http://rsb.info.nih.gov/ij/
Mendeley	http://www.mendeley.com/
MicroManager	Wayne Rasband (NIH, USA) http://rsb.info.nih.gov/ij/
Microsoft Office	Microsoft (Redmond, USA)
pubmed	http://www.ncbi.nlm.nih.gov/pubmed/
Origin6.1G	OriginLab Corporation(Northampton, MA, USA)
Slide Book 5	Intelligent Imaging Innovations (Göttingen)
Volocity	Perkin Elmer (Rodgau)
Zen 2012	Carl Zeiss Microscopy Software (Jena)

2.4 Biochemistry

2.4.1 Preparation of cell lysates

Cell lysates were prepared to biochemically analyze protein levels. HeLa cells were grown in 6-well plates, washed on ice three times in ice cold phosphate-buffered saline (PBS) and harvested in 1 ml PBS using a cell scraper. To separate the buffer from the cells, the suspension was spun for 5 min at 4°C, 1000 xg. For lysis 50 to 100 µl cell lysis buffer was added and the cells incubated for 30 to 45 min on ice. Cell lysates were cleared by centrifugation for 10 min at 4°C 17000 xg. After determination of protein concentrations using the Bradford assay, sample buffer was added and the cell lysates boiled for 5 min at 95°C.

2.4.2 Protein concentration determination (Bradford assay)

This analytical procedure is dependent on the amino acid composition of the measured protein. The principle of this colorimetric assay (Bradford, 1976) is based on an absorbance shift of the dye Coomassie Brilliant Blue G-250 under acidic conditions. Protein concentration were determined by mixing 2–4 µl of cell lysate with 500 µl water and 500 µl 2x Bradford reagent. The mixture was then incubated for 5 min at room temperature in the dark, and the absorbance measured at 595 nm blanked against diluted Bradford reagent (1x Bradford solution). All samples were measured in duplicate and the protein concentration was calculated from a standard curve using BSA in the range of 1 µg to 10 µg as reference.

2.4.3 SDS polyacrylaminde gel electrophoresis (SDS-PAGE)

Protein mixtures can be separated by SDS-PAGE under denaturing conditions according to their molecular mass (Laemmli, 1970). β-mercaptoethanol and sodium dodecyl sulfate (SDS) are used to infere with the protein structure. Disulfide bonds are reduced by β-mercaptoethanol, while non-covalent protein interactions are disrupted by the anionic detergent SDS. SDS binds the denatured protein thereby building a SDS-protein complex with a large net negative charge. As this complex is proportional to the proteins mass it can be separated by electrophoresis.

SDS polyacrylamide gels were prepared with different polymerization degrees for the separation gel varying from 8 % to 13 % according to the protein to be detected and 3.8 % for the stacking gel. All gels were run in Tris-glycine based 1x SDS-PAGE running buffer (Laemmli) at 20 – 25 mA for the stacking gel and 10 – 15 mA for the separating gel. The following recipe is sufficient for two small SDS-gels:

	Separating gel (15 ml)			**Stacking gel (5 ml)**
	8 %	10 %	13 %	3.8 %
ddH_2O	7 ml	6 ml	4.5 ml	3.25 ml
4x separating gel buffer	3.75 ml	3.75 ml	3.75 ml	-
4x stacking gel buffer	-	-	-	1.25 ml

30 % acrylamide/ 0.8 % bis-acrylamide	4 ml	5 ml	6.5 ml	0.625 ml
10 % APS	75 µl	75 µl	75 µl	75 µl
TEMED	7.5 µl	7.5 µl	7.5 µl	7.5 µl

2.4.4 Immunoblotting

This immunoassay technique, also called Western blotting (Towbin et al, 1979), is routinely used to detect very small protein quantities. After subjecting the samples to electrophoresis on a SDS-gel the separated proteins were transferred to a nitrocellulose (Whatman Biometra) or to a PVDF (Millipore) membrane using either a semi-dry or wet transfer blotting system. Whatman filter papers were soaked in transfer buffer and assembled together with the membrane and the SDS-gel in a blotting apparatus (bottom to top: three layers of Whatman paper, membrane, SDS-gel, and three additional layers of Whatman paper). For the wet transfer two layers of Whatman paper on each side were sufficient. The semi-dry electrotransfer was run for 3 – 4 h at 45 mA per gel. The wet transfer was performed in the coldroom at 450 mA for 1 h. After blotting, the membrane was stained in Ponceau staining solution to visualize the transfer efficiency and destained in 1 % acetic acid. To reduce unspecific antibody binding, the membrane was incubated in IB blocking solution for 1 h at room temperature, then washed three times for 10 min in 1x TBS. Primary antibody was incubated in IB antibody solution for 1 h at room temperature or overnight at 4°C, and then washed in TBS three times for 10 min. Secondary antibody coupled to horseradish peroxidase (HRP) was diluted in 3 % milk powder in TBS and incubated for 1 h at room temperature. To reduce unspecific secondary antibody binding, the membrane was washed three times in TBS. Enhanced chemoluminescence (ECL) Western Blotting Detection Reagent (GE Healthcare) was used to detect the antibodies on the membrane. The reaction of hydrogen peroxide (HRP) with luminol (ECL) results in the emission of a luminescent signal. This signal was visualized by exposing the membrane to a light sensitive film (Hyperfilm ECL, Amersham Biosciences). The gel analysis plugin for ImageJ was used to quantify western blot signals. For redecoration of membranes, antibodies were stripped from the membrane by applying IB stripping buffer for 30 min at 55°C. After one wash in H_2O and three washing steps in TBS, each 10 min, membranes were blocked in IB blocking solution and re-decorated with antibodies.

2.4.5 EGFR-signaling

HeLa cells at a confluence of 90 % were washed in PBS and incubated with 20 µg/ ml silica nanoparticles in cell culture medium for 4 h, whereas control cells were incubated in cell culture medium only. All samples were then washed, subjected to starvation for 2 h in DMEM and stimulated for 0 and 30 min with 500 ng/ ml unlabelled EGF in DMEM supplemented with 10 µg/ ml cycloheximide. Subsequently cells were washed three times in ice cold PBS and lysed in lysis buffer (1 % Triton X-100, PMSF and protease inhibitor cocktail were added freshly). Phosphatase inhibitor cocktail (Sigma) was added for the analysis of phosphorylated proteins. Lysates were spun at 20.000 xg for 10 minutes to separate cell nuclei and debris. After determination of the protein concentration the supernatants were mixed with 6x SDS-PAGE sample buffer, boiled for 5 min at 95°C, and then analyzed by SDS/PAGE and immunoblotting.

2.4.6 Autophagic flux (LC3-I to LC3-II conversion & mTOR)

Cells were washed in PBS and incubated for 24 h in cell culture medium supplemented with 20 µg/ ml and 100 µg/ ml silica nanoparticles, respectively. Control cells were incubated for the same time in cell culture medium only. 4 h before cell lysis, 100 nM Bafilomycin A1 (Sigma) was directly added to the corresponding samples and the starvation control was induced by addition of HBSS. After washing three times in ice cold PBS, HeLa cells were lysed on ice for 30–60 minutes in lysis buffer (2 % Triton X-100, PMSF and protease inhibitor cocktail were added freshly before use). Phosphatase inhibitor cocktail (Sigma) was added for the analysis of phosphorylated proteins. The protein concentration was determined from crude cell lysates. Samples were mixed with 6x SDS-PAGE sample buffer, boiled for 5 min at 95°C and analyzed by SDS-PAGE and immunoblotting.

2.5 Cell Biology

2.5.1 Mammalian cell culture

HeLa cells were cultured at 37°C and 5 % CO_2 in a humidified incubator in low-glucose Dulbecco's modified Eagle's medium (DMEM containing 1 g/ l glucose; Lonza) supplemented with 10 % (v/v) heat-inactivated (30 min, 56°C) fetal bovine serum (FBS), 1 % glutamine and 1 % penicillin/ streptomycin (50 units/ ml penicillin, 50 µg/ ml streptomycin). Cells were passaged every two to four days up to passage number 35. For passaging,

confluent cells were washed once in PBS and incubated with Trypsin / EDTA for 5 min at 37°C for detachment. After resuspension in cell culture medium cells were plated in 1:5 to 1:40 dilutions on a new cell culture dish.

2.5.2 Transfection of mammalian cells with siRNA

For specific depletion of a protein of interest, small interfering RNA was transfected into cells using Oligofectamine according to the manufacturer's protocol. The exogenous double-stranded 20 – 25 base pairs RNA sequence binds to mRNA of complementary sequence, leading to their degradation thus interfering with protein translation (Hamilton & Baulcombe, 1999). For knockdown experiments HeLa cells were grown to 40 – 50 % confluence and transfected with siRNA on day 1. SiRNA and Oligofectamine were each mixed with Optimem in two separate polystyrol snapcap tubes and both incubated for 5 min at room temperature. Then the siRNA mix and the Oligofectamine mix were combined and incubated for 20 min at room temperature. Cells were washed in PBS once and put into Optimem. The transfection mix was added drop wise and the cells were incubated at 37°C and 5 % CO_2 in a humidified incubator. After 4 h, the transfection mix was replaced by antibiotic free cell culture medium. On day 2, the cells were passaged on a new cell culture dish for a second round of transfection on day 3. Cells were split on coverslips on day 4 and used for experiments on day 5.

Culture vessel	siRNA mix		Oligofectamine mix		Plating medium (Optimem)
	Volume of siRNA (stock 100 µM)	Volume of Optimem	Volume of Oligofectamine™	Volume of Optimem	
12-well	1 µl	85 µl	2 µl	10 µl	400 µl
6-well	2 µl	175 µl	6 µl	44 µl	800 µl
6 cm	4 µl	350 µl	12 µl	88 µl	1600 µl

2.5.3 Disruption of cytoskeletal elements

HeLa cells were grown overnight on coverslips to reach 80 % confluence. The cells were then washed in PBS once and incubated with 5 µM cytochalasin D (4 mM stock in EtOH) or 10 µg/ ml nocodazole (6 mg/ ml stock in DMSO) in cell culture medium at 37°C. Control

cells were incubated with the according amounts of EtOH or DMSO, respectively. After 30 min, freshly sonicated silica nanoparticles were directly added into the wells at a concentration of 20 µg/ ml and cells were incubated for 4 h at 37°C. Cells were then washed three times for 5 min in ice cold PBS supplemented with 10 mM $MgCl_2$ and fixed. Cytochalasin D-treated cells were fixed 10 min at room temperature in fixation buffer and nocodazole-treated cells were fixed in methanol at -20°C for 5 min. For immunofluorescence experiments, samples were decorated with fluorescently labeled phalloidin and anti-tubulin antibody to detect actin and microtubules, respectively. Images were acquired using a laser-scanning microscope LSM780 (Carl Zeiss Micro Imaging GmbH, Jena, Germany) with a 63x/1.4 numerical aperture oil-immersion objective and processed with Zen 2012 software (Zeiss).

2.5.4 Cell viability (MTT assay)

The MTT [3-(4,5-dimethyl-2-thiazolyl)-2,5-diphenyl-2*H*-tetrazolium bromide] assay is a colorimetric assay widely used to assess cell viability or cytotoxicity (Mosmann, 1983). The test is based on the reduction of yellow water-soluble 3-(4,5-dimethyl-2-thiazolyl)-2,5-diphenyltetrazolium bromide (MTT) to purple colored insoluble formazan by enzymes in living cells. After solubilization of the product, absorbance measurements of the colored solution are accessible at wavelengths between 500 and 600 nm.

HeLa cells were seeded in 96-well plates at a density of 10,000 cells per well. The next day cells were incubated for 24 h at 37°C and 5 % CO_2 with different concentrations of silica nanoparticles (+/- FITC) in phenol red-free cell culture medium (Invitrogen). Cells were washed twice in PBS and the buffer replaced with 100 µl fresh phenol red-free DMEM. After addition of 10 µl MTT (12 mM stock in sterile PBS) to each well, cells were incubated for 4 h at 37°C and 5 % CO_2. Then 100 µl of the SDS-HCl solubilization solution was added to each well and thoroughly mixed. The microplate was incubated for additional 16-17 h at 37°C and 5 % CO_2 in a humidified incubator and the absorbance measured at 562 nm using the Safire2 plate reader (Tecan AG). All samples were prepared and measured in triplicates. See also the manufacturer's instructions (Invitrogen).

2.5.5 Immunofluorescence Staining

HeLa cells were seeded on poly-L-lysine-coated glass coverslips (Thermo Scientific) and grown overnight to a confluence of 60-80 %. For colocalization studies, cells were washed

once in PBS and incubated at 37°C and 5 % CO_2 for 4 h in cell culture medium containing freshly sonicated 20 µg/ ml silica nanoparticles. After three washing steps in ice cold PBS (+10 mM $MgCl_2$), cells were fixed in fixation buffer for 10 min and blocked in GSDB for 30 min at room temperature to reduce unspecific binding. After three 5 min washes in IF washing buffer, the samples were decorated with primary antibodies in GSDB and incubated for 1 h at room temperature. To remove unbound antibodies, the cells were washed three times for 10 min in IF washing buffer. A solution with a 1:100 dilution of species-specific fluorescently labeled secondary antibodies in GSDB was then prepared to incubate the samples for 1 h at room temperature. After additional three 10 min washes in IF washing buffer the samples were mounted onto glass slides using Immu-Mount solution (Thermo Scientific) supplemented with 5 µg/ ml DAPI (Sigma). Samples were as far as possible processed in the dark to avoid bleaching of the fluorophores and stored at 4°C.

2.5.6 Degradation of epidermal growth factor

60-80 % confluent HeLa cells, grown on poly-L-lysine-coated coverslips, were washed in PBS and incubated with 20 µg/ ml silica nanoparticles in cell culture medium for 4 h at 37°C and 5 % CO_2 in a humidified incubator. Control cells were incubated for the same time in cell culture medium only. Samples were then rinsed three times in PBS, starved in DMEM for 2 h followed by incubation with 100 ng/ ml EGF^{647} in DMEM for 30 min on ice. Cells were then washed twice in ice cold PBS to remove unbound EGF and incubated in DMEM at 37°C. After 30, 60 and 120 min cells were washed in PBS on ice, fixed in fixation solution and processed for immunocytochemistry. To evaluate EGF surface levels, coverslips were fixed at timepoint 0 min, right after the 30 min EGF^{647} prebinding on ice. Images were acquired using a spinning disc confocal microscope (Perkin Elmer).

2.5.7 Transferrin/ epidermal growth factor uptake

HeLa cells were seeded on poly-L-lysine-coated glass coverslips and grown to a confluence of 60−70 %. After one washing step in PBS, cells were incubated for 4 h with 20 µg/ ml silica nanoparticles in cell culture medium in a humidified incubator at 37°C and 5 % CO_2. Control cells were incubated for the same time in cell culture medium only. All samples were washed three times in PBS and preincubated on ice for 30 min with 20 µg/ ml Tf^{647} or 100 ng/ ml EGF^{647}. To allow internalization, cell dishes were shifted to 37°C for 15 min. Subsequently, the cells were placed on ice, washed three times for 5 min in ice cold PBS

buffer containing 10 mM $MgCl_2$ and fixed in fixation solution for 10 min. After fixation, cells were washed twice in PBS and mounted onto glass slides using Immu-Mount solution (Thermo Scientific) supplemented with 1 µg/ ml DAPI. A spinning disc confocal microscope was used to acquire images (Perkin Elmer).

2.5.8 Recycling of transferrin

60-80 % confluent HeLa cells grown on glass coverslips were incubated in cell culture medium and cell culture medium supplemented with 20 µg/ ml silica nanoparticles for 4 h, subsequently washed three times in PBS, and starved for 1 h in DMEM followed by incubation with 20 µg/ ml Tf^{647} for 30 min on ice. Cells were then washed twice in ice cold PBS and incubated in DMEM for 5, 15 and 60 min at 37°C. Immediately afterwards, cells were washed on ice, fixed in fixation solution for 10 min at room temperature and processed for immunocytochemistry. To evaluate Tf surface levels, coverslips were fixed at timepoint 0 min, right after the 30 min Tf^{647} prebinding on ice. Images were acquired using a spinning disc confocal microscope (Perkin Elmer).

2.5.9 Autophagy assay

HeLa cells at a confluence of 50 % were incubated for 24 h at 37°C in cell culture medium supplemented with 20 µg/ ml and 100 µg/ ml silica nanoparticles, respectively. Control cells were incubated for the same time in cell culture medium only. The next day, 4 h before incubation was stopped, 100 nM Bafilomycin A1 (Sigma) was added directly to the corresponding samples to disrupt fusion of autophagosomes with lysosomes. In addition, cell culture medium in the starvation control was replaced by HBSS. After washing in ice cold PBS, cells were fixed in fixation solution for 10 min at room temperature and prepared for immunostaining with LC3 and p62, respectively. Digitonin (100 µg/ µl in PBS; Invitrogen) was used instead of Triton X-100 to permeabilize the cells for LC3 staining. Image acquisition was performed on a spinning disc confocal microscope (Perkin Elmer).

2.5.10 Internalization of dendritic polyglycerol nanoparticles and release of doxorubicin

HeLa cells were seeded on glass coverslips (Thermo Scientific) and cultured overnight at 37°C and 5 % CO_2. Cells were washed once in PBS and incubated for 2 h in cell culture

medium together with 10 µM TMP or non-cleavable ctrl (stated in Dox equivalents). After two PBS washing steps, coverslips were fixed in fixation solution for 10 min at room temperature, and mounted using Immu-Mount (Thermo Scientific). Images were acquired using the Nikon Eclipse Ti epifluorescence microscope with a 40x/1.3 numerical aperture oil-immersion objective, excitation filter BL HC 494/41, dichroic mirror HC BS 520, emission filter BL HC 582/75 (all from Semrock). Image processing was performed using MicroManager.

2.6 Fluorescence microscopy

This microscopy technique is based on the principle of absorption and subsequent re-radiation of light. Organic or inorganic probes are thereby excited into a higher energetic state by light of a specific wavelength. Emission of a photon, light of a shorter wavelength than the absorbed light, results in relaxation of the fluorophore back to the electronic ground state. Fluorescent probes as well as genetically encoded fluorescent proteins can be used to visualize proteins in fixed or living cells.

2.6.1 Epifluorescence microscopes

Conventional microscopy that uses illumination from above the sample is termed epifluorescence microscopy. A mercury arc lamp is usually used as a high-intensity light source that emits light in a broad spectrum ranging from ultraviolet to near-infrared light. Fluorescence filter cubes, consisting of excitation filter, dichroic mirror (beam splitter) and emission filter, are implemented into the light path to limit light transmission to a narrow wavelength range.

The epifluorescence microscope Axiovert 200M from Zeiss was equipped with a DG4 excitation unit and a Coolsnap HQ2 EM- CCD camera (Roper Scientific). The system was operated by Slidebook software (Intelligent Imaging Innovations).

The Nikon Eclipse Ti epifluorescence microscope was equipped with an Andor Neo sCMOS camera, a motorized high precision stage from Märzhäuser (Wetzlar) and auto focus system (PFS, Nikon). The system was operated by MicroManager (Edelstein et al, 2010).

2.6.2 Confocal microscopes

Confocal microscopy uses point illumination (Hofmann et al) and a pinhole in front of the detector to eliminate the out-of-focus fluorescence signal. This results in a higher resolution in the z-axis. While laser scanning confocal microscopes scan a sample point-by-point, spinning disk confocal microscopes use a series of moving pinholes on a disc, which enables scanning of an area in parallel thereby reducing excitation energy and increasing imaging time. Thus, spinning disk confocal microscopy is a preferred system for live cell imaging.

Laser scanning confocal microscope

Micrographs were acquired with point-by-point scanning using a LSM780 from Carl Zeiss MicroImaging GmbH, Jena, Germany with a 63x/1.4 numerical aperture oil-immersion objective. The system was operated by Zen 2012 software (Zeiss).

Spinning disc confocal microscope

The Axiovert 200M microscope from Zeiss connected to a dual spinning-disk system Ultra View ERS Rapid confocal Imager (Perkin Elmer Life Sciences), and equipped with an EM-CCD camera (Hamamatsu) was used for image acquisition. The system was operated by Volocity software (Improvision).

2.6.3 Live cell imaging

Lysotracker

HeLa cells were grown overnight on coverslips, washed once in PBS and incubated with 20 µg/ ml silica nanoparticles and 50 nM LysoTracker® Red DND-99 (Invitrogen) in cell culture medium for 4 h at 37°C. Afterwards cells were washed thoroughly in PBS and subjected to live imaging on a spinning disc confocal microscope in imaging buffer at 37°C and 5 % CO_2.

Cathepsin B/ L - protease activity

Cells were seeded on MatTek glass bottom dishes (MatTek Corporation) and cultured overnight at 37°C and 5 % CO_2. After washing in PBS and incubation for 4 h with 20 µg/ml silica nanoparticles in cell culture medium, cells were thoroughly washed in PBS and subsequently treated with 20 µl of 26x Magic Red™ Cathepsin B/L solution (frozen 260x stock of Magic Red™ Cathepsin B/L was diluted 1:10 in PBS immediately before use) in

500 µl cell culture medium. The total incubation time with Magic Red™ Cathepsin B/L (both from Immunochemistry Technologies) was 60 min at 37°C and 5 % CO_2. Hoechst was added directly to cells 15 min prior to imaging. Cells were washed thoroughly in PBS and subjected to live imaging on a spinning disc confocal microscope in imaging buffer at 37°C and 5 % CO_2.

Lysosomal pH

The lysosomal pH was determined by ratiometric fluorescence imaging using a pH sensitive Oregon Green® 488 dye coupled to a 10 kDa dextran (OGD, Molecular Probes). A standard pulse-chase protocol was used to specifically target the fluorophore to lysosomes. Cells were grown on MatTek glass bottom dishes to a confluence of 80 %. The PBS washed cells were treated with 20 µg/ ml silica nanoparticles (-FITC) for 4 h in cell culture medium. After two additional PBS washing steps, 0.5 mg/ ml OGD was loaded onto the cells and incubated overnight in cell culture medium. The next day, cells were washed in PBS and the pH sensitive dye chased into lysosomes for 2 h at 37°C in cell culture medium. Control experiments were conducted to prove the localization of Oregon Green to LAMP1- and CD63-positive structures. The fluorophore was excited at a wavelength of 440 and 488 nm, respectively, and ratiometric fluorescence images were acquired with an inverted microscope (Zeiss Axiovert 200 equipped with a 100x 1.30 NA oil immersion objective) connected to a Polychrom II monochromator (TILL photonics). After passing a 535±20 nm filter, the emitted light was captured with a Sensicam CCD camera (PCO). For each sample (ctrl and +SiNPs, respectively) at least 10 different cells were measured in imaging solution (10 mM glucose, 2 mM $CaCl_2$, 1 mM $MgCl_2$, 135 mM NaCl, 5 mM KCl, 10 mM HEPES pH 7.4). Image analysis was performed using a self-programmed Macro for Fiji ImageJ (Schindelin et al, 2012). Regions of interest (ROIs) were defined as areas above a certain fluorescence threshold in the acquired images at 488 nm excitation. The ratio of the mean intensity of the 488 and the 440 channel was calculated for each ROI. To finally evaluate the pH for each measurement, an *in situ* pH calibration was conducted at the end of each experiment by treating the cells with isotonic K^+-based solutions (5 mM NaCl, 1 mM $CaCl_2$, 115 mM KCl, 1.2 mM $MgSO_4$, 10 mM glucose, 25 mM of either HEPES, MES or potassium acetate) ranging in pH from 3.5 to 7.0 and supplemented with 10 µM of both nigericin (Tocris Bioscience) and monensin (Sigma). The resulting fluorescence intensity ratio (488 nm/ 440 nm) was fitted with a sigmoidal function and used to interpolate the pH value from the experimental ratio data.

TMP – Doxorubicin release

HeLa cells were seeded on MatTek glass bottom dishes (MatTek Corporation) and cultured overnight at 37°C and 5 % CO_2. Before live imaging, cells were washed once in PBS and placed in a heating unit. Immediately after addition of imaging buffer supplemented with 10 µM polymer conjugate (concentration stated in Dox equivalents) images were acquired using the laser-scanning microscope LSM780 (Carl Zeiss MicroImaging GmbH, Jena, Germany) with a 63x/1.4 numerical aperture oil-immersion objective, λ_{ex} = 488 nm, detection window 508 – 690 nm, pinhole 599 µm. Images were acquired for 60 min with a frame rate of 1 image every 10 min. After 120 min of conjugate addition, cells were washed in PBS and fixed in fixation solution for 10 min at room temperature. Fixed samples were washed in PBS and subjected again to imaging using the same settings as stated above. Quantification analysis was performed using Fiji ImageJ software (Schindelin et al, 2012).

2.7 Data analysis and statistics

Fluorescence microscopy images were analyzed using Volocity software for spinning disc confocal data, and Zen software for laser scanning confocal data. Fiji Image J software was used to quantify images attained with the Nikon epifluorescence microscope, and Slidebook software for Zeiss epifluorescence microscopy images. Quantitative data were processed with Excel (Microsoft Office). Statistics for the entire experimental pool were done using the unpaired *t*-test (GraphPad software). All data are presented as mean with standard error of the mean (s.e.m.), wirth n indicating the number of independent experiments. Significance is indicated by asterisks (ns, non-significant $p > 0.05$; *$p < 0.05$; **$p<0.01$; ***$p<0.001$).

3 RESULTS

Part I – Silica nanoparticles

Silica nanomaterials are often used as model systems in biomedical studies. Aside from the physicochemical properties, such as optical transparency, chemical inertness, mechanic stability or biocompatibility, there is the manageability that makes silica the material of choice (Iler, 1979). Well-established protocols allow the synthesis of dye- or QD-labeled silica nanoparticles with a low polydispersity (Graf et al, 2006; Ketelson et al, 1995; Liu & Han, 2005; van Blaaderen & Vrij, 1992). In addition, surface functionalization and the adjustment of size and shape are fairly easy to achieve with silica.

3.1 Surface properties are crucial for nanoparticle stability in biological media

Besides shape and size of nanomaterials, there is also the issue of surface functionalization of nanoparticles that contributes significantly to the interaction with cells. Therefore, a systematic study on surface stabilization was performed in collaboration with the Rühl group (FU Berlin). Spherical silica nanoparticles with variable surface functionalizations were investigated with regard to aggregation in physiological media and cell interaction. We used several methods, such as dynamic light scattering (DLS), zeta potential measurements, and transmission electron microscopy (TEM), to determine their colloidal stability in standard buffers as well as in cell culture media (Graf et al, 2012).

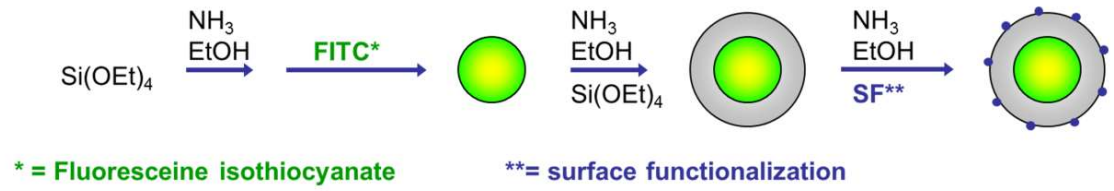

Scheme 1 Preparation of silica nanoparticles (SiNPs). The scheme illustrates the synthesis of surface-functionalized SiNPs using the microemulsion and Stöber technique. Modified from Schütz et al., 2016

Silica nanoparticles were generated based on a modified microemulsion process (Scheme 1) (Ow et al, 2005). The resulting spherical silica cores of 50 ± 3 nm in diameter were then covalently labeled with fluoresceine isothiocyanate (FITC) and subsequently used as seeds

to grow a 3 nm thick silica shell using the Stöber method (Stöber et al, 1968; van Blaaderen et al, 1992). The resulting core/ shell silica nanoparticles with an average TEM-diameter of 55 ± 2 nm or approx 65 nm DLS-diameter (see alsoTable 3.1) were surface-functionalized either by adsorption or by covalent binding to different silane agents, such as (3-aminopropyl)trimethoxysilane (APS), *N*-(6-aminohexyl)-aminopropyl-trimethoxysilane (AHAPS), and 2-[methoxy-(polyethyleneoxy)propyl]trimethoxysilane (PEG silane). In addition, APS [(3-aminopropyl)-trimethoxysilane]-coupled probes were modified with 1-*H*-pyrazole-1- carboxamidine hydrochloride (N-guanylpyrazole, GP) to obtain GP-coupled particles (Figure 3.1 A).

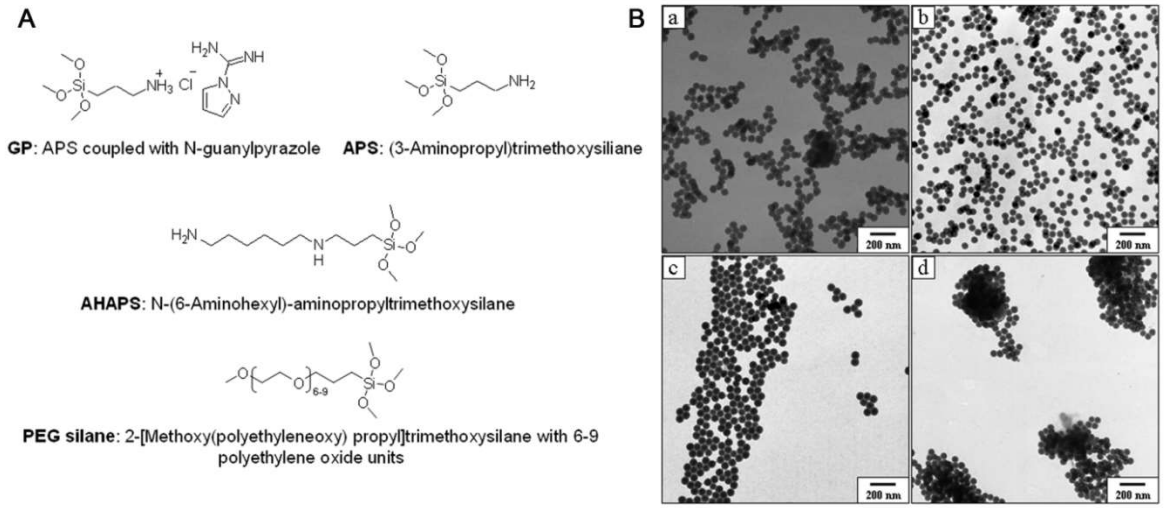

Figure 3.1 SiNPs with variable surface functionalizations. (**A**) Chemical formulae of surface functionalization agents used in this study. (**B**) TEM images after 14 h of exposure to cell culture medium of (a) non-functionalized, (b) AHAPS functionalized, (c) PEG-functionalized, and (d) APS-functionalized silica particles. Modified from (Graf et al, 2012)

Zeta potentials of the differently functionalized particles in ethanol varied from highly negative for the non- and PEG-functionalized samples (-43 ± 2 mV and -56 ± 2 mV, respectively) to highly positive values for the particles bearing amino groups on the surface (+41 ± 3 mV (AHAPS), +64 ± 3 mV (APS), and +43 ± 2 mV (GP), respectively) (

Table 3.1; ethanol). Both, the stable diameter and zeta potential values are an indication of successful surface functionalization and high colloidal stability in ethanol.

Table 3.1 Zeta potentials and diameters of different surface-functionalized NPs in various media. Diameter determined by dynamic light scattering (DLS) and transmission electron microscopy (TEM). All data are averaged values from at least five independent measurements performed within the first hour after transfer into the corresponding medium. Modified from (Graf et al, 2012)

	Ethanol			Water		DMEM (+ 10 % FCS)	
	Ø [nm] (TEM)	Ø [nm] (DLS)	ζ [mV]	Ø [nm] (DLS)	ζ [mV]	Ø [nm] (DLS)	ζ [mV]
NPs-non	55 ± 2	65 ± 2	-43 ± 2	69 ± 2	-35 ± 3	97 ± 3	-16 ± 2
NPs-AHAPS	55 ± 2	65 ± 2	+41 ± 3	71 ± 2	+23 ± 2	78 ± 7	+15 ± 2
NPs-PEG	55 ± 2	65 ± 2	-56 ± 2	76 ± 3	-49 ± 1	57 ± 3	-10 ± 1
NPs-APS	55 ± 2	64 ± 3	+64 ± 3	108 ± 3	+16 ± 2	[a]	[a]
NPs-GP	55 ± 2	66 ± 3	+43 ± 2	104 ± 8	+21 ± 2	[a]	[a]

[a]Severe aggregation of the silica nanoparticles.

Interestingly, the colloidal stability changes significantly for particles functionalized with APS or GP after transfer from ethanol into pure water or cell culture medium leading to severe aggregation (Table 3.1). This is indicated by a dramatic increase in hydrodynamic diameters (DLS) and a decrease in zeta potentials (see Table 3.1 water or DMEM). Little to severe aggregation can also be observed in TEM images for non-functionalized and APS-coupled nanoparticles 14 h after transfer from ethanol to cell culture medium (see Figure 3.1 B a and d, respectively). Only AHAPS- or PEG-functionalized silica nanoparticles remain fairly stable after transfer (Figure 3.1 B b and c, respectively).

Additionally, we investigated the effect on colloidal stability of these differently surface functionalized silica nanoparticles in interaction with eukaryotic cells. First, the nanoparticles were transferred from ethanol into pure water by several centrifugation steps, subsequently diluted in cell culture medium and incubated with HeLa cells, an immortal human cervix carcinoma cell line, for 4 h at 37°C. Alexa 568-labeled transferrin (Tf^{568}), a cargo specifically internalized via clathrin-mediated endocytosis (Hanover et al, 1984), was co-incubated as a positive control. Cells were then extensively washed in PBS to remove non-internalized material and fixed. Nuclei were stained with DAPI. Confocal microscopy images revealed just little internalization of non-functionalized particles (green, Figure 3.2 A) in contrast to positively charged AHAPS particles (green, Figure 3.2 B). A more efficient uptake of positively compared to negatively charged nanoparticles is in agreement with earlier studies

(Oh W. K. et al, 2010; Rancan et al, 2012) and with the fact that binding to the predominant negatively charged cell surface is the first step of nanoparticle-cell-interaction. Furthermore, we could observe partial colocalization (yellow spots in the left-hand image in Figure 3.2 B) of FITC-labeled (green channel) AHAPS-functionalized particles with Tf^{568} (red channel) indicating that after 4 h of treatment at least a fraction of these particles resides in transferrin-positive endosomes.

Confocal microscopy images displayed no sign of PEG particles in or on HeLa cells although DLS and zeta potential values predicted high colloidal stability (Figure 3.2 C). Similarly, inhibitory effects of PEG coating resulted from repulsion caused by membrane proteins on the cell surface (Zhang F. et al, 2001). By contrast, images of particles with an APS surface moiety showed large aggregates in the perinuclear area (most likely extracellular) when incubated in cell culture medium for 4 h at 37°C (Figure 3.2 D), suggesting that adsorption of these positively charged particles to the cell membrane takes place. A 3D reconstruction revealed that at least a small fraction of APS-functionalized particles was internalized into the cells (Graf et al, 2012). Since DLS and zeta potential measurements in cell culture medium already indicated colloidal instability, aggregation had to be expected, possibly due to continuous loss of amino groups from the cell surface as discussed in (Asenath-Smith & Chen, 2008). Aggregation was even more pronounced for GP particles, which carry an APS-based surface functionalization (Figure 3.2 E).

Taken together, we conclude that AHAPS-functionalized nanoparticles are efficiently taken up into HeLa, indicating that efficient cellular uptake is dependent on high colloidal stability in cell culture media and a highly positive zeta potential.

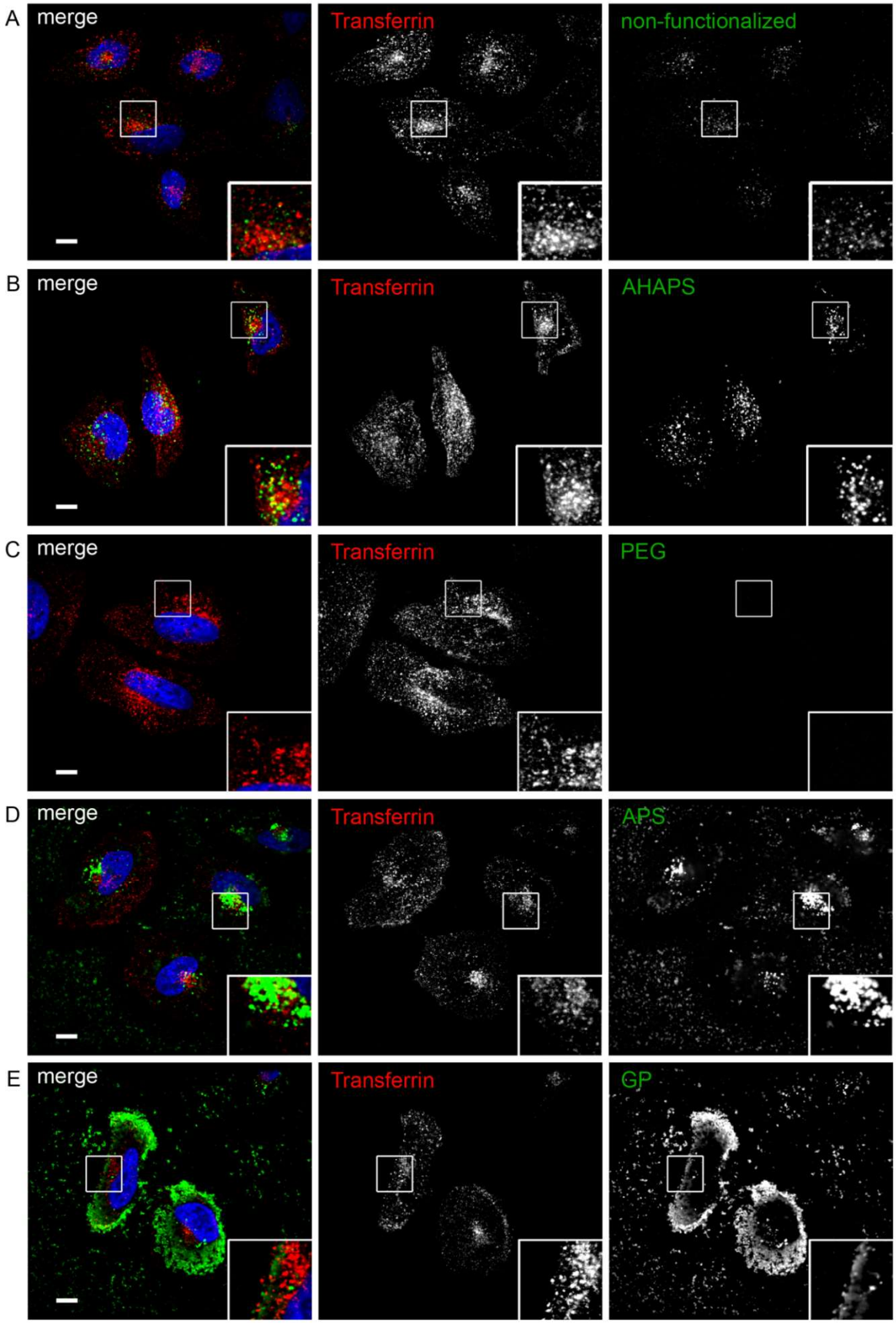

Figure 3.2 Representative spinning disk confocal microscopy images of HeLa cells show the degree of NP uptake. Cells were incubated for 4 h at 37°C in DMEM (+10 % FCS) supplemented

with 100 µg/ ml FITC-labeled SiNPs (green, right column) without surface functionalization(**A**) or with AHAPS (**B**), PEG (**C**), APS (**D**), and GP (**E**) functionalization and subsequently treated with Alexa568-labeled transferrin (red, middle column). Cell nuclei were labeled with DAPI (blue). The left column represents overlays of red, blue, and green fluorescence channels. Scale bars, 10 µm. Modified from (Graf et al, 2012)

3.2 Uptake of SiNP-AHAPS into HeLa cells

Based on our previous results (Graf et al, 2012), we decided to perform a detailed biological study in HeLa cells. All cell biological and biochemical experiments were done with silica nanoparticles bearing the positively charged AHAPS surface functionalization (SiNPs). For this purpose, a new batch of SiNPs, with and without fluorescent label, was synthesized and characterized by TEM, DLS and zeta potential measurements (Figure 3.3 and Table 3.2).

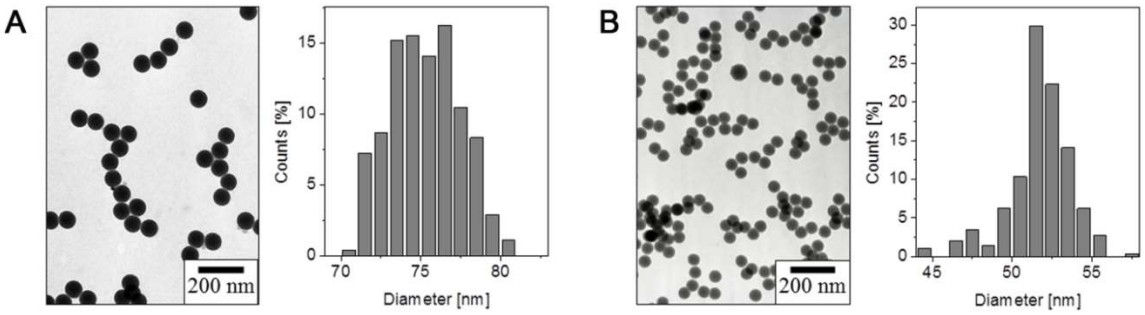

Figure 3.3 Most promising candidate for cell studies: silica nanoparticle with AHAPS surface functionalization. Displayed are a transmission electron microscopy image and the corresponding size distribution histogram of FITC-labeled (**A**, left) and non-labeled (**B**, right) SiNPs. Scale bar, 200 nm. Taken from Schütz et al., 2016

The manufactured particles were of spherical shape and largely monodisperse (as shown in the size distribution diagram in Figure 3.3) with similar average DLS diameters of about 105 nm for both SiNPs (measured in ethanol, Table 3.2). Positive zeta potential values of +51 ± 1 mV for FITC-labeled and +37 ± 7 mV for FITC-unlabeled SiNPs (measured in ethanol, Table 3.2) verified the successful surface functionalization with positively charged amino groups. Transfer into water or cell culture medium just slightly decreased zeta potentials or increased DLS values.

In summary, all characteristics were in full agreement with previous measurements (chapter 3.1) and therefore confirmed colloidal stability for these silica nanoparticles.

Table 3.2 Characterization of AHAPS-functionalized nanoparticles with (+) and without (-) FITC in the core. Diameter determined by dynamic light scattering (DLS) and transmission electron microscopy (TEM). All data are averaged values from at least five independent measurements, performed within the first hour after transfer into the corresponding medium. Taken from Schütz et al., 2016

	Ethanol			**Water**		**DMEM (+ 10 % FCS)**
	Ø [nm] (TEM)	Ø [nm] (DLS)	ζ [mV]	Ø [nm] (DLS)	ζ [mV]	Ø [nm] (DLS)
SiNPs(+FITC)	75 ± 2	107 ± 1	+51 ± 1	119 ± 2	+25 ± 1	245 ± 4
SiNPs(-FITC)	52 ± 2	105 ± 3	+37 ± 7	118 ± 6	+33 ± 2	150 ± 15

3.2.1 Internalization proceeds largely via dynamin 2-dependent caveolar uptake

To unravel the mechanism of cellular uptake of SiNPs, we used small interfering RNAs in order to deplete endogenous protein levels of key components known to be involved in three separate endocytic pathways (Doherty & McMahon, 2009). For that purpose, HeLa cells were treated with siRNAs against clathrin heavy chain, an essential coat protein involved in clathrin-mediated endocytosis, flotillin 1 (also called reggie 2), an integral membrane protein suggested to facilitate clathrin-independent fluid-phase uptake via the CLIC/ GEEC pathway (Glebov et al, 2006), and caveolin 1, which is beside sphingolipids and cholesterol the main structural element of caveolae (Simons & Ikonen, 1997). Caveolin-mediated endocytosis might be the best-characterized dynamin-dependent clathrin-independent pathway. Knockdown efficiency was determined by semi-quantitative immunoblotting. There, expression levels of the target proteins were about 85 – 95 % downregulated. By contrast, the levels of control proteins (Hsc70 and actin) remained unchanged (Figure 3.4 A). Silenced HeLa cells were incubated with FITC-labeled SiNPs for 4 h at 37°C, washed extensively in PBS (+10 mM $MgCl_2$) and fixed. Cell nuclei were stained with DAPI. The relative fluorescence intensity of internalized SiNPs was then evaluated using confocal microscopy. Cells lacking clathrin heavy chain were inperturbed and just a

small though significant reduction in SiNP-uptake was observed in flotillin 1-depleted cells (Figure 3.4 B and C). The greatest decline in SiNP-fluorescence to about 50 – 60 % of control cells (treated with scrambled siRNA) was determined upon knockdown of caveolin 1 (using either single or smart pool siRNA) and dynamin 2 (Figure 3.4 B and C), suggesting that caveolin-mediated dynamin 2-dependent endocytosis is the major internalization pathway of these SiNPs.

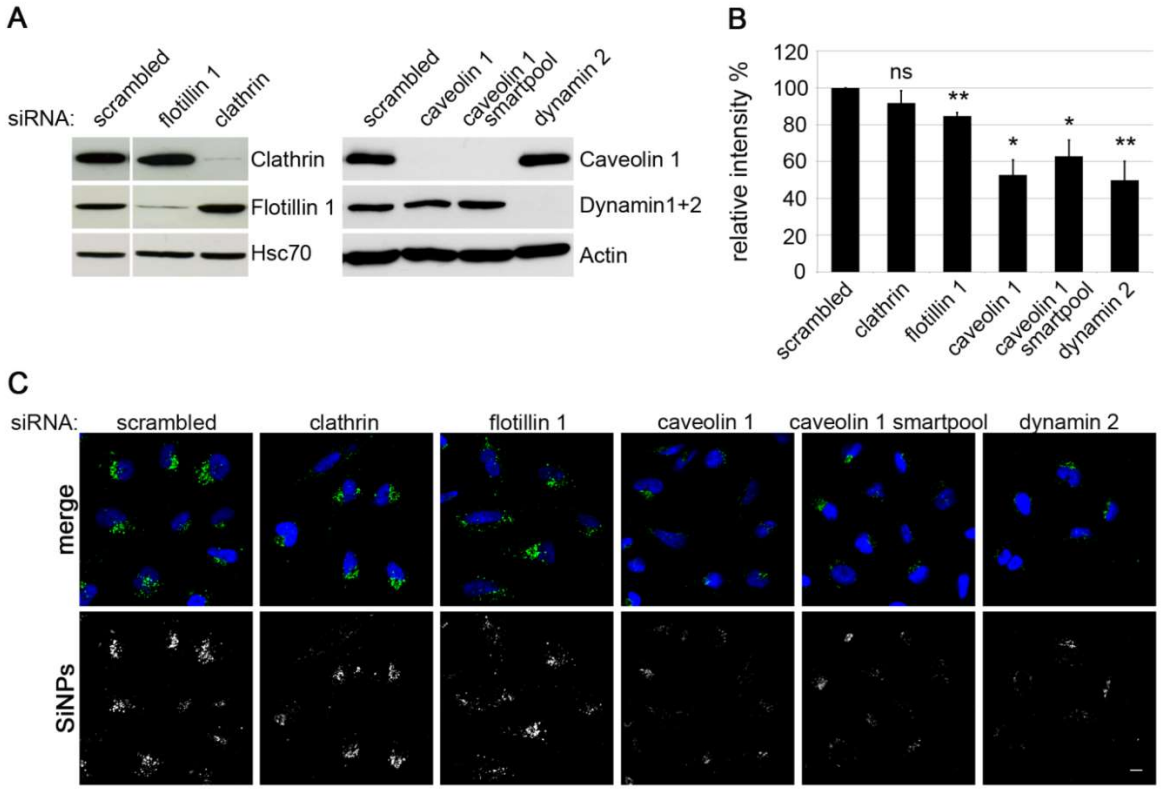

Figure 3.4 SiNPs are internalized largely via dynamin 2-mediated caveolar endocytosis. (**A**) Representative immunoblots of HeLa cell lysates after treatment with siRNA. Protein levels for clathrin (4.9 ± 2.6 % of ctrl), flotillin 1 (15.0 ± 0.9 % of ctrl), caveolin 1 (5.1 ± 0.9 % of ctrl) or caveolin 1 smartpool (4.4 ± 3.6 % of ctrl) and dynamin 2 (5 % of ctrl) were determined using Image J software. (**B**) Quantification of SiNP-uptake as shown in (C). Depicted is the mean SiNP-fluorescence intensity of HeLa cells treated with siRNAs against clathrin (91.8 ± 6.8 %), flotillin 1 (84.7 ± 2.0 %), caveolin 1 (52.8 ± 8.2 % for single and 62.9 ± 8.8 % for smartpool siRNA, respectively), or dynamin 2 (49.9 ± 10.3 %) (mean ± s.e.m.; n = 3-10 independent experiments; *p< 0.05; **p<0.01). (**C**) Representative confocal microscopy images of HeLa cells incubated with SiNPs following depletion of clathrin, flotillin 1, caveolin 1 (single or smartpool siRNA), or dynamin 2. Scale bar, 10 µm. Taken from Schütz et al., 2016

3.2.2 Role of the actin- and microtubule-based cytoskeleton

Furthermore, we investigated whether elements of the cytoskeletal network might affect the internalization of SiNPs, as it was shown before for other nanoparticles (Dausend et al, 2008). Cytochalasin D, a mycotoxin, was reported to induce disruption of actin filaments within seconds (Schliwa, 1982), whereas the antimitotic agent nocodazole inhibits the polymerization of microtubules (Correia, 1991). For that purpose, HeLa cells were grown on glass cover slips, preincubated with either cytochalasin D or nocodazole (5 µM and 10 µg/ ml, respectively) for 30 min, and immediately treated with FITC-labeled SiNPs for 4 h in presence of inhibitors. After extensive washing in PBS (+10 mM $MgCl_2$), cells were fixed and stained for either actin or microtubules using Alexa568-labeled phalloidin and a specific anti-tubulin antibody, respectively (Figure 3.5). Confocal microscopy images of control cells (-Cyt D) displayed a considerable network of actin-positive filaments, which did not colocalize with internalized SiNPs. By contrast, actin fibers were disrupted in HeLa cells treated with cytochalasin D (+Cyt D, Figure 3.5 A). Also microtubules (-Noc, Figure 3.5 B), stained with antibodies against tubulin, were dissipated in cells treated with inhibitor (+Noc). Fluorescence intensity analysis revealed in both cytochalasin D- and nocodazole-treated cells a diminished amount of internalized SiNPs (26,1 ± 1.4 % in Cyt D- and 27.4 ± 9.0 % in nocodazole-treated cells, respectively as shown on the right-hand side of Figure 3.5). This leads to the conclusion that both actin filaments and microtubules are essential for accumulation of internalized SiNPs.

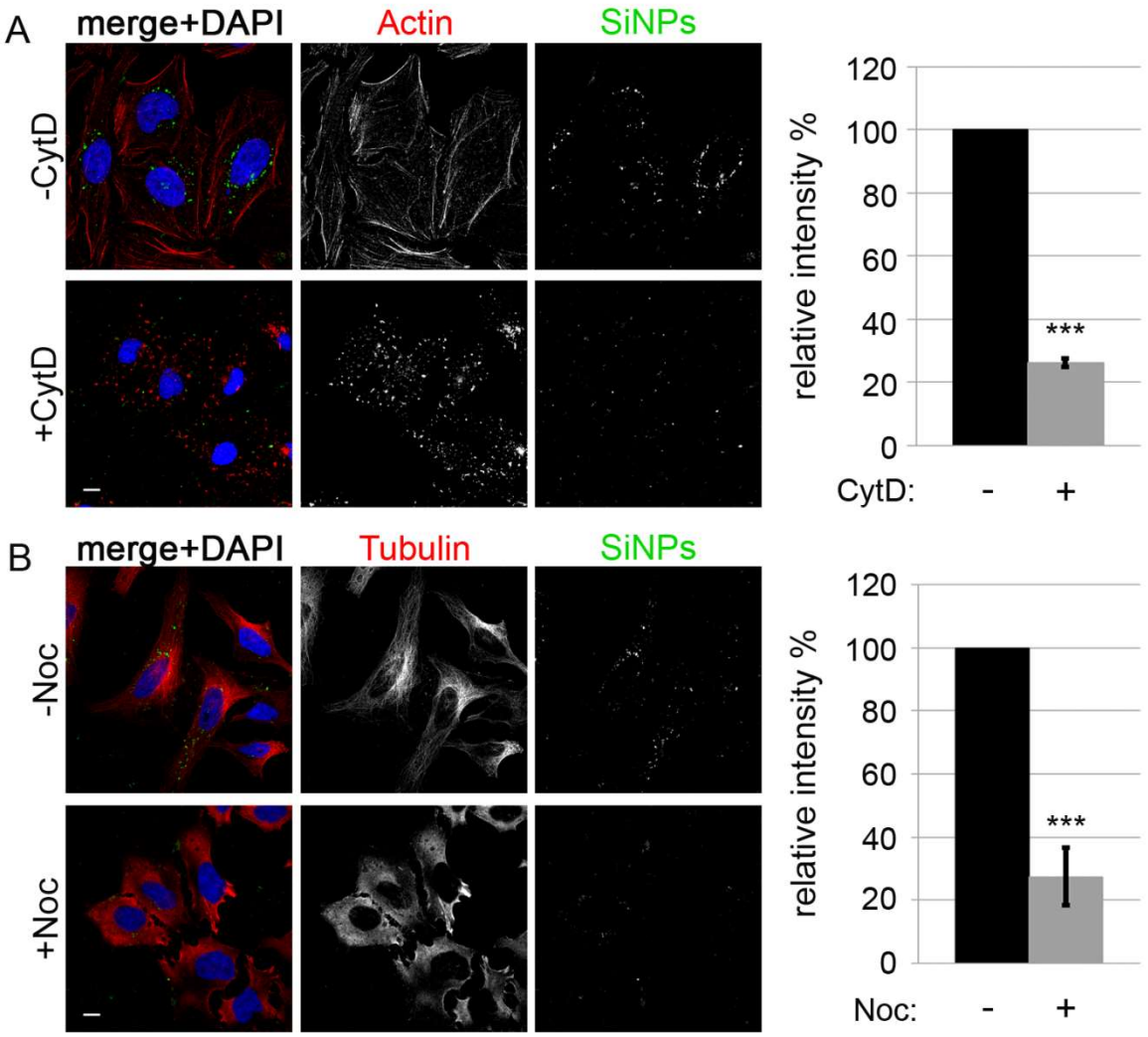

Figure 3.5 Impact of perturbing the actin- and microtubule-based cytoskeleton on the intracellular accumulation of SiNPs in HeLa cells. (**A**) Confocal microscopy images show HeLa cells treated with 5 µM cytochalasin D (+Cyt D) and a corresponding amount of EtOH (-Cyt D), respectively for 30 min at 37°C followed by incubation with 20 µg/ ml SiNPs (green chanel) in cell culture medium for 4 h. Actin filaments were stained with Alexa568-coupled phalloidin (red chanel). Quantification on the right-hand side represents a reduced intensitiy of FITC fluorescence (26,1 ± 1.4 %) compared to EtOH treated (set to 100 %) cells (mean ± s.e.m.; n = 3 independent experiments; *** p<0.001). (**B**) Representative images of HeLa cells after 30 min nocodazole or DMSO treatment (10 µg/ ml) and subsequent SiNP (green chanel)-incubation for 4 h in cell culture medium at 37°C. Microtubules, stained with an anti-tubulin antibody, are depicted in red. Quantification reveals a strongly reduced FITC fluorescence (27.4 ± 9.0 %) in SiNP-treated cells compared to DMSO control, which was set to 100 % (mean ± s.e.m.; n = 4 independent experiments; *** p<0.001). DAPI stained nuclei are shown in blue. Scale bars, 10 µm. Taken from Schütz et al., 2016

3.3 Accumulation of SiNPs in late endosomes/ lysosomes

When testing silica nanoparticles with regard to their ability for uptake in HeLa cells (as discussed earlier in chapter 3.1 and 3.2.1), we could observe a perinuclear distribution of AHAPS-functionalized nanoparticles, suggesting their accumulation in intracellular organelles. Hence, we wanted to clarify the SiNPs' cellular destiny after 4 h. Therefore, HeLa cells were incubated with FITC-labeled SiNPs in cell culture medium at 37°C, washed extensively in PBS (+10 mM $MgCl_2$) to remove non-internalized material, and fixed. After permeabilization, the cells were immunolabeled with various marker proteins for the endolysosomal system. Antibodies against caveolin 1, an abundant component of caveolae, and EEA1 (early endosomal protein) were applied to visualize early constituents of the endosomal regime. AP-1 (adaptor protein 1), a member of the heterotetrameric family of adaptor proteins, and M6PR (mannose 6-phosphate receptor)-stained proteins that cycle between endosomes and the trans-Golgi network. Furthermore, we used antibodies against LAMP1 (lysosome-associated membrane protein 1) and CD63 (member of the tetraspanin family) to illustrate late endosomal/ lysosomal compartments (Figure 3.6 A)(Saftig & Klumperman, 2009; Schwake et al, 2013). Analysis of the Pearson's correlation coefficient revealed no colocalization of SiNPs with components of the early endosomal machinery (0.068 ± 0.001 for caveolin 1 and 0.080 ± 0.014 for EEA1, respectively) and only very little with AP-1 (0.161 ± 0.032) and M6PR (0.212 ± 0.008) after 4 h. The most abundant overlap between SiNP- and marker protein-channel was observed for the late endosomal/ lysosomal system (0.396 ± 0.023 for LAMP1 and 0.474 ± 0.012 for CD63, Figure 3.6 B). A profound colocalization of SiNPs with late endosomes/ lysosomes was not just pronounced in fixed cells, but also in living cells after incubation with Lysotracker Red (0.439 ± 0.021), a fluorescent acidotropic probe that accumulates within the lumen of acidic organelles (Mesa et al, 2001) (see Figure 3.6 B and Figure 3.19). Additionally, ultrastructural analysis of glutaraldehyd fixed cells confirmed the prominent accumulation of SiNPs within the lumen of lysosomes (Figure 3.6 C). These results indicate that SiNPs are targeted to the late endosomal system, where they accumulate within lysosomes.

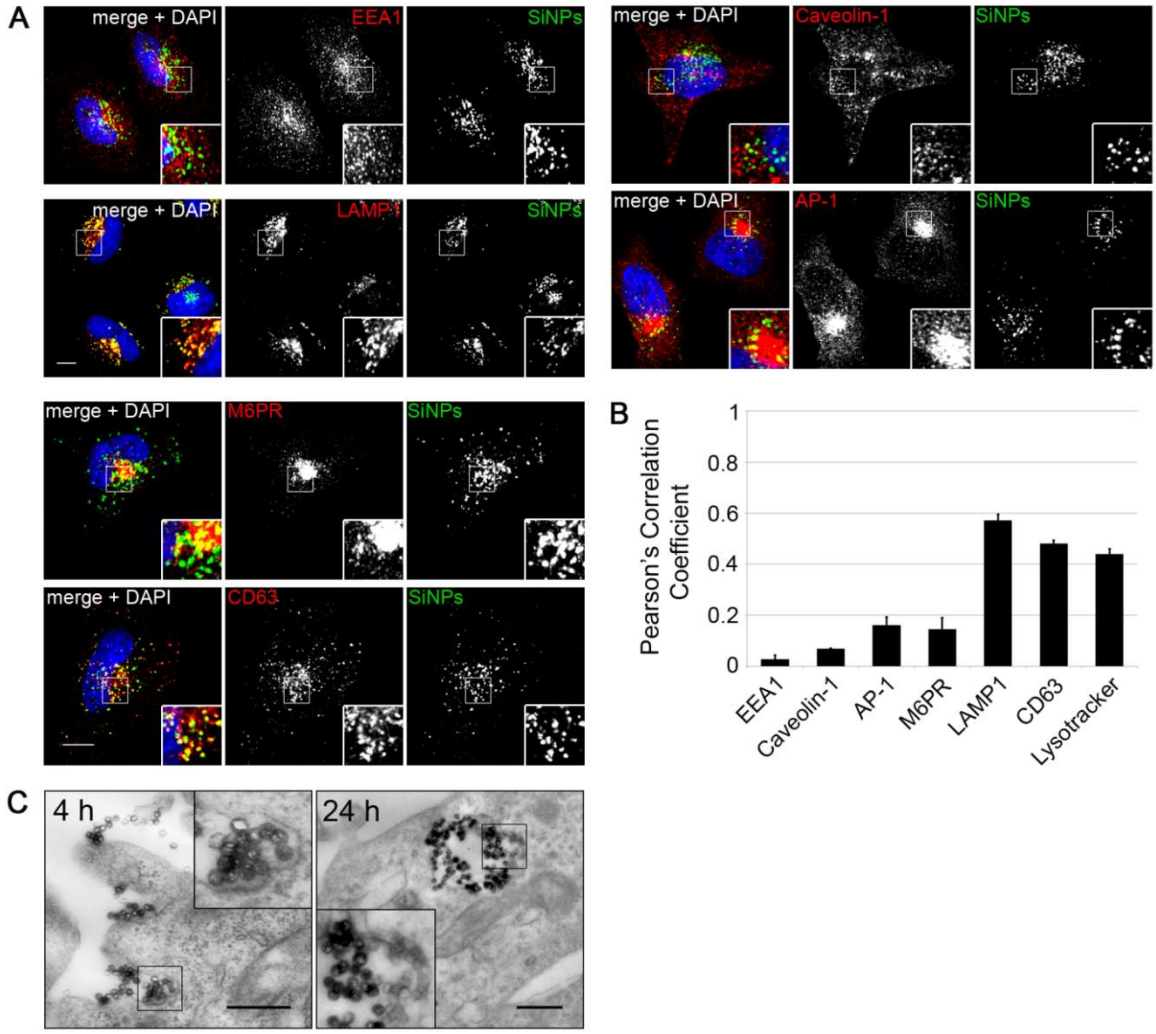

Figure 3.6 SiNPs accumulate in late endosomes/ lysosomes. (**A**) Confocal microscopy images of HeLa cells illustrating the subcellular localization of internalized SiNPs (green chanel) and various organellar markers (red chanels) such as EEA1 (early endosomal protein), LAMP1 (late endosomal/ lysosomal marker protein), M6PR (trans-Golgi network/ endosomes), CD63 (late endosomes/ lysosomes), Caveolin 1 (caveolae), and AP-1 (trans-Golgi network/ recycling endosomes). Scale bar, 10 µm. (**B**) Pearson's correlation coefficients of SiNPs with different organellar markers: EEA1 (early endosomes), 0.080 ± 0.014; Caveolin 1 (caveolae), 0.068 ± 0.001; AP-1 (trans-Golgi network/ recycling endosomes), 0.161 ± 0.032; mannose 6-phosphate receptor, M6PR (trans-Golgi network/ endosomes), 0.212 ± 0.008; LAMP1 (late endosomes/ lysosomes), 0.396 ± 0.023; CD63 (late endosomes/ lysosomes), 0.474 ± 0.012; Lysotracker (lysosomes), 0.439 ± 0.021) for at least n = 3 independent experiments (mean ± s.e.m.). (**C**) SiNPs accumulate in lysosomes at the ultrastructural level. Electron micrographs of HeLa cells were acquired after 4 h (left) or 24 h (right) of incubation with SiNPs. Scale bars, 500 nm. Taken from Schütz et al., 2016

3.4 Reduced cell viability

To assess cell viability after nanoparticle exposure, we performed standard MTT assays for both the FITC-labeled and –unlabeled SiNPs. Therefore, HeLa cells were grown in 96-well plates and incubated in cell culture medium containing SiNP-concentrations ranging from 2 µg/ ml to 100 µg/ ml. Absorbance was measured at 562 nm 24 h after exposure to nanoparticles. Both FITC-labeled and –unlabeled SiNPs induced a similar decline in cell viability down to 60 % in cells treated with 20 µg/ ml (62.3 ± 4.8 % (-FITC) and 63.2 ± 2.9 % (+FITC), respectively) or 100 µg/ ml SiNPs (55.8 ± 4.0 % (-FITC) and 58.0 ± 2.6 % (+FITC), respectively) compared to untreated control cells (0 µg/ ml set to 100 %, Figure 3.7). Taken together, we conclude that reduced cell viability is likely caused by the accumulation of silica nanoparticles in late endosomes/ lysosomes.

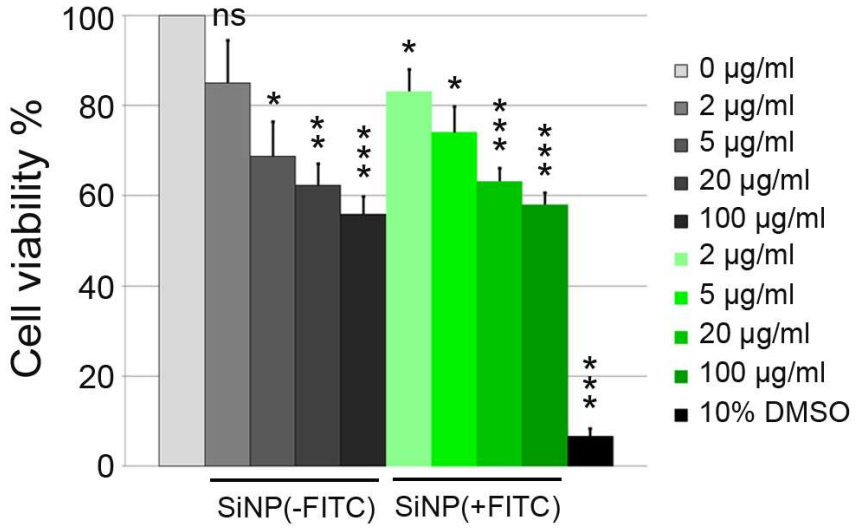

Figure 3.7 Reduced viability of SiNP-treated HeLa cells. HeLa cells were incubated with SiNPs (with or without FITC) for 24 h before MTT addition. Viability was determined for cells treated with 2 µg/ ml SiNPs (85.0 ± 9.4 % (-FITC) and 83.1 ± 4.9 % (+FITC), respectively), with 5 µg/ ml SiNPs (68.8 ± 7.6 % (-FITC) and 74.0 ± 5.8 % (+FITC), respectively), with 20 µg/ ml SiNPs (62.3 ± 4.8 % (-FITC) and 63.2 ± 2.9 % (+FITC), respectively), and 100 µg/ ml SiNPs (55.8 ± 4.0 % (-FITC) and 58.0 ± 2.6 % (+FITC), respectively). The value for untreated cells was set to 100 %. Cells treated with 10 % DMSO served as a positive control (triplicates shown as mean ± s.e.m. for n = 3 independent experiments; ns, non-significant; *p< 0.05; **p<0.01; ***p<0.001. Taken from Schütz et al., 2016

3.5 Unaltered cargo internalization

One important issue we needed to address is whether SiNP-accumulation interferes with trafficking events in cells. Thus, we analyzed in more detail two well-studied cargo proteins, i.e. transferrin, which follows the recycling pathway (see also chapter 3.6) and EGF, which is involved in the degradative pathway (Huang et al, 2006; Maxfield & McGraw, 2004) (see also chapter 3.8).

3.5.1 Transferrin

Transferrin is known to enter cells via clathrin-mediated endocytosis upon binding to its receptor, and recycle back to the plasma membrane (Abe et al, 2008).

To investigate potential effects of SiNP-accumulation on trafficking, we first performed transferrin uptake experiments. HeLa cells were treated with FITC-labeled SiNPs for 4 h at 37°C, and subsequently incubated with 20 µg/ ml transferrin conjugated with Alexa647 (Tf^{647}) for 15 min. Cells were then thoroughly rinsed in PBS (+10 mM $MgCl_2$) and fixed. In addition, samples were permeabilized and stained for the early endosomal marker EEA1 to affirm the colocalization with transferrin (Figure 3.8 A). The analysis of confocal microscopy images revealed no significant difference in transferrin intensity levels in SiNP-loaded compared to control (ctrl) cells (Figure 3.8 B).

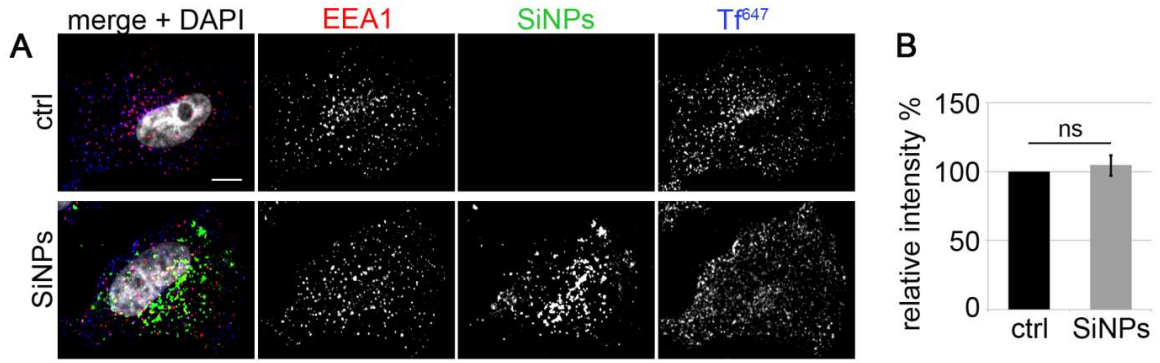

Figure 3.8 SiNP-accumulation does not affect Tf uptake. (**A**) Confocal microscopy images display transferrin (Tf^{647}, blue channel) levels after 15 min uptake in control (upper panel) and SiNP-pretreated (green channel) HeLa cells. Additionally, cells were stained for the early endosomal marker EEA1 (red channel) to confirm the localization of Tf but not SiNPs in early endosomes. Nuclei were stained with DAPI (shown in grey). Scale bar, 10 µm. (**B**) Unaltered levels of Tf fluorescence intensity in control (set to 100 %) and SiNP-treated HeLa cells (105 ± 7 %). Cells were incubated

with Tf^{647} at 4°C to allow for TfR engagement in the absence of internalization, washed extensively, and analyzed by immunofluorescence microscopy. Data represent mean ± s.e.m. for n = 3 independent experiments; ns, non-significant p> 0.05.

3.5.2 Epidermal growth factor

The internalization of EGFR, a subfamily member of RTKs, is triggered upon ligand binding. After receptor kinase-dependent sorting into MVBs and fusion with lysosomes, ligand-bound receptors are degraded by lysosomal proteases (Alwan et al, 2003).

Prior to the examination of EGF degradation, we performed uptake experiments to exclude alteration caused by SiNPs accumulation early in the degradative pathway. HeLa cells were incubated with SiNPs for 4 h at 37°C, followed by a 15 min treatment with 100 ng/ ml Alexa647-labeled EGF (EGF^{647}). The cells were immediately washed, fixed and immunolabeled (Figure 3.9 A). The accumulation of SiNPs in late endosomes/ lysosomes was visualized by a staining with specific antibodies against LAMP1. As with transferrin uptake, no siginificant discrepancy of fluorescence intensities in SiNP-loaded compared to control cells could be determined, signifying unaltered EGF internalization (Figure 3.9 B).

Taken together, these data indicate that lysosomal SiNP-accumulation does not impact on the internalization of CME-specific cargo. This is in agreement with the clathrin-independent endocytosis of SiNPs, thus, suggesting a lack of competition between SiNPs and cargo proteins.

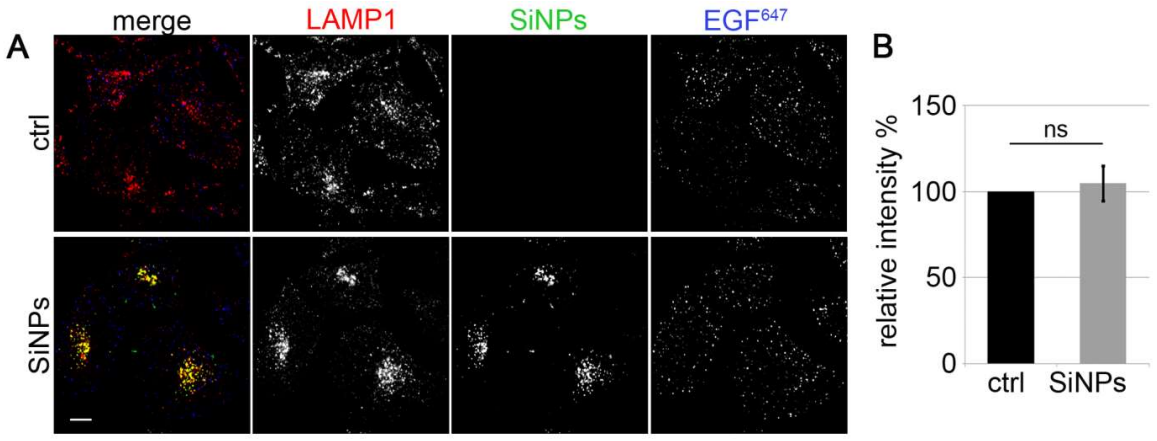

Figure 3.9 SiNP-accumulation does not affect EGF uptake. (**A**) Confocal microscopy images show EGF^{647} (blue channel) levels after 15 min uptake in control (upper panel) and SiNP-loaded HeLa cells (lower panel). Additionally, cells were stained for the late endosomal/ lysosomal marker

LAMP1 (red channel) to visualize the localization of SiNPs (green channel). Scale bar, 10 µm. (**B**) Quantification displays unaltered levels of EGF fluorescence intensity in SiNP-treated cells (105 ± 10 %) compared to the control (set to 100 %). Data represent mean ± s.e.m. for n = 3 independent experiments; ns, non-significant p> 0.05.

3.6 Transferrin recycling remains unperturbed

We further tested whether SiNP-accumulation might interfere with transferrin recycling. After treatment with SiNPs for 4 h at 37°C, HeLa cells were starved for 1 h in serum-depleted cell culture medium. Alexa647-conjugated transferrin was then added to the cells at 4°C to allow prebinding to transferrin receptor without internalization. By shifting the cells to 37°C, receptor-engaged Tf^{647} was internalized and chased for 5, 15 and 60 min. Subsequently samples were rinsed and fixed at the indicated timepoints (Figure 3.10 A). Quantification of confocal microscopy images revealed that already 15 min post-chase the levels of Tf^{647} were reduced by about 50 % in both control and SiNP-treated cells, respectively (see graph in Figure 3.10 A). Further decline of fluorescence levels continued alike in both samples. Also, surface levels of prebound Tf^{647} were unaltered (Figure 3.10 B).

These data suggest that intralysosomal accumulation of SiNPs does not interfere with early trafficking routes in HeLa cells.

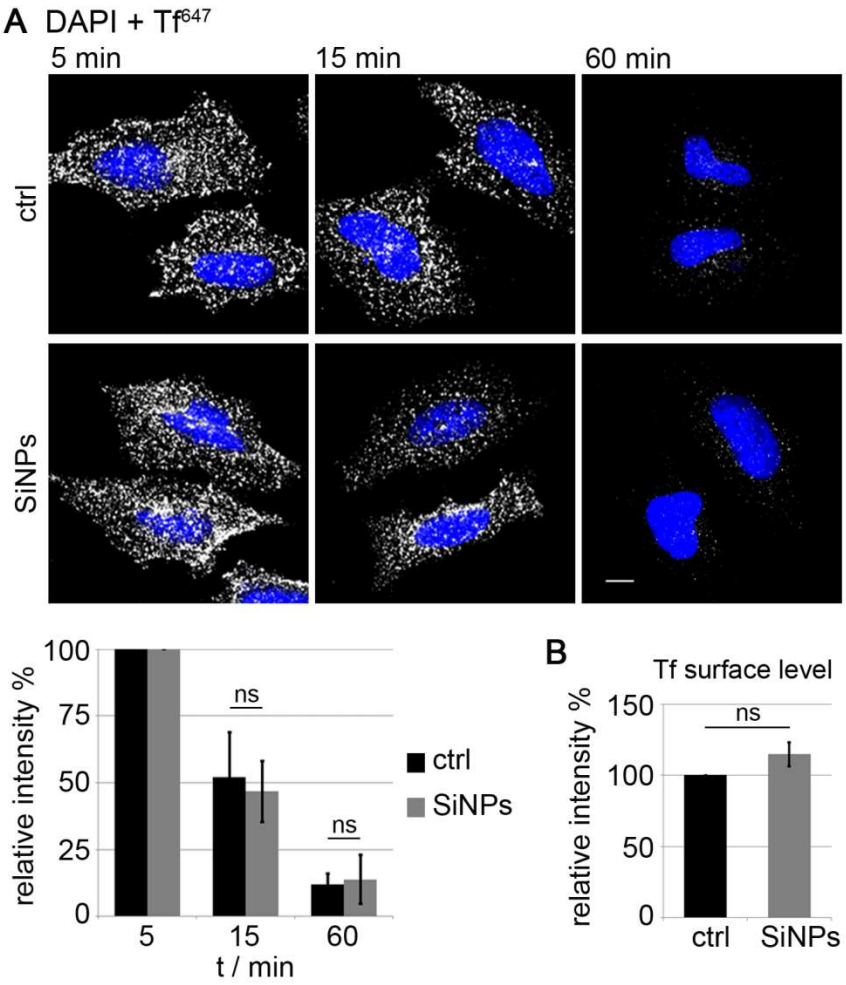

Figure 3.10 SiNP-accumulation does not affect Tf recycling, or surface Tf levels. (**A**) Confocal microscopy images show Tf^{647} levels in control (upper panel) and SiNP-treated HeLa cells (lower panel) at three different timepoints. Nuclei were stained with DAPI (blue). Quantified is the Tf^{647} fluorescence intensity in cells incubated with SiNPs compared to control cells. Intensity values at 5 min were set to 100 % to monitor the continuing recycling process. 15 min post-chase the levels of Tf^{647} were reduced to 52 ± 17 % in control cells vs. 47 ± 11 % in SiNP-treated cells. 60 min post-chase the levels of Tf^{647} were reduced to 12 ± 4 % in control cells vs. 14 ± 9 % in SiNP-treated cells. Data represent mean ± s.e.m. for n = 3 independent experiments; ns, non-significant p> 0.05. Scale bar, 10 µm. (**B**) HeLa cells were incubated with Tf^{647} at 4°C to allow for TfR engagement in the absence of internalization, washed extensively, and analyzed by immunofluorescence microscopy. Quantification shows unaltered surface levels of TfR in control (set to 100 %) and SiNP-treated HeLa cells (115 ± 8 %). Data represent mean ± s.e.m. for n = 4 independent experiments; ns, non-significant p> 0.05. Taken from Schütz et al., 2016

3.7 Epidermal growth factor receptor signaling is not affected

Binding of external ligands, i.e. EGF, to EGFR, not only leads to internalization and degradation, but also induces autophosphorylation of RTKs and subsequent activation of signal transduction pathways that are involved in various regulatory processes, such as proliferation, differentiation and cell survival (Herbst, 2004). Extracellular signal-regulated kinase 1 and 2 (Erk1 and Erk2) are important downstream components of the MAPK/ ERK pathway.

To address the issue of potential impact on EGFR signaling caused by lysosomal SiNP-accumulation, we stimulated control and SiNP-treated HeLa cells with EGF and subjected the cell lysates to immunoblotting (Figure 3.11). Similar EGFR levels were observed before (timepoint 0') and after stimulation with EGF (timepoint 30') in both control and SiNP-pretreated cells, respectively. Also, the signaling response of the key components Erk1/2 proceeded unperturbed prior to (timepoint 0') and upon ligand binding (timepoint 30').

In contrast to observations from other studies using different nanoparticles, we conclude that these AHAPS-functionalized silica nanoparticles do not adversely affect EGFR signaling (Duan et al, 2014).

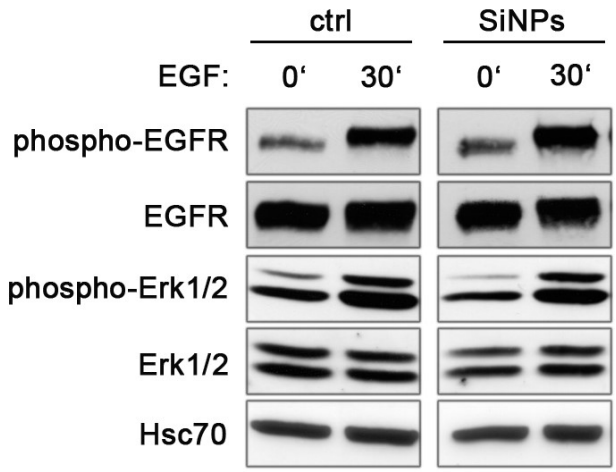

Figure 3.11 Immunoblot analysis of EGF signalling responses in control or SiNP-treated HeLa cells. Cells were treated with EGF for the indicated time and subjected to immunoblotting for phosphorylated EGF receptor (pEGFR), total EGF receptor (EGFR), phosphorylated Erk 1/2 kinase (pErk 1/2), and total Erk 1/2 kinase (Erk 1/2). Hsc70 served as loading control. Blots are representative for 3 independent experiments. Taken from Schütz et al., 2016

3.8 Effects on EGF degradation upon SiNP-treatment

In addition to internalization and signaling, we examined potential consequences on the trafficking route of fluorescently labeled epidermal growth factor, which after ubiquitination of its receptor takes the degradative route (Huotari & Helenius, 2011).

3.8.1 Impaired EGF degradation

To monitor EGF degradation, HeLa cells were first incubated with 20 µg/ ml SiNPs in cell culture medium for 4 h and then starved for 2 h. Afterwards, Alexa647-conjugated EGF was added to the cells at 4°C for prebinding to its receptor. To allow internalization, cells were shifted to 37°C. EGF^{647} was then chased for 30, 60 and 120 min followed by extensive washing and fixation. Confocal microscopy images revealed that in control cells about 90 % of the initial EGF^{647} amount was already degraded after 60 min (Figure 3.12 A, upper panel). In contrast, the reduction of EGF^{647} in SiNP-loaded cells was determined to be around 50 % (SiNPs(+FITC)) and 60 % (SiNPs(-FITC)), respectively for nanoparticles with and without fluorescent label (Figure 3.12 A, lower panel). Even after 120 min, about 25 % of initially internalized EGF^{647} remained undegraded in HeLa cells pretreated with SiNPs. EGF surface levels, on the other hand, were unaltered as shown in Figure 3.12 B. Similar observations were made for EGFR surface levels (data not shown).

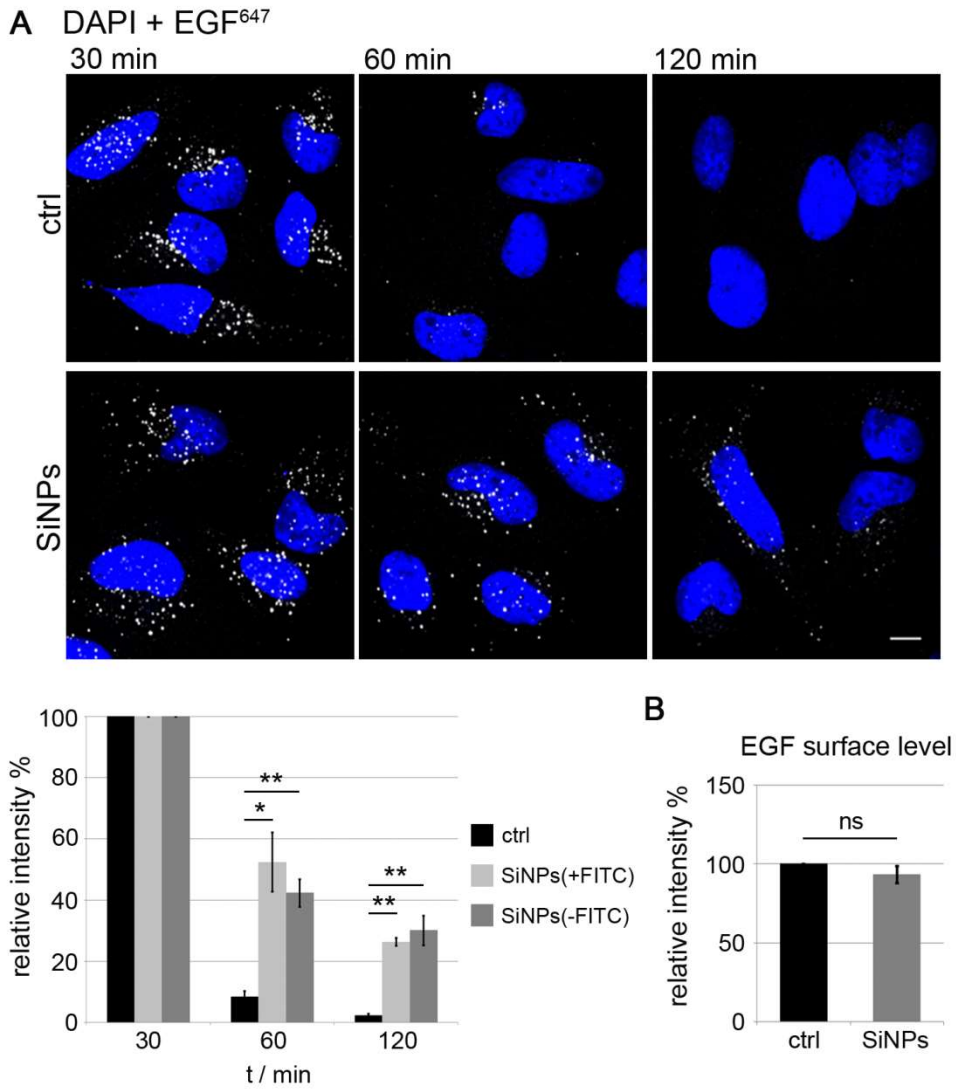

Figure 3.12 Lysosomal accumulation of SiNPs impairs EGF degradation. (**A**) Confocal microscopy images of EGF^{647} internalized into control (upper panel) or SiNP-treated HeLa cells (lower panel) chased for the indicated timepoints post-internalization. Nuclei were stained with DAPI (blue). Quantitative analysis of EGF^{647} fluorescence intensity of control or SiNP-treated HeLa cells [SiNPs, either FITC-labeled (+FITC) or unlabeled (-FITC)] chased for the indicated timepoints post-internalization. Intensity values at 30 min were set to 100 %. Note the impaired degradation of EGF at 60 min [EGF remaining: ctrl, 8.4 ± 1.9 % vs. SiNPs(+FITC), 52.4 ± 9.6 % and SiNPs(-FITC), 42.3 ± 4.5 %] and 120 min of chase [EGF remaining: ctrl, 2.2 ± 0.7 % vs. SiNPs(+FITC), 26.3 ± 1.3 % and SiNPs(-FITC), 30.1 ± 4.8 %] in SiNP-treated cells. Data represent mean ± s.e.m. for n = 3 independent experiments; *p< 0.05; **p<0.01. Scale bar, 10 µm. (**B**) Unaltered surface levels of EGF in control (set to 100 %) and SiNP-treated HeLa cells (SiNPs(+FITC), 93.3 ± 5.3 %. HeLa cells were incubated with EGF^{647} at 4°C to allow for EGFR engagement in the absence of internalization, washed extensively, and analyzed by immunofluorescence microscopy. Data represent mean ± s.e.m. for n = 4 independent experiments; ns, non-significant p> 0.05. Taken from Schütz et al., 2016

3.8.2 Non-degraded EGF accumulates in late endosomes/ lysosomes

As previously determined in chase experiments, about 25 % of the originally internalized EGF^{647} persisted within punctuate structures in HeLa cells incubated with SiNPs (Figure 3.12 A). To identify these structures, we fixed cells 120 min post-chase and stained various cell compartments using specific antibodies against late endosomes/ lysosomes (LAMP1 and CD63, respectively), early endosomes (EEA1), trans-Golgi network/ endosomes (M6PR) and autophagosomes (p62 and LC3, respectively) (Figure 3.13 A). About 50 % of total non-degraded EGF was located in the late endosomal/ lysosomal compartment (47.79 ± 0.09 % in LAMP1- and 55.38 ± 0.08 % in CD63-positive organelles; Figure 3.13 B). Only little amounts were present in early endosomes and autophagosomes. Even more striking was the accumulation of non-degraded EGF in late endosomes/ lysosomes under constant supply of EGF^{647} for 2 h (78.6 ± 11.7 % in LAMP1- or 89.7 ± 1.3 % in CD63-labeled compartments, respectively; Figure 3.13 C).

These data indicate that intralysosomal SiNP-accumulation in HeLa cells disrupts the lysosomal degradation of internalized EGF. Non-degraded EGF remains within punctuate structures identified as LAMP-1 and CD63-positive late endosomes.

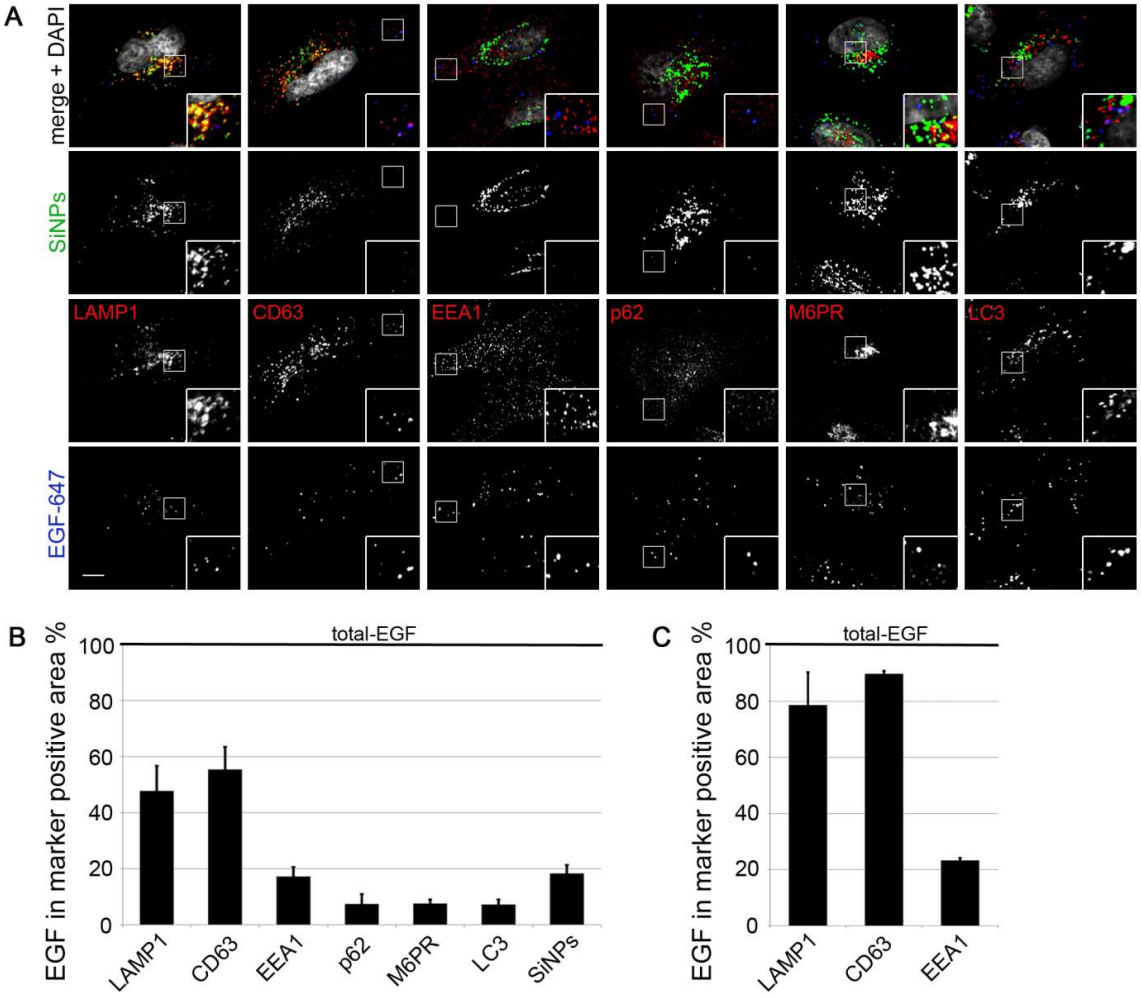

Figure 3.13 Non-degraded EGF accumulates in late endosomes/ lysosomes. (**A**) Representative confocal images of EGF^{647} internalized into SiNP-treated HeLa cells chased for 120 min post-internalization. To assess the localization of non-degraded EGF, cells were counterstained for different organellar markers: LAMP1 (late endosomes/ lysosomes), CD63 (late endosomes/ lysosomes), EEA1 (early endosomes), p62 (autophagosomes), M6PR (trans-Golgi network/ endosomes), or LC3 (autophagosomes). Nuclei were stained with DAPI. Scale bar, 10 µm. (**B**) Quantitative analysis of the localization of non-degraded EGF^{647} in SiNP-treated HeLa cells, chased for 120 min post-internalization. Depicted is the fraction of EGF^{647} present in compartments immunopositive for the indicated marker: LAMP1 (late endosomes/ lysosomes), 47.79 ± 0.09 %; CD63 (late endosomes/ lysosomes), 55.38 ± 0.08 %; EEA1 (early endosomes), 17.22 ± 0.03 %; p62 (autophagosomes), 7.43 ± 3.42 %; M6PR (trans-Golgi network/ endosomes), 7.48 ± 1.49 %; LC3 (autophagosomes), 7.16 ± 1.83 %. Data represent mean ± s.e.m. for n = 3 independent experiments. (**C**) Quantitative analysis of the localization of non-degraded EGF^{647} accumulated in SiNP-treated HeLa cells after 120 min of permanent EGF^{647} uptake. Note the higher fraction of EGF colocalizing with late endosomal/ lysosomal marker LAMP1 (78.6 ± 11.7 %) or CD63 (89.7 ± 1.3 %) compared to the early endosomal marker EEA1 (23.1 ± 1.0 %), which remained similar to the amount of EGF^{647} post-chase. Data represent mean ± s.e.m. for n = 2 independent experiments. Taken from Schütz et al., 2016

3.9 Effects on autophagy in SiNP-loaded cells

In the last few years, nanoparticles have been frequently reported to be connected with irregularities leading to lysosomal dysfunction and autophagy (Halamoda Kenzaoui et al, 2012; Stern et al, 2012; Yu et al, 2014).

Autophagy is one major intracellular pathway responsible for the turnover of proteins and disposal of damaged organelles or invading bacteria. The initial compartment of an autophagosome is the phagophore, which expands around cytoplasmic material, thereby forming a double-membrane organelle. Autophagosomes eventually fuse with lysosomes to deliver their content for degradation (see chapter 1.3).

For the investigation of autophagy, we included following conditions: untreated cells (non-starved), nutrient deprivation (starved) leading to autophagy induction, addition of bafilomycin A1, a V-ATPase inhibitor that blocks lysosomal degradation by dissipating the proton gradient across the lysosomal membrane, and incubation with SiNPs in presence or without bafilomycin A1. DIC images of living HeLa cells treated under various conditions are displayed in Figure 3.14. Cells were incubated for 24 h with SiNPs in cell culture medium. Starvation in HBSS buffer and treatment with bafilomycin A1 was carried out for 4 h before image acquisition. Interestingly, we observed a concentration-dependent increase of vacuoles in cells treated with SiNPs (Figure 3.14, lower panel), suggesting an increasing level of autophagic vacuole formation.

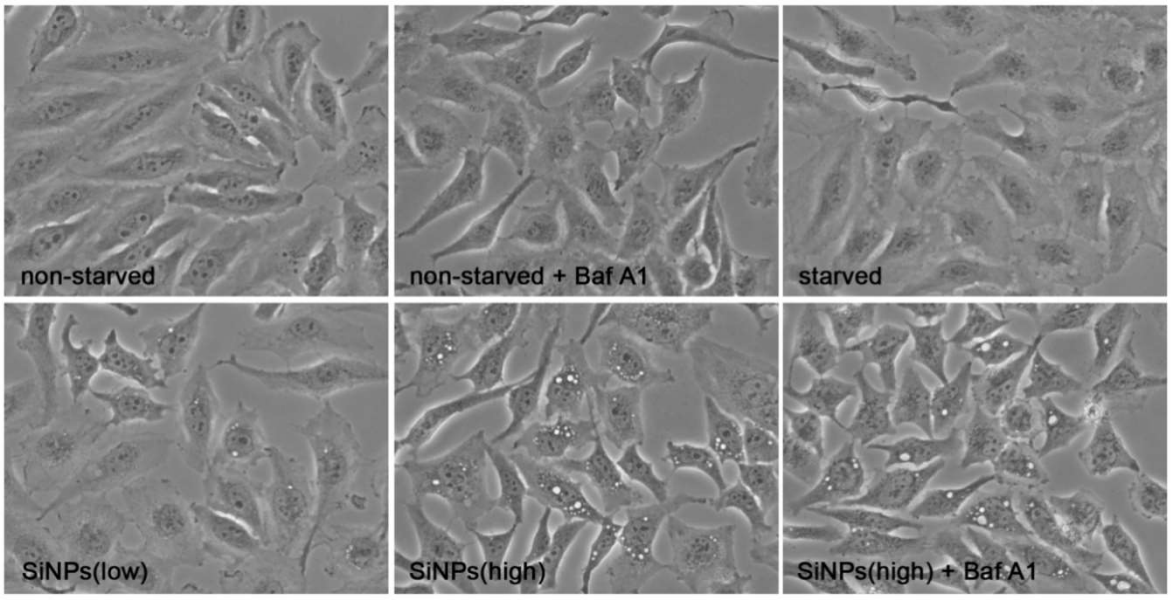

Figure 3.14 Vacuole-like structures form in SiNP-treated cells. DIC images of living HeLa cells display control (non-starved or starved, upper panel) or 24 h SiNP-treatment conditions (SiNPs(low)

and SiNPs(high), lower panel). Where indicated, bafilomycin A1 was added 4 h before image acquisition. Note the increasing amount in vacuolar structures in cells preincubated with SiNPs.

3.9.1 Enhanced levels of autophagosomal marker LC3

Microtubule-associated protein light chain 3 (LC3) is widely used to monitor autophagy. During autophagy, the cytoplasmic LC3-I protein undergoes posttranslational lipidation with phosphatidylethanolamine (PE) to become LC3-PE (also termed LC3-II), a compound tightly associated with membranes and linked to autophagosome formation. Subsequently, autophagosomes containing LC3-II fuse with lysosomes to enable breakdown of the engulfed material (see chapter 1.3).

To determine whether SiNPs affect cellular processes connected to autophagy, we subjected HeLa cells to a 24 h treatment with 20 µg/ ml (SiNPs(low)) and 100 µg/ ml (SiNPs(high)) nanoparticles, respectively. Untreated (non-starved) and serum-depleted (starved) cells served as controls. In addition, all experiments were performed in presence of 100 nM bafilomycin A1. The starvation in HBSS buffer and inhibitor treatment was carried out 4 h prior to fixation. Samples were then immuno-labeled with a specific antibody against LC3 and analyzed by confocal microscopy (Figure 3.15). We observed elevated levels of LC3 in SiNP-treated cells (SiNPs(low), 129.1 ± 4.6 %) compared to untreated cells (non-starved set to 100 % and starved, 69.3 ± 9.9 %), which showed a basal degree of autophagosomes. Even higher LC3 fluorescence intensity levels were examined in cells incubated with 100 µg/ ml SiNPs (SiNPs(high), 274.8 ± 58.6 %) (Figure 3.15 A, -Baf A1). Furthermore, addition of bafilomycin A1 led to an increase in LC3-positive structures in control cells (non-starved + Baf A1, 141.4 ± 18.4 % and starved + Baf A1, 197.0 ± 24.9 %, respectively) as well as in SiNPs(low)-treated cells (SiNPs(low) + Baf A1, 222.9 ± 12.1 %) (Figure 3.15 A, +Baf A1) compared to samples without inhibitor treatment. Just in SiNPs(high)-treated cells (SiNPs(high) + Baf A1, 283.7 ± 38.5 %) the inhibition of autophagosome-lysosome fusion did not induce a further increase of LC3 intensity levels, suggesting an existant disruption of lysosomal degradation in these cells. The quantification of LC3 SD intensity for all conditions is shown in Figure 3.15 B.

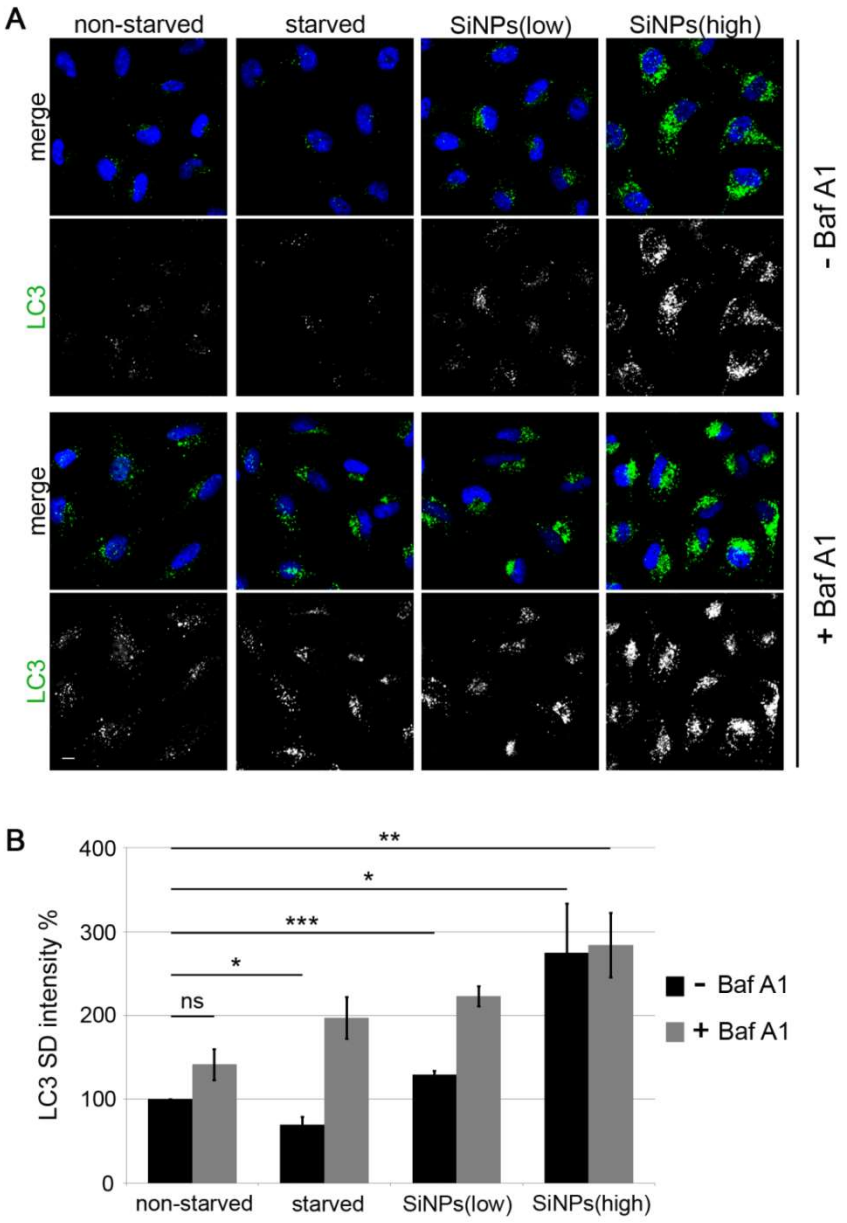

Figure 3.15 LC3-positive structures are strongly increased in SiNP-treated cells. (**A**) Confocal microscopy images of control (non-starved and starved) or SiNP-treated (low and high) HeLa cells stained for the autophagosomal marker LC3 (green chanel). The two panels above show the merged and LC3 channels for samples without bafilomycin A1 treatment (-Baf A1). Whereas the two panels below illustrate the merged and LC3 channels of HeLa cells treated with bafilomycin A1 (+Baf A1). Nuclei were stained with DAPI. Scale bar, 10 µm. (**B**) Quantification shows LC3 SD intensity levels of samples displayed in (A): control cells (non-starved, set to 100 % and starved, 69.3 ± 9.9 %, respectively), cells treated with bafilomycin A1 (non-starved + Baf A1, 141.4 ± 18.4 % and starved + Baf A1, 197.0 ± 24.9 %, respectively), or cells incubated with low (SiNPs(low), 129.1 ± 4.6 %) or high concentrations of SiNPs in the absence (SiNPs(high), 274.8 ± 58.6 %) or presence of bafilomycin A1 (SiNPs(low) + Baf A1, 222.9 ± 12.1 % and SiNPs(high) + Baf A1, 283.7 ± 38.5 %). Values represent mean ± s.e.m. for n = 4 independent experiments; *p< 0.05; **p<0.01; ***p<0.001. Modified from Schütz et al., 2016

3.9.2 Enhanced levels of autophagosomal cargo protein p62

SQSTM1, better known as p62, was identified to interact with LC3. It is trapped by LC3 and transported selectively into autophagosomes (Pankiv et al, 2007). As another component of autophagosomes and thus, a substrate for autophagy-mediated lysosomal protein turnover, p62 accumulates in cells in case autophagy or downstream processes, such as autophagosome-lysosome fusion or lysosomal degradation, are impaired.

We incubated HeLa cells for 24 h with 20 µg/ ml and 100 µg/ ml SiNPs (low and high, respectively) in cell culture medium. After extensive washing, cells were fixed and stained with a specific antibody against p62. Where indicated, 100 nM bafilomycin A1 was added to the cells 4 h before fixation. Confocal microscopy images revealed elevated p62 levels in SiNP-treated cells (Figure 3.16 A). p62 fluorescence intensities were increased up to three-fold in cells treated with nanoparticles (260.9 ± 42.4 % for SiNPs(low) and 313.3 ± 55.4 % SiNPs(high), respectively) compared to control cells (non-starved set to 100 %; Figure 3.16 B). Interestingly, cells supplemented with inhibitor (both control and SiNPs(high)) did not show a significant increase in p62 SD intensity levels compared to inhibitor-untreated samples (non-starved + Baf A1, 84.9 ± 21.4 % and SiNPs(high) + Baf A1, 384.3 ± 128.1 %). This might be due to the overall high cytosolic p62 fluorescence signal.

In conclusion, these data indicate that SiNP-treatment leads to an accumulation of p62 in HeLa cells, similar to that observed for LC3.

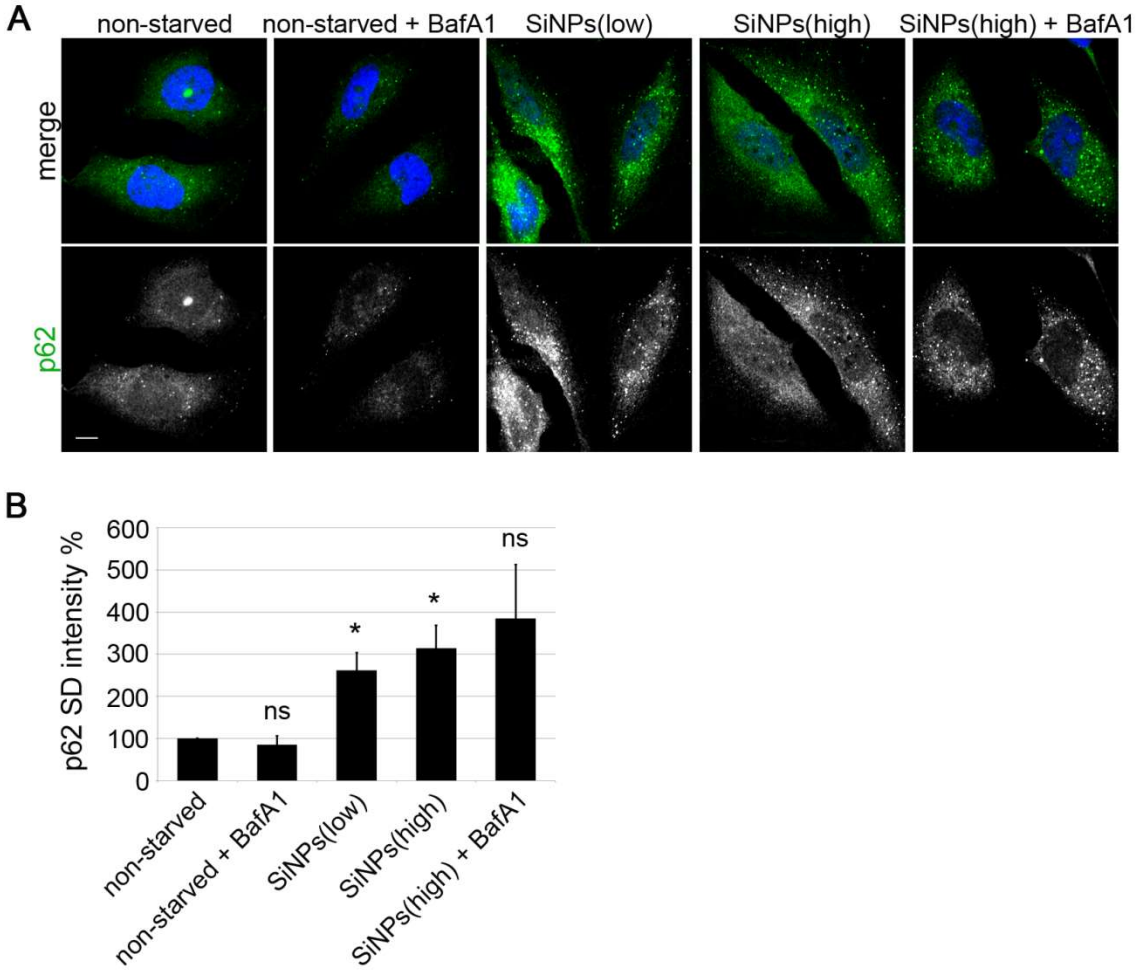

Figure 3.16 Accumulation of p62 in SiNP-treated cells. (**A**) Confocal microscopy images of non-starved control or SiNP-treated (low and high) HeLa cells stained for the autophagosomal component p62 (green channel). Cells were treated with bafilomycin A1 where indicated. Nuclei were stained with DAPI. Scale bar, 10 µm. (**B**) Quantified are p62 SD intensity levels of samples shown in (A): ctrl cells (non-starved, set to 100 %), non-starved + Baf A1 (84.9 ± 21.4 %), cells treated with low (260.9 ± 42.4 %), high concentrations of SiNPs (313.3 ± 55.4 %), or high concentrations SiNPs + Baf A1 (384.3 ± 128.1 %). Values represent mean ± s.e.m. for n = 3 independent experiments; ns, non-significant $p > 0.05$, *$p < 0.05$. Modified from Schütz et al., 2016

3.9.3 Autophagic flux is impaired in SiNP-treated cells

Elevated LC3-II and p62 levels were also detectable by SDS-PAGE and immunoblot analyses from HeLa cells incubated with SiNPs for 24 h (Figure 3.17 left-hand side). While control cells (non-starved and starved) showed a normal turnover of LC3-II protein as illustrated by the vanishing LC3-II band, this was not the case when bafilomycin A1 was supplemented to the cell culture medium such that lysosomal degradation was disabled. By contrast, LC3-II levels were already elevated in nanoparticle-treated cells (SiNPs(low) and

SiNPs(high)) compared to control samples, even without inhibitor treatment. The turnover of LC3-II was quantified by semi-quantitative immunoblotting as ratio of LC3-II to LC3-I (Figure 3.17 right-hand side). Low ratio values for the conversion of LC3-I into LC3-II indicate a normal functional turnover of LC3-II protein (non-starved, set to 1). After addition of inhibitor, the value rises due to higher LC3-II levels, indicating abolished of protein degradation (non-starved + Baf A1, 3.2 ± 0.7). Under starvation conditions, when autophagy is induced, both LC3-I and LC3-II first rise (at earlier timepoints), but then gradually decline due to protein degradation (starved, 2.2 ± 0.4) (Mizushima & Yoshimori, 2007). Three-fold and five-fold increased ratio values for SiNPs(low) (3.1 ± 0.9) and SiNPs(high) (5.0 ± 1.2), respectively, suggest a missing LC3-II turnover.

Similar results were observed for p62, which was degraded in control cells (non-starved and starved, respectively) but not in SiNP-treated cells, also indicating an impairment of autophagic flux.

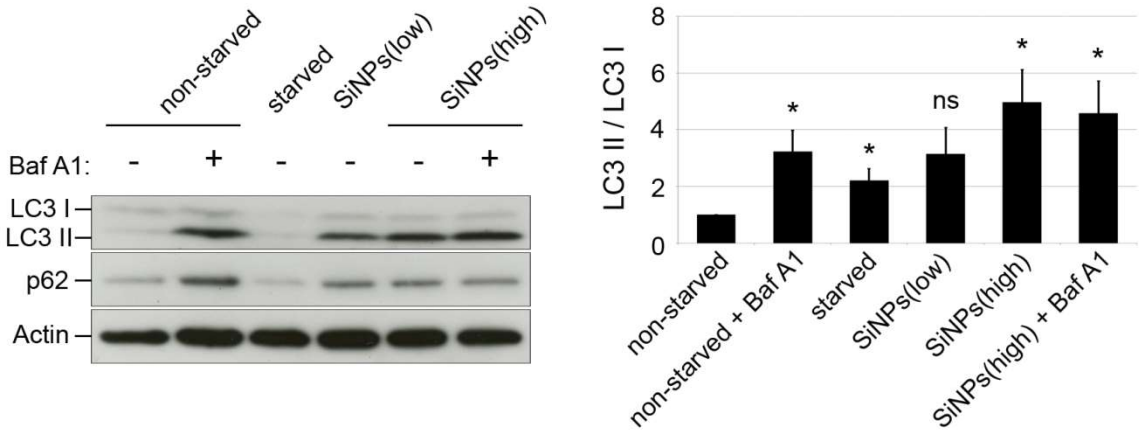

Figure 3.17 Autophagic flux is impaired upon SiNP-treatment. Control cells (non-starved and starved) or cells treated with SiNPs (low and high) were subjected to immunoblotting for LC3-I (the inactive precursor form), LC3-II (the active autophagosome-associated form), or the autophagosomal component p62. Bafilomycin A1 (100 nM) was added to the medium (for 4 h) where indicated. Actin served as loading control. The turnover of LC3-II was quantified as the ratio of LC3-II to LC3-I (non-starved, set to 1; non-starved + Baf A1, 3.2 ± 0.7; starved, 2.2 ± 0.4; SiNPs(low), 3.1 ± 0.9; SiNPs(high), 5.0 ± 1.2; SiNPs(high) + Baf A1, 4.6 ± 1.1) for 4 independent experiments; ns, non-significant $p > 0.05$, *$p < 0.05$). Taken from Schütz et al., 2016

3.9.4 SiNP-accumulation does not induce autophagy

mTOR signaling is a key regulatory pathway of autophagy. Under nutrient-rich conditions, the active mTOR complex 1 stimulates growth-related processes such as protein translation by phosphorylation of S6K (mitogen-activated protein kinase that phosphorylates the S6 protein of the 40S ribosomal unit), while simultaneously inhibiting autophagy by phosphorylating ULK1 at Ser757 (Alers et al, 2012; Kim J. et al, 2011).

To investigate whether elevated levels of LC3-II and p62 in SiNP-treated cells are a consequence of altered mTOR signaling, we analyzed the phosphorylation levels of two downstream components.

HeLa cells were incubated with SiNPs for 24 h in cell culture medium, and then washed thoroughly to remove non-internalized material. Starvation of control cells in HBSS or the supply of bafilomycin A1 (where indicated in Figure 3.18) was started four hours prior to the end of incubation. After harvesting and lysis, total cell lysates were analyzed by SDS-PAGE and immunoblotting. Protein levels of phospho-ULK1, phosphorylated at serine 757 (S757), and phospho-S6K, modified at threonine 389 (T389), remained unaltered for non-starved control or SiNP-treated cells (p-ULK1 and p-S6K set to 1 for non-starved control; SiNPs(high): 1.12 ± 0.08 (p-ULK1) and 0.93 ± 0.10 (p-S6K); see Figure 3.18, left-hand side). In contrast, phospho-levels of both ULK1 (S757) and S6K (T389) were significantly diminished under nutrient deprivation, as inactivated mTORC1 was unable to modify these amino acid residues by phosphorylation (p-ULK1, starved 0.22 ± 0.08; p-S6K, starved 0.40 ± 0.07; Figure 3.18, left-hand side). However, total protein levels of ULK1 and S6K remained unchanged as shown in the quantification (Figure 3.18, right-hand side). All values were normalized to actin, which served as loading control in each experiment.

Taken together, we conclude that SiNP-treatment causes an accumulation of LC3- and p62-positive autophagosomes. Further, SiNP-accumulation impairs autophagic flux. However, mTOR signaling is not altered in SiNP-loaded HeLa cells. We therefore conclude that fusion of autophagosomes and lysosomes is impaired.

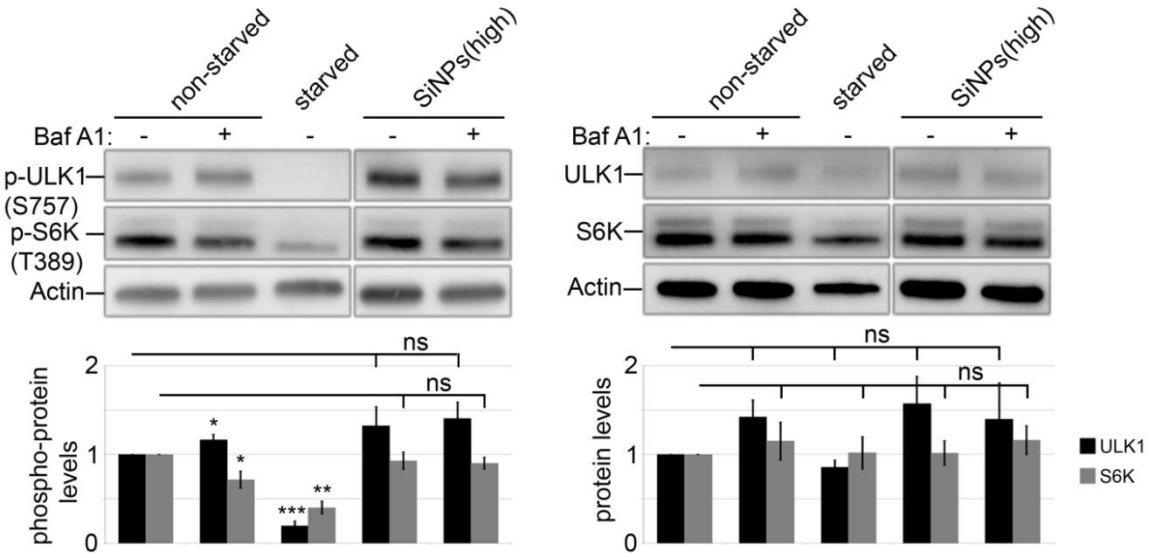

Figure 3.18 mTOR signaling is not inhibited in SiNP-treated HeLa cells. Control cells (non-starved and starved) or cells treated with SiNPs(high) were subjected to immunoblotting for ULK1 and S6K (right-hand side) or their phosphorylated forms (phospho-ULK1 (S757) and phospho-S6K (T389) (left-hand side), respectively. Baf A1 (100 nM) was added to the medium (for 4 h) where indicated. Actin served as loading control. The protein levels of total ULK1 (non-starved, set to 1; non-starved + Baf A1, 1.4 ± 0.2; starved 0.9 ± 0.1; SiNPs(high), 1.6 ± 0.3; SiNPs(high) + Baf A1, 1.4 ± 0.4) and total S6K (non-starved, set to 1; non-starved + Baf A1, 1.2 ± 0.2; starved 1.0 ± 0.2; SiNPs(high), 1.0 ± 0.1; SiNPs(high) + Baf A1, 1.2 ± 0.2), as well as the levels of their phosphorylated forms phospho-ULK1 (S757) (non-starved, set to 1; non-starved + Baf A1, 1.12 ± 0.06; starved 0.22 ± 0.08; SiNPs(high), 1.12 ± 0.08; SiNPs(high) + Baf A1, 1.26 ± 0.19) and phospho-S6K (non-starved, set to 1; non-starved + Baf A1, 0.72 ± 0.10; starved 0.40 ± 0.07; SiNPs(high), 0.93 ± 0.10; SiNPs(high) + Baf A1, 0.90 ± 0.07) were quantified. Data is presented as mean ± s.e.m. for n = 3 independent experiments; ns, non-significant p> 0.05; *p<0.05; **p<0.01; ***p<0.001). Taken from Schütz et al., 2016

3.10 Lysosomal function in SiNP-treated cells

As shown by confocal microscopy in both living and fixed HeLa cells, SiNPs accumulate in late endosomal/ lysosomal compartments. Figure 3.19 (upper panel) displays live cell images of SiNPs profoundly colocalizing with the acidotropic fluorescent probe Lysotracker Red, while LAMP2A, a protein tightly associated with lysosomal membranes, surrounds SiNP-positive organelles (lower panel).

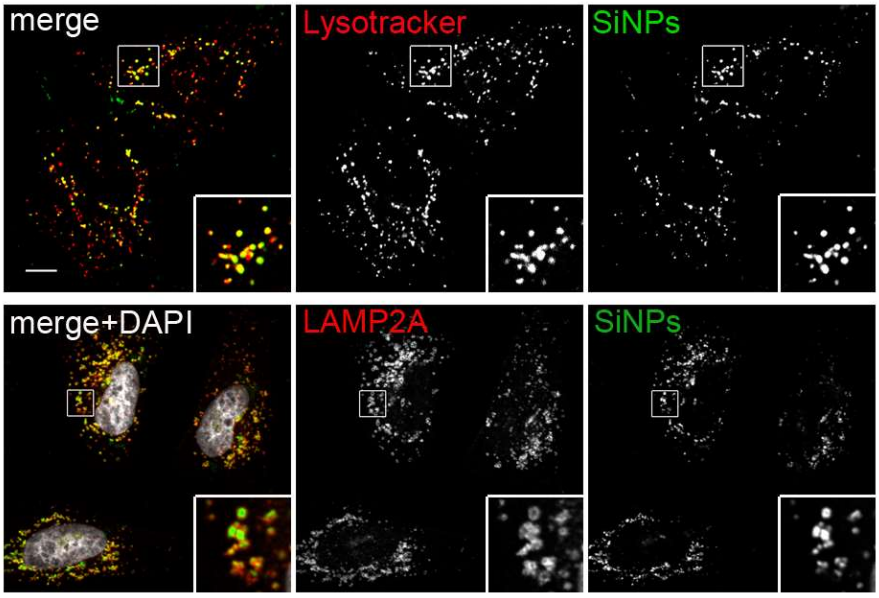

Figure 3.19 SiNPs accumulate in lysosomes. Upper panel: confocal live images of SiNP-treated (green channel) HeLa cells incubated with the lysosomal tracer Lysotracker Red. Lower panel: images of fixed HeLa cells treated with SiNPs (green channel) and stained for the lysosomal membrane protein LAMP2A (red channel). Nuclei were labeled with DAPI (grey). Scale bar, 10 µm.

Pulse-chase experiments revealed that lysosomal degradation of internalized EGF^{647} is disrupted in SiNP-filled cells. Furthermore, we demonstrated that intralysosomal accumulation of SiNPs leads to the accumulation of p62-containing LC3-positive autophagosomes that apparently fail to undergo further lysosomal degradation.

In search of an explanation for impaired lysosomal fusion and degradation, we analyzed the lysosomal integrity in SiNP-loaded HeLa cells.

3.10.1 Lysosomal acidification remains functional

Many cellular processes as for example the degradation of macromolecules in lysosomes depend on the intraluminal pH of organelles. The highly acidic pH (less than pH 5.0) facilitates the digestive function of intralysosomal hydrolases, while impaired acidification can result in severe diseases (see chapter 1.4).

Fluorescent indicators like pH sensitive dyes are very suitable for the investigation of lysosomal pH (Han & Burgess, 2010). We used Oregon Green488 coupled to 10 kDa dextran (OGD) to perform dual-excitation ratiometric imaging. Image analysis using a self-programmed Macro for Fiji ImageJ revealed an intralysosomal pH of 4.5 ± 0.1 in control

cells and of 3.9 ± 0.1 in cells treated with SiNPs (-FITC) (Figure 3.20 A). In addition, we conducted control experiments to verify the localization of OGD to LAMP1- and CD63-positive structures (Figure 3.20 B left-hand side). Cells were fixed and immuno-labeled with specific antibodies against CD63/ OGD and LAMP1/ OGD, respectively. Confocal microscopy images display control (upper panel) and nanoparticle-incubated (lower panel) HeLa cells stained for CD63 (red channel). The quantification of the Pearson's correlation coefficient disclosed a similar overlap of OGD/ CD63 and OGD/ LAMP1 in both control and SiNP-filled cells, respectively (Figure 3.20 B right-hand side).

These data clearly demonstrate that accumulated SiNPs do not prevent intralysosomal acidification in HeLa cells. The slightly lower pH of SiNP-loaded lysosomes possibly is a secondary consequence resulting from the failure of these lysosomes to degrade intracellular proteins, which serve as the main lumenal buffer for protons.

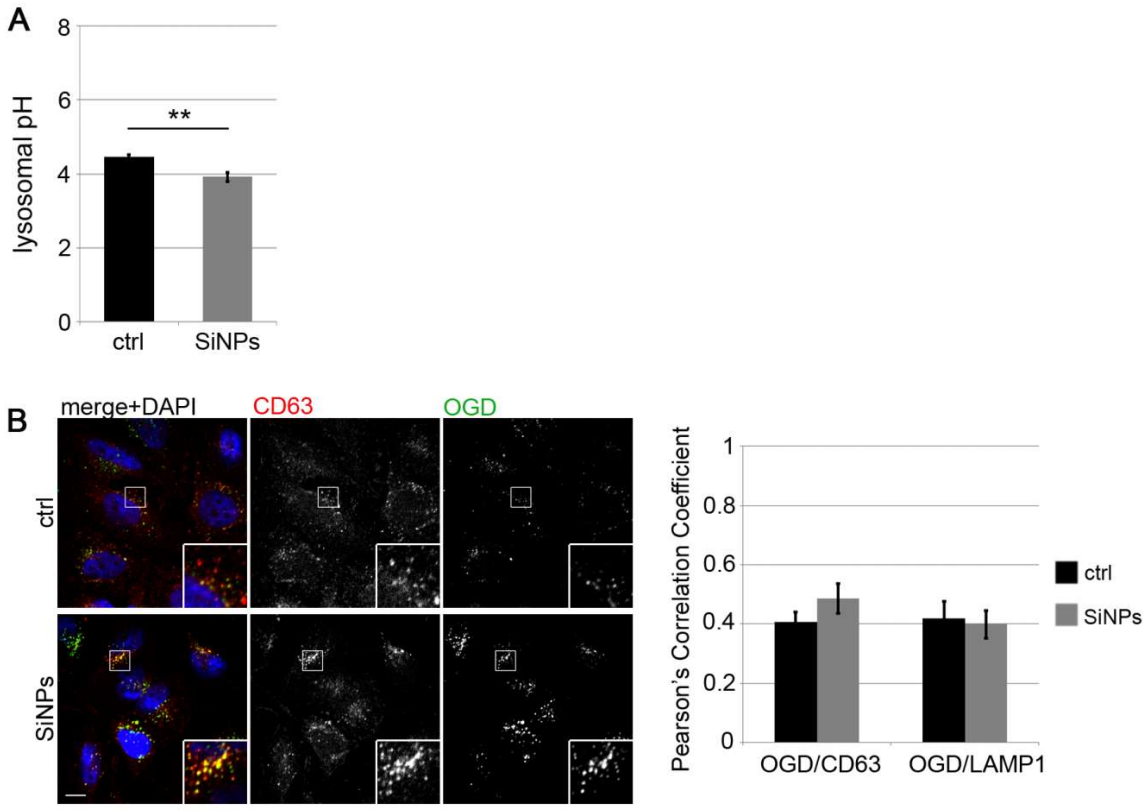

Figure 3.20 SiNP-accumulation in lysosomes results in slightly enhanced lysosomal acidification. (**A**) Ratiometric measurement of intralysosomal pH of control (pH = 3.9 ± 0.1) or SiNP-treated (SiNPs, pH = 4.5 ± 0.1) HeLa cells. Data represent mean ± s.e.m.; n = 5 independent experiments; **p<0.01. (**B**) Confocal microscopy images of HeLa cells confirm profound colocalization of Oregon Green Dextran (OGD) with late endosomes/ lysosomes in control as well as in SiNP-treated cells. Pearson's correlation coefficients were determined for OGD and CD63 (ctrl, 0.41 ± 0.03 and SiNPs, 0.49 ± 0.05, respectively) or OGD and LAMP1 (ctrl, 0.42 ± 0.06 and SiNPs,

0.40 ± 0.05, respectively). Data shown as mean ± s.e.m.; n = 3 independent experiments. Scale bar, 10 µm. Taken from Schütz et al., 2016

3.10.2 Increased lysosomal protease activity

Changes in lysosomal pH are often accompanied by alterations in lysosomal protein activity (Guha & Padh, 2008). Hence, we tested the protease activity of two widely expressed cathepsins, cathepsin B and L, using fluorogenic peptide substrates. Both MR-$(RR)_2$ and MR-$(FR)_2$ coupled to the dye cresyl violet served as non-fluorescent substrate peptides. Upon cleavage mediated by cathepsin B and cathepsin L, respectively the released dye becomes fluorescent and thus, allows monitoring of cathepsin activity in living cells. For that purpose, control and SiNP-treated cells were loaded with substrate peptides for 1 h at 37°C to allow trafficking to lysosomes and then analyzed by live cell imaging. Fluorescence intensity levels of released cresyl violet (red channel) were enhanced in SiNP-treated cells as observed by confocal microscopy (Figure 3.21 A and B, left-hand side). This is true for both substrate peptides (red channels labeled as CathepsinB and CathepsinL, respectively), indicating increased protease activities in SiNP-filled HeLa cells. The quantification of cresyl violet fluorescence revealed up to three-fold higher protease activity levels in SiNP-treated HeLa cells (Figure 3.21 A and B, right-hand side). This agrees well with a decrease in intralysosomal pH.

These results show that protease activity in SiNP-filled lysosomes remains functional. In fact, the elevated hydrolase activity is in full agreement with a decrease of intralysosomal pH. We therefore conclude that the observed dysfunction of SiNP-loaded lysosomes does not result from an impaired lysosomal acidification or perturbed intralysosomal hydrolase activity.

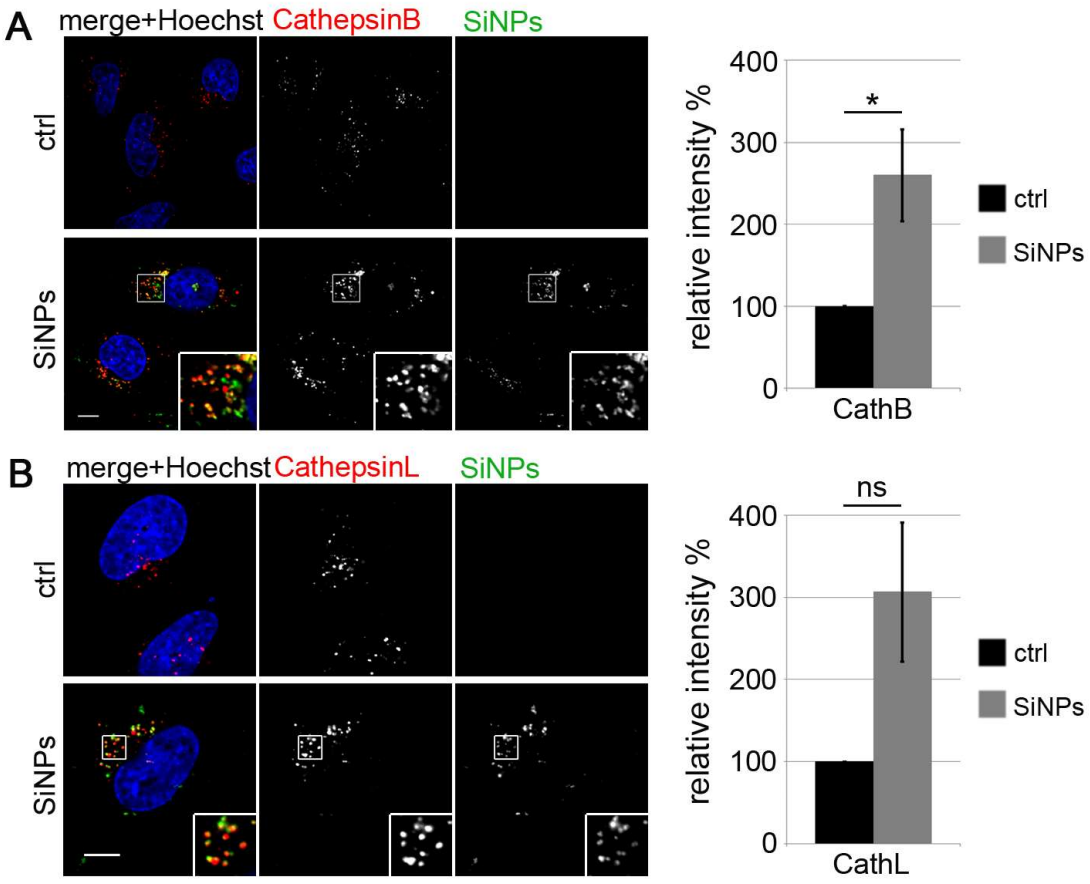

Figure 3.21 Cathepsin activity is not inhibited after SiNP-incubation. (**A**) Live cell confocal images show the localization of hydrolyzed fluorescent cathepsin B product (red channel) in control (upper panel) and SiNP-treated (green chanel) HeLa cells (SiNPs, lower panel). Nuclei were stained with Hoechst (blue). Quantitative analysis indicates an increased activity of cathepsin B (259.8 ± 56.1%) in SiNP-treated HeLa cells compared to controls (set to 100%). Data represent mean ± s.e.m. ,n = 3 independent experiments; *p< 0.05. (**B**) Images from live cell microscopy show hydrolysed fluorescent cathepsin L product (red chanel) in control (upper panel) and SiNP-treated (green chanel) HeLa cells (SiNPs, lower panel). Nuclei were stained with Hoechst (blue). Quantitative analysis on the right-hand side also indicates an increased activity for cathepsin L in SiNP-treated (306.5 ± 84.5 %) HeLa cells compared to control (set to 100 %). Data shown as mean ± s.e.m., n = 3 independent experiments; ns, non-significant p> 0.05. Scale bars, 10 µm. Taken from Schütz et al., 2016

3.10.3 Impaired cargo delivery to lysosomes

As our data showed that intralysosomal acidification and hydrolase activity was not impaired in SiNP-filled lysosomes, we finally tested whether perturbed degradation of autophagic and internalized substrates might be a consequence of inhibited fusion between lysosomes and upstream compartments. In this case we would expect a lack of colocalization between

compartments filled with substrates destined for lysosomal proteolysis, such as LC3-II, p62, and internalized EGF and compartments positive for SiNPs as well as functional lysosomal hydrolases (positive for cathepsin B or cathepsin L). As expected, confocal microscopy imaging revealed an almost complete lack of colocalization between non-degraded EGF^{647}, LC3, and p62 with accumulated SiNPs (Figure 3.22 left-hand side). SiNPs, on the other hand, profoundly overlapped with lysosomal cathepsin B and L hydrolase activities (Figure 3.21 A and B, left-hand side).

Taken together, these data demonstrate that impaired autophagic flux and degradation of internalized EGF^{647} in SiNP-loaded HeLa cells is not a consequence of impaired acidification or perturbed protease activity. We rather conclude that failed degradation of internalized and cytoplasmic substrates results from inhibited fusion between autophagosomes and late endosomes with SiNP-filled lysosomes.

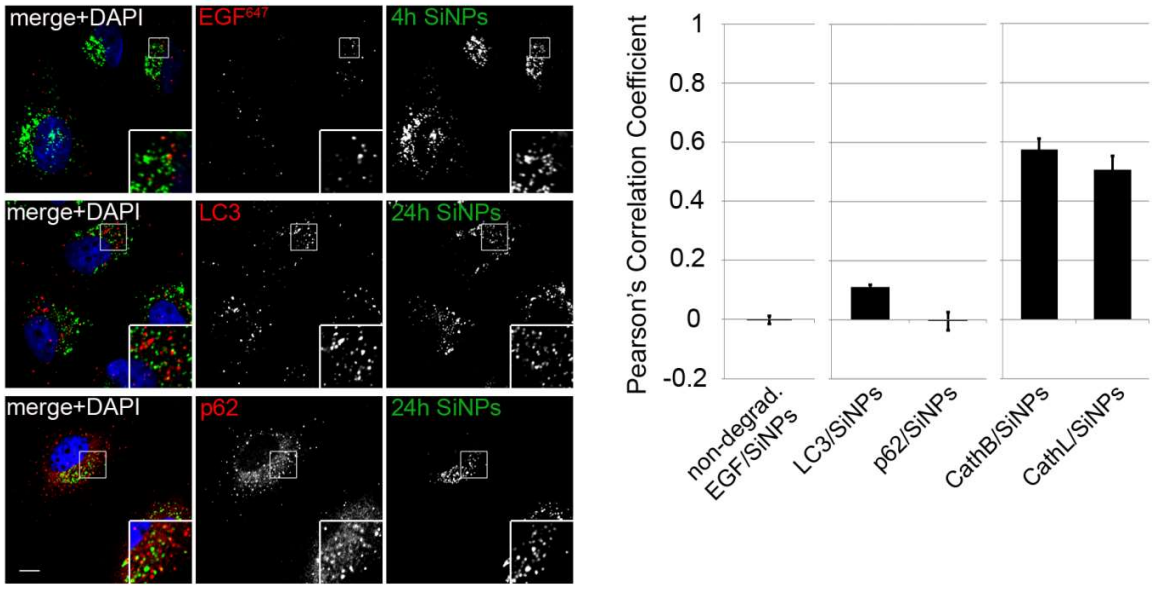

Figure 3.22 Accumulated cargo does not colocalize with SiNP-positive lysosomes. Representative confocal microscopy images depict the distribution of non-degraded EGF^{647} (red, top panel), LC3 (red, middle panel), and p62 (red, bottom panel) in SiNP-treated (green, right column) HeLa cells. Pearson's correlation analysis demonstrates the clear lack of colocalization between non-degraded EGF (-0.002 ± 0.014), LC3 (0.111 ± 0.006), and p62 (-0.005 ± 0.031) with SiNP-positive organelles. By contrast, fluorescent cathepsin products strongly colocalize with SiNPs (0.58 ± 0.04 for cathepsin B and 0.51 ± 0.05 for cathepsin L). Data represent mean ± s.e.m., n = 3 independent experiments. Scale bar, 10 µm. Taken from Schütz et al., 2016

Part II – Dendritic polyglycerol nanoparticles

Theranostics, as they combine both therapeutic and diagnostic tools, can not only be applied to treat diseases, but also to help monitoring intracellular drug release or elucidate trafficking pathways, delivery kinetics, and therapeutic efficacy (Kelkar & Reineke, 2011).

To gain information about the intracellular pH-triggered cleavage of Dox from its delivery vehicle, we used a FRET-based theranostic macromolecular prodrug, synthesized by the Calderón group (FU Berlin) following a three-step strategy. A 200 kDa dendritic polyglycerol nanocarrier served as the delivery system, equipped with Dox and IDCC, both connected to the carrier via a tri-functional linker. Importantly, the chemotherapeutic drug was attached to the carrier through a pH-sensitive hydrazone bond (Figure 3.23). Furthermore, we included non-cleavable and unquenched control conjugates in the experimental procedure (see also chapter 3.12) (Krüger et al, 2014).

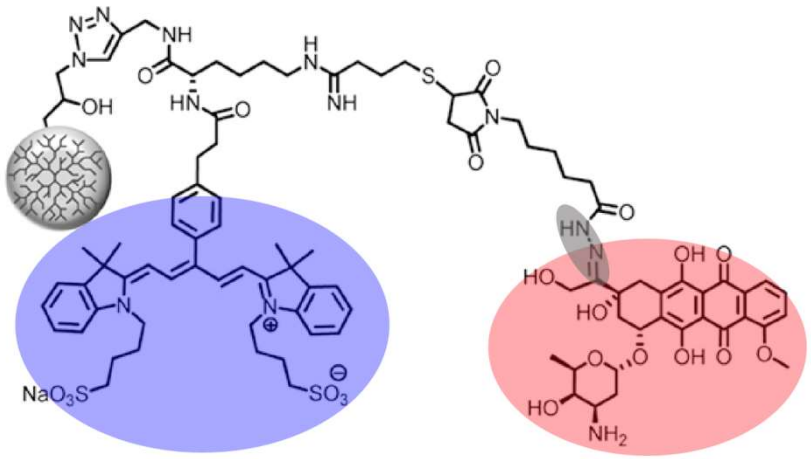

Figure 3.23 Chemical structure of the TMP. The therapeutic molecule Dox (red) is linked via a hydrazone bond (grey) to the dendritic polyglycerol nanocarrier. The diagnostic tool IDCC (blue) is located in close proximity to Dox to enable FRET. Taken from (Krüger et al, 2014)

3.11 TMP is cell permeable and releases doxorubicin

First, we aimed at confirming that the synthesized theranostic conjugates are taken up by cells as published earlier for almost identical dendritic polyglycerol nanoparticles (Reichert et al, 2011). We incubated HeLa cells for 2 h in cell culture medium supplemented with exact concentrations (stated in Dox equivalents) of TMP and non-cleavable control, respectively. Cells were then washed and immediately fixed. Images obtained by epifluorescence microscopy verified the intracellular localization of both TMP and non-

cleavable control conjugates (IDCC channel (green), upper row and lower row, respectively) (Figure 3.24). In addition, images showing the Dox fluorescence (Dox channel (red), middle of upper row) indicated the capability of the TMP to release Dox, as shown by the intense nuclear staining. In contrast, only very low levels of fluorescence intensity could be determined for the Dox channel upon incubation with non-cleavable control compound (Dox channel (red) in the middle of the lower row).

These data indicate that the TMP is cleavable and quenched, which is in full agreement with results obtained by fluorescence spectroscopy and gel permeation chromatography (Krüger et al, 2014).

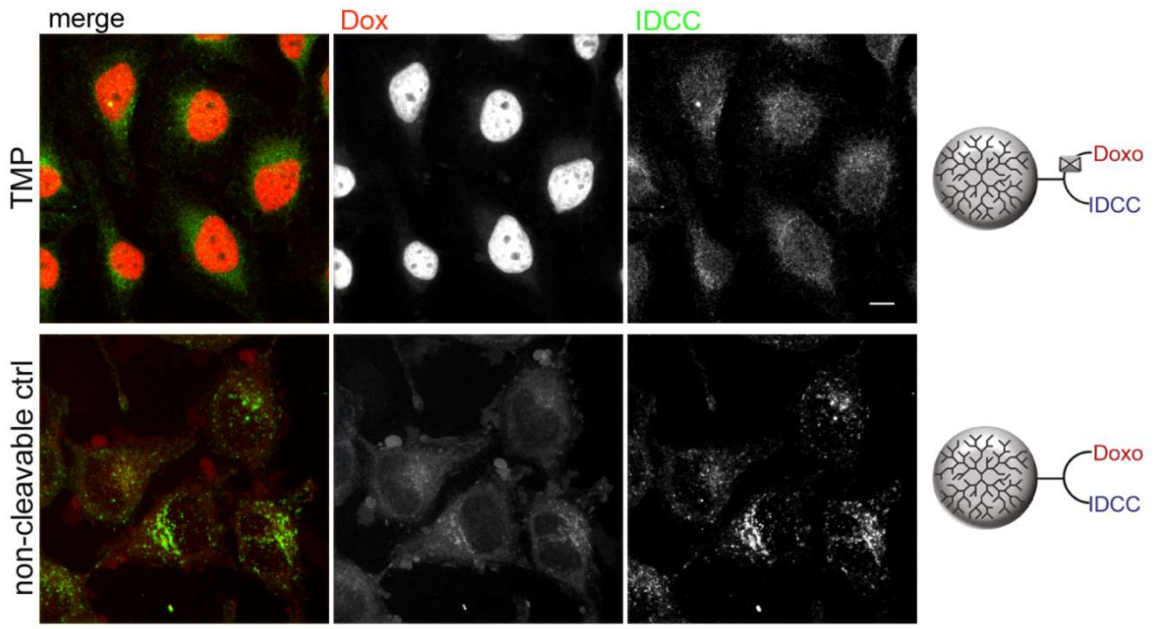

Figure 3.24 Dendritic polyglycerol conjugates are cell permeable. Representative images show fixed HeLa cells 2 h after incubation with TMP (upper row) and non-cleavable control (lower row), respectively. Both channels (dox in red, IDCC in green) were imaged separately using an epifluorescence microscope. Scale bar, 10 µm. Modified from (Krüger et al, 2014) (see supplementary information for chemical structure of the non-cleavable construct)

3.12 Monitoring doxorubicin cleavage from the TMP via FRET

FRET is a non-radiative energy transfer from an excited donor state to a proximal acceptor ground state based on long-range dipole-dipole interactions between two molecules. Necessary prerequisites for FRET are the spectral overlap of the fluorescence emission of the donor with the fluorescence absorption of the acceptor, the relative orientation of the

transition dipoles, and importantly, the distance between donor and acceptor molecules (1-10 nm) (Förster, 1948; Sapsford et al, 2006).

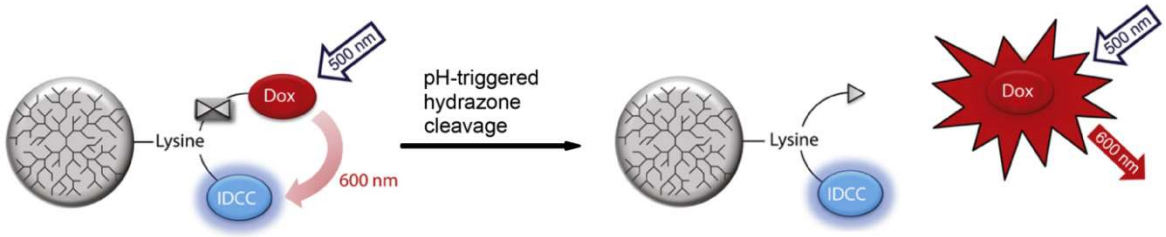

Figure 3.25 Monitoring of Dox before and after pH-triggered hydrazone cleavage. Fluorescence of Dox is quenched when in close proximity to IDCC. Upon pH-triggered release and enhanced spatial separation of donor and acceptor, fluorescence emission of Dox becomes detectable. Taken from (Krüger et al, 2014)

To monitor the intracellular drug release in real time, we measured by live cell imaging the increase in Dox fluorescence emission. HeLa cells were incubated with 10 µM TMP (concentration stated in Dox equivalents) accompanied by an immediate start of a time lapse series for 60 min with a frame rate of 1 image every 10 min. The samples were excited at 488 nm and Dox fluorescence detected in the range from 512 nm to 684 nm. Figure 3.26 displays typical images of HeLa cells at 5, 30 and 60 min after addition of TMP. Notably, the Dox signal visibly accumulates in the nucleus at timepoint 60 min.

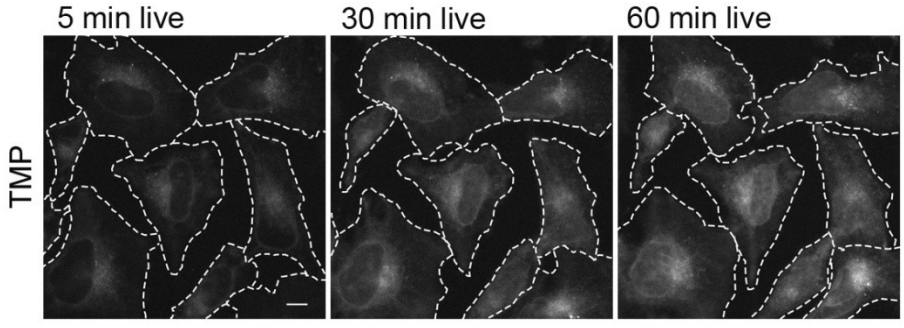

Figure 3.26 Dox release from TMP in HeLa cells. Visualization of Dox fluorescence upon intracellular cleavage of the drug. Dashed lines mark individual cells. Scale bar, 10 µm. Image taken from (Krüger et al, 2014)

To ensure FRET-based quenching of Dox fluorescence intensity within the TMP probe, we included two control conjugates, one non-cleavable and quenched, the other one cleavable and not quenched by FRET (non-cleavable ctrl and non-quenched ctrl, respectively). The equivalent experimental procedure was conducted for all conjugates and the cumulated fluorescence intensity (normalized to the non-cleavable control) was analyzed using the same thresholds (Figure 3.27). Quantifications for the timepoints 5 and 120 min are plotted on the left side of Figure 3.27 B. As the Dox fluorescence is quenched in case of the TMP and the non-cleavable control conjugate, the initial signal is rather weak compared to the non-quenched control (see timepoint 5 min live in Figure 3.27 B). In contrast, the fluorescence signal for the non-quenched control was already enhanced at 5 min, because a large distance between Dox and IDCC (>10 nm) prevented FRET. The fluorescence signal increased further as more conjugate was internalized. Compared to the non-cleavable control, the cumulated fluorescence intensity of the TMP samples increased significantly at 120 min and likely reflects the cleavage of Dox from the prodrug, resulting in effective de-quenching. We further quantified the drug release and its subsequent nuclear accumulation after intracellular cleavage by applying masks covering the cytosol and the nuclear region, respectively. The resulting ratios of nuclear-to-cytosol fluorescence intensity values clearly demonstrated the growing nuclear accumulation of Dox in TMP-treated cells, whereas the ratios remained unchanged for the non-cleavable and non-quenched controls (Figure 3.27 B right hand side).

Taken together, we conclude that Dox fluorescence is quenched when in close proximity to IDCC. Dequenching of Dox fluorescence results upon pH-triggered release from the prodrug. Cleavage of Dox is likely accelerated when facing low intracellular pH values like they exist in endolysosomal compartments of living cells.

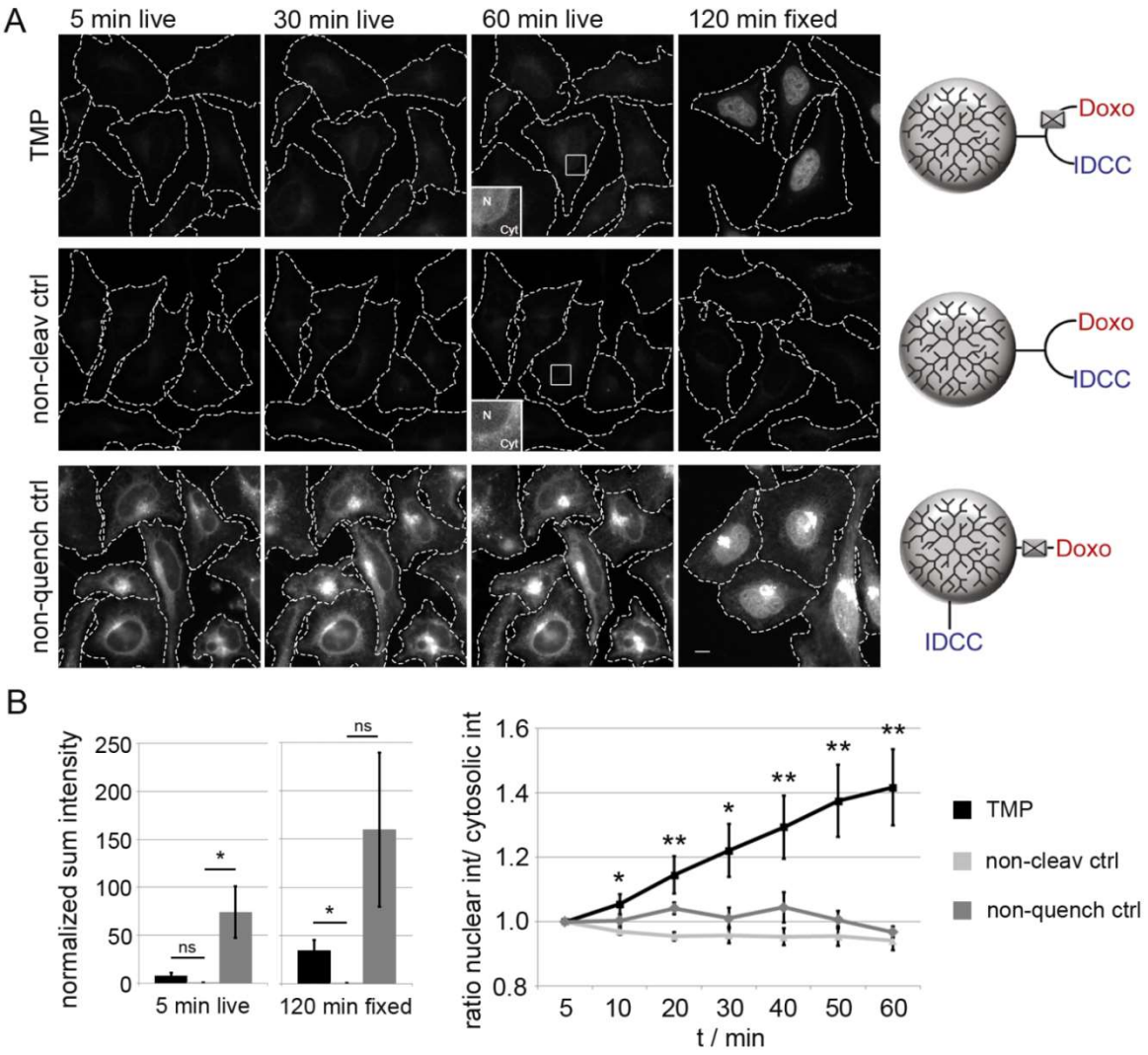

Figure 3.27 Live cell imaging of HeLa cells incubated with various polyglycerol conjugates. (**A**) Laser scanning microscopy images show Dox fluorescence in cells incubated with TMP (upper row), non-cleavable control (middle row) and non-quenched control (lower row). Images were acquired during live cell imaging at 5, 30 and 60 min, respectively, whereas images at 120 min were taken after PFA fixation. Blow ups of indicated areas for TMP and non-cleavable control at 60 min were 5 % depth corrected to illustrate the intracellular distribution of Dox fluorescence either in the nucleus (N) or in the cytosol (Cyt). Dashed lines indicate cell edges. Scale bar, 10 µm. (**B**) Quantification on the left hand side shows normalized Dox sum intensities for two timepoints: 5 min in live (non-cleav ctrl was set to 1; TMP, 7.5 ± 3.6; non-quench ctrl, 74.1 ± 26.9) and 120 min in fixed cells (non-cleav ctrl was set to 1; TMP, 34.3 ± 11.4; non-quench ctrl, 159.9 ± 79.8). The plot on the right hand side displays the calculated ratios of nuclear-to-cytosolic intensities for all three conjugates. Values represent mean ± s.e.m. for n = 5-6 independent experiments; ns, non-significant p> 0.05; *p< 0.05; **p<0.01. Modified from (Krüger et al, 2014)

4 DISCUSSION

In this work, we describe adverse cellular effects resulting from the interaction of positively charged amino-functionalized silica nanoparticles with HeLa cells. SiNPs are internalized mainly via dynamin 2-dependent caveolar endocytosis and targeted to late endosomal/ lysosomal compartments, where they accumulate resulting in impaired cell viability. Moreover, degradation of exogenous ligands such as growth factors is tremendously altered in SiNP-loaded HeLa cells, while endosomal recycling proceeds unperturbed. Additionally, levels of autophagosomal marker and cytosolic cargo protein are highly elevated, both of which usually undergo degradation via the autophagy-lysosome pathway. However, lysosomal acidification and intralysosomal protease activity were not the cause for the dysfunction of lysosomes in SiNP-treated HeLa cells. We argue that the accumulation of non-degraded proteins in late endosomes and autophagosomes results from inhibition of fusion between lysosomes and upstream compartments. Our data clearly demonstrate the necessity of further investigations of nanoparticle interactions with cells at the subcellular and cellular level.

4.1 Internalization of positively charged silica nanoparticles

We have demonstrated that the surface properties of silica nanoparticles are crucial for their colloidal stability and cell uptake. As the colloidal stability of GP- and APS-functionalized NPs (both positively charged) dramatically decreases already after transfer from ethanol into water, it is not surprising to observe severe aggregation after transfer into cell culture medium, thus preventing cell uptake. Otherwise, non-functionalized, PEG-, and AHAPS-functionalized silica NPs, although fairly stable in biological media, showed major differences in their individual cell uptake efficiency (Figure 3.2). Only poor internalization for non-functionalized and no uptake for PEG-functionalized NPs (both negatively charged) was observed after incubation with cells in cell culture medium. Positively charged AHAPS-functionalized NPs, on the other hand, were readily taken up. As most cells express a net negative surface charge due to proteoglycans on the outer membrane, cellular uptake of stable positively charged particles is in agreement with our expectations. This is in accordance with numerous cell biological studies, which compare internalization efficiencies between positively and negatively charged NPs (Harush-Frenkel et al, 2007; Slowing I. et al, 2006).

After all, despite the various features that are addressed in nanoparticle surface design, it is rather difficult to predict which particular pathway a specific nanoparticle will take. As every cell type has its own and very specific biological content that contributes to the protein corona built around any external nanomaterial, we were highly interested in unravelling the uptake mechanism of AHAPS-functionalized NPs (SiNPs) into HeLa cells (Nel et al, 2009). We therefore chose to investigate several independent internalization mechanisms involving clathrin, a key component of clathrin-mediated endocytosis, caveolin, the main structural component of caveolar membrane invaginations that undergo dynamin-mediated fission, and flotillin, an integral membrane protein thought to contribute to clathrin-independent fluid-phase endocytosis via the CLIC/ GEEC pathway (Wieffer et al, 2009). The most straightforward approach to acutely interfere with NP internalization is the use of pharmacological compounds, such as pitstop or dynasore (Macia et al, 2006; von Kleist et al, 2011). Notably, many inhibitors have been reported to be functional only in serum-depleted medium. Following this approach, we observed severe aggregation of SiNPs in serum-depleted cell culture medium (data not shown), which prevented any further analysis. Also, other studies report that inhibitors often used to interfere with caveolin-mediated uptake, such as methyl-β-cyclodextrin (MβCD) or genistein, either show contradictory results (Hao et al, 2012; Lee J. et al, 2013) or a broad spectrum of biological effects and therefore lack specificity (Vercauteren et al, 2010; von Kleist & Haucke, 2012). Hence, we decided to use small interfering RNA to deplete cells of endogenous dynamin 2, clathrin heavy chain, flotillin 1, and of caveolin 1 (Doherty & McMahon, 2009). We observed strongly reduced endocytosis of SiNPs in HeLa cells depleted of caveolin 1 or of dynamin 2. While SiNP-internalization proceeded unperturbed in the absence of clathrin, flotillin 1 knockdown resulted in a small though statistically significant reduction in SiNP-uptake (Figure 3.4). Our data clearly indicate that SiNPs are mainly, but not exclusively internalized via dynamin 2-dependent caveolae-mediated endocytosis.

A caveolin 1-dependent internalization has been reported elsewhere as an important uptake mechanism for diverse nanomaterials (El-Sayed & Harashima, 2013; Hao et al, 2012; Thorley et al, 2014). For instance and also in agreement with our data, positively charged silica-coated iron oxide NPs exhibited reduced endocytosis in cells depleted of caveolin 1, while NP internalization was neither affected upon clathrin nor flotillin 1 knockdown. Interestingly in contrast to our data, depletion of dynamin 2 showed no effect on the internalization of these NPs (Bohmer & Jordan, 2015). Furthermore, clathrin-mediated endocytosis has often been described as the major uptake route for NPs, both targeted and non-targeted (Harush-Frenkel et al, 2007; Mickler et al, 2012). However, as chemical inhibitors were used in most of the published studies, it remains debatable whether

this uptake route can be considered specific due to additional pharmacological activities of such inhibitors (Chithrani & Chan, 2007; Gao et al, 2013; Treiber et al, 2009).

Since cellular import via caveolin-mediated endocytosis includes a contribution of the cytoskeleton, we evaluated the involvement of cytoskeletal elements on the internalization of SiNPs into HeLa cells. Prior to incubation with SiNPs, we used cytochalasin D and nocodazole to interrupt actin filaments and microtubules, respectively. Our results reveal a strong reduction of SiNP-internalization compared to control cells with an intact cytoskeleton (Figure 3.5). As caveolin-mediated endocytosis and the intracellular transport of endocytosed vesicles are dependent on a functioning cytoskeletal network (Doherty & McMahon, 2008; Lim et al, 2014), these data agree at least partly with results gained from knockdown experiments. The discrepancy in the decrease of SiNP-uptake when comparing knockdown and inhibitor experiments might result from additional pharmacological effects of the inhibitors on cellular processes due to a lack of specificity (von Kleist & Haucke, 2012).

4.2 Lysosomal accumulation of SiNPs leads to reduced cell viability

Internalized SiNPs display a punctuate distribution and are often enriched in the perinuclear area, suggesting their accumulation within intracellular organelles. To determine the identity of these organelles, various marker proteins of the endolysosomal system were labeled by immunofluorescence staining. We observed a profound colocalization with late endosomal/ lysosomal compartments (LAMP1, CD63), whereas little or no overlap was found with early endosomes (EEA1) and proteins that cycle between endosomes and the TGN (AP-1, M6PR), respectively (Figure 3.6). Also, colocalization with caveolin 1-labeled structures was not visible after 4 h treatment with SiNPs. In contrast, other studies show the accumulation of NPs in compartments other than late endosomes and lysosomes. For example, internalized conjugated polymer NPs strongly overlapped with caveolin 1-positive organelles 24 h after exposure, indicating their accumulation in the early endosomal system (Lee J. et al, 2013). Furthermore, plain silica nanoparticles with an average size of 70 nm (the smallest NPs tested in this study) accumulated in the nucleus, where they induced aberrant clusters of topoisomerase I, a nuclear protein that regulates topology during DNA replication, polyQ, and huntingtin (Chen M. & von Mikecz, 2005). The majority of reports in the literature, however, confirm our finding that internalized NPs strongly overlap with or

even accumulate in late endosomes and lysosomes, respectively; two exemplary references are (Al-Rawi et al, 2011; Shi H. et al, 2010).

We also analyzed whether cell viability was affected in SiNP-filled HeLa cells. We indeed observed a reduction to 60 % after 24 h treatment with SiNPs in the MTT assay (Figure 3.7). Similar to our results, several other studies examined cytotoxic effects after incubation with silica-based nanomaterials (Ahmad et al, 2012; Halamoda Kenzaoui et al, 2012; Napierska et al, 2009). Interestingly, Fisichella and coworkers discovered that endocytosed mesoporous silica nanoparticles (MSNs) interfere with the MTT test in HeLa cells resulting in an overestimation of cytotoxicity (Fisichella et al, 2009). They speculate that MSNs interfere with forming of the insoluble formazan crystals by accelerating their exocytosis. However, as many other studies report no effects on cell viability after incubation with silica NPs using the MTT test, the question remains whether all kinds of silica-based nanoparticles cause false effects in MTT assays (Chu et al, 2011; Gan et al, 2012; Tang et al, 2012). Therefore, additional tests for the verification of cytotoxicity data, such as LDH (lactate dehydrogenase) activity assay, should be included. Other alternatives to the MTT test would be WST-1, XTT or INT test as their resulting formazan salts are water-soluble, thus avoiding interference with internalized nanoparticles (Worle-Knirsch et al, 2006).

4.3 Intracellular trafficking in SiNP-loaded cells

Considering that SiNPs accumulate in lysosomes and likely induce cytotoxic effects, we were wondering whether intracellular trafficking might be affected in SiNP-loaded HeLa cells. We therefore used well established fluorescently labeled cargo proteins to investigate endocytic recycling and degradation (see also chapter 1.2). Internalization of both Tf^{647} and EGF^{647} proceeded unaltered irrespective of whether these cells had been incubated with SiNPs prior to ligand addition (Figure 3.8 and Figure 3.9). Also, recycling of fluorescent Tf was not affected (Figure 3.10).

Until today, no other reports exist on endocytic recycling of Tf in cells that accumulate NPs. In nanoparticle studies that use fluorescently labeled ligands, Tf was applied either to investigate the endocytic mechanism of NP-entry into cells or to identify Tf-positive compartments that possibly colocalize with internalized NPs (Lunov et al, 2011a; Mickler et al, 2012). Sandin and coworkers used rapid multicolor 3D confocal microscopy in live cells combined with transient overexpression of small GTPases marking various endocytic membranes to study the kinetics of nanoparticle trafficking through Rab-associated compartments (Sandin et al, 2012). They report that NPs, after passing early endosomes

(Rab5-positive), were rapidly transferred to late endosomes/ lysosomes (Rab9- and Rab7-positive), whereas only few NPs were able to access the endocytic recycling pathway as determined by colocalization of NPs with Rab11-positive organelles. Although Tf recycling per se was not investigated in this study, the authors did not observe direct interference with the trafficking of recycling vesicles.

We further tested the import into and degradation of EGF^{647} in HeLa cells. SiNP-treated cells were incapable of entirely degrading EGF^{647} during the post-endocytic chase period of 60 or 120 min, although EGF^{647} binding to the cells as judged by EGF^{647} surface levels remained unchanged compared to control cells (Figure 3.12). Instead of being rapidly degraded, a significant fraction of internalized EGF^{647} remained within punctuate structures. Using specific antibodies, we could indentify these organelles as LAMP1- and CD63-positive late endosomes/ lysosomes (Figure 3.13). The attenuation or block of EGF^{647} degradation can be specifically located to the lysosomal system as endocytosis and recycling of Tf, a protein not degraded in lysosomes, proceeded unperturbed. Thus, intralysosomal accumulation of SiNPs in HeLa cells disrupts the degradation of internalized EGF^{647}.

Similarly, gold-NPs (AuNPs) were internalized in normal rat kidney (NRK) cells, where they accumulated in lysosomes causing an impairment of lysosome degradation capacity. In particular, lysosomes in AuNP-treated cells failed to degrade DQ-BSA (derivative-quenched BSA). In contrast to our findings, the cause for lysosomal dysfunction in these cells was determined to be an alkalinization of the lysosomal pH (Ma et al, 2011).

In a recent study, Jakhria and colleagues were aiming at unravelling the pathological mechanisms of β_2-microglobulin amyloid fibrils that cause amyloid diseases (Jakhria et al, 2014). They could show that fragmented amyloid fibrils, resulting in nanoscaled fibrilar particles, not only reduced cell viability (measured by MTT), but also accumulated in lysosomes leading to altered trafficking of lysosomal membrane proteins. Furthermore, these nano-fibrils inhibited the degradation of fluorescently labeled ovalbumin, a model protein substrate, which is endocytosed and degraded in lysosomes (Zhang T. et al, 2000).

Taken together, trafficking of diverse NPs through the degradative system was often shown as indicated by NP-colocalization with or NP-accumulation in LEs/ lysosomes (see chapter 4.3) (Hofmann et al, 2014; Lerch et al, 2015). However, whether or not and how intralysosomal NP-accumulation affects intracellular trafficking, particularly recycling of Tf and degradation of EGF, respectively, was not investigated so far.

4.4 Lysosomal SiNP-accumulation causes adverse effects on autophagy

As autophagy results in the lysosomal degradation of intracellularly engulfed material upon autophagosome-lysosome fusion, we investigated whether SiNP-accumulation in HeLa cells also affects this important process. Autophagy requires the posttranslational lipidation of cytoplasmic LC3 protein with phosphatidylethanolamine (termed LC3-II), resulting in its association with membranes and autophagosome formation (chapter 1.3). We observed a concomitant increase in the number of LC3-positive autophagosomes after incubation of HeLa cells with increasing concentrations of SiNPs (Figure 3.15). Moreover, not only LC3 levels were highly elevated, cellular accumulation in SiNP-filled cells was also seen for p62 (Figure 3.16), another component of autophagosomes and substrate for autophagy-mediated lysosomal protein turnover. Similarly, several cell biological studies reported an enhanced autophagosome formation upon NP exposure. These investigations were performed in diverse cell lines using various NPs, including silica, polymer, gold and copper NPs (Loos et al, 2014; Ma et al, 2011; Sun T. et al, 2012; Yu et al, 2014).

Since autophagosomes constitute intermediate structures in a dynamic process, the number of autophagosomes observed at any particular time point represents a snapshot of newly generated autophagosomes and freshly converted autolysosomes. Hence, autophagosome accumulation can either result from autophagy induction or from block of autophagic flux. Early studies on nanomaterial-related autophagosome formation focused only on autophagy induction, while entirely ignoring the possibility of an autophagic flux blockade (Seleverstov et al, 2006; Yamawaki & Iwai, 2006). However, autophagy induction in cells treated with NPs can originate from different sources, such as enhanced cellular ROS production or perturbed mTOR signaling, a key regulatory pathway of autophagy (Halamoda Kenzaoui et al, 2012; Loos et al, 2014). Furthermore, aside from various mTOR-independent pathways, the PI3K pathway, a major signaling cascade controlling mTORC1, and protein kinases like AMPK were reported to regulate autophagy in mammalian cells (Ravikumar et al, 2010).

We were able to demonstrate that LC3 and p62 accumulation was not a consequence of altered mTOR signaling, as the levels of phospho-S6K (T389) or phospho-ULK1 (S757) were not altered in SiNP-filled cells (Figure 3.18). Similarly, Ma et al as well as Khan et al evaluated levels of phosphorylated S6K to determine the status of mTOR signaling (Khan et al, 2012; Ma et al, 2011). Alternatively, one could detect phospho-mTOR levels or phospho-protein levels of upstream components of the mTOR signaling pathway (Li C. et al, 2009; Loos et al, 2014). Yet, by measuring the LC3 protein levels and evaluating the

turnover of LC3-I to LC3-II species, we determined significantly elevated LC3-II/ LC3-I ratios, indicating a defective autophagic flux in SiNP-treated HeLa cells (Figure 3.17). We therefore conclude that intralysosomal accumulation of SiNPs leads to the accumulation of p62-containing LC3-positive autophagosomes that fail to undergo lysosomal degradation.

Another possibility to measure autophagic flux requires comparing LC3-II levels in the presence and absence of lysosomal inhibitors, such as bafilomycin A1 that prevents lysosomal degradation by inhibiting the v-type H^+-ATPase (Figure 3.15); unchanged LC3-II levels indicate then a block in autophagy at the terminal stages (Klionsky et al, 2012). Furthermore, transfection of a tandem monomeric RFP-GFP-tagged LC3 would be the most straight forward approach to monitor autophagic flux in live cells by fluorescence microscopy. As the GFP signal is sensitive to acidic conditions, it strongly decreases in the intralysosomal environment, whereas the RFP signal remains stable; higher colocalization of RFP and GFP indicates defective autophagic flux or acidification (see also chapter 4.6) (Kimura et al, 2007). Assuming that the fusion of autophagosomes with SiNP-loaded lysosomes is blocked, one would expect a higher ratio of GFP/RFP-positive punctae (autophagosomes) in relation to total RFP-levels (autophagosomes and autolysosomes) compared to control cells. Lower ratios would be expected for non-starved and starved control cells as autophagy and lysosomal degradation remain functional, whereas equal or even higher ratios should occur in Baf A1-treated cells as lysosomal degradation is disrupted. The monitoring of autophagic flux in tandem-GFP-RFP-transfected SiNP-treated (without FITC label) HeLa represents a potential next step, but goes beyond the scope of this study.

Meanwhile, a substantial body of literature links autophagy dysfunction to nanomaterial toxicity (Stern et al, 2012). In particular, both autophagy induction and block of autophagic flux were identified as emerging consequences of oxidative stress (e.g. ER stress, mitochondrial damage) caused by NP-incubation (Khan et al, 2012; Lee J. et al, 2012b; Li J. J. et al, 2010; Li N. et al, 2008).

Interestingly, autophagy induction can also be a desirable effect. Wei and coworkers observed that europium hydroxide nanorods, while not being cytotoxic, induce autophagy in cell lines expressing mutant huntingtin (with 74 polyQ repeats), a protein implicated in Huntington's disease, leading to an accelerated clearance of aggregated protein (Wei et al, 2014).

4.5 Intralysosomal function is not affected

So what might be the reason for the failure of SiNP-filled lysosomes to degrade cytoplasmic autophagic substrates as well as internalized EGF? Explanations for lysosomal dysfunction could be either the disruption of their proton gradient due to the accumulation of charge, a sequestration of ions required for acidification (i.e. Cl^-), or loss of membrane integrity. Such changes would eventually result in the inactivity of intralysosomal hydrolases (Settembre et al, 2013). Using ratiometric imaging, we first tested whether the lysosomal pH is affected in SiNP-treated HeLa cells. We observed indeed a slight but significant drop of the intralysosomal pH compared to control cells (Figure 3.20). The lower pH of SiNP-filled lysosomes might be a consequence from failure of these lysosomes to degrade intracellular proteins, which otherwise serve as the main lumenal buffer for protons. In addition, we observed elevated activities for both cathepsin B and L in SiNP-loaded cells (Figure 3.21). This is consistent with the fact that most lysosomal hydrolases are activated at low pH (Mego, 1971).

Our observations agree well with reports on positively charged polymer NPs delivered to lysosomes, where they acidified the lysosomal pH leading to enhanced hydrolase activity as shown for cathepsin D (Baltazar et al, 2012). In contrast, PAMAM dendrimers surface-functionalized with amino groups were shown to accumulate in lysosomal compartments, but cause an increase in lysosomal pH possibly based on the ‘proton sponge’ effect (or pH-buffering effect) (Akinc et al, 2005; Liang & Lam, 2012). A following induction of mitochondria-mediated apoptosis was likely the result of lysosomal alkalinization (Thomas et al, 2009). Further, Ma and coworkers could demonstrate that internalized AuNPs are targeted to lysosomes, where they accumulate resulting in alkalinization of the intralysosomal pH. They also revealed that the observed autophagosome accumulation was a result of impaired lysosomal degradation of LC3- as well as p62-positive organelles (Ma et al, 2011).

Inhibition of protein degradation (as observed for internalized EGF and cytoplasmic material) might also result from nanomaterial-induced membrane destabilization. Lysosomal destabilization can be identified by measuring the cytosolic accumulation of lysosomotropic dyes or lysosomal enzymes (Thibodeau et al, 2004). Depending on the degree of membrane damage, two forms may occur, either lysosomal membrane permeabilization (LMP) or lysosomal membrane rupture (LMR). While partial LMP results in mitochondrial permeabilization that can induce the generation of ROS and apoptosis, severe LMP (LMR) may cause necrosis and cytosolic acidification upon release of degradative lysosomal enzymes into the cytoplasm (Villamil Giraldo et al, 2014; Wan et al,

2013). Interestingly, inflammatory responses upon NP- treatment have been proposed to result from cathepsin B-mediated activation of the NLRP3 (Nod-like receptor family protein 3) inflammasome following LMP (Lunov et al, 2011b; Meunier et al, 2012). However, there is evidence that autophagy is intertwined with NLRP3 inflammasome activation (Shi C. S. et al, 2012). As inflammation is a key factor in the development of a variety of diseases, it would be highly interesting to investigate if and how our SiNPs influence inflammatory processes.

4.6 Dysfunctional lysosomal degradation may result from impaired autophagosome-lysosome fusion

Another explanation for the failure of SiNP-filled lysosomes to degrade cytoplasmic autophagic substrates as well as internalized EGF might be the inability to fuse with upstream donor compartments such as autophagosomes and late endosomes. Spatial segregation of lysosomes from their target substrates might occur resulting from failure of their limiting membrane to undergo remodeling required for fusion. Thus, we tested whether impaired lysosomal degradation of autophagic and internalized cargo results from the inhibition of fusion between lysosomes and upstream compartments by determining colocalization coefficients. Substrates for lysosomal proteolysis such as LC3, p62, and EGF should then accumulate in organelles lacking SiNPs as well as functional hydrolases. Evaluation of Pearson's correlation coefficients indeed confirmed this hypothesis. While colocalization between LC3, p62, or non-degraded EGF and SiNPs-containing lysosomes was almost completely lacking, SiNPs displayed a profound overlap with lysosomal cathepsin B and L hydrolase activities (Figure 3.22). These data suggest that inhibited fusion of autophagosomes with lysosomes likely caused the impaired autophagic flux and incomplete degradation of internalized EGF. To confirm an inhibition of fusion with SiNP-loaded lysosomes and therefore of autophagic flux, one could use a tandem monomeric RFP-GFP-tagged LC3 construct to monitor flux in live cells pretreated with unlabeled SiNPs. Alternatively, one could transfect an RFP-tagged LC3 construct in FITC-labeled SiNP-filled cells, followed by the incubation with Lysotracker Deep Red (fluorescent in the near infrared) for live cell imaging or by employing specific antibodies against autophagosomes and late endosomes/ lysosomes for the investigation of fixed samples. The three labels would not only allow monitoring autophagic flux in SiNP-labeled cells, but also to simultaneously distinguish SiNP-filled organelles from autophagosomes and autolysosomes, respectively. In case of defective autophagic flux, we would first of all expect a higher number of autophagsosomes (as shown in Figure 3.15), and secondly a

lower proportion thereof to colocalize with late endsosomes/ lysosomes compared to untreated control samples. Similarly, one would expect higher colocalization values for non-degraded EGF with LAMP1-/ CD63-positive compartments lacking SiNPs, when constantly loaded with fluorescently labeled EGF (in contrast to a pulse and chase experiment) (as shown in Figure 3.13 C). Furthermore, syntaxin 17 (Stx17) has been identified as the autophagosomal SNARE required for fusion with the endosome/ lysosome (Itakura et al, 2012). As depletion of Stx17 results in autophagosome accumulation without degradation, it represents an additional target to investigate autophagosome-lysosome fusion in further detail.

Interestingly, lysosomal overload by particulates from cigarette smoke and asbestos was shown to result in vacuole accumulation and block of autophagic flux (Monick et al, 2010; Montgomery et al, 1991). Similar effects were observed in patients with lysosomal storage disorders, where lysosomal overload induces destabilization of lysosomal membranes and leads to defects in intracellular trafficking (Futerman & van Meer, 2004). Accumulating evidence indicates that lysosomal and autophagy dysfunction is one of the main mechanisms underlying neurodegenerative diseases such as Parkinsons's disease, Alzheimer's disease, and Huntington's disease (Lee J. H. et al, 2010; Settembre et al, 2013; Wong & Cuervo, 2010).

Autophagy and lysosomal dysfunction might also be exploited as therapeutic mechanisms. For instance, alumina NPs are being developed into a novel therapeutic vaccine that transports antigens required by dendritic cells to activate T cells. The alumina NPs deliver these antigens to autophagosomes of dendritic cells, which then present them to T cells through autophagy (Li H. et al, 2011). Furthermore, iron oxide NPs appear to selectively kill cancer cells through an autophagy-related mechanism (Wu Y. N. et al, 2011b).

4.7 Model illustrating the effect of SiNP-treatment

Based on our results obtained from biochemical and cell biological experiments we developed a simplified model that visualizes how SiNP-treatment affects processes in HeLa cells (Figure 4.1). In untreated cells (scenario on the left side), internalized EGF that remains bound to its receptor becomes sorted into intralumenal vesicles (ILVs) inside of early endosomes (EEs). While undergoing a multitude of changes, including conversion of membrane components and intralumenal acidification, EEs mature to late endosomes

(LEs), which eventually fuse with lysosomes for degradation. In addition, a basal level of autophagy is maintained, as cytoplasmic material such as p62 is engulfed into newly forming autophagosomes (positive for LC3). Their content is subsequently delivered for degradation upon fusion with lysosomes.

In contrast, while internalization and sorting of EGF and its receptor proceed unaltered in cells that accumulate SiNPs in lysosomes (scenario on the right side), their degradation is impaired. Furthermore, autophagosomes (positive for p62 and LC3) strongly accumulate in SiNP-filled cells. Failed lysosomal proteolysis of EGF or autophagosomal substrates does not result from altered mTOR signaling, elevated intralysosomal pH, general damage of lysosomal membranes, or inhibition of lysosomal protease activity. We favor a model according to which lysosomes containing high levels of SiNPs fail to undergo fusion with LEs and autophagosomes resulting in a lack of colocalization between non-degraded EGF or p62 and lysosomal proteases. It seems conceivable that the rigid structure of SiNPs may prevent membrane-remodeling processes that are required for SNARE-mediated fusion with LEs and autophagosomes.

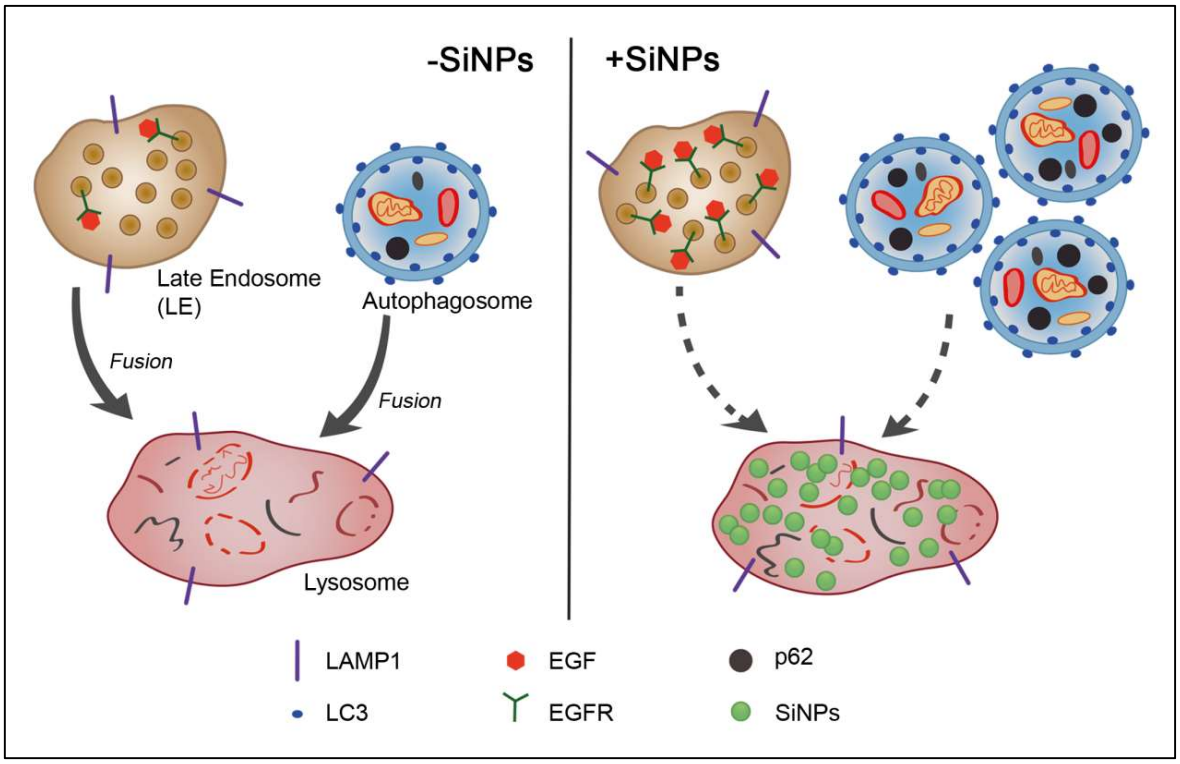

Figure 4.1 Schematic model illustrating the effect of SiNPs on the endolysosomal system. Under control conditions (-SiNPs, left), receptor-bound EGF is sorted into LEs, which eventually fuse with lysosomes. LC3- and p62-containing autophagosomes also fuse with lysosomes for degradation. SiNP-accumulation in lysosomes (+SiNPs, right) inhibits fusion of both LEs and

autophagosomes with lysosomes, resulting in impaired degradation of EGF/ EGFR and elevated levels of LC3- and p62-positive autophagosomes.

4.8 Visualization of intracellular drug release by live cell imaging

Theranostic nanomedical tools hold great promise for the understanding and development of personalized medicine as they allow simultaneous detection and treatment of diseases. Using a FRET-based theranostic macromolecular prodrug (TMP), we investigated the intracellular drug release in HeLa cells in real time. Similar to other prevalent polymeric drug conjugates, we chose dendritic polyglycerol as a biocompatible nanocarrier (Calderón et al, 2010). The anticancer drug Dox, linked via a pH-sensitive hydrazone bond, was attached in close proximity to IDCC via a trifunctional linker (Figure 3.23). IDCC dye was considered a perfectly suitable FRET acceptor for Dox due to its photopyhsical properties, i.e. degree of spectral overlap of Dox fluorescence and IDCC absorption and spatial separation of the emission wavelengths for accurate detection. First, we demonstrated that the TMP was cell permeable as published for almost identical dendritic polyglycerol NPs (Reichert et al, 2011). We also observed the release probability of the TMP in fixed cells as cleaved Dox became fluorescent and accumulated in cell nuclei (Figure 3.24, upper row). In contrast, while being cell permeable (as visible by the intracellular IDCC fluorescence), the non-cleavable control conjugate did not release Dox as its fluorescence remained almost entirely quenched via FRET (Figure 3.24, lower row). Next, we monitored the drug release from the TMP in real time by measuring the recovered Dox fluorescence over time (Figure 3.26). We quantified drug release and its subsequent nuclear accumulation after intracellular cleavage by evaluating nuclear-to-cytosol fluorescence ratios of TMP in comparison to a non-cleavable and an unquenched control (Figure 3.27 B right). Our results suggest that the TMP undergoes rapid cleavage after cellular internalization, followed by a nuclear accumulation of released Dox. Cleavage of the drug most likely occurs in acidic organelles such as endosomes and lysosomes.

Chen and coworkers investigated a similar FRET system except that Dox and Cy5 were used as a FRET-donor-acceptor pair (Chen K. J. et al, 2011). Cy5 dyes were conjugated to N-palmitoylated chitosan chains that were able to self-assemble into NPs in dilute aqueous media, thereby entrapping Dox molecules. A proper balance between charge repulsion (derived from the cationic polysaccharide chitosan) and hydrophobic interaction (mediated by the hydrophobic palmitoyl sidechains) enabled these polyelectrolytes to undergo a fast hydrogelation triggered by their environmental pH. At neutral pH, as encapsulated Dox remained in close proximity to Cy5, energy transfer took place resulting in quenched Dox

fluorescence. At low pH, however, the amino groups of the N-palmitoylated chitosan became protonated leading to an expansion of the backbone due to charge repulsion, Dox was released and dequenching occured.

Dendritic polyglycerol-based theranostic systems like those applied in our study can be used to further improve therapeutic efficacy by specifically targeting e.g. cancer cells using the SNAP-Tag technology. For this purpose, a recombinant antibody fragment of EGFR was fused to an engineered version of the human DNA-repair enzyme O^6-alkylguanine DNA alkyltransferase (AGT; also known as SNAP-Tag) to facilitate a site-specific conjugation to the NP surface (Crivat & Taraska, 2012; Hussain et al, 2013).

Interestingly, as most of the commonly used dendrimer therapeutics are non-degradable under physiological conditions, design of biodegradable dendrimers for theranostic applications have come to the fore (Leiro et al, 2015). For instance, degradable polyester dendrimers conjugated to Dox via an acid-labile hydrazone bond show a pH-dependent drug release and alter the drug's pharmacokinetics (Padilla De Jesus et al, 2002). Another example is the encapsulation of highly hydrophobic drugs such as camptothecins into dendritic structures that was established using biocompatible polyester dendrimers composed of glycerol and succinic acid (Morgan et al, 2006).

5 CONCLUSION AND OUTLOOK

The dissertation presented here focuses on the interaction of nanoparticles with HeLa cells. Two aspects of nanoparticle interaction with these cells were studied: firstly, we evaluated potential consequences of a SiNP-treatment for health and safety and secondly, we monitored drug release from a FRET-based theranostic macromolecular prodrug in real time.

The investigation of SiNP-interaction with cells in the first part demonstrates that positively charged SiNPs enter HeLa cells mainly via dynamin 2-dependent caveolin-mediated endocytosis. SiNPs accumulate in lysosomes over extended periods of time causing severe lysosomal dysfunction. This conclusion is based on the evidence that LC3- and p62-positive autophagosomes accumulate and apparently fail to undergo lysosomal degradation in SiNP-filled cells. While endosomal recycling proceeds unperturbed in these cells, internalized growth factors accumulate in late endosomes indicating that SiNP-induced alterations specifically affect degradative sorting. Failed lysosomal proteolysis of EGF and autophagosomal substrates does not result from altered mTOR signaling, elevated intralysosomal pH, general damage of lysosomal membranes, or inhibition of lysosomal protease activity. We assume that SiNP-loaded lysosomes fail to undergo fusion with late endosomes and autophagosomes as a spatial segregation of non-degraded EGF or p62 and lysosomal proteases is observed. Given that lysosomal function is crucial for many aspects of cell physiology, most notably the clearance of aggregated or otherwise malfunctional proteins, we hypothesize that the adverse effects of SiNP-treatment are a direct consequence of lysosomal dysfunction.

Next experimental steps would include further *in vitro* studies such as the investigation of ROS production, inflammatory responses, or apoptosis. Also, the question whether chronic cell damage occurs upon longtime exposure with SiNPs remains to be answered. Interestingly, a study investigating the effects of NP-treatment on the cell cycle has shown that internalized NPs (assuming that exocytosis is negligible) are distributed between the daughter cells. This ‘NP dilution effect’ will likely be enhanced in rapidly dividing tumour cells resulting in a re-consideration of the potential use of NPs as drug carriers (Kim J. A. et al, 2012). As autophagy has been linked to a variety of diseases (see chapter 1.3.3), it would be highly interesting to elucidate whether SiNPs potentiate the adverse effects caused by malfunctioning autophagy. *In vivo* studies in various organisms have shown opposite health effects upon treatment with silica nanoparticles (see chapter 1.3.3). SiNPs

seem not to penetrate skin (Ostrowski et al, 2014), whereas uptake and potential health effects caused by SiNPs upon oral or pulmonary administration still need to be elucidated.

In the second part, we explore a novel approach to monitor intracellular drug release from a TMP. We demonstrate that the Dox fluorescence is quenched via FRET, through the attachment of an acceptor dye in close proximity. Upon intracellular cleavage of the hydrazone bond Dox becomes fluorescent and cytotoxic (Krüger et al, 2014). This probe not only allows monitoring drug release and translocation to the nucleus, but also enables direct tracking of the nanocarrier in real time. Using such a system could help to quickly obtain important intracellular parameters possibly leading toward an improvement of the prodrug performance. Such a delivery system can also be equipped with an immunoconjugate that specifically targets and kills cancer cells (Fang et al, 2014; Hussain et al, 2013; Parodi et al, 2013). A sustainable approach of such drug delivery systems would be the use of biodegradable materials for the development of theranostics (Perner-Nochta et al, 2009).

The development of novel systems in the field of nanotechnology is currently undergoing an impressive expansion. However, most research efforts have been dedicated to their applicability, rather than environmental health and safety issues. As a consequence the assessment of potential nanomaterial-related risks must be accurately conducted. Toxicological studies must not only include a comprehensive physicochemical characterization of the nanoparticle (e.g. size, surface area, surface charge), but also the consideration of potential routes of exposure (e.g. lung, gastrointestinal tract, skin), a justification of nanoparticle concentrations, and importantly inclusion of benchmark controls.

6 BIBLIOGRAPHY

Abe N., Inoue T., Galvez T., Klein L. and Meyer T. (2008). Dissecting the role of PtdIns(4,5)P2 in endocytosis and recycling of the transferrin receptor. *Journal of cell science* **121:** 1488-1494

Affentranger S., Martinelli S., Hahn J., Rossy J. and Niggli V. (2011). Dynamic reorganization of flotillins in chemokine-stimulated human T-lymphocytes. *BMC cell biology* **12:** 28

Ahmad J., Ahamed M., Akhtar M.J., Alrokayan S.A., Siddiqui M.A. et al (2012). Apoptosis induction by silica nanoparticles mediated through reactive oxygen species in human liver cell line HepG2. *Toxicology and applied pharmacology* **259:** 160-168

Aisen P. (2004). Transferrin receptor 1. *The international journal of biochemistry & cell biology* **36:** 2137-2143

Akinc A., Thomas M., Klibanov A.M. and Langer R. (2005). Exploring polyethylenimine-mediated DNA transfection and the proton sponge hypothesis. *The journal of gene medicine* **7:** 657-663

Al-Jamal W.T., Al-Jamal K.T., Tian B., Lacerda L., Bomans P.H. et al (2008). Lipid-quantum dot bilayer vesicles enhance tumor cell uptake and retention in vitro and in vivo. *ACS nano* **2:** 408-418

Al-Rawi M., Diabate S. and Weiss C. (2011). Uptake and intracellular localization of submicron and nano-sized SiO(2) particles in HeLa cells. *Archives of toxicology* **85:** 813-826

Al Rawi S., Louvet-Vallee S., Djeddi A., Sachse M., Culetto E. et al (2011). Postfertilization autophagy of sperm organelles prevents paternal mitochondrial DNA transmission. *Science* **334:** 1144-1147

Alers S., Löffler A.S., Wesselborg S. and Stork B. (2012). Role of AMPK-mTOR-Ulk1/2 in the regulation of autophagy: cross talk, shortcuts, and feedbacks. *Molecular and cellular biology* **32:** 2-11

Alwan H.A. and van Leeuwen J.E. (2007). UBPY-mediated epidermal growth factor receptor (EGFR) de-ubiquitination promotes EGFR degradation. *The Journal of biological chemistry* **282:** 1658-1669

Alwan H.A., van Zoelen E.J. and van Leeuwen J.E. (2003). Ligand-induced lysosomal epidermal growth factor receptor (EGFR) degradation is preceded by proteasome-dependent EGFR de-ubiquitination. *The Journal of biological chemistry* **278:** 35781-35790

Amaravadi R.K., Lippincott-Schwartz J., Yin X.M., Weiss W.A., Takebe N. et al (2011). Principles and current strategies for targeting autophagy for cancer treatment. *Clinical cancer research : an official journal of the American Association for Cancer Research* **17:** 654-666

Ambrogio M.W., Thomas C.R., Zhao Y.L., Zink J.I. and Stoddart J.F. (2011). Mechanized silica nanoparticles: a new frontier in theranostic nanomedicine. *Accounts of chemical research* **44:** 903-913

Andrejewski N., Punnonen E.L., Guhde G., Tanaka Y., Lullmann-Rauch R. et al (1999). Normal lysosomal morphology and function in LAMP-1-deficient mice. *The Journal of biological chemistry* **274:** 12692-12701

Andrews N.W. (2000). Regulated secretion of conventional lysosomes. *Trends in cell biology* **10:** 316-321

Ascenzi P., Bocedi A., Heptonstall J., Capobianchi M.R., Di Caro A. et al (2008). Ebolavirus and Marburgvirus: insight the Filoviridae family. *Molecular aspects of medicine* **29:** 151-185

Asenath-Smith E. and Chen W. (2008). How to prevent the loss of surface functionality derived from aminosilanes. *Langmuir : the ACS journal of surfaces and colloids* **24:** 12405-12409

Asterholm I.W., Mundy D.I., Weng J., Anderson R.G. and Scherer P.E. (2012). Altered mitochondrial function and metabolic inflexibility associated with loss of caveolin-1. *Cell metabolism* **15:** 171-185

Axe E.L., Walker S.A., Manifava M., Chandra P., Roderick H.L. et al (2008). Autophagosome formation from membrane compartments enriched in phosphatidylinositol 3-phosphate and dynamically connected to the endoplasmic reticulum. *The Journal of cell biology* **182:** 685-701

Babst M., Odorizzi G., Estepa E.J. and Emr S.D. (2000). Mammalian tumor susceptibility gene 101 (TSG101) and the yeast homologue, Vps23p, both function in late endosomal trafficking. *Traffic* **1:** 248-258

Bache K.G., Raiborg C., Mehlum A. and Stenmark H. (2003). STAM and Hrs are subunits of a multivalent ubiquitin-binding complex on early endosomes. *The Journal of biological chemistry* **278:** 12513-12521

Ballabio A. and Gieselmann V. (2009). Lysosomal disorders: from storage to cellular damage. *Biochimica et biophysica acta* **1793:** 684-696

Baltazar G.C., Guha S., Lu W., Lim J., Boesze-Battaglia K. et al (2012). Acidic nanoparticles are trafficked to lysosomes and restore an acidic lysosomal pH and degradative function to compromised ARPE-19 cells. *PloS one* **7:** e49635

Barandeh F., Nguyen P.L., Kumar R., Iacobucci G.J., Kuznicki M.L. et al (2012). Organically modified silica nanoparticles are biocompatible and can be targeted to neurons in vivo. *PloS one* **7:** e29424

Bargal R., Avidan N., Ben-Asher E., Olender Z., Zeigler M. et al (2000). Identification of the gene causing mucolipidosis type IV. *Nature genetics* **26:** 118-123

Barik T.K., Sahu B. and Swain V. (2008). Nanosilica-from medicine to pest control. *Parasitology research* **103:** 253-258

Bauer S. and Kaltenbrunner M. (2014). Built to disappear. *ACS nano* **8:** 5380-5382

Behnia R. and Munro S. (2005). Organelle identity and the signposts for membrane traffic. *Nature* **438:** 597-604

Benesch S., Polo S., Lai F.P., Anderson K.I., Stradal T.E. et al (2005). N-WASP deficiency impairs EGF internalization and actin assembly at clathrin-coated pits. *Journal of cell science* **118:** 3103-3115

Berlin I., Schwartz H. and Nash P.D. (2010). Regulation of epidermal growth factor receptor ubiquitination and trafficking by the USP8.STAM complex. *The Journal of biological chemistry* **285:** 34909-34921

Bishop N., Horman A. and Woodman P. (2002). Mammalian class E vps proteins recognize ubiquitin and act in the removal of endosomal protein-ubiquitin conjugates. *The Journal of cell biology* **157:** 91-101

Bocking T., Aguet F., Harrison S.C. and Kirchhausen T. (2011). Single-molecule analysis of a molecular disassemblase reveals the mechanism of Hsc70-driven clathrin uncoating. *Nature structural & molecular biology* **18:** 295-301

Boettner D.R., Chi R.J. and Lemmon S.K. (2012). Lessons from yeast for clathrin-mediated endocytosis. *Nature cell biology* **14:** 2-10

Bohmer N. and Jordan A. (2015). Caveolin-1 and CDC42 mediated endocytosis of silica-coated iron oxide nanoparticles in HeLa cells. *Beilstein journal of nanotechnology* **6:** 167-176

Bonifacino J.S. and Hurley J.H. (2008). Retromer. *Current opinion in cell biology* **20:** 427-436

Boya P., Reggiori F. and Codogno P. (2013). Emerging regulation and functions of autophagy. *Nature cell biology* **15:** 713-720

Bradford M.M. (1976). A rapid and sensitive method for the quantitation of microgram quantities of protein utilizing the principle of protein-dye binding. *Analytical biochemistry* **72:** 248-254

Brandt D.T., Marion S., Griffiths G., Watanabe T., Kaibuchi K. et al (2007). Dia1 and IQGAP1 interact in cell migration and phagocytic cup formation. *The Journal of cell biology* **178:** 193-200

Braulke T. and Bonifacino J.S. (2009). Sorting of lysosomal proteins. *Biochimica et biophysica acta* **1793:** 605-614

Breen M.R., Camps M., Carvalho-Simoes F., Zorzano A. and Pilch P.F. (2012). Cholesterol depletion in adipocytes causes caveolae collapse concomitant with proteosomal degradation of cavin-2 in a switch-like fashion. *PloS one* **7:** e34516

Brodsky F.M. (2012). Diversity of clathrin function: new tricks for an old protein. *Annual review of cell and developmental biology* **28:** 309-336

Brown M.D. and Sacks D.B. (2006). IQGAP1 in cellular signaling: bridging the GAP. *Trends in cell biology* **16:** 242-249

Calderón M., Quadir M.A., Sharma S.K. and Haag R. (2010). Dendritic polyglycerols for biomedical applications. *Advanced materials* **22:** 190-218

Calderón M., Welker P., Licha K., Fichtner I., Graeser R. et al (2011). Development of efficient acid cleavable multifunctional prodrugs derived from dendritic polyglycerol with a

poly(ethylene glycol) shell. *Journal of controlled release : official journal of the Controlled Release Society* **151:** 295-301

Campellone K.G. and Welch M.D. (2010). A nucleator arms race: cellular control of actin assembly. *Nature reviews Molecular cell biology* **11:** 237-251

Cang C., Zhou Y., Navarro B., Seo Y.J., Aranda K. et al (2013). mTOR regulates lysosomal ATP-sensitive two-pore Na(+) channels to adapt to metabolic state. *Cell* **152:** 778-790

Canton I. and Battaglia G. (2012). Endocytosis at the nanoscale. *Chemical Society reviews* **41:** 2718-2739

Cao H., Orth J.D., Chen J., Weller S.G., Heuser J.E. et al (2003). Cortactin is a component of clathrin-coated pits and participates in receptor-mediated endocytosis. *Molecular and cellular biology* **23:** 2162-2170

Carcea I., Ma'ayan A., Mesias R., Sepulveda B., Salton S.R. et al (2010). Flotillin-mediated endocytic events dictate cell type-specific responses to semaphorin 3A. *The Journal of neuroscience : the official journal of the Society for Neuroscience* **30:** 15317-15329

Carstea E.D., Morris J.A., Coleman K.G., Loftus S.K., Zhang D. et al (1997). Niemann-Pick C1 disease gene: homology to mediators of cholesterol homeostasis. *Science* **277:** 228-231

Champion J.A. and Mitragotri S. (2006). Role of target geometry in phagocytosis. *Proceedings of the National Academy of Sciences of the United States of America* **103:** 4930-4934

Chan E.Y., Kir S. and Tooze S.A. (2007). siRNA screening of the kinome identifies ULK1 as a multidomain modulator of autophagy. *The Journal of biological chemistry* **282:** 25464-25474

Chao W.T. and Kunz J. (2009). Focal adhesion disassembly requires clathrin-dependent endocytosis of integrins. *FEBS letters* **583:** 1337-1343

Chapman S., Dobrovolskaia M., Farahani K., Goodwin A., Joshi A. et al (2013). Nanoparticles for cancer imaging: The good, the bad, and the promise. *Nano today* **8:** 454-460

Chaudhuri A., Battaglia G. and Golestanian R. (2011). The effect of interactions on the cellular uptake of nanoparticles. *Physical biology* **8:** 046002

Chen K.J., Chiu Y.L., Chen Y.M., Ho Y.C. and Sung H.W. (2011). Intracellularly monitoring/imaging the release of doxorubicin from pH-responsive nanoparticles using Forster resonance energy transfer. *Biomaterials* **32:** 2586-2592

Chen M. and von Mikecz A. (2005). Formation of nucleoplasmic protein aggregates impairs nuclear function in response to SiO2 nanoparticles. *Experimental cell research* **305:** 51-62

Cheng Z., Al Zaki A., Hui J.Z., Muzykantov V.R. and Tsourkas A. (2012). Multifunctional nanoparticles: cost versus benefit of adding targeting and imaging capabilities. *Science* **338:** 903-910

Chernousova S. and Epple M. (2013). Silver as antibacterial agent: ion, nanoparticle, and metal. *Angewandte Chemie* **52:** 1636-1653

Chithrani B.D. and Chan W.C. (2007). Elucidating the mechanism of cellular uptake and removal of protein-coated gold nanoparticles of different sizes and shapes. *Nano letters* **7:** 1542-1550

Chithrani B.D., Ghazani A.A. and Chan W.C. (2006). Determining the size and shape dependence of gold nanoparticle uptake into mammalian cells. *Nano letters* **6:** 662-668

Cho E.C., Xie J., Wurm P.A. and Xia Y. (2009). Understanding the role of surface charges in cellular adsorption versus internalization by selectively removing gold nanoparticles on the cell surface with a I2/KI etchant. *Nano letters* **9:** 1080-1084

Choi W.I., Kim J.Y., Kang C., Byeon C.C., Kim Y.H. et al (2011). Tumor regression in vivo by photothermal therapy based on gold-nanorod-loaded, functional nanocarriers. *ACS nano* **5:** 1995-2003

Chou L.Y., Ming K. and Chan W.C. (2011). Strategies for the intracellular delivery of nanoparticles. *Chemical Society reviews* **40:** 233-245

Chu Z., Huang Y., Tao Q. and Li Q. (2011). Cellular uptake, evolution, and excretion of silica nanoparticles in human cells. *Nanoscale* **3:** 3291-3299

Clague M.J. and Urbe S. (2006). Endocytosis: the DUB version. *Trends in cell biology* **16:** 551-559

Claus V., Jahraus A., Tjelle T., Berg T., Kirschke H. et al (1998). Lysosomal enzyme trafficking between phagosomes, endosomes, and lysosomes in J774 macrophages. Enrichment of cathepsin H in early endosomes. *The Journal of biological chemistry* **273:** 9842-9851

Collins A., Warrington A., Taylor K.A. and Svitkina T. (2011). Structural organization of the actin cytoskeleton at sites of clathrin-mediated endocytosis. *Current biology : CB* **21:** 1167-1175

Collins B.M., Davis M.J., Hancock J.F. and Parton R.G. (2012). Structure-based reassessment of the caveolin signaling model: do caveolae regulate signaling through caveolin-protein interactions? *Developmental cell* **23:** 11-20

Collins B.M., McCoy A.J., Kent H.M., Evans P.R. and Owen D.J. (2002). Molecular architecture and functional model of the endocytic AP2 complex. *Cell* **109:** 523-535

Conner S.D. and Schmid S.L. (2003). Regulated portals of entry into the cell. *Nature* **422:** 37-44

Conus S. and Simon H.U. (2008). Cathepsins: key modulators of cell death and inflammatory responses. *Biochemical pharmacology* **76:** 1374-1382

Correia J.J. (1991). Effects of antimitotic agents on tubulin-nucleotide interactions. *Pharmacology & therapeutics* **52:** 127-147

Couleaud P., Morosini V., Frochot C., Richeter S., Raehm L. et al (2010). Silica-based nanoparticles for photodynamic therapy applications. *Nanoscale* **2:** 1083-1095

Cox T.M. and Cachon-Gonzalez M.B. (2012). The cellular pathology of lysosomal diseases. *The Journal of pathology* **226:** 241-254

Cremona O., Di Paolo G., Wenk M.R., Luthi A., Kim W.T. et al (1999). Essential role of phosphoinositide metabolism in synaptic vesicle recycling. *Cell* **99:** 179-188

Crivat G. and Taraska J.W. (2012). Imaging proteins inside cells with fluorescent tags. *Trends in biotechnology* **30:** 8-16

Cuervo A.M. (2008). Autophagy and aging: keeping that old broom working. *Trends in genetics : TIG* **24:** 604-612

Cureton D.K., Massol R.H., Saffarian S., Kirchhausen T.L. and Whelan S.P. (2009). Vesicular stomatitis virus enters cells through vesicles incompletely coated with clathrin that depend upon actin for internalization. *PLoS pathogens* **5:** e1000394

Damm E.M., Pelkmans L., Kartenbeck J., Mezzacasa A., Kurzchalia T. et al (2005). Clathrin- and caveolin-1-independent endocytosis: entry of simian virus 40 into cells devoid of caveolae. *The Journal of cell biology* **168:** 477-488

Das M., Saxena N. and Dwivedi P.D. (2009). Emerging trends of nanoparticles application in food technology: Safety paradigms. *Nanotoxicology* **3:** 10-18

Dasgupta S., Auth T. and Gompper G. (2014). Shape and orientation matter for the cellular uptake of nonspherical particles. *Nano letters* **14:** 687-693

Daumke O., Lundmark R., Vallis Y., Martens S., Butler P.J. et al (2007). Architectural and mechanistic insights into an EHD ATPase involved in membrane remodelling. *Nature* **449:** 923-927

Dausend J., Musyanovych A., Dass M., Walther P., Schrezenmeier H. et al (2008). Uptake mechanism of oppositely charged fluorescent nanoparticles in HeLa cells. *Macromolecular bioscience* **8:** 1135-1143

Dekkers S., Krystek P., Peters R.J., Lankveld D.P., Bokkers B.G. et al (2011). Presence and risks of nanosilica in food products. *Nanotoxicology* **5:** 393-405

Deneka M., Neeft M., Popa I., van Oort M., Sprong H. et al (2003). Rabaptin-5alpha/rabaptin-4 serves as a linker between rab4 and gamma(1)-adaptin in membrane recycling from endosomes. *The EMBO journal* **22:** 2645-2657

Dhal P.K., Polomoscanik S.C., Avila L.Z., Holmes-Farley S.R. and Miller R.J. (2009). Functional polymers as therapeutic agents: concept to market place. *Advanced drug delivery reviews* **61:** 1121-1130

Dietzen D.J., Hastings W.R. and Lublin D.M. (1995). Caveolin is palmitoylated on multiple cysteine residues. Palmitoylation is not necessary for localization of caveolin to caveolae. *The Journal of biological chemistry* **270:** 6838-6842

Dobbins J.T., 3rd, Ergun D.L., Rutz L., Hinshaw D.A., Blume H. et al (1995). DQE(f) of four generations of computed radiography acquisition devices. *Medical physics* **22:** 1581-1593

Docter D., Bantz C., Westmeier D., Galla H.J., Wang Q. et al (2014). The protein corona protects against size- and dose-dependent toxicity of amorphous silica nanoparticles. *Beilstein journal of nanotechnology* **5:** 1380-1392

Doherty G.J. and McMahon H.T. (2008). Mediation, modulation, and consequences of membrane-cytoskeleton interactions. *Annual review of biophysics* **37:** 65-95

Doherty G.J. and McMahon H.T. (2009). Mechanisms of endocytosis. *Annual review of biochemistry* **78:** 857-902

Dolnik O., Kolesnikova L. and Becker S. (2008). Filoviruses: Interactions with the host cell. *Cellular and molecular life sciences : CMLS* **65:** 756-776

Dong M., Richards D.A., Goodnough M.C., Tepp W.H., Johnson E.A. et al (2003). Synaptotagmins I and II mediate entry of botulinum neurotoxin B into cells. *The Journal of cell biology* **162:** 1293-1303

Dong X.P., Cheng X., Mills E., Delling M., Wang F. et al (2008). The type IV mucolipidosis-associated protein TRPML1 is an endolysosomal iron release channel. *Nature* **455:** 992-996

Duan J., Yu Y., Shi H., Tian L., Guo C. et al (2013). Toxic effects of silica nanoparticles on zebrafish embryos and larvae. *PloS one* **8:** e74606

Duan J., Yu Y., Yu Y., Li Y., Huang P. et al (2014). Silica nanoparticles enhance autophagic activity, disturb endothelial cell homeostasis and impair angiogenesis. *Particle and fibre toxicology* **11:** 50

Dulhunty A.F. and Franzini-Armstrong C. (1975). The relative contributions of the folds and caveolae to the surface membrane of frog skeletal muscle fibres at different sarcomere lengths. *The Journal of physiology* **250:** 513-539

Duncan R. (2003). The dawning era of polymer therapeutics. *Nature reviews Drug discovery* **2:** 347-360

Duncan R. and Vicent M.J. (2010). Do HPMA copolymer conjugates have a future as clinically useful nanomedicines? A critical overview of current status and future opportunities. *Advanced drug delivery reviews* **62:** 272-282

Duncan R. and Vicent M.J. (2013). Polymer therapeutics-prospects for 21st century: the end of the beginning. *Advanced drug delivery reviews* **65:** 60-70

Dwivedi P.D., Misra A., Shanker R. and Das M. (2009). Are nanomaterials a threat to the immune system? *Nanotoxicology* **3:** 19-26

Echarri A., Muriel O., Pavon D.M., Azegrouz H., Escolar F. et al (2012). Caveolar domain organization and trafficking is regulated by Abl kinases and mDia1. *Journal of cell science* **125:** 3097-3113

Edelstein A., Amodaj N., Hoover K., Vale R. and Stuurman N. (2010). Computer control of microscopes using microManager. *Current protocols in molecular biology / edited by Frederick M Ausubel [et al]* **Chapter 14:** Unit14 20

El-Sayed A. and Harashima H. (2013). Endocytosis of gene delivery vectors: from clathrin-dependent to lipid raft-mediated endocytosis. *Molecular therapy : the journal of the American Society of Gene Therapy* **21:** 1118-1130

Errico A. (2013). New technology: nanotechnology targets cancer cells. *Nature reviews Clinical oncology* **10:** 667

Escola J.M., Kleijmeer M.J., Stoorvogel W., Griffith J.M., Yoshie O. et al (1998). Selective enrichment of tetraspan proteins on the internal vesicles of multivesicular endosomes and on exosomes secreted by human B-lymphocytes. *The Journal of biological chemistry* **273:** 20121-20127

Etienne-Manneville S. (2013). Microtubules in cell migration. *Annual review of cell and developmental biology* **29:** 471-499

Ewers H., Romer W., Smith A.E., Bacia K., Dmitrieff S. et al (2010). GM1 structure determines SV40-induced membrane invagination and infection. *Nature cell biology* **12:** 11-18; sup pp 11-12

Ezratty E.J., Bertaux C., Marcantonio E.E. and Gundersen G.G. (2009). Clathrin mediates integrin endocytosis for focal adhesion disassembly in migrating cells. *The Journal of cell biology* **187:** 733-747

Ezratty E.J., Partridge M.A. and Gundersen G.G. (2005). Microtubule-induced focal adhesion disassembly is mediated by dynamin and focal adhesion kinase. *Nature cell biology* **7:** 581-590

Faelber K., Posor Y., Gao S., Held M., Roske Y. et al (2011). Crystal structure of nucleotide-free dynamin. *Nature* **477:** 556-560

Fang R.H., Hu C.M., Luk B.T., Gao W., Copp J.A. et al (2014). Cancer cell membrane-coated nanoparticles for anticancer vaccination and drug delivery. *Nano letters* **14:** 2181-2188

Ferguson K.M., Berger M.B., Mendrola J.M., Cho H.S., Leahy D.J. et al (2003). EGF activates its receptor by removing interactions that autoinhibit ectodomain dimerization. *Molecular cell* **11:** 507-517

Ferguson S.M., Raimondi A., Paradise S., Shen H., Mesaki K. et al (2009). Coordinated actions of actin and BAR proteins upstream of dynamin at endocytic clathrin-coated pits. *Developmental cell* **17:** 811-822

Fernandez-Rojo M.A., Restall C., Ferguson C., Martel N., Martin S. et al (2012). Caveolin-1 orchestrates the balance between glucose and lipid-dependent energy metabolism: implications for liver regeneration. *Hepatology* **55:** 1574-1584

Ferrari M. (2008). Nanogeometry: beyond drug delivery. *Nature nanotechnology* **3:** 131-132

Fisichella M., Dabboue H., Bhattacharyya S., Saboungi M.L., Salvetat J.P. et al (2009). Mesoporous silica nanoparticles enhance MTT formazan exocytosis in HeLa cells and astrocytes. *Toxicology in vitro : an international journal published in association with BIBRA* **23:** 697-703

Flannery A.R., Czibener C. and Andrews N.W. (2010). Palmitoylation-dependent association with CD63 targets the Ca2+ sensor synaptotagmin VII to lysosomes. *The Journal of cell biology* **191:** 599-613

Fleming M.D., Romano M.A., Su M.A., Garrick L.M., Garrick M.D. et al (1998). Nramp2 is mutated in the anemic Belgrade (b) rat: evidence of a role for Nramp2 in endosomal iron transport. *Proceedings of the National Academy of Sciences of the United States of America* **95:** 1148-1153

Förster T. (1948). Zwischenmolekulare Energiewanderung und Fluoreszenz. *Annalen der Physik* **6:** 2

Ford M.G., Mills I.G., Peter B.J., Vallis Y., Praefcke G.J. et al (2002). Curvature of clathrin-coated pits driven by epsin. *Nature* **419:** 361-366

Forgac M. (2007). Vacuolar ATPases: rotary proton pumps in physiology and pathophysiology. *Nature reviews Molecular cell biology* **8:** 917-929

Frick M., Bright N.A., Riento K., Bray A., Merrified C. et al (2007). Coassembly of flotillins induces formation of membrane microdomains, membrane curvature, and vesicle budding. *Current biology : CB* **17:** 1151-1156

Fröhlich E. (2012). The role of surface charge in cellular uptake and cytotoxicity of medical nanoparticles. *International journal of nanomedicine* **7:** 5577-5591

Fujita A., Cheng J., Tauchi-Sato K., Takenawa T. and Fujimoto T. (2009). A distinct pool of phosphatidylinositol 4,5-bisphosphate in caveolae revealed by a nanoscale labeling technique. *Proceedings of the National Academy of Sciences of the United States of America* **106:** 9256-9261

Futerman A.H. and van Meer G. (2004). The cell biology of lysosomal storage disorders. *Nature reviews Molecular cell biology* **5:** 554-565

Galvez T., Gilleron J., Zerial M. and O'Sullivan G.A. (2012). SnapShot: Mammalian Rab proteins in endocytic trafficking. *Cell* **151:** 234-234 e232

Gan Q., Dai D., Yuan Y., Qian J., Sha S. et al (2012). Effect of size on the cellular endocytosis and controlled release of mesoporous silica nanoparticles for intracellular delivery. *Biomedical microdevices* **14:** 259-270

Gao H., Yang Z., Zhang S., Cao S., Shen S. et al (2013). Ligand modified nanoparticles increases cell uptake, alters endocytosis and elevates glioma distribution and internalization. *Scientific reports* **3:** 2534

Geng J. and Klionsky D.J. (2008). The Atg8 and Atg12 ubiquitin-like conjugation systems in macroautophagy. 'Protein modifications: beyond the usual suspects' review series. *EMBO reports* **9:** 859-864

Ghosh P., Dahms N.M. and Kornfeld S. (2003). Mannose 6-phosphate receptors: new twists in the tale. *Nature reviews Molecular cell biology* **4:** 202-212

Gilleron J., Querbes W., Zeigerer A., Borodovsky A., Marsico G. et al (2013). Image-based analysis of lipid nanoparticle-mediated siRNA delivery, intracellular trafficking and endosomal escape. *Nature biotechnology* **31:** 638-646

Glebov O.O., Bright N.A. and Nichols B.J. (2006). Flotillin-1 defines a clathrin-independent endocytic pathway in mammalian cells. *Nature cell biology* **8:** 46-54

Goetz J.G., Minguet S., Navarro-Lerida I., Lazcano J.J., Samaniego R. et al (2011). Biomechanical remodeling of the microenvironment by stromal caveolin-1 favors tumor invasion and metastasis. *Cell* **146:** 148-163

Goh L.K., Huang F., Kim W., Gygi S. and Sorkin A. (2010). Multiple mechanisms collectively regulate clathrin-mediated endocytosis of the epidermal growth factor receptor. *The Journal of cell biology* **189:** 871-883

Graf C., Dembski S., Hofmann A. and Rühl E. (2006). A general method for the controlled embedding of nanoparticles in silica colloids. *Langmuir : the ACS journal of surfaces and colloids* **22:** 5604-5610

Graf C., Gao Q., Schütz I., Noufele C.N., Ruan W. et al (2012). Surface functionalization of silica nanoparticles supports colloidal stability in physiological media and facilitates internalization in cells. *Langmuir : the ACS journal of surfaces and colloids* **28:** 7598-7613

Grant B.D. and Donaldson J.G. (2009). Pathways and mechanisms of endocytic recycling. *Nature reviews Molecular cell biology* **10:** 597-608

Gratton S.E., Ropp P.A., Pohlhaus P.D., Luft J.C., Madden V.J. et al (2008). The effect of particle design on cellular internalization pathways. *Proceedings of the National Academy of Sciences of the United States of America* **105:** 11613-11618

Griffiths G., Hoflack B., Simons K., Mellman I. and Kornfeld S. (1988). The mannose 6-phosphate receptor and the biogenesis of lysosomes. *Cell* **52:** 329-341

Gruenberg J. (2001). The endocytic pathway: a mosaic of domains. *Nature reviews Molecular cell biology* **2:** 721-730

Guha S. and Padh H. (2008). Cathepsins: fundamental effectors of endolysosomal proteolysis. *Indian journal of biochemistry & biophysics* **45:** 75-90

Gupta B., Levchenko T.S. and Torchilin V.P. (2005). Intracellular delivery of large molecules and small particles by cell-penetrating proteins and peptides. *Advanced drug delivery reviews* **57:** 637-651

Gustincich S., Vatta P., Goruppi S., Wolf M., Saccone S. et al (1999). The human serum deprivation response gene (SDPR) maps to 2q32-q33 and codes for a phosphatidylserine-binding protein. *Genomics* **57:** 120-129

Haag R. and Kratz F. (2006). Polymer therapeutics: concepts and applications. *Angewandte Chemie* **45:** 1198-1215

Halamoda Kenzaoui B., Chapuis Bernasconi C., Guney-Ayra S. and Juillerat-Jeanneret L. (2012). Induction of oxidative stress, lysosome activation and autophagy by nanoparticles in human brain-derived endothelial cells. *The Biochemical journal* **441:** 813-821

Hamilton A.J. and Baulcombe D.C. (1999). A species of small antisense RNA in posttranscriptional gene silencing in plants. *Science* **286:** 950-952

Han J. and Burgess K. (2010). Fluorescent indicators for intracellular pH. *Chemical reviews* **110:** 2709-2728

Hanover J.A., Willingham M.C. and Pastan I. (1984). Kinetics of transit of transferrin and epidermal growth factor through clathrin-coated membranes. *Cell* **39:** 283-293

Hansen C.G., Howard G. and Nichols B.J. (2011). Pacsin 2 is recruited to caveolae and functions in caveolar biogenesis. *Journal of cell science* **124:** 2777-2785

Hansen C.G. and Nichols B.J. (2009). Molecular mechanisms of clathrin-independent endocytosis. *Journal of cell science* **122:** 1713-1721

Hansen C.G. and Nichols B.J. (2010). Exploring the caves: cavins, caveolins and caveolae. *Trends in cell biology* **20:** 177-186

Hao X., Wu J., Shan Y., Cai M., Shang X. et al (2012). Caveolae-mediated endocytosis of biocompatible gold nanoparticles in living Hela cells. *Journal of physics Condensed matter : an Institute of Physics journal* **24:** 164207

Harush-Frenkel O., Debotton N., Benita S. and Altschuler Y. (2007). Targeting of nanoparticles to the clathrin-mediated endocytic pathway. *Biochemical and biophysical research communications* **353:** 26-32

Hayer A., Stoeber M., Bissig C. and Helenius A. (2010). Biogenesis of caveolae: stepwise assembly of large caveolin and cavin complexes. *Traffic* **11:** 361-382

Helgeson L.A. and Nolen B.J. (2013). Mechanism of synergistic activation of Arp2/3 complex by cortactin and N-WASP. *eLife* **2:** e00884

Henley J.R., Krueger E.W., Oswald B.J. and McNiven M.A. (1998). Dynamin-mediated internalization of caveolae. *The Journal of cell biology* **141:** 85-99

Henne W.M., Boucrot E., Meinecke M., Evergren E., Vallis Y. et al (2010). FCHo proteins are nucleators of clathrin-mediated endocytosis. *Science* **328:** 1281-1284

Henne W.M., Buchkovich N.J. and Emr S.D. (2011). The ESCRT pathway. *Developmental cell* **21:** 77-91

Herbst R.S. (2004). Review of epidermal growth factor receptor biology. *International journal of radiation oncology, biology, physics* **59:** 21-26

Herd H.L., Malugin A. and Ghandehari H. (2011). Silica nanoconstruct cellular toleration threshold in vitro. *Journal of controlled release : official journal of the Controlled Release Society* **153:** 40-48

Hernandez S.E., Krishnaswami M., Miller A.L. and Koleske A.J. (2004). How do Abl family kinases regulate cell shape and movement? *Trends in cell biology* **14:** 36-44

Herrero M.A., Toma F.M., Al-Jamal K.T., Kostarelos K., Bianco A. et al (2009). Synthesis and characterization of a carbon nanotube-dendron series for efficient siRNA delivery. *Journal of the American Chemical Society* **131:** 9843-9848

Heuser J.E. and Anderson R.G. (1989). Hypertonic media inhibit receptor-mediated endocytosis by blocking clathrin-coated pit formation. *The Journal of cell biology* **108:** 389-400

Hill M.M., Bastiani M., Luetterforst R., Kirkham M., Kirkham A. et al (2008). PTRF-Cavin, a conserved cytoplasmic protein required for caveola formation and function. *Cell* **132:** 113-124

Hill T.A., Gordon C.P., McGeachie A.B., Venn-Brown B., Odell L.R. et al (2009). Inhibition of dynamin mediated endocytosis by the dynoles--synthesis and functional activity of a family of indoles. *Journal of medicinal chemistry* **52:** 3762-3773

Hinrichsen L., Meyerholz A., Groos S. and Ungewickell E.J. (2006). Bending a membrane: how clathrin affects budding. *Proceedings of the National Academy of Sciences of the United States of America* **103:** 8715-8720

Hinshaw J.E. and Schmid S.L. (1995). Dynamin self-assembles into rings suggesting a mechanism for coated vesicle budding. *Nature* **374:** 190-192

Hofmann D., Tenzer S., Bannwarth M.B., Messerschmidt C., Glaser S.F. et al (2014). Mass spectrometry and imaging analysis of nanoparticle-containing vesicles provide a mechanistic insight into cellular trafficking. *ACS nano* **8:** 10077-10088

Holmberg C.G. and Laurell C.B. (1947). Investigations in serum copper; nature of serum copper and its relation to the iron-binding protein in human serum. *Acta chemica Scandinavica* **1:** 944-950

Huang F., Kirkpatrick D., Jiang X., Gygi S. and Sorkin A. (2006). Differential regulation of EGF receptor internalization and degradation by multiubiquitination within the kinase domain. *Molecular cell* **21:** 737-748

Huotari J. and Helenius A. (2011). Endosome maturation. *The EMBO journal* **30:** 3481-3500

Hurley J.H. and Stenmark H. (2011). Molecular mechanisms of ubiquitin-dependent membrane traffic. *Annual review of biophysics* **40:** 119-142

Hussain A.F., Krüger H.R., Kampmeier F., Weissbach T., Licha K. et al (2013). Targeted delivery of dendritic polyglycerol-doxorubicin conjugates by scFv-SNAP fusion protein suppresses EGFR+ cancer cell growth. *Biomacromolecules* **14:** 2510-2520

Hutter E., Boridy S., Labrecque S., Lalancette-Hebert M., Kriz J. et al (2010). Microglial response to gold nanoparticles. *ACS nano* **4:** 2595-2606

Huynh K.K., Eskelinen E.L., Scott C.C., Malevanets A., Saftig P. et al (2007). LAMP proteins are required for fusion of lysosomes with phagosomes. *The EMBO journal* **26:** 313-324

Iler R.K. (1979). The Chemistry of Silica: Solubility, Polymerization, Colloid and Surface Properties and Biochemistry of Silica. Wiley: New York

Ishizaki T., Morishima Y., Okamoto M., Furuyashiki T., Kato T. et al (2001). Coordination of microtubules and the actin cytoskeleton by the Rho effector mDia1. *Nature cell biology* **3:** 8-14

Itakura E., Kishi-Itakura C. and Mizushima N. (2012). The hairpin-type tail-anchored SNARE syntaxin 17 targets to autophagosomes for fusion with endosomes/lysosomes. *Cell* **151:** 1256-1269

Itakura E. and Mizushima N. (2010). Characterization of autophagosome formation site by a hierarchical analysis of mammalian Atg proteins. *Autophagy* **6:** 764-776

Jahn R. and Scheller R.H. (2006). SNAREs--engines for membrane fusion. *Nature reviews Molecular cell biology* **7:** 631-643

Jakhria T., Hellewell A.L., Porter M.Y., Jackson M.P., Tipping K.W. et al (2014). beta2-microglobulin amyloid fibrils are nanoparticles that disrupt lysosomal membrane protein trafficking and inhibit protein degradation by lysosomes. *The Journal of biological chemistry* **289:** 35781-35794

Jandl J.H., Inman J.K., Simmons R.L. and Allen D.W. (1959). Transfer of iron from serum iron-binding protein to human reticulocytes. *The Journal of clinical investigation* **38:** 161-185

Jensen J.P., Bates P.W., Yang M., Vierstra R.D. and Weissman A.M. (1995). Identification of a family of closely related human ubiquitin conjugating enzymes. *The Journal of biological chemistry* **270:** 30408-30414

Jiang W., Kim B.Y., Rutka J.T. and Chan W.C. (2008). Nanoparticle-mediated cellular response is size-dependent. *Nature nanotechnology* **3:** 145-150

Johansen T. and Lamark T. (2011). Selective autophagy mediated by autophagic adapter proteins. *Autophagy* **7:** 279-296

Kaksonen M., Sun Y. and Drubin D.G. (2003). A pathway for association of receptors, adaptors, and actin during endocytic internalization. *Cell* **115:** 475-487

Kasper D., Planells-Cases R., Fuhrmann J.C., Scheel O., Zeitz O. et al (2005). Loss of the chloride channel ClC-7 leads to lysosomal storage disease and neurodegeneration. *The EMBO journal* **24:** 1079-1091

Kaufmann A., Beier V., Franquelim H.G. and Wollert T. (2014). Molecular mechanism of autophagic membrane-scaffold assembly and disassembly. *Cell* **156:** 469-481

Kaushik S. and Cuervo A.M. (2012). Chaperone-mediated autophagy: a unique way to enter the lysosome world. *Trends in cell biology* **22:** 407-417

Ke J.H., Lin J.J., Carey J.R., Chen J.S., Chen C.Y. et al (2010). A specific tumor-targeting magnetofluorescent nanoprobe for dual-modality molecular imaging. *Biomaterials* **31:** 1707-1715

Kelkar S.S. and Reineke T.M. (2011). Theranostics: combining imaging and therapy. *Bioconjugate chemistry* **22:** 1879-1903

Ketelson H.A., Brook M.A. and Pelton R.H. (1995). Sterically stabilized silica colloids: Radical grafting of poly(methylmethacrylate) and hydrosilylative grafting of silicones to functionalized silica. *Polymers for Advanced Technologies* **6:** 335-344

Khan M.I., Mohammad A., Patil G., Naqvi S.A., Chauhan L.K. et al (2012). Induction of ROS, mitochondrial damage and autophagy in lung epithelial cancer cells by iron oxide nanoparticles. *Biomaterials* **33:** 1477-1488

Khandare J., Calderón M., Dagia N.M. and Haag R. (2012). Multifunctional dendritic polymers in nanomedicine: opportunities and challenges. *Chemical Society reviews* **41:** 2824-2848

Kim C.S., Duncan B., Creran B. and Rotello V.M. (2013). Triggered Nanoparticles as Therapeutics. *Nano today* **8:** 439-447

Kim J., Kundu M., Viollet B. and Guan K.L. (2011). AMPK and mTOR regulate autophagy through direct phosphorylation of Ulk1. *Nature cell biology* **13:** 132-141

Kim J.A., Aberg C., Salvati A. and Dawson K.A. (2012). Role of cell cycle on the cellular uptake and dilution of nanoparticles in a cell population. *Nature nanotechnology* **7:** 62-68

Kimura S., Noda T. and Yoshimori T. (2007). Dissection of the autophagosome maturation process by a novel reporter protein, tandem fluorescent-tagged LC3. *Autophagy* **3:** 452-460

Kinchen J.M. and Ravichandran K.S. (2010). Identification of two evolutionarily conserved genes regulating processing of engulfed apoptotic cells. *Nature* **464:** 778-782

Kirkham M. and Parton R.G. (2005). Clathrin-independent endocytosis: new insights into caveolae and non-caveolar lipid raft carriers. *Biochimica et biophysica acta* **1746:** 349-363

Klionsky D.J., Abdalla F.C., Abeliovich H., Abraham R.T., Acevedo-Arozena A. et al (2012). Guidelines for the use and interpretation of assays for monitoring autophagy. *Autophagy* **8:** 445-544

Knauer S.K. and Stauber R.H. (2009). Kontroverse im „Nanohype“: Nanopartikel - Freund oder Feind? *Deutsche Zeitung für Klinische Forschung (DZKF) – Nanotechnologie* **5/6**-2009

Koblinski J.E., Ahram M. and Sloane B.F. (2000). Unraveling the role of proteases in cancer. *Clinica chimica acta; international journal of clinical chemistry* **291:** 113-135

Komatsu M. and Ichimura Y. (2010). Physiological significance of selective degradation of p62 by autophagy. *FEBS letters* **584:** 1374-1378

Komatsu M., Waguri S., Ueno T., Iwata J., Murata S. et al (2005). Impairment of starvation-induced and constitutive autophagy in Atg7-deficient mice. *The Journal of cell biology* **169:** 425-434

Krüger H.R., Schütz I., Justies A., Licha K., Welker P. et al (2014). Imaging of doxorubicin release from theranostic macromolecular prodrugs via fluorescence resonance energy transfer. *Journal of controlled release : official journal of the Controlled Release Society* **194:** 189-196

Kuma A., Hatano M., Matsui M., Yamamoto A., Nakaya H. et al (2004). The role of autophagy during the early neonatal starvation period. *Nature* **432:** 1032-1036

Laemmli U.K. (1970). Cleavage of structural proteins during the assembly of the head of bacteriophage T4. *Nature* **227:** 680-685

Lakadamyali M., Rust M.J. and Zhuang X. (2006). Ligands for clathrin-mediated endocytosis are differentially sorted into distinct populations of early endosomes. *Cell* **124:** 997-1009

Lamark T. and Johansen T. (2012). Aggrephagy: selective disposal of protein aggregates by macroautophagy. *International journal of cell biology* **2012:** 736905

Lamb C.A., Yoshimori T. and Tooze S.A. (2013). The autophagosome: origins unknown, biogenesis complex. *Nature reviews Molecular cell biology* **14:** 759-774

Langhorst M.F., Solis G.P., Hannbeck S., Plattner H. and Stuermer C.A. (2007). Linking membrane microdomains to the cytoskeleton: regulation of the lateral mobility of reggie-1/flotillin-2 by interaction with actin. *FEBS letters* **581:** 4697-4703

Laplante M. and Sabatini D.M. (2012). mTOR signaling in growth control and disease. *Cell* **149:** 274-293

Lee H., Lytton-Jean A.K., Chen Y., Love K.T., Park A.I. et al (2012a). Molecularly self-assembled nucleic acid nanoparticles for targeted in vivo siRNA delivery. *Nature nanotechnology* **7:** 389-393

Lee J., Giordano S. and Zhang J. (2012b). Autophagy, mitochondria and oxidative stress: cross-talk and redox signalling. *The Biochemical journal* **441:** 523-540

Lee J., Twomey M., Machado C., Gomez G., Doshi M. et al (2013). Caveolae-mediated endocytosis of conjugated polymer nanoparticles. *Macromolecular bioscience* **13:** 913-920

Lee J.H., Jang J.T., Choi J.S., Moon S.H., Noh S.H. et al (2011). Exchange-coupled magnetic nanoparticles for efficient heat induction. *Nature nanotechnology* **6:** 418-422

Lee J.H., Yu W.H., Kumar A., Lee S., Mohan P.S. et al (2010). Lysosomal proteolysis and autophagy require presenilin 1 and are disrupted by Alzheimer-related PS1 mutations. *Cell* **141:** 1146-1158

Leiro V., Garcia J.P., Tomas H. and Pego A.P. (2015). The Present and the Future of Degradable Dendrimers and Derivatives in Theranostics. *Bioconjugate chemistry*

Lerch S., Ritz S., Bley K., Messerschmidt C., Weiss C.K. et al (2015). Nanoprobing the acidification process during intracellular uptake and trafficking. *Nanomedicine : nanotechnology, biology, and medicine*

Levkowitz G., Waterman H., Zamir E., Kam Z., Oved S. et al (1998). c-Cbl/Sli-1 regulates endocytic sorting and ubiquitination of the epidermal growth factor receptor. *Genes & development* **12:** 3663-3674

Li C., Liu H., Sun Y., Wang H., Guo F. et al (2009). PAMAM nanoparticles promote acute lung injury by inducing autophagic cell death through the Akt-TSC2-mTOR signaling pathway. *Journal of molecular cell biology* **1:** 37-45

Li H., Li Y., Jiao J. and Hu H.M. (2011). Alpha-alumina nanoparticles induce efficient autophagy-dependent cross-presentation and potent antitumour response. *Nature nanotechnology* **6:** 645-650

Li J.J., Hartono D., Ong C.N., Bay B.H. and Yung L.Y. (2010). Autophagy and oxidative stress associated with gold nanoparticles. *Biomaterials* **31:** 5996-6003

Li N., Xia T. and Nel A.E. (2008). The role of oxidative stress in ambient particulate matter-induced lung diseases and its implications in the toxicity of engineered nanoparticles. *Free radical biology & medicine* **44:** 1689-1699

Liang W. and Lam J.K. (2012). Endosomal Escape Pathways for Non-Viral Nucleic Acid Delivery Systems, Molecular Regulation of Endocytosis, Dr. Brian Ceresa (Ed.), ISBN: 978-953-51-0662-3*, InTech*, DOI: 10.5772/46006

Lim J.S., Shin M., Kim H.J., Kim K.S., Choy H.E. et al (2014). Caveolin-1 mediates Salmonella invasion via the regulation of SopE-dependent Rac1 activation and actin reorganization. *The Journal of infectious diseases* **210:** 793-802

Lindmo K., Brech A., Finley K.D., Gaumer S., Contamine D. et al (2008). The PI 3-kinase regulator Vps15 is required for autophagic clearance of protein aggregates. *Autophagy* **4:** 500-506

Liu B., Du H., Rutkowski R., Gartner A. and Wang X. (2012). LAAT-1 is the lysosomal lysine/arginine transporter that maintains amino acid homeostasis. *Science* **337:** 351-354

Liu L., Brown D., McKee M., Lebrasseur N.K., Yang D. et al (2008). Deletion of Cavin/PTRF causes global loss of caveolae, dyslipidemia, and glucose intolerance. *Cell metabolism* **8:** 310-317

Liu S. and Han M. (2005). Synthesis, functionalization, and bioconjugation of monodisperse, silica-coated gold nanoparticles: robust bioprobes. *Advanced Functional Materials* **15:** 961-967

Lloyd-Evans E., Morgan A.J., He X., Smith D.A., Elliot-Smith E. et al (2008). Niemann-Pick disease type C1 is a sphingosine storage disease that causes deregulation of lysosomal calcium. *Nature medicine* **14:** 1247-1255

Loos C., Syrovets T., Musyanovych A., Mailänder V., Landfester K. et al (2014). Amino-functionalized nanoparticles as inhibitors of mTOR and inducers of cell cycle arrest in leukemia cells. *Biomaterials* **35:** 1944-1953

LoPresti C., Massignani M., Fernyhough C., Blanazs A., Ryan A.J. et al (2011). Controlling polymersome surface topology at the nanoscale by membrane confined polymer/polymer phase separation. *ACS nano* **5:** 1775-1784

Lu F., Wu S.H., Hung Y. and Mou C.Y. (2009). Size effect on cell uptake in well-suspended, uniform mesoporous silica nanoparticles. *Small* **5:** 1408-1413

Ludwig A., Otto G.P., Riento K., Hams E., Fallon P.G. et al (2010). Flotillin microdomains interact with the cortical cytoskeleton to control uropod formation and neutrophil recruitment. *The Journal of cell biology* **191:** 771-781

Lundmark R., Doherty G.J., Howes M.T., Cortese K., Vallis Y. et al (2008). The GTPase-activating protein GRAF1 regulates the CLIC/GEEC endocytic pathway. *Current biology : CB* **18:** 1802-1808

Lunov O., Syrovets T., Loos C., Beil J., Delacher M. et al (2011a). Differential uptake of functionalized polystyrene nanoparticles by human macrophages and a monocytic cell line. *ACS nano* **5:** 1657-1669

Lunov O., Syrovets T., Loos C., Nienhaus G.U., Mailänder V. et al (2011b). Amino-functionalized polystyrene nanoparticles activate the NLRP3 inflammasome in human macrophages. *ACS nano* **5:** 9648-9657

Luo D. and Saltzman W.M. (2000). Enhancement of transfection by physical concentration of DNA at the cell surface. *Nature biotechnology* **18:** 893-895

Luzio J.P., Gray S.R. and Bright N.A. (2010). Endosome-lysosome fusion. *Biochemical Society transactions* **38:** 1413-1416

Luzio J.P., Parkinson M.D., Gray S.R. and Bright N.A. (2009). The delivery of endocytosed cargo to lysosomes. *Biochemical Society transactions* **37:** 1019-1021

Luzio J.P., Pryor P.R. and Bright N.A. (2007). Lysosomes: fusion and function. *Nature reviews Molecular cell biology* **8:** 622-632

Ma X., Wu Y., Jin S., Tian Y., Zhang X. et al (2011). Gold nanoparticles induce autophagosome accumulation through size-dependent nanoparticle uptake and lysosome impairment. *ACS nano* **5:** 8629-8639

Macia E., Ehrlich M., Massol R., Boucrot E., Brunner C. et al (2006). Dynasore, a cell-permeable inhibitor of dynamin. *Developmental cell* **10:** 839-850

Madshus I.H. and Stang E. (2009). Internalization and intracellular sorting of the EGF receptor: a model for understanding the mechanisms of receptor trafficking. *Journal of cell science* **122:** 3433-3439

Magadan J.G., Barbieri M.A., Mesa R., Stahl P.D. and Mayorga L.S. (2006). Rab22a regulates the sorting of transferrin to recycling endosomes. *Molecular and cellular biology* **26:** 2595-2614

Malaga-Trillo E., Solis G.P., Schrock Y., Geiss C., Luncz L. et al (2009). Regulation of embryonic cell adhesion by the prion protein. *PLoS biology* **7:** e55

Malerod L., Stuffers S., Brech A. and Stenmark H. (2007). Vps22/EAP30 in ESCRT-II mediates endosomal sorting of growth factor and chemokine receptors destined for lysosomal degradation. *Traffic* **8:** 1617-1629

Mamaeva V., Sahlgren C. and Linden M. (2013). Mesoporous silica nanoparticles in medicine--recent advances. *Advanced drug delivery reviews* **65:** 689-702

Margadant C., Monsuur H.N., Norman J.C. and Sonnenberg A. (2011). Mechanisms of integrin activation and trafficking. *Current opinion in cell biology* **23:** 607-614

Marshansky V. and Futai M. (2008). The V-type H+-ATPase in vesicular trafficking: targeting, regulation and function. *Current opinion in cell biology* **20:** 415-426

Massignani M., LoPresti C., Blanazs A., Madsen J., Armes S.P. et al (2009). Controlling cellular uptake by surface chemistry, size, and surface topology at the nanoscale. *Small* **5:** 2424-2432

Massol R.H., Boll W., Griffin A.M. and Kirchhausen T. (2006). A burst of auxilin recruitment determines the onset of clathrin-coated vesicle uncoating. *Proceedings of the National Academy of Sciences of the United States of America* **103:** 10265-10270

Mathew R., Karantza-Wadsworth V. and White E. (2007). Role of autophagy in cancer. *Nature reviews Cancer* **7:** 961-967

Matsunaga K., Morita E., Saitoh T., Akira S., Ktistakis N.T. et al (2010). Autophagy requires endoplasmic reticulum targeting of the PI3-kinase complex via Atg14L. *The Journal of cell biology* **190:** 511-521

Maxfield F.R. and McGraw T.E. (2004). Endocytic recycling. *Nature reviews Molecular cell biology* **5:** 121-132

Maxfield F.R. and Yamashiro D.J. (1987). Endosome acidification and the pathways of receptor-mediated endocytosis. *Advances in experimental medicine and biology* **225:** 189-198

Mayle K.M., Le A.M. and Kamei D.T. (2012). The intracellular trafficking pathway of transferrin. *Biochimica et biophysica acta* **1820:** 264-281

Mayor S. and Pagano R.E. (2007). Pathways of clathrin-independent endocytosis. *Nature reviews Molecular cell biology* **8:** 603-612

McCullough J., Clague M.J. and Urbe S. (2004). AMSH is an endosome-associated ubiquitin isopeptidase. *The Journal of cell biology* **166:** 487-492

McMahon H.T. and Boucrot E. (2011). Molecular mechanism and physiological functions of clathrin-mediated endocytosis. *Nature reviews Molecular cell biology* **12:** 517-533

Medina D.L., Fraldi A., Bouche V., Annunziata F., Mansueto G. et al (2011). Transcriptional activation of lysosomal exocytosis promotes cellular clearance. *Developmental cell* **21:** 421-430

Mego J.L. (1971). The effect of pH on cathepsin activities in mouse liver heterolysosomes. *The Biochemical journal* **122:** 445-452

Meister M. and Tikkanen R. (2014). Endocytic trafficking of membrane-bound cargo: a flotillin point of view. *Membranes* **4:** 356-371

Merrifield C.J., Feldman M.E., Wan L. and Almers W. (2002). Imaging actin and dynamin recruitment during invagination of single clathrin-coated pits. *Nature cell biology* **4:** 691-698

Mesa R., Salomon C., Roggero M., Stahl P.D. and Mayorga L.S. (2001). Rab22a affects the morphology and function of the endocytic pathway. *Journal of cell science* **114:** 4041-4049

Meunier E., Coste A., Olagnier D., Authier H., Lefevre L. et al (2012). Double-walled carbon nanotubes trigger IL-1beta release in human monocytes through Nlrp3 inflammasome activation. *Nanomedicine : nanotechnology, biology, and medicine* **8:** 987-995

Mickler F.M., Mockl L., Ruthardt N., Ogris M., Wagner E. et al (2012). Tuning nanoparticle uptake: live-cell imaging reveals two distinct endocytosis mechanisms mediated by natural and artificial EGFR targeting ligand. *Nano letters* **12:** 3417-3423

Mijaljica D., Prescott M. and Devenish R.J. (2011). Microautophagy in mammalian cells: revisiting a 40-year-old conundrum. *Autophagy* **7:** 673-682

Milici A.J., Watrous N.E., Stukenbrok H. and Palade G.E. (1987). Transcytosis of albumin in capillary endothelium. *The Journal of cell biology* **105:** 2603-2612

Minchinton A.I. and Tannock I.F. (2006). Drug penetration in solid tumours. *Nature reviews Cancer* **6:** 583-592

Mindell J.A. (2012). Lysosomal acidification mechanisms. *Annual review of physiology* **74:** 69-86

Mislick K.A. and Baldeschwieler J.D. (1996). Evidence for the role of proteoglycans in cation-mediated gene transfer. *Proceedings of the National Academy of Sciences of the United States of America* **93:** 12349-12354

Mizushima N. (2010). The role of the Atg1/ULK1 complex in autophagy regulation. *Current opinion in cell biology* **22:** 132-139

Mizushima N. and Komatsu M. (2011). Autophagy: renovation of cells and tissues. *Cell* **147:** 728-741

Mizushima N. and Levine B. (2010). Autophagy in mammalian development and differentiation. *Nature cell biology* **12:** 823-830

Mizushima N., Levine B., Cuervo A.M. and Klionsky D.J. (2008). Autophagy fights disease through cellular self-digestion. *Nature* **451:** 1069-1075

Mizushima N. and Yoshimori T. (2007). How to interpret LC3 immunoblotting. *Autophagy* **3:** 542-545

Mizushima N., Yoshimori T. and Levine B. (2010). Methods in mammalian autophagy research. *Cell* **140:** 313-326

Mizushima N., Yoshimori T. and Ohsumi Y. (2011). The role of Atg proteins in autophagosome formation. *Annual review of cell and developmental biology* **27:** 107-132

Monick M.M., Powers L.S., Walters K., Lovan N., Zhang M. et al (2010). Identification of an autophagy defect in smokers' alveolar macrophages. *Journal of immunology* **185:** 5425-5435

Montgomery R.R., Webster P. and Mellman I. (1991). Accumulation of indigestible substances reduces fusion competence of macrophage lysosomes. *Journal of immunology* **147:** 3087-3095

Mooren O.L., Galletta B.J. and Cooper J.A. (2012). Roles for actin assembly in endocytosis. *Annual review of biochemistry* **81:** 661-686

Moren B., Shah C., Howes M.T., Schieber N.L., McMahon H.T. et al (2012). EHD2 regulates caveolar dynamics via ATP-driven targeting and oligomerization. *Molecular biology of the cell* **23:** 1316-1329

Morgan M.T., Nakanishi Y., Kroll D.J., Griset A.P., Carnahan M.A. et al (2006). Dendrimer-encapsulated camptothecins: increased solubility, cellular uptake, and cellular retention affords enhanced anticancer activity in vitro. *Cancer research* **66:** 11913-11921

Morrow I.C. and Parton R.G. (2005). Flotillins and the PHB domain protein family: rafts, worms and anaesthetics. *Traffic* **6:** 725-740

Mosmann T. (1983). Rapid colorimetric assay for cellular growth and survival: application to proliferation and cytotoxicity assays. *Journal of immunological methods* **65:** 55-63

Motley A., Bright N.A., Seaman M.N. and Robinson M.S. (2003). Clathrin-mediated endocytosis in AP-2-depleted cells. *The Journal of cell biology* **162:** 909-918

Müller S., Dennemarker J. and Reinheckel T. (2012). Specific functions of lysosomal proteases in endocytic and autophagic pathways. *Biochimica et biophysica acta* **1824:** 34-43

Mundy D.I., Machleidt T., Ying Y.S., Anderson R.G. and Bloom G.S. (2002). Dual control of caveolar membrane traffic by microtubules and the actin cytoskeleton. *Journal of cell science* **115:** 4327-4339

Muriel O., Echarri A., Hellriegel C., Pavon D.M., Beccari L. et al (2011). Phosphorylated filamin A regulates actin-linked caveolae dynamics. *Journal of cell science* **124:** 2763-2776

Nabeshi H., Yoshikawa T., Matsuyama K., Nakazato Y., Tochigi S. et al (2011). Amorphous nanosilica induce endocytosis-dependent ROS generation and DNA damage in human keratinocytes. *Particle and fibre toxicology* **8:** 1

Nakai T., Kanamori T., Sando S. and Aoyama Y. (2003). Remarkably size-regulated cell invasion by artificial viruses. Saccharide-dependent self-aggregation of glycoviruses and its consequences in glycoviral gene delivery. *Journal of the American Chemical Society* **125:** 8465-8475

Napierska D., Thomassen L.C., Lison D., Martens J.A. and Hoet P.H. (2010). The nanosilica hazard: another variable entity. *Particle and fibre toxicology* **7:** 39

Napierska D., Thomassen L.C., Rabolli V., Lison D., Gonzalez L. et al (2009). Size-dependent cytotoxicity of monodisperse silica nanoparticles in human endothelial cells. *Small* **5:** 846-853

Nassoy P. and Lamaze C. (2012). Stressing caveolae new role in cell mechanics. *Trends in cell biology* **22:** 381-389

Nel A.E., Madler L., Velegol D., Xia T., Hoek E.M. et al (2009). Understanding biophysicochemical interactions at the nano-bio interface. *Nature materials* **8:** 543-557

Nichols B.J. (2002). A distinct class of endosome mediates clathrin-independent endocytosis to the Golgi complex. *Nature cell biology* **4:** 374-378

Nickerson D.P., Brett C.L. and Merz A.J. (2009). Vps-C complexes: gatekeepers of endolysosomal traffic. *Current opinion in cell biology* **21:** 543-551

Niedergang F. and Chavrier P. (2004). Signaling and membrane dynamics during phagocytosis: many roads lead to the phagos(R)ome. *Current opinion in cell biology* **16:** 422-428

Nishino I., Fu J., Tanji K., Yamada T., Shimojo S. et al (2000). Primary LAMP-2 deficiency causes X-linked vacuolar cardiomyopathy and myopathy (Danon disease). *Nature* **406:** 906-910

Nixon R.A. (2013). The role of autophagy in neurodegenerative disease. *Nature medicine* **19:** 983-997

Obara K., Noda T., Niimi K. and Ohsumi Y. (2008). Transport of phosphatidylinositol 3-phosphate into the vacuole via autophagic membranes in Saccharomyces cerevisiae. *Genes to cells : devoted to molecular & cellular mechanisms* **13:** 537-547

Oberdörster G., Elder A. and Rinderknecht A. (2009). Nanoparticles and the brain: cause for concern? *Journal of nanoscience and nanotechnology* **9:** 4996-5007

Oda K., Matsuoka Y., Funahashi A. and Kitano H. (2005). A comprehensive pathway map of epidermal growth factor receptor signaling. *Molecular systems biology* **1:** 2005 0010

Odorizzi G., Babst M. and Emr S.D. (1998). Fab1p PtdIns(3)P 5-kinase function essential for protein sorting in the multivesicular body. *Cell* **95:** 847-858

OECD (2005). Screening information data set (Synthetic amourphous silica and silicates, CAS-No. 7631-86-9, CAS-No. 112945-52-5, CAS-No. 112926-00-8, CAS-No. 1344-00-9, CAS-No. 1344-95-2)

Oh P., McIntosh D.P. and Schnitzer J.E. (1998). Dynamin at the neck of caveolae mediates their budding to form transport vesicles by GTP-driven fission from the plasma membrane of endothelium. *The Journal of cell biology* **141:** 101-114

Oh W.K., Kim S., Choi M., Kim C., Jeong Y.S. et al (2010). Cellular uptake, cytotoxicity, and innate immune response of silica-titania hollow nanoparticles based on size and surface functionality. *ACS nano* **4:** 5301-5313

Ohsaki M., Okuda T., Wada A., Hirayama T., Niidome T. et al (2002). In vitro gene transfection using dendritic poly(L-lysine). *Bioconjugate chemistry* **13:** 510-517

Okamoto K. (2014). Organellophagy: eliminating cellular building blocks via selective autophagy. *The Journal of cell biology* **205:** 435-445

Okamoto T., Schlegel A., Scherer P.E. and Lisanti M.P. (1998). Caveolins, a family of scaffolding proteins for organizing "preassembled signaling complexes" at the plasma membrane. *The Journal of biological chemistry* **273:** 5419-5422

Onodera J. and Ohsumi Y. (2005). Autophagy is required for maintenance of amino acid levels and protein synthesis under nitrogen starvation. *The Journal of biological chemistry* **280:** 31582-31586

Orrenius S., Kaminskyy V.O. and Zhivotovsky B. (2013). Autophagy in toxicology: cause or consequence? *Annual review of pharmacology and toxicology* **53:** 275-297

Orsi A., Razi M., Dooley H.C., Robinson D., Weston A.E. et al (2012). Dynamic and transient interactions of Atg9 with autophagosomes, but not membrane integration, are required for autophagy. *Molecular biology of the cell* **23:** 1860-1873

Osaki F., Kanamori T., Sando S., Sera T. and Aoyama Y. (2004). A quantum dot conjugated sugar ball and its cellular uptake. On the size effects of endocytosis in the subviral region. *Journal of the American Chemical Society* **126:** 6520-6521

Ostrowski A., Nordmeyer D., Boreham A., Brodwolf R., Mundhenk L. et al (2014). Skin barrier disruptions in tape stripped and allergic dermatitis models have no effect on dermal penetration and systemic distribution of AHAPS-functionalized silica nanoparticles. *Nanomedicine : nanotechnology, biology, and medicine* **10:** 1571-1581

Otto G.P. and Nichols B.J. (2011). The roles of flotillin microdomains--endocytosis and beyond. *Journal of cell science* **124:** 3933-3940

Ow H., Larson D.R., Srivastava M., Baird B.A., Webb W.W. et al (2005). Bright and stable core-shell fluorescent silica nanoparticles. *Nano letters* **5:** 113-117

Padilla De Jesus O.L., Ihre H.R., Gagne L., Frechet J.M. and Szoka F.C., Jr. (2002). Polyester dendritic systems for drug delivery applications: in vitro and in vivo evaluation. *Bioconjugate chemistry* **13:** 453-461

Pankiv S., Clausen T.H., Lamark T., Brech A., Bruun J.A. et al (2007). p62/SQSTM1 binds directly to Atg8/LC3 to facilitate degradation of ubiquitinated protein aggregates by autophagy. *The Journal of biological chemistry* **282:** 24131-24145

Park B., Martin P.A., Harris C., Guest H., Whittingham A. et al (2009). Preliminary *in vitro* investigation of the potential health effects of Optisol^{TM}, a nanoparticulate manganese modified titanium dioxide UV-filter used in certain sunscreen products. *Nanotoxicology* **3:** 73-90

Parodi A., Quattrocchi N., van de Ven A.L., Chiappini C., Evangelopoulos M. et al (2013). Synthetic nanoparticles functionalized with biomimetic leukocyte membranes possess cell-like functions. *Nature nanotechnology* **8:** 61-68

Parton R.G. and del Pozo M.A. (2013). Caveolae as plasma membrane sensors, protectors and organizers. *Nature reviews Molecular cell biology* **14:** 98-112

Pasut G. and Veronese F.M. (2012). State of the art in PEGylation: the great versatility achieved after forty years of research. *Journal of controlled release : official journal of the Controlled Release Society* **161:** 461-472

Pearson G., Robinson F., Beers Gibson T., Xu B.E., Karandikar M. et al (2001). Mitogen-activated protein (MAP) kinase pathways: regulation and physiological functions. *Endocrine reviews* **22:** 153-183

Pechstein A., Bacetic J., Vahedi-Faridi A., Gromova K., Sundborger A. et al (2010). Regulation of synaptic vesicle recycling by complex formation between intersectin 1 and the clathrin adaptor complex AP2. *Proceedings of the National Academy of Sciences of the United States of America* **107:** 4206-4211

Peer D., Karp J.M., Hong S., Farokhzad O.C., Margalit R. et al (2007). Nanocarriers as an emerging platform for cancer therapy. *Nature nanotechnology* **2:** 751-760

Pelkmans L., Kartenbeck J. and Helenius A. (2001). Caveolar endocytosis of simian virus 40 reveals a new two-step vesicular-transport pathway to the ER. *Nature cell biology* **3:** 473-483

Perner-Nochta I., Krumov N., Oder S., Angelov A. and Posten C. (2009). Biopartikel: Eine Alternative zur Produktion nanoskaliger anorganischer Partikel. *Chemie Ingenieur Technik* **81:** 685-697

Perrais D. and Merrifield C.J. (2005). Dynamics of endocytic vesicle creation. *Developmental cell* **9:** 581-592

Perumal O.P., Inapagolla R., Kannan S. and Kannan R.M. (2008). The effect of surface functionality on cellular trafficking of dendrimers. *Biomaterials* **29:** 3469-3476

Pfeffer S.R. (2009). Multiple routes of protein transport from endosomes to the trans Golgi network. *FEBS letters* **583:** 3811-3816

Pols M.S. and Klumperman J. (2009). Trafficking and function of the tetraspanin CD63. *Experimental cell research* **315:** 1584-1592

Posor Y., Eichhorn-Gruenig M., Puchkov D., Schöneberg J., Ullrich A. et al (2013). Spatiotemporal control of endocytosis by phosphatidylinositol-3,4-bisphosphate. *Nature* **499:** 233-237

Poteryaev D., Datta S., Ackema K., Zerial M. and Spang A. (2010). Identification of the switch in early-to-late endosome transition. *Cell* **141:** 497-508

Pryor P.R., Mullock B.M., Bright N.A., Lindsay M.R., Gray S.R. et al (2004). Combinatorial SNARE complexes with VAMP7 or VAMP8 define different late endocytic fusion events. *EMBO reports* **5:** 590-595

Qiu Y., Liu Y., Wang L., Xu L., Bai R. et al (2010). Surface chemistry and aspect ratio mediated cellular uptake of Au nanorods. *Biomaterials* **31:** 7606-7619

Rabolli V., Thomassen L.C., Princen C., Napierska D., Gonzalez L. et al (2010). Influence of size, surface area and microporosity on the in vitro cytotoxic activity of amorphous silica nanoparticles in different cell types. *Nanotoxicology* **4:** 307-318

Raiborg C., Malerod L., Pedersen N.M. and Stenmark H. (2008). Differential functions of Hrs and ESCRT proteins in endocytic membrane trafficking. *Experimental cell research* **314:** 801-813

Raiborg C. and Stenmark H. (2009). The ESCRT machinery in endosomal sorting of ubiquitylated membrane proteins. *Nature* **458:** 445-452

Rajendran L., Beckmann J., Magenau A., Boneberg E.M., Gaus K. et al (2009). Flotillins are involved in the polarization of primitive and mature hematopoietic cells. *PloS one* **4:** e8290

Rancan F., Gao Q., Graf C., Troppens S., Hadam S. et al (2012). Skin penetration and cellular uptake of amorphous silica nanoparticles with variable size, surface functionalization, and colloidal stability. *ACS nano* **6:** 6829-6842

Rao S.K., Huynh C., Proux-Gillardeaux V., Galli T. and Andrews N.W. (2004). Identification of SNAREs involved in synaptotagmin VII-regulated lysosomal exocytosis. *The Journal of biological chemistry* **279:** 20471-20479

Rapoport I., Boll W., Yu A., Böcking T. and Kirchhausen T. (2008). A motif in the clathrin heavy chain required for the Hsc70/auxilin uncoating reaction. *Molecular biology of the cell* **19:** 405-413

Ravikumar B., Sarkar S., Davies J.E., Futter M., Garcia-Arencibia M. et al (2010). Regulation of mammalian autophagy in physiology and pathophysiology. *Physiological reviews* **90:** 1383-1435

Reczek D., Schwake M., Schröder J., Hughes H., Blanz J. et al (2007). LIMP-2 is a receptor for lysosomal mannose-6-phosphate-independent targeting of beta-glucocerebrosidase. *Cell* **131:** 770-783

Reddy A., Caler E.V. and Andrews N.W. (2001). Plasma membrane repair is mediated by Ca(2+)-regulated exocytosis of lysosomes. *Cell* **106:** 157-169

Reichert S., Welker P., Calderón M., Khandare J., Mangoldt D. et al (2011). Size-dependant cellular uptake of dendritic polyglycerol. *Small* **7:** 820-829

Rejman J., Oberle V., Zuhorn I.S. and Hoekstra D. (2004). Size-dependent internalization of particles via the pathways of clathrin- and caveolae-mediated endocytosis. *The Biochemical journal* **377:** 159-169

Ren M., Xu G., Zeng J., De Lemos-Chiarandini C., Adesnik M. et al (1998). Hydrolysis of GTP on rab11 is required for the direct delivery of transferrin from the pericentriolar recycling compartment to the cell surface but not from sorting endosomes. *Proceedings of the National Academy of Sciences of the United States of America* **95:** 6187-6192

Ren Q., Ye S. and Whiteheart S.W. (2008). The platelet release reaction: just when you thought platelet secretion was simple. *Current opinion in hematology* **15:** 537-541

Richter T., Floetenmeyer M., Ferguson C., Galea J., Goh J. et al (2008). High-resolution 3D quantitative analysis of caveolar ultrastructure and caveola-cytoskeleton interactions. *Traffic* **9:** 893-909

Rink J., Ghigo E., Kalaidzidis Y. and Zerial M. (2005). Rab conversion as a mechanism of progression from early to late endosomes. *Cell* **122:** 735-749

Rodriguez A., Webster P., Ortego J. and Andrews N.W. (1997). Lysosomes behave as Ca2+-regulated exocytic vesicles in fibroblasts and epithelial cells. *The Journal of cell biology* **137:** 93-104

Rojas R., van Vlijmen T., Mardones G.A., Prabhu Y., Rojas A.L. et al (2008). Regulation of retromer recruitment to endosomes by sequential action of Rab5 and Rab7. *The Journal of cell biology* **183:** 513-526

Rossy J., Schlicht D., Engelhardt B. and Niggli V. (2009). Flotillins interact with PSGL-1 in neutrophils and, upon stimulation, rapidly organize into membrane domains subsequently accumulating in the uropod. *PloS one* **4:** e5403

Rothberg K.G., Heuser J.E., Donzell W.C., Ying Y.S., Glenney J.R. et al (1992). Caveolin, a protein component of caveolae membrane coats. *Cell* **68:** 673-682

Rothnie A., Clarke A.R., Kuzmic P., Cameron A. and Smith C.J. (2011). A sequential mechanism for clathrin cage disassembly by 70-kDa heat-shock cognate protein (Hsc70) and auxilin. *Proceedings of the National Academy of Sciences of the United States of America* **108:** 6927-6932

Roux A., Uyhazi K., Frost A. and De Camilli P. (2006). GTP-dependent twisting of dynamin implicates constriction and tension in membrane fission. *Nature* **441:** 528-531

Roy D., Liston D.R., Idone V.J., Di A., Nelson D.J. et al (2004). A process for controlling intracellular bacterial infections induced by membrane injury. *Science* **304:** 1515-1518

Rubinsztein D.C. (2006). The roles of intracellular protein-degradation pathways in neurodegeneration. *Nature* **443:** 780-786

Rubinsztein D.C., Codogno P. and Levine B. (2012a). Autophagy modulation as a potential therapeutic target for diverse diseases. *Nature reviews Drug discovery* **11:** 709-730

Rubinsztein D.C., Shpilka T. and Elazar Z. (2012b). Mechanisms of autophagosome biogenesis. *Current biology : CB* **22:** R29-34

Ruedas-Rama M.J., Walters J.D., Orte A. and Hall E.A. (2012). Fluorescent nanoparticles for intracellular sensing: a review. *Analytica chimica acta* **751:** 1-23

Russell R.C., Tian Y., Yuan H., Park H.W., Chang Y.Y. et al (2013). ULK1 induces autophagy by phosphorylating Beclin-1 and activating VPS34 lipid kinase. *Nature cell biology* **15:** 741-750

Rust M.J., Lakadamyali M., Zhang F. and Zhuang X. (2004). Assembly of endocytic machinery around individual influenza viruses during viral entry. *Nature structural & molecular biology* **11:** 567-573

Saftig P. and Klumperman J. (2009). Lysosome biogenesis and lysosomal membrane proteins: trafficking meets function. *Nature reviews Molecular cell biology* **10:** 623-635

Sahay G., Querbes W., Alabi C., Eltoukhy A., Sarkar S. et al (2013). Efficiency of siRNA delivery by lipid nanoparticles is limited by endocytic recycling. *Nature biotechnology* **31:** 653-658

Sahu R., Kaushik S., Clement C.C., Cannizzo E.S., Scharf B. et al (2011). Microautophagy of cytosolic proteins by late endosomes. *Developmental cell* **20:** 131-139

Saitoh T., Fujita N., Hayashi T., Takahara K., Satoh T. et al (2009). Atg9a controls dsDNA-driven dynamic translocation of STING and the innate immune response. *Proceedings of the National Academy of Sciences of the United States of America* **106:** 20842-20846

Saitoh T., Fujita N., Jang M.H., Uematsu S., Yang B.G. et al (2008). Loss of the autophagy protein Atg16L1 enhances endotoxin-induced IL-1beta production. *Nature* **456:** 264-268

Sajid M. and McKerrow J.H. (2002). Cysteine proteases of parasitic organisms. *Molecular and biochemical parasitology* **120:** 1-21

Salata O. (2004). Applications of nanoparticles in biology and medicine. *Journal of nanobiotechnology* **2:** 3

Sandin P., Fitzpatrick L.W., Simpson J.C. and Dawson K.A. (2012). High-speed imaging of Rab family small GTPases reveals rare events in nanoparticle trafficking in living cells. *ACS nano* **6:** 1513-1521

Sandri M., Coletto L., Grumati P. and Bonaldo P. (2013). Misregulation of autophagy and protein degradation systems in myopathies and muscular dystrophies. *Journal of cell science* **126:** 5325-5333

Santra S., Kaittanis C., Santiesteban O.J. and Perez J.M. (2011). Cell-specific, activatable, and theranostic prodrug for dual-targeted cancer imaging and therapy. *Journal of the American Chemical Society* **133:** 16680-16688

Sapsford K.E., Berti L. and Medintz I.L. (2006). Materials for fluorescence resonance energy transfer analysis: beyond traditional donor-acceptor combinations. *Angewandte Chemie* **45:** 4562-4589

Sardiello M., Palmieri M., di Ronza A., Medina D.L., Valenza M. et al (2009). A gene network regulating lysosomal biogenesis and function. *Science* **325:** 473-477

Sato M. and Sato K. (2011). Degradation of paternal mitochondria by fertilization-triggered autophagy in C. elegans embryos. *Science* **334:** 1141-1144

Scheele U., Kalthoff C. and Ungewickell E. (2001). Multiple interactions of auxilin 1 with clathrin and the AP-2 adaptor complex. *The Journal of biological chemistry* **276:** 36131-36138

Schindelin J., Arganda-Carreras I., Frise E., Kaynig V., Longair M. et al (2012). Fiji: an open-source platform for biological-image analysis. *Nature methods* **9:** 676-682

Schlessinger J. (2002). Ligand-induced, receptor-mediated dimerization and activation of EGF receptor. *Cell* **110:** 669-672

Schliwa M. (1982). Action of cytochalasin D on cytoskeletal networks. *The Journal of cell biology* **92:** 79-91

Schlossman D.M., Schmid S.L., Braell W.A. and Rothman J.E. (1984). An enzyme that removes clathrin coats: purification of an uncoating ATPase. *The Journal of cell biology* **99:** 723-733

Schmidt M.H. and Dikic I. (2005). The Cbl interactome and its functions. *Nature reviews Molecular cell biology* **6:** 907-918

Schwake M., Schröder B. and Saftig P. (2013). Lysosomal membrane proteins and their central role in physiology. *Traffic* **14:** 739-748

Scott C.C., Vacca F. and Gruenberg J. (2014). Endosome maturation, transport and functions. *Seminars in cell & developmental biology* **31:** 2-10

Seleverstov O., Zabirnyk O., Zscharnack M., Bulavina L., Nowicki M. et al (2006). Quantum dots for human mesenchymal stem cells labeling. A size-dependent autophagy activation. *Nano letters* **6:** 2826-2832

Senju Y., Itoh Y., Takano K., Hamada S. and Suetsugu S. (2011). Essential role of PACSIN2/syndapin-II in caveolae membrane sculpting. *Journal of cell science* **124:** 2032-2040

Settembre C., Di Malta C., Polito V.A., Garcia Arencibia M., Vetrini F. et al (2011). TFEB links autophagy to lysosomal biogenesis. *Science* **332:** 1429-1433

Settembre C., Fraldi A., Medina D.L. and Ballabio A. (2013). Signals from the lysosome: a control centre for cellular clearance and energy metabolism. *Nature reviews Molecular cell biology* **14:** 283-296

Settembre C., Zoncu R., Medina D.L., Vetrini F., Erdin S. et al (2012). A lysosome-to-nucleus signalling mechanism senses and regulates the lysosome via mTOR and TFEB. *The EMBO journal* **31:** 1095-1108

Shan Y., Ma S., Nie L., Shang X., Hao X. et al (2011). Size-dependent endocytosis of single gold nanoparticles. *Chemical communications* **47:** 8091-8093

Shapero K., Fenaroli F., Lynch I., Cottell D.C., Salvati A. et al (2011). Time and space resolved uptake study of silica nanoparticles by human cells. *Molecular bioSystems* **7:** 371-378

Sharma D.K., Brown J.C., Choudhury A., Peterson T.E., Holicky E. et al (2004). Selective stimulation of caveolar endocytosis by glycosphingolipids and cholesterol. *Molecular biology of the cell* **15:** 3114-3122

Shi C.S., Shenderov K., Huang N.N., Kabat J., Abu-Asab M. et al (2012). Activation of autophagy by inflammatory signals limits IL-1beta production by targeting ubiquitinated inflammasomes for destruction. *Nature immunology* **13:** 255-263

Shi H., He X., Yuan Y., Wang K. and Liu D. (2010). Nanoparticle-based biocompatible and long-life marker for lysosome labeling and tracking. *Analytical chemistry* **82:** 2213-2220

Shvets E., Ludwig A. and Nichols B.J. (2014). News from the caves: update on the structure and function of caveolae. *Current opinion in cell biology* **29:** 99-106

Sies H. (1999). Glutathione and its role in cellular functions. *Free radical biology & medicine* **27:** 916-921

Sigismund S., Woelk T., Puri C., Maspero E., Tacchetti C. et al (2005). Clathrin-independent endocytosis of ubiquitinated cargos. *Proceedings of the National Academy of Sciences of the United States of America* **102:** 2760-2765

Simons K. and Ikonen E. (1997). Functional rafts in cell membranes. *Nature* **387:** 569-572

Singh N., Karambelkar A., Gu L., Lin K., Miller J.S. et al (2011). Bioresponsive mesoporous silica nanoparticles for triggered drug release. *Journal of the American Chemical Society* **133:** 19582-19585

Sinha B., Koster D., Ruez R., Gonnord P., Bastiani M. et al (2011). Cells respond to mechanical stress by rapid disassembly of caveolae. *Cell* **144:** 402-413

Slowing, Ll, Vivero-Escoto J.L., Wu C.W. and Lin V.S. (2008). Mesoporous silica nanoparticles as controlled release drug delivery and gene transfection carriers. *Advanced drug delivery reviews* **60:** 1278-1288

Slowing I., Trewyn B.G. and Lin V.S. (2006). Effect of surface functionalization of MCM-41-type mesoporous silica nanoparticles on the endocytosis by human cancer cells. *Journal of the American Chemical Society* **128:** 14792-14793

Solinger J.A. and Spang A. (2013). Tethering complexes in the endocytic pathway: CORVET and HOPS. *The FEBS journal* **280:** 2743-2757

Solis G.P., Hoegg M., Munderloh C., Schrock Y., Malaga-Trillo E. et al (2007). Reggie/flotillin proteins are organized into stable tetramers in membrane microdomains. *The Biochemical journal* **403:** 313-322

Soppina V., Rai A.K., Ramaiya A.J., Barak P. and Mallik R. (2009). Tug-of-war between dissimilar teams of microtubule motors regulates transport and fission of endosomes.

Proceedings of the National Academy of Sciences of the United States of America **106:** 19381-19386

Sorkina T., Huang F., Beguinot L. and Sorkin A. (2002). Effect of tyrosine kinase inhibitors on clathrin-coated pit recruitment and internalization of epidermal growth factor receptor. *The Journal of biological chemistry* **277:** 27433-27441

Sou Y.S., Waguri S., Iwata J., Ueno T., Fujimura T. et al (2008). The Atg8 conjugation system is indispensable for proper development of autophagic isolation membranes in mice. *Molecular biology of the cell* **19:** 4762-4775

Soubeyran P., Kowanetz K., Szymkiewicz I., Langdon W.Y. and Dikic I. (2002). Cbl-CIN85-endophilin complex mediates ligand-induced downregulation of EGF receptors. *Nature* **416:** 183-187

Steere A.N., Byrne S.L., Chasteen N.D. and Mason A.B. (2012). Kinetics of iron release from transferrin bound to the transferrin receptor at endosomal pH. *Biochimica et biophysica acta* **1820:** 326-333

Stern S.T., Adiseshaiah P.P. and Crist R.M. (2012). Autophagy and lysosomal dysfunction as emerging mechanisms of nanomaterial toxicity. *Particle and fibre toxicology* **9:** 20

Stinchcombe J., Bossi G. and Griffiths G.M. (2004). Linking albinism and immunity: the secrets of secretory lysosomes. *Science* **305:** 55-59

Stöber W., Fink A. and Bohn E. (1968). Controlled growth of monodisperse silica spheres in the micron size range. *Journal of Colloid and Interface Science* **26:** 62-69

Stoeber M., Stoeck I.K., Hanni C., Bleck C.K., Balistreri G. et al (2012). Oligomers of the ATPase EHD2 confine caveolae to the plasma membrane through association with actin. *The EMBO journal* **31:** 2350-2364

Sun Q., Fan W., Chen K., Ding X., Chen S. et al (2008). Identification of Barkor as a mammalian autophagy-specific factor for Beclin 1 and class III phosphatidylinositol 3-kinase. *Proceedings of the National Academy of Sciences of the United States of America* **105:** 19211-19216

Sun T., Yan Y., Zhao Y., Guo F. and Jiang C. (2012). Copper oxide nanoparticles induce autophagic cell death in A549 cells. *PloS one* **7:** e43442

Sundborger A., Soderblom C., Vorontsova O., Evergren E., Hinshaw J.E. et al (2011). An endophilin-dynamin complex promotes budding of clathrin-coated vesicles during synaptic vesicle recycling. *Journal of cell science* **124:** 133-143

Suzuki K., Kubota Y., Sekito T. and Ohsumi Y. (2007). Hierarchy of Atg proteins in pre-autophagosomal structure organization. *Genes to cells : devoted to molecular & cellular mechanisms* **12:** 209-218

Sweitzer S.M. and Hinshaw J.E. (1998). Dynamin undergoes a GTP-dependent conformational change causing vesiculation. *Cell* **93:** 1021-1029

Taguchi-Atarashi N., Hamasaki M., Matsunaga K., Omori H., Ktistakis N.T. et al (2010). Modulation of local PtdIns3P levels by the PI phosphatase MTMR3 regulates constitutive autophagy. *Traffic* **11:** 468-478

Tang L. and Cheng J. (2013). Nonporous Silica Nanoparticles for Nanomedicine Application. *Nano today* **8:** 290-312

Tang L., Fan T.M., Borst L.B. and Cheng J. (2012). Synthesis and biological response of size-specific, monodisperse drug-silica nanoconjugates. *ACS nano* **6:** 3954-3966

Taylor M.J., Perrais D. and Merrifield C.J. (2011). A high precision survey of the molecular dynamics of mammalian clathrin-mediated endocytosis. *PLoS biology* **9:** e1000604

Tebar F., Sorkina T., Sorkin A., Ericsson M. and Kirchhausen T. (1996). Eps15 is a component of clathrin-coated pits and vesicles and is located at the rim of coated pits. *The Journal of biological chemistry* **271:** 28727-28730

Teckchandani A., Toida N., Goodchild J., Henderson C., Watts J. et al (2009). Quantitative proteomics identifies a Dab2/integrin module regulating cell migration. *The Journal of cell biology* **186:** 99-111

Thibodeau M.S., Giardina C., Knecht D.A., Helble J. and Hubbard A.K. (2004). Silica-induced apoptosis in mouse alveolar macrophages is initiated by lysosomal enzyme activity. *Toxicological sciences : an official journal of the Society of Toxicology* **80:** 34-48

Thomas T.P., Majoros I., Kotlyar A., Mullen D., Holl M.M. et al (2009). Cationic poly(amidoamine) dendrimer induces lysosomal apoptotic pathway at therapeutically relevant concentrations. *Biomacromolecules* **10:** 3207-3214

Thorley A.J., Ruenraroengsak P., Potter T.E. and Tetley T.D. (2014). Critical determinants of uptake and translocation of nanoparticles by the human pulmonary alveolar epithelium. *ACS nano* **8:** 11778-11789

Towbin H., Staehelin T. and Gordon J. (1979). Electrophoretic transfer of proteins from polyacrylamide gels to nitrocellulose sheets: procedure and some applications. *Proceedings of the National Academy of Sciences of the United States of America* **76:** 4350-4354

Traer C.J., Rutherford A.C., Palmer K.J., Wassmer T., Oakley J. et al (2007). SNX4 coordinates endosomal sorting of TfnR with dynein-mediated transport into the endocytic recycling compartment. *Nature cell biology* **9:** 1370-1380

Traub L.M. (2009). Tickets to ride: selecting cargo for clathrin-regulated internalization. *Nature reviews Molecular cell biology* **10:** 583-596

Treiber C., Quadir M.A., Voigt P., Radowski M., Xu S. et al (2009). Cellular copper import by nanocarrier systems, intracellular availability, and effects on amyloid beta peptide secretion. *Biochemistry* **48:** 4273-4284

Trewyn B.G., Slowing, II, Giri S., Chen H.T. and Lin V.S. (2007). Synthesis and functionalization of a mesoporous silica nanoparticle based on the sol-gel process and applications in controlled release. *Accounts of chemical research* **40:** 846-853

Tsukamoto S., Kuma A., Murakami M., Kishi C., Yamamoto A. et al (2008). Autophagy is essential for preimplantation development of mouse embryos. *Science* **321:** 117-120

Tulsiani D.R., Abou-Haila A., Loeser C.R. and Pereira B.M. (1998). The biological and functional significance of the sperm acrosome and acrosomal enzymes in mammalian fertilization. *Experimental cell research* **240:** 151-164

Turk B., Turk D. and Turk V. (2000). Lysosomal cysteine proteases: more than scavengers. *Biochimica et biophysica acta* **1477:** 98-111

Ullrich O., Reinsch S., Urbe S., Zerial M. and Parton R.G. (1996). Rab11 regulates recycling through the pericentriolar recycling endosome. *The Journal of cell biology* **135:** 913-924

Umebayashi K., Stenmark H. and Yoshimori T. (2008). Ubc4/5 and c-Cbl continue to ubiquitinate EGF receptor after internalization to facilitate polyubiquitination and degradation. *Molecular biology of the cell* **19:** 3454-3462

Ungewickell E., Ungewickell H., Holstein S.E., Lindner R., Prasad K. et al (1995). Role of auxilin in uncoating clathrin-coated vesicles. *Nature* **378:** 632-635

Urbe S., McCullough J., Row P., Prior I.A., Welchman R. et al (2006). Control of growth factor receptor dynamics by reversible ubiquitination. *Biochemical Society transactions* **34:** 754-756

van Blaaderen A., van Geest J. and Vrij A. (1992). Monodisperse colloidal silica spheres from tetraalkoxysilanes: particle formation and growth mechanism. *Journal of Colloid and Interface Science* **154:** 481-501

van der Sluijs P., Hull M., Webster P., Male P., Goud B. et al (1992). The small GTP-binding protein rab4 controls an early sorting event on the endocytic pathway. *Cell* **70:** 729-740

van Meel E. and Klumperman J. (2008). Imaging and imagination: understanding the endo-lysosomal system. *Histochemistry and cell biology* **129:** 253-266

Veiga E. and Cossart P. (2005). Listeria hijacks the clathrin-dependent endocytic machinery to invade mammalian cells. *Nature cell biology* **7:** 894-900

Veiga E., Guttman J.A., Bonazzi M., Boucrot E., Toledo-Arana A. et al (2007). Invasive and adherent bacterial pathogens co-Opt host clathrin for infection. *Cell host & microbe* **2:** 340-351

Velikkakath A.K., Nishimura T., Oita E., Ishihara N. and Mizushima N. (2012). Mammalian Atg2 proteins are essential for autophagosome formation and important for regulation of size and distribution of lipid droplets. *Molecular biology of the cell* **23:** 896-909

Vercauteren D., Vandenbroucke R.E., Jones A.T., Rejman J., Demeester J. et al (2010). The use of inhibitors to study endocytic pathways of gene carriers: optimization and pitfalls. *Molecular therapy : the journal of the American Society of Gene Therapy* **18:** 561-569

Vergne I., Roberts E., Elmaoued R.A., Tosch V., Delgado M.A. et al (2009). Control of autophagy initiation by phosphoinositide 3-phosphatase Jumpy. *The EMBO journal* **28:** 2244-2258

Verhage M. and Toonen R.F. (2007). Regulated exocytosis: merging ideas on fusing membranes. *Current opinion in cell biology* **19:** 402-408

Verma A. and Stellacci F. (2010). Effect of surface properties on nanoparticle-cell interactions. *Small* **6:** 12-21

Verma A., Uzun O., Hu Y., Hu Y., Han H.S. et al (2008). Surface-structure-regulated cell-membrane penetration by monolayer-protected nanoparticles. *Nature materials* **7:** 588-595

Vicinanza M., D'Angelo G., Di Campli A. and De Matteis M.A. (2008). Function and dysfunction of the PI system in membrane trafficking. *The EMBO journal* **27:** 2457-2470

Villamil Giraldo A.M., Appelqvist H., Ederth T. and Ollinger K. (2014). Lysosomotropic agents: impact on lysosomal membrane permeabilization and cell death. *Biochemical Society transactions* **42:** 1460-1464

von Kleist L. and Haucke V. (2012). At the crossroads of chemistry and cell biology: inhibiting membrane traffic by small molecules. *Traffic* **13:** 495-504

von Kleist L., Stahlschmidt W., Bulut H., Gromova K., Puchkov D. et al (2011). Role of the clathrin terminal domain in regulating coated pit dynamics revealed by small molecule inhibition. *Cell* **146:** 471-484

Wan J., Savas J.N., Roth A.F., Sanders S.S., Singaraja R.R. et al (2013). Tracking brain palmitoylation change: predominance of glial change in a mouse model of Huntington's disease. *Chemistry & biology* **20:** 1421-1434

Wang A.Z., Bagalkot V., Vasilliou C.C., Gu F., Alexis F. et al (2008). Superparamagnetic iron oxide nanoparticle-aptamer bioconjugates for combined prostate cancer imaging and therapy. *ChemMedChem* **3:** 1311-1315

Wang C.W., Stromhaug P.E., Shima J. and Klionsky D.J. (2002). The Ccz1-Mon1 protein complex is required for the late step of multiple vacuole delivery pathways. *The Journal of biological chemistry* **277:** 47917-47927

Wang T., Ming Z., Xiaochun W. and Hong W. (2011). Rab7: role of its protein interaction cascades in endo-lysosomal traffic. *Cellular signalling* **23:** 516-521

Warheit D.B. (2010). Debunking some misconceptions about nanotoxicology. *Nano letters* **10:** 4777-4782

Watanabe N., Kato T., Fujita A., Ishizaki T. and Narumiya S. (1999). Cooperation between mDia1 and ROCK in Rho-induced actin reorganization. *Nature cell biology* **1:** 136-143

Watanabe Y., Kobayashi T., Yamamoto H., Hoshida H., Akada R. et al (2012). Structure-based analyses reveal distinct binding sites for Atg2 and phosphoinositides in Atg18. *The Journal of biological chemistry* **287:** 31681-31690

Waters S., Marchbank K., Solomon E., Whitehouse C. and Gautel M. (2009). Interactions with LC3 and polyubiquitin chains link nbr1 to autophagic protein turnover. *FEBS letters* **583:** 1846-1852

Wehling J., Dringen R., Zare R.N., Maas M. and Rezwan K. (2014). Bactericidal activity of partially oxidized nanodiamonds. *ACS nano* **8:** 6475-6483

Wei P.F., Zhang L., Nethi S.K., Barui A.K., Lin J. et al (2014). Accelerating the clearance of mutant huntingtin protein aggregates through autophagy induction by europium hydroxide nanorods. *Biomaterials* **35:** 899-907

Weidberg H., Shvets E. and Elazar Z. (2011). Biogenesis and cargo selectivity of autophagosomes. *Annual review of biochemistry* **80:** 125-156

Weinert S., Jabs S., Supanchart C., Schweizer M., Gimber N. et al (2010). Lysosomal pathology and osteopetrosis upon loss of H+-driven lysosomal Cl- accumulation. *Science* **328:** 1401-1403

White E. (2012). Deconvoluting the context-dependent role for autophagy in cancer. *Nature reviews Cancer* **12:** 401-410

Wickström S.A., Lange A., Hess M.W., Polleux J., Spatz J.P. et al (2010). Integrin-linked kinase controls microtubule dynamics required for plasma membrane targeting of caveolae. *Developmental cell* **19:** 574-588

Wieffer M., Maritzen T. and Haucke V. (2009). SnapShot: endocytic trafficking. *Cell* **137:** 382 e381-383

Wigge P., Kohler K., Vallis Y., Doyle C.A., Owen D. et al (1997). Amphiphysin heterodimers: potential role in clathrin-mediated endocytosis. *Molecular biology of the cell* **8:** 2003-2015

Wilke S., Krausze J. and Bussow K. (2012). Crystal structure of the conserved domain of the DC lysosomal associated membrane protein: implications for the lysosomal glycocalyx. *BMC biology* **10:** 62

Witsch E., Sela M. and Yarden Y. (2010). Roles for growth factors in cancer progression. *Physiology* **25:** 85-101

Wong E. and Cuervo A.M. (2010). Autophagy gone awry in neurodegenerative diseases. *Nature neuroscience* **13:** 805-811

Wörle-Knirsch J.M., Pulskamp K. and Krug H.F. (2006). Oops they did it again! Carbon nanotubes hoax scientists in viability assays. *Nano letters* **6:** 1261-1268

Wu S.H., Hung Y. and Mou C.Y. (2011a). Mesoporous silica nanoparticles as nanocarriers. *Chemical communications* **47:** 9972-9985

Wu Y.N., Yang L.X., Shi X.Y., Li I.C., Biazik J.M. et al (2011b). The selective growth inhibition of oral cancer by iron core-gold shell nanoparticles through mitochondria-mediated autophagy. *Biomaterials* **32:** 4565-4573

Xia T., Kovochich M., Brant J., Hotze M., Sempf J. et al (2006). Comparison of the abilities of ambient and manufactured nanoparticles to induce cellular toxicity according to an oxidative stress paradigm. *Nano letters* **6:** 1794-1807

Xia T., Kovochich M., Liong M., Zink J.I. and Nel A.E. (2008). Cationic polystyrene nanosphere toxicity depends on cell-specific endocytic and mitochondrial injury pathways. *ACS nano* **2:** 85-96

Xie Z. and Klionsky D.J. (2007). Autophagosome formation: core machinery and adaptations. *Nature cell biology* **9:** 1102-1109

Xing Y., Bocking T., Wolf M., Grigorieff N., Kirchhausen T. et al (2010). Structure of clathrin coat with bound Hsc70 and auxilin: mechanism of Hsc70-facilitated disassembly. *The EMBO journal* **29:** 655-665

Yamamoto H., Kakuta S., Watanabe T.M., Kitamura A., Sekito T. et al (2012). Atg9 vesicles are an important membrane source during early steps of autophagosome formation. *The Journal of cell biology* **198:** 219-233

Yamashita K., Yoshioka Y., Higashisaka K., Mimura K., Morishita Y. et al (2011). Silica and titanium dioxide nanoparticles cause pregnancy complications in mice. *Nature nanotechnology* **6:** 321-328

Yamawaki H. and Iwai N. (2006). Cytotoxicity of water-soluble fullerene in vascular endothelial cells. *American journal of physiology Cell physiology* **290:** C1495-1502

Yang P., Gai S. and Lin J. (2012). Functionalized mesoporous silica materials for controlled drug delivery. *Chemical Society reviews* **41:** 3679-3698

Yang Z. and Klionsky D.J. (2010a). Eaten alive: a history of macroautophagy. *Nature cell biology* **12:** 814-822

Yang Z. and Klionsky D.J. (2010b). Mammalian autophagy: core molecular machinery and signaling regulation. *Current opinion in cell biology* **22:** 124-131

Yarden Y. (2001). The EGFR family and its ligands in human cancer. signalling mechanisms and therapeutic opportunities. *European journal of cancer* **37 Suppl 4:** S3-8

Yarden Y. and Sliwkowski M.X. (2001). Untangling the ErbB signalling network. *Nature reviews Molecular cell biology* **2:** 127-137

Yogalingam G., Bonten E.J., van de Vlekkert D., Hu H., Moshiach S. et al (2008). Neuraminidase 1 is a negative regulator of lysosomal exocytosis. *Developmental cell* **15:** 74-86

Yoo J.W. and Mitragotri S. (2010). Polymer particles that switch shape in response to a stimulus. *Proceedings of the National Academy of Sciences of the United States of America* **107:** 11205-11210

Yu Y., Duan J., Yu Y., Li Y., Liu X. et al (2014). Silica nanoparticles induce autophagy and autophagic cell death in HepG2 cells triggered by reactive oxygen species. *Journal of hazardous materials* **270:** 176-186

Zerial M. and McBride H. (2001). Rab proteins as membrane organizers. *Nature reviews Molecular cell biology* **2:** 107-117

Zhang F., Kang E.T., Neoh K.G., Wang P. and Tan K.L. (2001). Surface modification of stainless steel by grafting of poly(ethylene glycol) for reduction in protein adsorption. *Biomaterials* **22:** 1541-1548

Zhang T., Maekawa Y., Hanba J., Dainichi T., Nashed B.F. et al (2000). Lysosomal cathepsin B plays an important role in antigen processing, while cathepsin D is involved in degradation of the invariant chain inovalbumin-immunized mice. *Immunology* **100:** 13-20

Zhong J., Zhang Y., Zhong Q., Hu Q., Hu B. et al (2014). Fiber-based generator for wearable electronics and mobile medication. *ACS Nano* **8:** 6273-80

Zhong Y., Wang Q.J., Li X., Yan Y., Backer J.M. et al (2009). Distinct regulation of autophagic activity by Atg14L and Rubicon associated with Beclin 1-phosphatidylinositol-3-kinase complex. *Nature cell biology* **11:** 468-476

Zhou C., Zhong W., Zhou J., Sheng F., Fang Z. et al (2012). Monitoring autophagic flux by an improved tandem fluorescent-tagged LC3 (mTagRFP-mWasabi-LC3) reveals that high-dose rapamycin impairs autophagic flux in cancer cells. *Autophagy* **8:** 1215-1226

Zoncu R., Bar-Peled L., Efeyan A., Wang S., Sancak Y. et al (2011a). mTORC1 senses lysosomal amino acids through an inside-out mechanism that requires the vacuolar H(+)-ATPase. *Science* **334:** 678-683

Zoncu R., Efeyan A. and Sabatini D.M. (2011b). mTOR: from growth signal integration to cancer, diabetes and ageing. *Nature reviews Molecular cell biology* **12:** 21-35

Zoncu R., Perera R.M., Sebastian R., Nakatsu F., Chen H. et al (2007). Loss of endocytic clathrin-coated pits upon acute depletion of phosphatidylinositol 4,5-bisphosphate. *Proceedings of the National Academy of Sciences of the United States of America* **104:** 3793-3798

Zorko M. and Langel U. (2005). Cell-penetrating peptides: mechanism and kinetics of cargo delivery. *Advanced drug delivery reviews* **57:** 529-545

7 APPENDIX

7.1 Abbreviations

Abl	Abelson murine leukemia
AHAPS	*N*-(6-aminohexyl)-aminopropyltrimethoxysilane
AMBRA1	activating molecule in Beclin 1-related autophagy 1
AMPK	AMP(5' adenosine monophophate)-activated protein kinase
AMSH	associated molecule with the SH3 domain (Src homology 3 domain) of STAM (signal transducing adapter molecule)
AP-1	adaptor protein 1
AP-2	adaptor protein 2
APS	1) (3-Aminopropyl)trimethoxysilane
	2) ammonium peroxodisulfate
Arf	ADP-ribosylation factor
ARP2/3	actin-related protein 2/3
ATG	autophagy-related
ATP	adenosine triphosphate
AuNP	gold nanoparticle
Baf A1	Bafilomycin A1
BAR	Bin-Amphiphysin-Rvs
Barkor	Beclin 1-associated autophagy-related key regulator
BSA	bovine serum albumine
c-Cbl	Casitas B-lineage lymphoma, E3 ubiquitin ligase
CCP	clathrin-coated pit
CCV	clathrin-coated vesicle
CD59	a glycoprotein also known as MAC-inhibitory protein (MAC-IP) or Homologous restriction factor (HRF)
CD63	member of the tetraspanin family; also known as LAMP3
CIN85	Cbl-interacting protein of 85 kDa
CLASP	clathrin-associated sorting protein
CLC	Chloride channel

CLIC	clathrin- and dynamin-independent carrier
CMA	chaperone-mediated autophagy
CME	clathrin-mediated endocytosis
CORVET	class C core vacuole/ endosome tethering
CPP	cell-penetrating peptide
ctrl	control
CTxB	cholera toxin B
Cy	cyanine dye
Cyt D	cytochalasin D
Dab-2	Disabled-2
DAPI	4', 6-Diamindino-2-phenylindole dihydrochloride
DFCP1	double FYVE-containing protein 1
DMEM	Dulbecco's modified Eagle's medium
DMSO	dimethyl sulfoxide
Dox	doxorubicin
DQ-BSA	derivative-quenched bovine serum albumin
DTM1	divalent metal transporter
DUB	deubiquitinating enzyme
ECL	enhanced chemoluminescence
ECM	extracellular matrix
EDTA	ethylene-diamine-tetraacetic acid
EE	early endosome
EEA1	early endosome antigen 1
EGF^{647}	epidermal growth factor labeled with Alexa-647 dye
EGFR	epidermal growth factor (EGF) receptor
EHD2	Eps-15 homology domain-containing protein 2
Eps15	EGFR pathway substrate 15
ER	endoplasmic reticulum
erbB	family member of receptor tyrosine kinases
ERC	endocytic recycling compartment
Erk	extracellular signal-regulated kinase

ESCRT	endosomal sorting complex required for transport
EtOH	ethanol
FBS	fetal bovine serum
FCHo1/2	FCH domain only proteins 1/2
FCS	Fetal calf serum
FIP200	FAK (focal adhesion kinase) family interacting protein of 200 kDa
FITC	fluoresceine isothiocyanate
FRET	fluorescence resonance energy transfer
FYVE	named after four cysteine-rich proteins: **F**ab 1 (yeast orthologue of PIKfyve), **Y**OTB, **V**ac 1 (vesicle transport protein), and **E**EA1
GABARAP	γ-aminobutyric-acid-type-A-receptor-associated protein
GATE-16	Golgi-associated ATPase enhancer of 16 kDa
GEEC	glycosyl phosphatidylinositol-anchored protein enriched early endosomal compartment
GFP	green fluorescent protein
GM1	monosialotetrahexosylganglioside
GP	APS coupled with N-guanylpyrazole
GPI	glycosyl phosphatidylinositol
GSDB	Goat serum dilution buffer
HBSS	Hank's balanced salt solution
HeLa	human cervix carcinoma cells
HEPES	4-(2-hydroxyethyl)-1-piperazine-ethanesulfonic acid
HOPS	homotypic fusion and vacuole protein sorting
HPMA	N-(2-Hydroxypropyl)methacrylamide
HRP	horseradish peroxidase
Hrs	hepatocyte growth factor-regulated tyrosine kinase substrate
Hsc70	heat shock cognate protein of 70 kDa
Hsp70	heat shock protein of 70 kDa
hVps	human vacuolar protein sorting
IB	immunoblotting
IDCC	indodicarbocyanine dye
IF	immunofluorescence

ILK	integrin-linked kinase
ILV	intralumenal vesicle
IM	isolation membrane or phagophore
INT	2-(4-iodophenyl)-3-(4-nitrophenyl)-5-phenyl-2*H*-tetrazolium chloride
IQGAP1	IQ motif-containing GTPase-activating protein 1
LAAT1	lysosomal amino acid transporter 1
LAMP	lysosome-associated membrane protein
LC3	microtubule-associated protein light chain 3
LDH	lactate dehydrogenase
LE	late endosome
LIMP2	lysosome integral membrane protein 2
LMP	1) lysosomal membrane permeabilization
	2) lysosomal membrane proteins
LMR	lysosomal membrane rupture
LSD	Lysosomal storage disorder
LYNUS	lysosome nutrient sensing
MAPK	mitogen-activated protein kinase
MCOLN1	Mucolipin 1
mDia1	mammalian diaphanous 1
MβCD	methyl-β-cyclodextrin
MPR	mannose 6-phosphate receptor
MRI	magnetic resonance imaging
MSN	mesoporous silica nanoparticles
MT	microtubule
MTMR	myotubularin-related phosphatase
mTOR	mammalian target of rapamycin
mTORC1	mammalian target of rapamycin complex 1
MTT	3-(4,5-dimethyl-2-thiazolyl)-2,5-diphenyl-2*H*-tetrazolium bromide
MVB	multivesicular body
NBR1	neighbor of Brca1 gene
NLRP3	Nod-like receptor family protein 3

Noc	nocodazole
NP	nanoparticle
NPC1	Niemann-Pick C1 protein 1
NPF	nucleation-promoting factor
N-WASP	neural Wiskott-Aldrich syndrome protein
OGD	Oregon Green® 488 dye coupled to a 10 kDa dextran
pacsin 2	PKC and casein kinase substrate in neurons 2 (also termed syndapin 2)
PAMAM	polyamidoamine
PAS	phagophore assembly site
PBS	phosphate-buffered saline
PDT	photodynamic therapy
PEG	1) 2-[Methoxy(polyethyleneoxy)propyl]trimethoxysilane 2) poly(ethylene glycol)
PFA	paraformaldehyde
PFS	perfect focus system
PG	dendritic polyglycerol
PI(3)K, PI3K	phosphatidylinositol 3-kinase
$PI(3,5)P_2$	phosphatidylinositol-3,5-bisphosphate
$PI(4,5)P_2$	phosphatidylinositol-4,5-bisphosphate
PI3P	phosphoinositol-3-phosphate
PIKfyve	FYVE finger-containing phosphoinositide kinase
PKCα	protein kinase C α
PLL	poly-L-lysine
PM	plasma membrane
PMSF	phenylmethanesulfonylfluoride
polyQ	glutamine repeat proteins
QD	quantum dot
Rab protein	member of the Ras superfamily of monomeric G proteins
RFP	red fluorescent protein
ROI	region of interest
ROS	reactive oxygen species

RTK	receptor tyrosine kinase
S6K	mitogen activated protein kinase that phosphorylates the S6 protein of the 40S ribosomal unit
SDS	sodium dodecyl sulfate
SDS-PAGE	SDS polyacrylaminde gel electrophoresis
SH3	SRC homology 3
SiNPs	silica nanoparticles
SiO_2	silicon dioxide/ silica
siRNA	small interfering RNA
SNAP-23	synaptosome-associated protein of 23 kDa
SNAP-Tag	human DNA-repair enzyme O^6-alkylguanine DNA alkyltransferase (also known as AGT)
SNARE	soluble *N*-ethylmaleimide-sensitive factor attachment receptor
SNX	sorting nexin
SQSTM1, p62	sequestosome 1
Stx17	syntaxin 17
SV40	Simian virus 40
Syt VII	synaptotagmin VII
TBS	tris-buffered saline
TEMED	tetramethyl-ethylene-diamine
Tf^{647}	transferrin labeled with Alexa-647 dye
TFEB	transcription factor EB
TfR	transferrin receptor
TGFα	transforming growth factor α
TGN	trans-Golgi network
TiO_2	titanium dioxide
TIRF	total internal reflection fluorescence
TMP	theranostic macromolecular prodrug
Ube2D1-4	Ubc4/5 homolog in yeast, E2 ubiquitin-conjugating enzymes
ULK	UNC-51-like kinase
USP8/UBPY	ubiquitin-specific protease 8
UV	ultra violet

v/v	volume per volume
VAMP	vesicle-associated membrane protein
v-ATPase	proton pumping vacuolar-type ATPase
(VIP)21	vesicular integral membrane protein (also called caveolin 1)
VTI1B	vesicle transport through interaction with t-SNAREs homolog 1B
w/o	without
w/v	weight per volume
WIPI	WD-repeat protein interacting with phosphoinositides
WST-1	2-(4-iodophenyl)-3-(4-nitrophenyl)-5-(2,4-disulfophenyl)-2*H*-tetrazolium
XTT	2,3-bis-(2-methoxy-4-nitro-5-sulfophenyl)-2*H*-tetrazolium-5-carboxanilide

7.2 List of Figures and Tables

7.3 Publications

Schütz I., Lopez-Hernandez T., Gao Q., Puchkov D., Jabs S., Nordmeyer D., Schmudde M., Rühl E., Graf C.M., Haucke V.: Lysosomal dysfunction caused by cellular accumulation of silica nanoparticles. *Journal of Biological Chemistry*, 2016, published online May 11.

Krüger H. & **Schütz I.**, Justies A., Licha K., Welker P., Haucke V., Calderón M.: Imaging of Doxorubicin Release from Theranostic Macromolecular Prodrugs via Fluorescence Resonance Energy Transfer. *Journal of Controlled Release*, 2014, **194**, 189-196.

Graf C., Gao Q., **Schütz I.**, Noufele C. N., Ruan W., Posselt U., Korotiansky E., Nordmeyer D., Rancan F., Hadam S., Vogt A., Lademann J., Haucke V., Rühl E.: Surface Functionalization of Silica Nanoparticles Supports Colloidal Stability in Physiological Media and Facilitates Internalization in Cells. *Langmuir*, 2012, **28**(20), 7598-613.

Waiczies S., Lepore S., Sydow K., Drechsler S., Ku M.-C., Martin C., Lorenz D., **Schütz I.**, Reimann H., Purfürst B., Dieringer M. A., Waiczies H., Dathe M., Pohlmann A., Niendorf T.: Anchoring Dipalmitoyl Phosphoethanolamine to Fluorine-rich Nanoparticles Boosts Cellular Uptake and ^{19}F Magnetic Resonance Signal. *Scientific Reports*, 2015, **5**, 8427.

Wieffer M., Cibrián Uhalte E., Posor Y., Otten C., Branz K., **Schütz I.**, Mössinger J., Schu P., Abdelilah-Seyfried S., Krauß M., Haucke V.: PI4K2β/AP-1-Based TGN-Endosomal sorting regulates Wnt Signaling. *Current Biology*, 2013, **23**(21), 2185-90.